UCRL-17468

cy. 2

University of California

Ernest O. Lawrence Radiation Laboratory

NUCLEAR DOUBLE RESONANCE DYNAMICS

David Alexander McArthur
(Ph. D. Thesis)

July 1967

DISCLAIMER

UCRL-17468

UNIVERSITY OF CALIFORNIA

Lawrence Radiation Laboratory
Berkeley, California

AEC Contract No. W-7405-eng-48

NUCLEAR DOUBLE RESONANCE DYNAMICS

David Alexander McArthur

(Ph. D. Thesis)

July 1967

TABLE OF CONTENTS

NUCLEAR DOUBLE RESONANCE DYNAMICS

David Alexander McArthur

Inorganic Materials Research Division, Lawrence Radiation Laboratory,
and Department of Physics,
University of California, Berkeley, California

ABSTRACT

This is the first detailed, quantitative study of the validity of the master equation with spin temperature assumption as used to describe the nuclear double resonance detection of a rare spin species.

The technique of nuclear double resonance following adiabatic demagnetization of F^{19} nuclei in the rotating frame (ADRF), has been used to study the resonance of .13% abundant Ca^{43} in CaF_2. Radio frequency (rf) pulses were applied near the Ca^{43} Larmor frequency after ADRF, and a study of cross-relaxation between F^{19} dipolar energy and Ca^{43} Zeeman energy in the rotating-frame effective field $\vec{H}_{eB}$, measured the F^{19} dipolar spectrum in CaF_2 for this kind of transition. The measured cross-relaxation rate decreases exponentially with increasing H_{eB} at $\theta = 90°$, $60°$, $45°$, and $30°$, and is proportional to $\sin^2\theta$ where θ is the angle between the laboratory magnetic field, $\vec{H}_o$, and $\vec{H}_{eB}$. A thermal-reservoir model of the cross-relaxation process, assuming slowly-varying spin temperatures for both the F^{19} and Ca^{43} nuclei, and assuming infinitely fast spin diffusion among F^{19} nuclei, agrees with experiment at all values of θ, if a five- to ten-degree misorientation of the crystal with respect to $\vec{H}_o$ is postulated. Audio saturation double resonance measurements of cross-relaxation rates yielded results in agreement with the pulsed experiments. Pulsed experiments showed no evidence of a finite F^{19} spin diffusion rate. The first-order change in the cross-relaxation rate for small random quadrupole

splittings of the Ca^{43} resonance line is shown to vanish, and the second-order correction is partially calculated. The first measurements using double resonance were made of the transverse (T_2) and longitudinal (T_1) relaxation times of a rare spin species (Ca^{43}). Audio saturation double resonance following ADRF was used to separate the dipolar and inhomogeneous broadening of the Ca^{43} resonance line; a method was also devised to measure the Ca^{43} free induction decay indirectly. Both these methods showed that motionally narrowed dipolar broadening of the Ca^{43} line was dominant for H_o parallel to the [111] and [110] directions in CaF_2, the quadrupolar contribution to the linewidth being only about 200 Hz. A method was devised to measure indirectly the spin-lattice relaxation time T_1 of Ca^{43} in CaF_2. The temperature dependence of T_1 agrees with the electric quadrupolar relaxation mechanism, and the values are: $T_1(300°K) = 236 \pm 27$ sec, $T_1(355°K) = 169 \pm 25$ sec.

The technique of double resonance following ADRF was also used to search for resonances of the rare spins D, O^{17}, Ca^{43} and S^{33} in gypsum, $CaSO_4 \cdot 2H_2O$. A double quantum spin transition of D was observed near the D Larmor frequency, and other resonances were observed which are tentatively associated with Ca^{43} and S^{33}.

I. INTRODUCTION

A. Definition of Nuclear Double Resonance

Many diamagnetic compounds contain more than one species of nucleus with nonvanishing spin, but some of the more interesting isotopes have very weak nuclear resonance signals because of their low natural abundance or small magnetic moments.[1] But many compounds contain in addition at least one nuclear species with a large natural abundance and magnetic moment (e.g., H^1, P^{31}, F^{19}, Na^{23}, Cl^{35}, Cl^{37}), which yields a large nuclear magnetic or quadrupole resonance signal. The nuclear double resonance method takes advantage of the presence of this abundant spin species to observe indirectly the interesting rare-spin nuclear resonance in the same compound.

The nuclear double resonance method first places the ensemble of abundant spins (the "A" spins) in an ordered magnetic state which persists for a time T_o seconds, of the order of the A spin-lattice relaxation time T_{1A}. This ordered magnetic state of the A spins can be a state of phase coherence (as when an A magnetization is "locked" along a radio frequency (rf) field[2]), or it can be an ordered dipolar state created by isentropic demagnetization in either the laboratory frame (LOW DOR),[3,4,5] or the reference frame rotating at the A Larmor frequency (ADRF-DR).[6,7] Then during the relatively long time $T_o \sim T_{1A}$ an rf field (the B rf field) is applied near the resonance frequency of the rare spin of interest (the "B" spin), which causes the B spins to modulate the nuclear dipole-dipole and exchange couplings between the A and B spins. This modulation represents a coupling which transfers energy between the A and B spin systems, until they reach a dynamic equilibrium, and A spin order is transferred to the B spins. If by some means this acquired B spin order is continually destroyed as the A-B cross-

relaxation proceeds, the modulation of the local field at the A spin sites near a B spin slowly destroys the ordered magnetic state of the A spins. The amount of A spin order remaining after this "double resonance process", lasting $\sim T_o$ seconds, can be sampled by techniques which depend on the nature of the ordered A spin state. Suppose the double resonance experiment is repeated many times, sweeping the frequency of the B rf field; then since the A-B coupling is strongly modulated only when the B rf field is near the B nuclear resonance frequency f_{Bo}, the double resonance indication is a sudden decrease in the remaining A signal, when the B rf frequency f_B is near the B spin resonance frequency f_{Bo} (see Fig. 1).

Hartmann and Hahn[2] developed the theory of spin-locked double resonance (SLDR), and experimentally verified the double-resonance line shape as a function of f_B, the exponential double resonance decay of the A signal, and the need to periodically destroy the B spin order to obtain a large double resonance signal if the B spins are rare. They studied the K^{39} and K^{41} resonances in $KClO_3$ in zero laboratory magnetic field, by using the Cl^{35} signal. Also in zero field, Redfield[3] measured the pure quadrupole resonances of Cu nuclei near Ag and Zn impurities in metallic Cu, and Slusher and Hahn[4] studied the pure quadrupole resonances of Na^{23} and Cl^{35} and Cl^{37} nuclei near rare impurities in NaCl.

Several double resonance studies have also been made in high field: Bloembergen and Sorokin[8] investigated cross-relaxation between two abundant spin species, Hartland[9] observed the high-field quadrupole splittings of K^{39} nuclei around impurities in KF via the F^{19} nuclear signal, and Schumacher[10] has observed quadrupole splittings around Ag impurities in the alkali halides.

The high-field double resonance work which is closest to that described in this thesis was done by Lurie and Slichter,[11] who tested a simple but

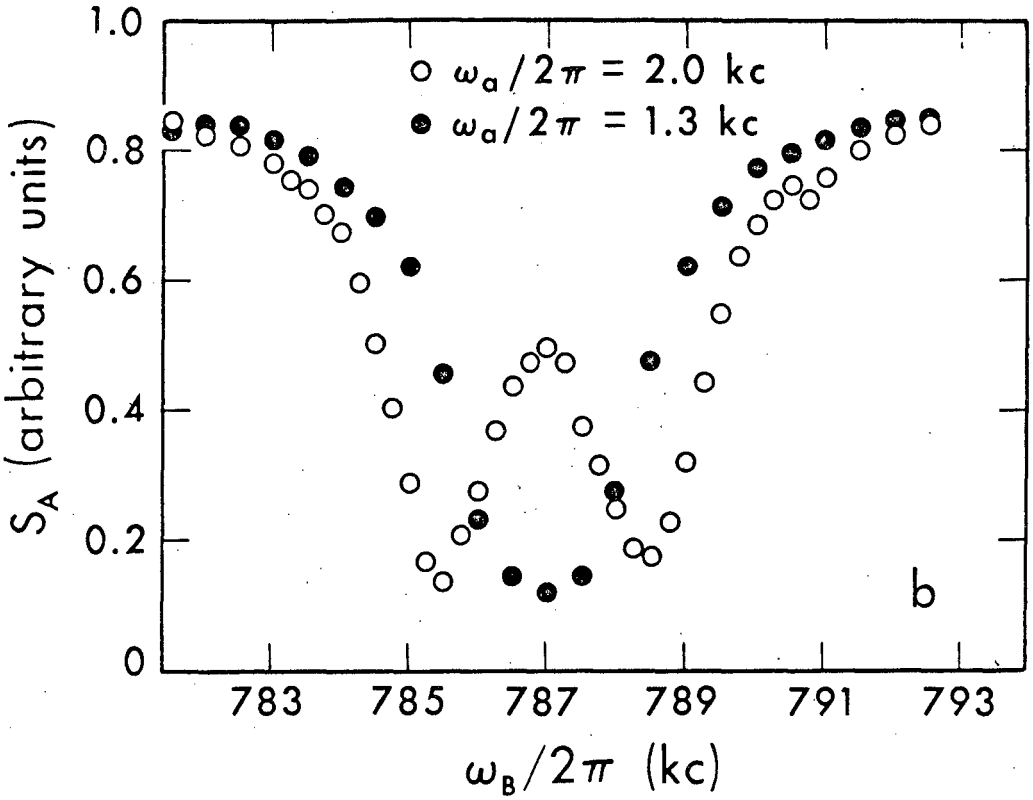

XBL 676-4148

Fig. 1 Typical double resonance signal $S_A(\omega_B)$; A spin is F^{19}, B spin is Ca^{43}, in CaF_2. Closed circles: single line for $\omega_{aud} \leq \gamma_B H_{1B}$; open circles: double line for $\omega_{aud} > \gamma_B H_{1B}$

exactly calculable equilibrium thermodynamic-reservoir model of the double resonance process by applying rf pulses at $f_B = f_{Bo}$ following spin locking or adiabatic demagnetization in the rotating frame (ADRF). They studied the resonance of 7.43% abundant Li^6 in Li metal using the 92.57% abundant Li^7; their theory of the double resonance process assumed that each B rf pulse lasted so long that the A and B systems came completely to thermal equilibrium with each other during the pulse. They derived an expression for the A-B cross-relaxation rate, assuming a Gaussian form for the A dipolar spectrum, and made a brief study of nonequilibrium effects, but they obtained experimental rates for large H_{1B} which were too large.

B. Purpose of This Investigation

There are at least three kinds of applications which can utilize the technique of nuclear double resonance: (1) Chemical studies which involve the observation of quadrupole splittings of rare spin species such as S^{33}, O^{17}, and D in a series of different chemical compounds,[12] (2) the direct measurement of the unknown electric quadrupole moment interaction of a rare spin species, and (3) studies of the spin dynamics of a rare spin species, which can in principle differ significantly from those of an abundant spin species.

The spin dynamics of a rare spin species in a solid is of interest because one of the approximations often valid for a system of abundant spins in a solid, the assumption of a slowly varying spin temperature during dynamic processes, is not necessarily valid for a rare spin species. The assumption of a spatially homogeneous spin temperature for an ensemble of nuclear spins requires a strong means of internal coupling which can restore internal thermal equilibrium in the ensemble faster than the external perturbation (spin-lattice relaxation, rf field, coupling to other species of nuclear spins) can disturb it from equilibrium. In a solid

this coupling consists of the nuclear dipole-dipole coupling between like spins: the $I_{+i}\ I_{-j}$ terms cause mutual spin flips between neighboring nuclei which are allowed because they conserve the Zeeman energy in the laboratory magnetic field.[13,14] This mutual spin flip process provides for spatial diffusion of spin energy and tends to restore a Boltzmann population distribution to the Zeeman levels if the distribution is disturbed.

But this dipole-dipole coupling is proportional to (r_{ij}^{-6}) where r_{ij} is the distance between neighboring like spins, so for the rare spins it is negligible. This means that theories of spin-lattice relaxation and cross-relaxation processes which assume spin temperatures for the nuclear species are not necessarily correct for the rare spins. Therefore it will be of interest to measure T_1, T_2, and cross-relaxation rates for a rare spin species. The double resonance process itself relies also upon the spin-diffusion process between abundant spins to carry the energy out from the isolated rare spin sites to the bulk of the abundant nuclei. If this spin diffusion process is not fast compared to A-B cross-relaxation rates, in calculating the double resonance rate it would be necessary to take into account the actual spin temperature distribution of the A spins around each B spin.

The bulk of this thesis will be concerned with the high-field double resonance dynamics of the B spin Ca^{43} in CaF_2, using as A spins the F^{19} nuclei (see Fig. 2 and Table I).

Table I. Properties of the nuclear species in CaF_2.

Nucleus	Spin	Abundance	$(\gamma_B/2\pi)$ (kHz/gauss)
Ca^{43}	7/2	0.13%	.2865
F^{19}	1/2	100%	4.0055

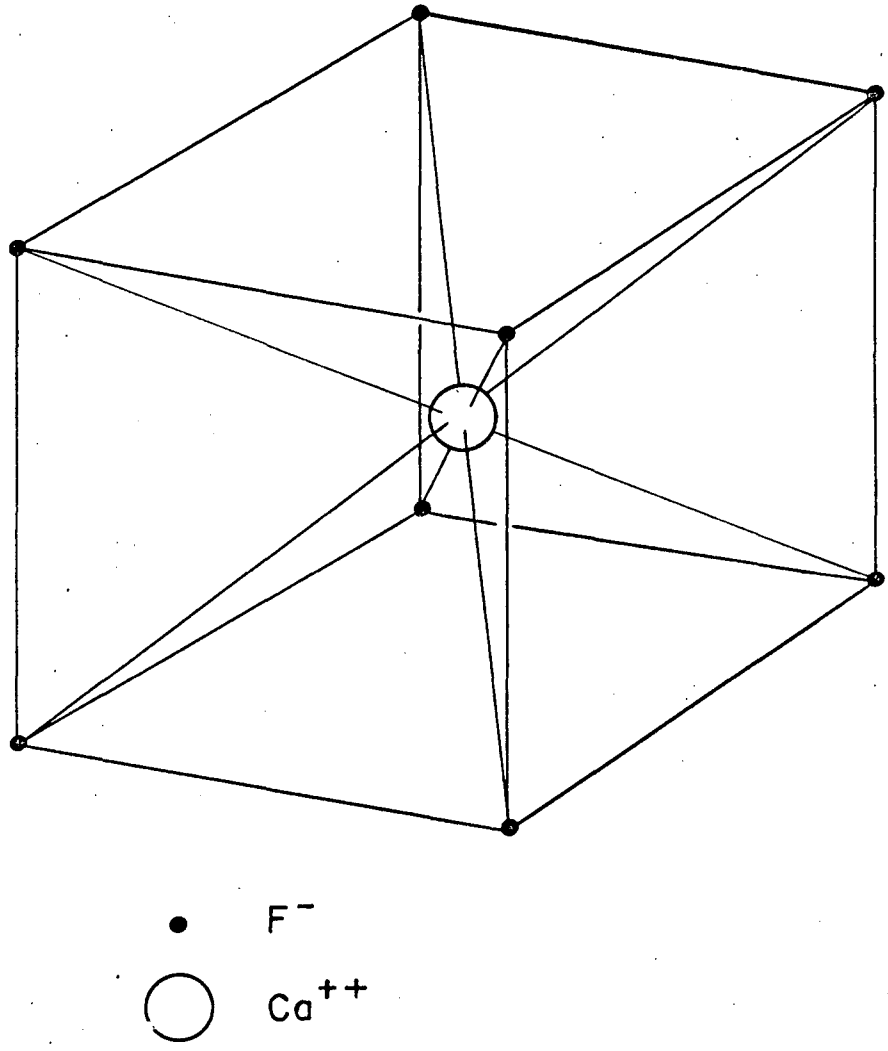

XBL 676-4149

Fig. 2 Lattice of CaF_2 near a Ca^{43} spin site, showing the eight nearest F^{19} neighbors; a is the edge of the cubic lattice of F^- ions

To test whether rare spins obey the same dynamics as abundant spins, we shall make our calculations assuming that the Ca^{43} spins are described by a spin temperature during cross-relaxation. We shall also assume (justifiably) infinitely fast spin diffusion among F^{19} spins, so the F^{19} spins will be described during A-B cross-relaxation by a spatially homogeneous spin temperature. Then if there is significant disagreement between theory and experiment, and if this disagreement cannot be completely explained by such perturbations as random quadrupole splittings, we shall have an idea of the importance of finite A spin diffusion rates, or lack of a B spin temperature in some processes.

The case of Ca^{43} in CaF_2 is particularly attractive because it should allow a precise comparision between theory and experiment:

(1) No other A or B spin species are present to complicate our calculations, and the average concentration of isolated Ca^{43} nuclei is accurately known because it is a naturally-occurring isotope rather than an impurity, which might form clusters.

(2) Because the spin = $\frac{1}{2}$ F^{19} nuclei have no quadrupole splittings near the ever-present crystalline imperfections, spin diffusion rates should be exactly calculable.[15] It is conceivable that the low relative abundance of Ca^{43} in CaF_2 would introduce spin diffusion effects which might be important for large cross-relaxation rates (see Appendix A for a discussion of this point). The experimental results, however, show no effects of diffusion in this case.

(3) Because CaF^2 is an insulator and readily available in large single crystals, our results will not be complicated by skin depth effects or powder averages.[11] We are also able to vary the A-B dipolar coupling over a wide range by rotating the crystal with respect to the laboratory magnetic field H_o.

(4) In high field H_o the A-A, A-B, and B-B spin-spin Hamiltonians simplify considerably, and since the relative abundance of Ca^{43} is about 10^{-2} of the relative abundance of Li^6 in Li metal, we can neglect the B-B coupling entirely.

(5) Because the environment of Ca^{43} in CaF_2 is cubic there will be no quadrupole splitting of the Ca^{43} resonance line (except by crystalline imperfections), so calculations can be carried out in an operator formalism, rather than dealing with explicit B eigenstates. On the other hand, it is fortunate for our investigation of B spin temperature effects that Ca^{43} possesses an electric quadrupole moment, because the presence or absence of a spin temperature during relaxation affects the details of the quadrupolar spin-lattice relaxation mechanism, which is expected to be dominant for Ca^{43} at room temperature.

In the work reported here the ordered A spin state was formed by adiabatic demagnetization in the rotating frame (ADRF), for three reasons: (1) Double resonance on this ordered state requires only one rf field, so only its amplitude and frequency require setting and monitoring. (2) Only with this ordered A spin state can one use the rotary saturation method of Redfield[16] and of Anderson and Hartmann[6] to destroy the B spin order, because only the ADRF state of the A spins is not affected directly by the applied audio field. (3) A study of the A dipolar - B Zeeman cross-relaxation rate traces out the A dipolar spectrum for this kind of cross-relaxation transition (see Fig. 5).

The following is a list of the original work reported in this thesis:

(1) A detailed study was made of the cross-relaxation process between F^{19} dipolar energy, and the Ca^{43} Zeeman energy of the Ca^{43} spins in the effective field H_{eB} in the rotating fraom (see Fig. 7). A digital computer

was used to extract the A-B cross-relaxation parameters from pulsed - B rf double resonance measurements related to those of Lurie and Slichter.[11] The exact cross-relaxation equations were used, including the effects of finite A spin-lattice relaxation and large B spin heat capacity. As a result the A dipolar spectrum for the cross-relaxation type of transition was obtained as a function of the angle θ which the effective field H_{eB} in the B rotating frame makes with the laboratory z-axis. This study confirms that the spin temperature assumption for the B spins during cross-relaxation is a good one, since the $\theta \neq 90°$ measurements show that first-order time dependent perturbation theory is sufficient to calculate the rates, and the first-order transition probabilities preserve a Boltzmann distribution during relaxation. The cross-relaxation spectra, which are usually assumed to be Gaussian in shape,[2,11] were measured to be accurately exponential for high frequency, which implies that the correlation function of the local field at a Ca^{43} spin site is Lorentzian in time, for short times.

(2) A small transient oscillation of the Ca^{43} magnetization along the field H_{eB}, at the beginning of each B rf pulse, was also studied. Analogues of this oscillation have been observed before,[17,18] but this is the first such case involving two different spin species, and it is relatively easy to calculate the expected shape of the oscillation. The decay of the oscillation is related to the local field correlation function mentioned above, and was found to be in agreement with theory.

(3) A detailed study has been made of the rotary saturation ("audio saturation") method of destroying the B spin order. Audio saturation double resonance was always used to measure the B effective field H_{eB} in the rotating frame, and the angle θ which the B effective field makes

with the laboratory magnetic field (see Fig. 7). Audio saturation was used to measure a cross-relaxation parameter which determines the maximum possible double resonance rate at a given H_{eB} and θ. A study was made of the audio saturation linewidths as a function of θ, which allows separation of the dipolar contribution from the quadrupolar and inhomogeneous contributions to the ordinary B spin linewidth.

(4) An indirect method of measuring the free induction decay of a Ca^{43} magnetization transverse to the laboratory field was developed, and this free induction decay was related to the A dipolar spectrum for the case of Ca^{43} in CaF_2.

(5) An indirect method of measuring the 0.13% abundant Ca^{43} spin-lattice relaxation time T_{1B} was devised to look for anisotropic or non-exponential relaxation of the Ca^{43} magnetization along H_o. No anisotropy was found, which confirmed certain properties of the noise spectrum which causes quadrupole relaxation. This is the first type of measurement in which spin-lattice relaxation of a low abundance nucelar species has been carried out.

(6) In addition to the work reported above on Ca^{43} in CaF_2, a search for rare-spin quadrupole resonances in gypsum ($CaSO_4 \cdot 2H_2O$) was made, using the protons in waters of hydration as the A spins. A double-quantum spin transition of naturally-occurring deuterium was observed, but no ordinary quadrupolar satellites. ~~Other double resonance lines~~ were observed which are probably associated with the rare spins Ca^{43} and S^{33}.

II. DOUBLE RESONANCE FOLLOWING ADIABATIC DEMAGNETIZATION IN THE ROTATING FRAME (ADRF)

A. Qualitative Description of ADRF Double Resonance

1. Definition of the A Dipolar System

Since we are interested in high-field nuclear double resonance, we shall restrict our discussion to the case of A and B nuclear spins in a laboratory magnetic field H_o much larger than the local fields (~1 gauss) produced at a nuclear spin site by neighboring nuclei, and much larger than any rf fields H_{1A} or H_{1B} which are applied to the sample. Then if we work with nuclear spin temperatures $T_s \gg 10^{-5}°K$, the high temperature approximation holds: $\hbar\omega_o/kT_s \ll 1$, where $\omega_o = \gamma H_o$, and γ is the A or B spin gyromagnetic ratio.

To describe the A dipolar state we shall assume that no audio or rf fields are applied to the sample, and consider only the effects of the laboratory magnetic field, and nuclear dipole-dipole coupling between the A and B spins. We also neglect A and B spin-lattice interaction, and assume that the A and B spins have no large electric quadrupole interactions, as is the case for Ca^{43} in CaF_2. We shall write our Hamiltonians in angular frequency units because of the many exponential operators used in the theory. Then the total Hamiltonian becomes:

$$\hbar\mathcal{H}_{Lab} = \hbar(\mathcal{H}_Z^A + \mathcal{H}_Z^B + \mathcal{H}_d^{AA} + \mathcal{H}_d^{AB})$$

where $\mathcal{H}_Z^A$ and $\mathcal{H}_Z^B$ are the Zeeman interactions of the A and B spins with H_o:

$$\mathcal{H}_Z^A = -\gamma_A H_o \sum_i I_{Zi} = -\omega_{Ao} I_Z,$$

$$\mathcal{H}_z^B = -\gamma_B H_o \sum_k S_{zk} = -\omega_{BO} S_z$$

and $\vec{I}_k \hbar$ and $\vec{S}_k \hbar$ are the angular momentum vectors for the kth, A and B spins, respectively. $\mathcal{H}_d^{AA}$ and $\mathcal{H}_d^{AB}$ are the nuclear dipole-dipole interactions among A spins, and between A and B spins.[19] We neglect dipole-dipole coupling between the rare B spins because they are on the average far from each other, and the dipolar field falls off as r^{-3}.

Because we are in high field, the dipolar terms are a small perturbation on $\mathcal{H}_z^A + \mathcal{H}_z^B$, so we can retain only the diagonal, or secular, parts of $\mathcal{H}_d^{AA} + \mathcal{H}_d^{AB}$ in the representation in which $(\mathcal{H}_Z^A + \mathcal{H}_Z^B)$ is diagonal. Therefore we separate each term in the dipolar Hamiltonian into secular (s) and non-secular (ns) parts:

$$\mathcal{H}_d^{AA} = \mathcal{H}_d^A(s) + \mathcal{H}_d^A(ns).$$

Then the approximate Hamiltonian including only the secular dipolar terms becomes:

$$\hbar \mathcal{H}_{Lab}^o = \hbar \left(\mathcal{H}_Z^A + \mathcal{H}_Z^B + \mathcal{H}_d^A(s) + \mathcal{H}_d^{AB}(s) \right),$$

where

$$\mathcal{H}_d^A(s) = \sum_{i<j} \left(A_{ij}^A I_{zi} I_{zj} + 2B_{ij}^A \left[I_{xi} I_{xj} + I_{yi} I_{yj} \right] \right),$$

$$\mathcal{H}_d^{AB}(s) = \sum_{i,k} A_{ik}^{AB} I_{zi} S_{zk},$$

$$A_{ij}^A = \gamma_A^2 \hbar \, (1-3\cos^2\theta_{ij}) r_{ij}^{-3},$$

and

$$A_{ik}^{AB} = \gamma_A \gamma_B \hbar \, (1-3\cos^2\theta_{ik}) r_{ik}^{-3}.$$

θ_{ij} is the angle between the laboratory magnetic field and the vector $\vec{r}_{ij}$ connecting the i th and j th nuclear spins.

Since by definition $\mathcal{H}_Z^A$ and $\mathcal{H}_d^A(s)$ commute, they are approximately independent, being coupled only weakly in high field by the non-secular perturbation $\mathcal{H}_d^A(ns)$. Philippot[20] has shown that if H_o is large and the high temperature condition above is satisfied, the Zeeman Hamiltonians $\mathcal{H}_Z^A$ and $\mathcal{H}_Z^B$ in the absence of rf fields can be assigned spin temperatures independently of the spin temperature of the "dipolar" Hamiltonian $\mathcal{H}_d^A(s) + \mathcal{H}_d^{AB}(s)$. $\mathcal{H}_d^A(s)$ is responsible for the close coupling among abundant spins mentioned above, since the $I_{xi}I_{xj}$ terms cause mutual spin flips between neighboring A spins.

If there are two species of abundant spins (A and A') in the sample, $\mathcal{H}_d^{AA'}(s)$ will strongly couple $\mathcal{H}_d^A(s)$ and $\mathcal{H}_d^{A'}(s)$ since it does not commute with either of them. This means that in the absence of rf fields there exists only a single secular "dipolar" reservoir for all the spins in the sample, with spin temperature T_{ss} and Hamiltonian $\mathcal{H}_d(s)$:

$$\mathcal{H}_d(s) = \mathcal{H}_d^A(s) + \mathcal{H}_d^{AA'}(s) + \mathcal{H}_d^{A'}(s) + \mathcal{H}_d^{AB}(s) + \mathcal{H}_d^{A'B}(s).$$

The presence of more than one A spin species in the sample may increase the sensitivity of ADRF double resonance, since all A spin species in the total dipolar reservoir will couple to the B spin of interest. Perhaps A'-B coupling will compensate for the weakness of A-B dipolar coupling for certain directions of H_o.

2. Formation of the Ordered Dipolar State

We assume that there is no quadrupole interaction in the A Hamiltonian, either because the A spin $I = \frac{1}{2}$, or because the crystal is cubic. If the A spin system is allowed to come into thermal equilibrium with the lattice,

$\mathcal{H}_d^A(s)$ and $\mathcal{H}_Z^A$ will be at the lattice temperature T_L. Because $\mathcal{H}_Z^A \gg \mathcal{H}_d^A(s)$, most of the A spin order will reside in the A magnetization, which is shown parallel to the laboratory z-axis in Fig. 3a.

If we now apply an rf field with rotating component H_{1A} at the A Larmor frequency, and view the A system from a reference frame rotating at this frequency, the effective field $H_{eA} = H_{1A}$ will be constant and perpendicular to H_o since we are on resonance. If $H_{1A} \gg H'_{LA}$ and is applied for a time $t_w = \frac{\pi}{2\omega_{1A}}$, where $\omega_{1A} = \gamma_A H_{1A}$, the A magnetization M_{oA} will rotate through 90° perpendicular to H_{1A}. If at time t_w the phase of the rf field is shifted by 90°, H_{1A} will lie along M_{oA}. According to Redfield's[16] hypothesis of a spin temperature in the rotating frame, the A dipolar interaction $\mathcal{H}_d^A(s)$ and $\mathcal{H}_{Arf}^A = -\omega_{1B} I_x$ will come into thermal equilibrium in the rotating frame, but this will not change M_A much if $H_{1A} \gg H'_{LA}$. This "spin locked" state will not decay except by A spin-lattice relaxation, in a time of order T_{1A}. If $H_{1A} \gg H'_{LA}$, the rotating frame A spin temperature in the "spin locked" state is then given by

$$T_A = \frac{C_A H_{eB}}{M_{oA}} = \frac{H_{1B}}{H_o} T_L \ll T_L.$$

If H_{1A} is now reduced to zero in a time long compared to T_{2A}, the internal thermal equilibration time of the A spin system, the demagnetization is isentropic and the A system spin temperature T_A obeys the law:[13]

$$T_A \propto \sqrt{H_{1A}^2 + H'^2_{LA}}$$

where

$$H'^2_{LA} \equiv T_r\left\{\mathcal{H}_d^A(s)^2\right\} \Big/ T_r\left\{M_x^{A^2}\right\}$$

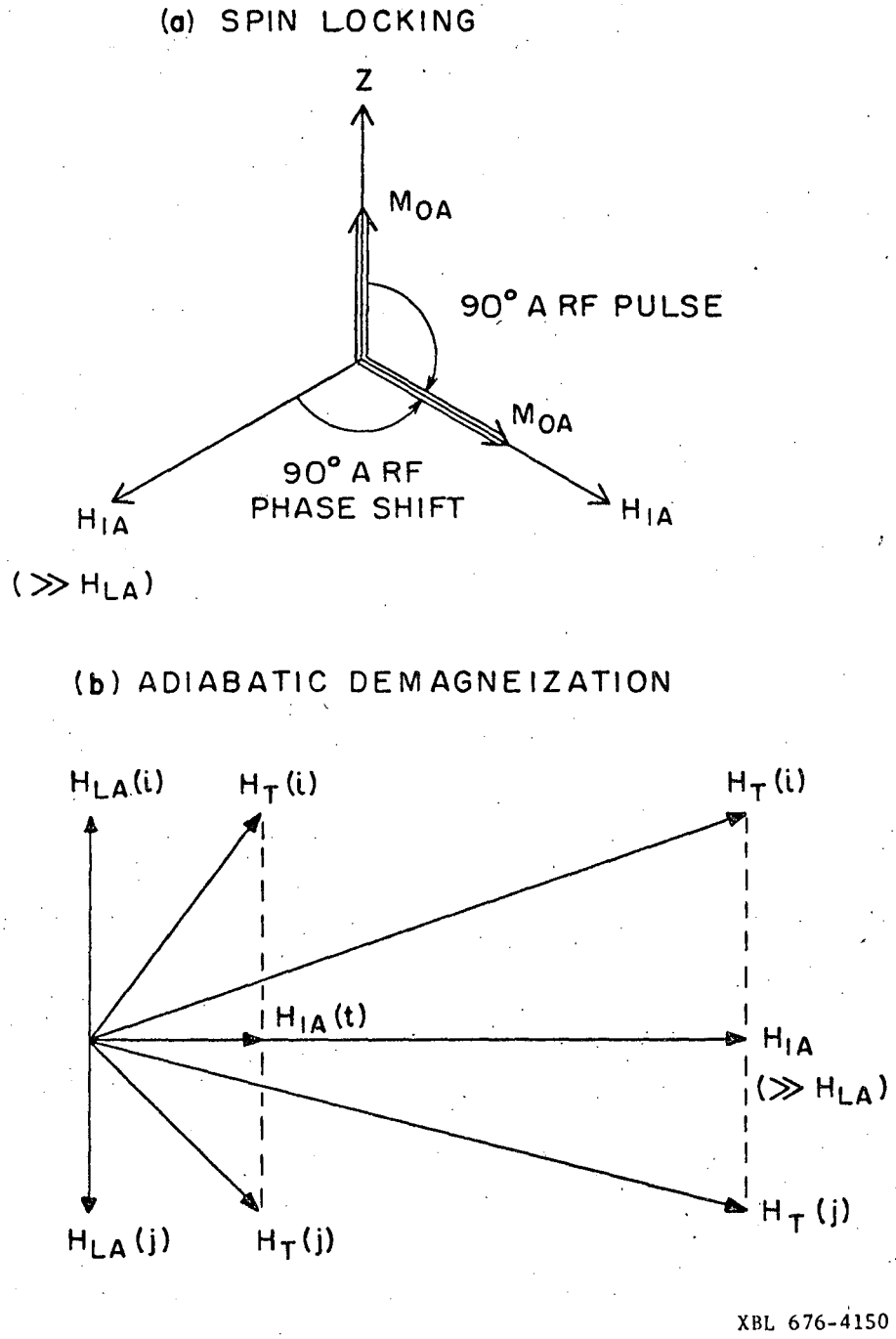

Fig. 3 ADRF process viewed from a frame rotating at the A spin Larmor frequency

and

$$M_x^A \equiv \gamma_A I_x .$$

The A dipolar spin temperature T_{Ai}, after ADRF, is thus

$$(T_{Ai}) \cong \frac{H'_{LA}}{\sqrt{H_{1A}^2 + H_{LA}'^2}} T_L \left(\frac{H_{1A}}{H_o}\right) \cong \left(\frac{H'_{LA}}{H_o}\right) T_L .$$

As can be seen in Fig. 3b, preferential alignment of each spin along H_{1A} has been converted by the adiabatic demagnetization process into preferential alignment along the local field each A spin sees at its spin site. Since these local fields are random there is no net magnetization associated with this ordered dipolar state. This process is called "adiabatic demagnetization in the rotating frame" (ADRF).[6]

To sample the order in the dipolar state an rf pulse of width θ° at the A larmor frequency can be applied $\left(\frac{\pi}{4} \leq \theta \leq \frac{\pi}{2}\right)$, which results in a "dipolar" free induction decay of a characteristic shape[6] (see Fig. 4b), 90° out of phase with the rf field producing it. The amplitude of this free induction decay is proportional to T_{Af}^{-1}, where T_{Af} is the A dipolar spin temperature following the double resonance process. Another way of sampling T_{Af} which is particularly useful for the case of several abundant spin species in the same sample is to reverse the adiabatic demagnetization process, increasing H_{1A} until it is $\gg H'_{LA}$, so that an A magnetization M_{fA} develops along H_{1A}. Then if H_{1A} is suddenly turned off, the A magnetization will produce an ordinary A Zeeman free induction decay, the amplitude of which is again proportional to T_{Af}^{-1}. Adiabatic remagnetization results in larger signals when there is more than one kind of A spin, because all A spin species contribute to the order in the magnetization M_{fA}.

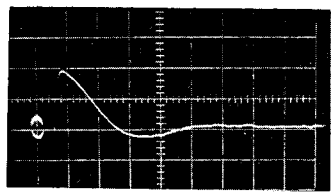

Fig. 4a F^{19} Zeeman signal at detector; horizontal: 20μsec/div.; vertical: 2 volts/div.; $H_o \parallel [111]$ in CaF_2

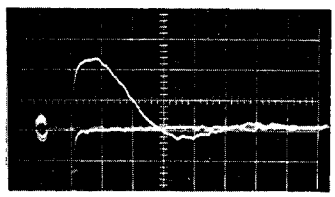

XBB 677-3643

Fig. 4b F^{19} dipolar signal at detector; horizontal: 20μsec/div.; vertical: 1 volt/div.; $H_o \parallel [111]$ in CaF_2

3. Mechanism of the ADRF Double Resonance Coupling

If an rf field with frequency f_{Bo} and amplitude $2H_{1B}$ large compared to local dipolar fields applied to the sample, $\mathcal{H}_d^{AB}(s)$ is no longer part of the "dipolar" Hamiltonian, but instead couples the Zeeman energy of the B spins in H_{1B} to the dipolar energy of the A system. The B rf field Hamiltonian can be written (neglecting the effect of H_{1B} on the A spins because $f_{Bo} \neq f_{Ao}$):

$$\mathcal{H}_{Brf}^{B} = -\gamma_B 2H_{1B} \cos(2\pi f_{Bo} t)\, S_x.$$

In a reference frame rotating around H_o at the frequency f_{Bo}, and in the same sense as the precession of the B spins around H_o, one of the rotating components H_{1B} of the oscillating B rf field is stationary. As the B spins precess around H_{1B} in the rotating frame, they produce local fields oscillating along the H_o direction at their A neighbors. These oscillating local fields induce transitions between the eigenstates of the A dipolar Hamiltonian $\mathcal{H}_d^A(s)$, causing cross-relaxation. If the crystal is thought of as broken up into subsystems, each subsystem containing one B spin plus the average number of A spins per B spin, then the dipolar eigenstates of $\mathcal{H}_d^A(s)$ will be unknown, but their energies should be well represented by a continuum, as in Fig. 5, because there are so many A spins per B spin (~1540 in CaF_2). Since $\mathcal{H}_d^{AB}(s)$ does not commute with either the B Zeeman Hamiltonian in the rotating frame $\mathcal{H}_{Brf}^{B'}$,

$$\mathcal{H}_{Brf}^{B'} = -\gamma_B H_{1B} S_x,$$

or $\mathcal{H}_d^A(s)$, $\mathcal{H}_d^{AB}(s)$ induces transitions in which the A dipolar system goes between two A dipolar levels separated in energy by $\hbar\gamma_B H_{1B}$ in the

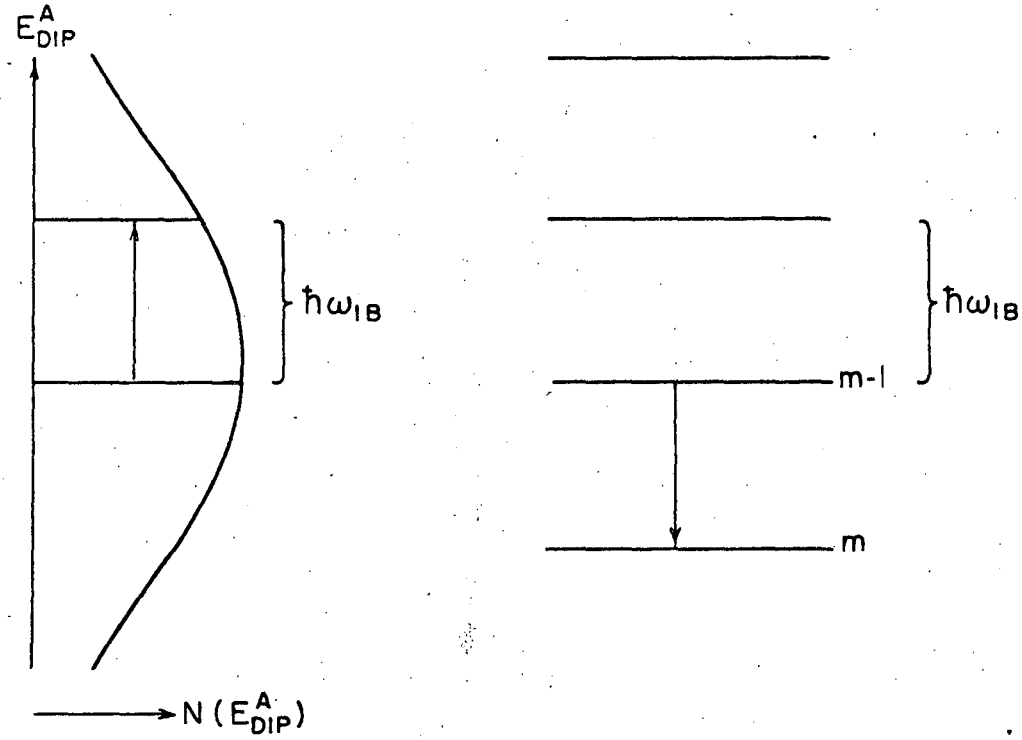

A
DIPOLAR ENERGY LEVELS.

B
ZEEMAN ENERGY LEVELS.

XBL 676-4152

Fig. 5 General type of A dipolar-B Zeeman cross-relaxation transition; $N(E^A_{DIP})$ is the density of A dipolar energy levels having A dipolar energy E^A_{DIP}

"continuum", and a B spin simultaneously makes a transition between two of its $2S + 1$ equally spaced Zeeman levels in H_{1B}. In this way energy is exchanged between the A and B systems until they reach a common spin temperature.

4. Thermal Reservoir Model of the A-B Cross-relaxation Process

Because there is strong dipolar coupling between A spins and because the A-B coupling is a small perturbation on the A dipolar system if the B spins are rare, it is reasonable to regard the A dipolar system as a thermal reservoir with a spin temperature $T_A(t)$ which changes slowly because of the A-B coupling. The B Zeeman system does not have a similar mechanism for restoring internal thermal equilibrium if the B system is disturbed from a Boltzmann population distribution. But it may be possible to describe the B system during cross-relaxation by a varying spin temperature $T_B(t)$, if the B system starts out in a Boltzmann distribution and the matrix elements of the A-B coupling are proportional to S_x, which preserves a high-temperature Boltzmann distribution. $T_B(t)$ is then really a parameter describing the approach of the B system toward the A spin temperature T_A, rather than a true spin temperature.

If we regard both the A and B spin systems as thermal reservoirs, the heat capacity of the A reservoir will be much larger than the B heat capacity because the B spins are rare. We define the coupling rate $W_{AB} = \tau_{AB}^{-1}$ for the exchange of energy between the reservoirs, and denote the ratio of heat capacities (at the same temperature) by ϵ:

$$\epsilon = \frac{C_B(T)}{C_A(T)} = \frac{C_B H_{1B}^2}{C_A H_{LA}^2} \ll 1.$$

The ADRF process places the A reservoir in a state of low spin temperature (see Fig. 6). When the B rf field is turned on the B reservoir is created, with T_B much higher than T_A, and if $f_B \cong f_{Bo}$ and H_{1B} is not too large, the resonant AB coupling transfers energy from the hot B Zeeman system to the cold A dipolar system with time constant τ_{AB}. If we can neglect A and B spin-lattice interaction, the total energy will be conserved:

$$E_A(t) + E_B(t) = \text{const.} \tag{1}$$

For $t \gg \tau_{AB}$, $T_B \cong T_A$, and the energy flow will stop; in this condition according to the definition of ϵ, since $E = -TC(T)$,

$$E_B = \epsilon E_A. \tag{2}$$

If our initial conditions were $E_B = 0$, $E_A = E_{Ao}$, Eqs. (1) and (2) imply:

$$E_A(t \gtrsim 3\tau_{AB}) \cong \frac{1}{1+\epsilon} E_{Ao}.$$

Thus a single contact between the cold A reservoir and the hot B reservoir will result in an unobservable change in the A signal if ϵ is small. It is therefore necessary to continually reheat the B reservoir and bring it into contact again and again. This reheating can be accomplished in several ways: (1) 180° phase shifting of the B rf about every τ_{AB} seconds,[2,4] (2) pulsing the B rf on for several τ_{AB} and then off for several T_{2B}^{11}, or (3) continually saturating the B magnetization in the rotating frame by an audio field parallel to H_o, which satisfies the Redfield rotary saturation condition $\omega_{aud} = \gamma_B H_{1B}$.[6,7] Methods (2) and (3) have been particularly useful for the case of Ca^{43} in CaF_2, for measuring ϵ and τ_{AB}. In a time $t \sim T_{1dip} \sim T_{1A}$, $N \cong t/3\,\tau_{AB}$ pulses can be applied (if $T_{2B} \ll \tau_{AB}$), resulting in the following decay of the A dipolar energy:

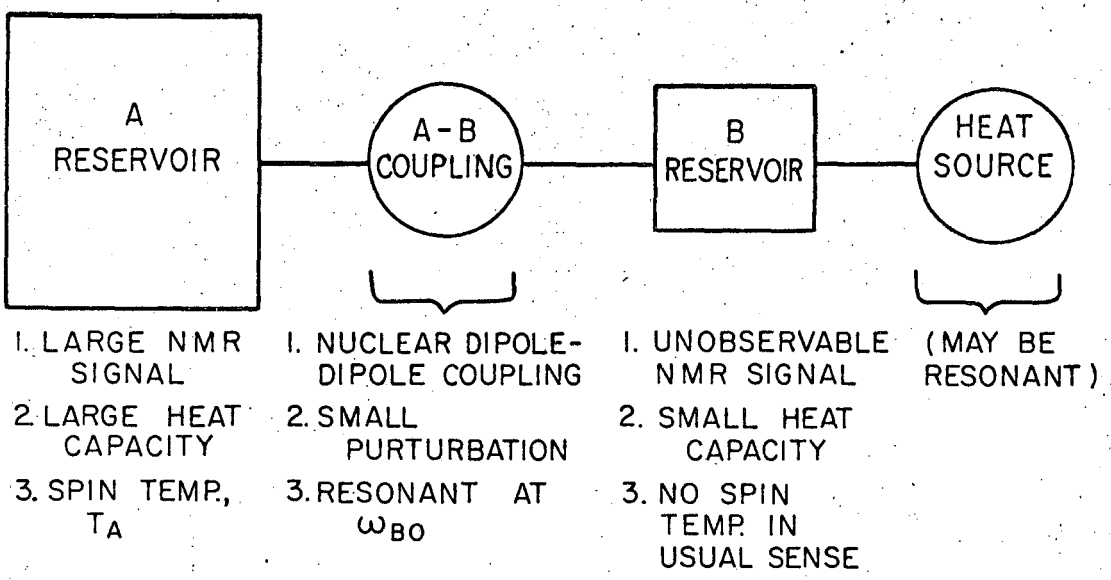

Fig. 6 Thermal reservoir model of the rare-spin double resonance process

$$\frac{E_A(N)}{E_{Ao}} \cong \left(\frac{1}{1+\epsilon}\right)^N \cong e^{-N} = e^{-t\epsilon/3\tau_{AB}}$$

Thus (ϵ/τ_{AB}) is a parameter characterizing the strength of the double resonance rate.

B. Derivation of the A Dipolar - B Zeeman Cross-Relaxation Equations

1. Laboratory Frame Hamiltonian

Now we proceed to calculate the equation which describes the cross relaxation between the Ca^{43} Zeeman energy in the rotating frame, and the F^{19} dipolar energy. Suppose that we are doing pulsed ADRF-DR, so that when an rf pulse is applied to the sample, the laboratory frame Hamiltonian $\hbar\mathcal{H}_L$ is given by

$$\hbar\mathcal{H}_L = \hbar\,\mathcal{H}_{ZA} + \mathcal{H}_{ZB} + \mathcal{H}_{dd}^{AA} + \mathcal{H}_{dd}^{AB} + \mathcal{H}_{Brf}^{B} + \mathcal{H}_{Brf}^{A}, \quad (3)$$

where we neglect the spin-lattice interaction of both the A and B spins, and neglect the dipole-dipole coupling of the rare B spins because the average distance between B spins is so large. $\mathcal{H}_{ZA}$ and $\mathcal{H}_{ZB}$ are the Zeeman interaction of the A and B spins with the laboratory magnetic field, $\mathcal{H}_{dd}^{AA}$ and $\mathcal{H}_{dd}^{AB}$ are the dipole-dipole interaction between abundant A spins and between abundant A and rare B spins, respectively, and $\mathcal{H}_{Brf}^{A}$ and $\mathcal{H}_{Brf}^{B}$ are the coupling of A and B spins with the rf field near the B resonance frequency. The laboratory frame density matrix obeys the equation:

$$\frac{d\rho_L}{dt} = -i\,[\mathcal{H}_L, \rho_L] \quad . \quad (4)$$

Since the A and B spins are assumed to have different resonance frequencies, the B rf pulse is far off resonance for the A spins and has no direct effect on them, so $\mathcal{H}^A_{Brf}$ can be dropped from the Hamiltonian.

2. Transformation to the Rotating Frame

The near-resonant B rf field in conjunction with the A-B cross-relaxation can cause a phase coherence to develop among the B spins, and thus a large component of B magnetization precessing perpendicular to the laboratory magnetic field. But this implies that the laboratory frame density matrix ρ_L will have large off diagonal components, so the B spin system cannot be described by a spin temperature in the laboratory frame. Therefore, in the presence of a resonant rf field it is necessary to transform to a frame rotating with the in-phase component of the rf field, in order to obtain an approximately time-independent Hamiltonian whose behavior can be described by slowly-varying spin temperatures.

The transformation to the rotating frame is accomplished by the operation

$$\rho'_R = T(t)\, \rho_L\, T^{-1}(t)$$

where ρ'_R is the rotating frame density matrix and

$$T(t) = \exp\ \{+i(\mathcal{H}^A_Z - \omega_B S_z)t\}\ . \qquad (5)$$

One can derive the equation of motion of ρ'_R by using the definition (5) of T(t) and the equation of motion (4) for ρ_L:

$$\frac{d\rho_R'}{dt} \cong -i[\mathcal{H}_R', \rho_R'] \,. \tag{5a}$$

The approximation in Eq. (5a) is the neglect of time dependent terms in $\mathcal{H}_R'$ which are non-secular because they oscillate at frequencies of the order of ω_{Ao}, ω_{Bo}, which are much greater than any rotating-frame resonance frequencies. $\mathcal{H}_R'$ is given by:

$$\mathcal{H}_R' = \mathcal{H}_Z^{B'} + \mathcal{H}_{Brf}^{B'} + \mathcal{H}_d^A(s) + \mathcal{H}_d^{AB}(s),$$

where

$$\mathcal{H}_Z^{B'} = -(\omega_{Bo} - \omega_B) \sum_k S_{zk},$$

$$\mathcal{H}_{Brf}^{B'} = -\gamma_B H_{1B} \sum_k S_{xk},$$

$$\mathcal{H}_d^A(s) = \sum_{i<j} \{A_{ij}^A I_{zi} I_{zj} + 2B_{ij}^A (I_{xi} I_{xj} + I_{yi} I_{yj})\}, \tag{6}$$

$$\mathcal{H}_d^{AB}(s) = \sum_{i,k} A_{ik}^{AB} I_{zi} S_{zk}, \tag{7}$$

and where

$$A_{ij}^A = \frac{\gamma_A^2 \hbar (1 - 3\cos^2\theta_{ij})}{r_{ij}^3} = -4B_{ij}^A, \tag{8}$$

and

$$A_{ik}^{AB} = \frac{\gamma_A \gamma_B \hbar (1 - 3\cos^2\theta_{ik})}{r_{ik}^3} \,. \tag{9}$$

γ_A and γ_B are the gyromagnetic ratios of the A and B spin species, θ_{ij} is the angle between the laboratory magnetic field and the vector $\vec{r}_{ij}$

connecting the ith and jth nuclear spins, and $\vec{I}_n$ and $\vec{S}_n$ are the A and B angular momentum vectors, respectively.

The two terms $\mathcal{H}_Z^{B'} + \mathcal{H}_{Brf}^{B'}$ form the effective field in the rotating frame, which makes an angle θ with the laboratory z-axis (Fig. 7). Since the rf field H_{1B} is chosen to be much larger than the local field at a B spin site due to its A neighbors, to a first approximation the strong Zeeman interaction with the effective field H_{eB} forms the B spin Hamiltonian in the rotating frame. Thus one must satisfy the larmor resonance condition in the rotating frame which corresponds to $\gamma_B H_{eB} = \omega_L$, not $\omega_L = \gamma_B H_{1B}$. The existence of a double peak as ω_B is swept (for the condition $\omega_{aud} > \gamma_B H_{1B}$), and the $\theta \neq 90°$ audio resonances confirm that $\mathcal{H}_{eB}$ is the correct zero-order Hamiltonian in the rotating frame, at least for large H_{1B} (see Fig. 1). It has been shown experimentally that this approximation breaks down for small H_{1B}.[21] In order to single out the zero-order (effective field H_{eB}) part of the B spin Hamiltonian, it is convenient to rotate the axis of quantization of the B spins through θ degrees about the y-axis in the rotating frame to lie along H_{eB}. Defining $\omega_{eB} = \sqrt{\Delta\omega_B^2 + \omega_{1B}^2}$, so that $\Delta\omega_B = \omega_{eB}\cos\theta$ and $\omega_{1B} = \omega_{eB}\sin\theta$, $\mathcal{H}_Z^{B'} + \mathcal{H}_{Brf}^{B'}$ can be rewritten:

$$\mathcal{H}_Z^{B'} + \mathcal{H}_{Brf}^{B'} = -\omega_{eB}(\cos\theta\, S_z + \sin\theta\, S_x)$$

$$= -\omega_{eB}\, e^{-i\theta S_y} S_z e^{+i\theta S_y}.$$

Thus the transformation $R = e^{i\theta S_y}$ will make the new z-axis lie along H_{eB}. Furthermore, since R is not a function of time and $[\mathcal{H}_d^A(s), S_y] = 0$, the new density matrix ρ_R and the new Hamiltonian $\mathcal{H}_R$ will be given by

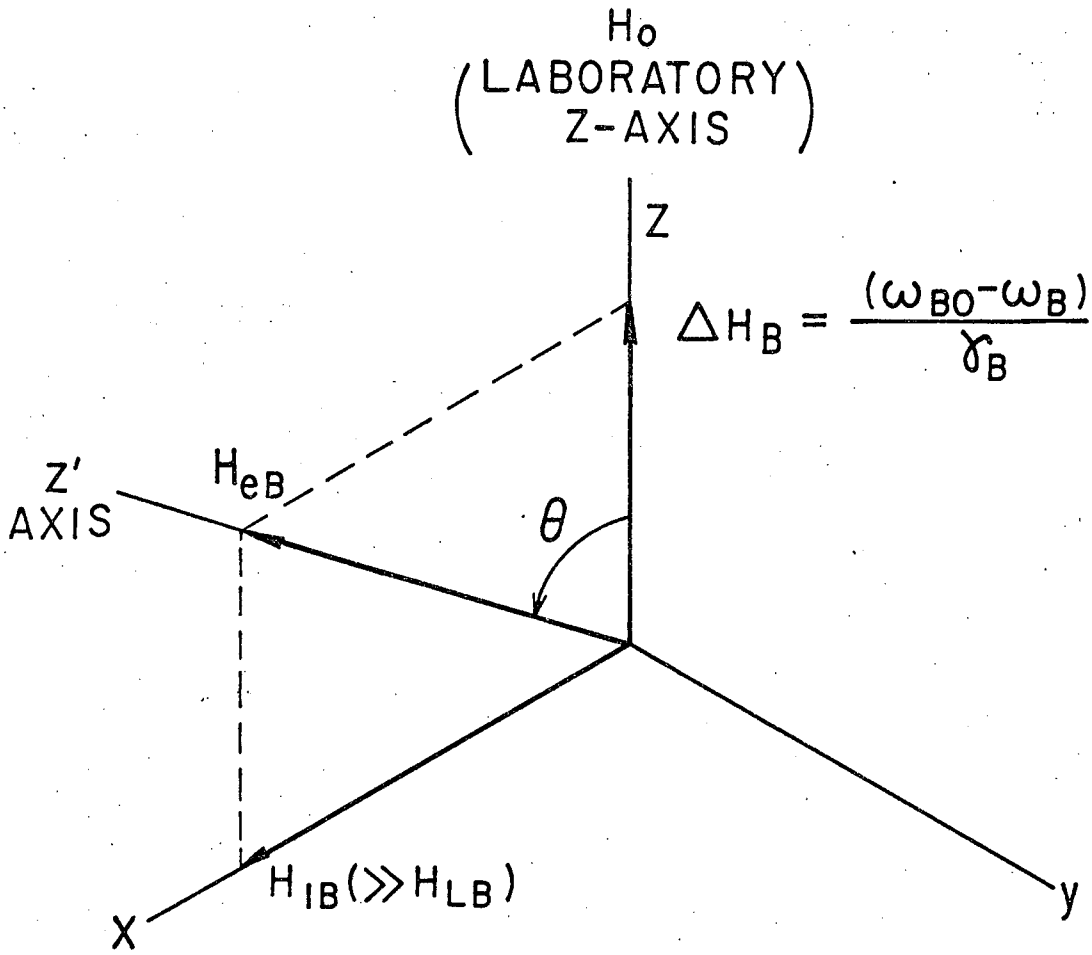

XBL 676-4154

Fig. 7 Definition of the B spin effective field in the rotating frame, H_{eB}, viewed from a frame rotating at the B rf frequency ω_B; the z' axis is the frame in which the zero-order B Hamiltonian is diagonal

$$\frac{d\rho_R}{dt} = -i[\mathcal{H}_R, \rho_R] \tag{10}$$

and

$$\mathcal{H}_R = R(\theta)\, \mathcal{H}'_R\, R^{-1}(\theta)$$

$$= \mathcal{H}^A_d(s) + \mathcal{H}^{AB}_{dz} + \mathcal{H}^{AB}_{dx} + \mathcal{H}^B_e,$$

where

$$\mathcal{H}^{AB}_{dz} = \left(\sum_{i,k} A^{AB}_{ik}\ I_{zi} S_{zk}\right) \cos\theta = \cos\theta\, \mathcal{H}_{lz}, \tag{11}$$

$$\mathcal{H}^{AB}_{dx} = -\left(\sum_{i,k} A^{AB}_{ik}\ I_{zi} S_{xk}\right) \sin\theta = -\sin\theta\, \mathcal{H}_{lx}, \tag{12}$$

and

$$\mathcal{H}^B_e = -\omega_{eB} S_z. \tag{13}$$

3. Spin Temperature Assumption During Cross-Relaxation

The question now arises as to whether both $\mathcal{H}^{AB}_{dz}$ and $\mathcal{H}^{AB}_{dx}$ are perturbations. Note that $\mathcal{H}^{AB}_{dz}$ is coupled strongly to $\mathcal{H}^A_d(s)$, since $\left[\mathcal{H}^A_d(s), \mathcal{H}^{AB}_{dz}\right] \neq 0$, but it is not coupled to $\mathcal{H}^B_e$. $\mathcal{H}^{AB}_{dz}$ corresponds to the component of the A local field which is parallel to H_{eB} at a B spin site. $\mathcal{H}^{AB}_{dz}$ does not transfer energy into $\mathcal{H}^B_e$, so it should be a good approximation to lump it with $\mathcal{H}^A_d(s)$ into a "spin-spin" reservoir $\mathcal{H}_{SS}$, with a spin temperature T_{SS}. The rest of the A-B coupling, $\mathcal{H}^{AB}_{dx}$, gives the local field component perpendicular to H_{eB}, and this component is the perturbation which is responsible for the cross-relaxation energy transfer.

At this point we must ask whether we can describe the energy changes which take place in the spin-spin and Zeeman reservoirs by slowly-varying spin temperatures. The spin-spin reservoir has a mechanism (in the form

of the A-A mutual spin flip) which can restore a Boltzmann population distribution if the spin-spin reservoir is disturbed from thermal equilibrium. As long as the cross relaxation rate is much smaller than the thermal equilibration rate of the spin-spin reservoir ($\tau_{AB}^{-1} \ll T_{2A}^{-1}$), we can use the spin temperature approximation for the change of $\mathcal{H}_{SS}$:

$$\rho_R \cong \rho_B \rho_{SS} \cong \rho_B \exp\left\{ \frac{-\hbar(\mathcal{H}_d^A(s) + \mathcal{H}_{dz}^{AB})}{k\, T_{SS}(t)} \right\} \Big/ Tr\{1\}. \qquad (14)$$

Note that the Eq. (14) implies a spatially uniform spin temperature for the A spins, which cannot be true for those A spins near a B spin, as discussed below in Appendix A. But this approximation is surprisingly well justified in CaF_2, as shown by the experimental results.

Now we come to the question of whether the growth of the B magnetization along H_{eB} can be described by a spin temperature, $T_B(t)$. When $\theta = 90°$, and the $\mathcal{H}_{dz}^{AB}$ term in the Hamiltonian vanishes, the transition probabilities (to the second order in $\mathcal{H}_{dx}^{AB}$) between the B Zeeman states in the rotating frams are proportional to $|\langle m | S_x | m' \rangle|^2$. But these matrix elements are the usual ones for rf saturation of a spin system and will preserve a Boltzmann population distribution if the B system starts out in one. Thus for $\theta = 90°$, and M_B(initial) = 0($T_B = \infty$, that is) we should be able to use a spin temperature for the B system during cross-relaxation, because the B system starts out in a Boltzmann distribution, is maintained in one by the perturbation, and tends toward a Boltzmann distribution as T_B approaches T_{SS}.

For $\theta \neq 90°$ the situation is not so clear. To second order in the small quantities $\mathcal{H}_{dx}^{AB}$, $\mathcal{H}_{dz}^{AB}$ the above arguments hold, but to third order there exists an interference between $\mathcal{H}_{dx}^{AB}$ and ($\mathcal{H}_{dz}^{AB}$ $\mathcal{H}_{dx}^{AB}$) which gives transition

probabilities proportional to $\langle m' | S_x | m \rangle \langle m' | S_z | m'' \rangle \langle m'' | S_x | m \rangle$.[22]

These matrix elements will not preserve a Boltzmann population distribution, but their effects may be small if the A-B coupling is really a small perturbation on the spin-spin system, so that perturbation theory to second order in $\mathcal{H}_{dx}^{AB}$ is a very good approximation. For the time being we will assume that the B spin system is still described by a spin temperature $T_B(t)$ during the cross-relaxation process, even for $\theta \neq 90°$.

To describe the cross-relaxation process, we will then assume that the density matrix of the ensemble of A and B spins is given approximately by:

$$\rho_R(t) \cong \exp \left\{ - \frac{\hbar}{k} \left(\frac{\mathcal{H}_{SS}}{T_{SS}(t)} + \frac{\mathcal{H}_e^B}{T_B(t)} \right) \right\} \Big/ \mathrm{Tr}\{1\}.$$

where

$$\mathcal{H}_{SS} = \mathcal{H}_d^A(s) + \mathcal{H}_{dz}^{AB}, \tag{15}$$

and $\mathcal{H}_e^B$ is given by Eq. (13). We are interested in calculating the change of $\mathcal{H}_{SS}$ caused by cross-relaxation, because the value of T_{SS} at the end of the B rf pulse determines the size of the dipolar signal obtained from the F^{19} nuclei (this neglects a small increase in T_{SS}, which occurs when $\mathcal{H}_{SS}$ comes into thermal equilibrium with $\mathcal{H}_{dx}^{AB}$ within a few T_{2A} following the end of the B rf pulse; this change is associated with transient oscillations described in Section II.C and is of the order of $(1 + \delta)$, where $\delta \lesssim (C_B H_{LB}^2 / C_A H_{LA}'^2) \lesssim 10^{-3})$.

4. Solution of the Density Matrix Equation

Since we are interested in calculating the change of one of the zero-order parts of the rotating frame Hamiltonion $\mathcal{H}_R$, it is possible to derive an equation of motion for the approximate density matrix $\rho_R(t)$, which is accurate to second order in the perturbation $\mathcal{H}_{dx}^{AB}$. This equation of motion

for ρ_R can then be used to derive equations for $\langle \mathcal{H}_{SS} \rangle$ and $\langle M_{Bz} \rangle$, which we can solve exactly and compare with our experimental results. To derive this equation it is useful to transform out the rapid time dependence of $\mathcal{H}_R$ caused by $\mathcal{H}_o = \mathcal{H}_{SS} + \mathcal{H}_e^B$, so we make a transformation to the interaction representation, where the density matrix (ρ^*) is given by:

$$\rho^*(t) = T_I(t)\, \rho_R\, T_I(t)^{-1} \quad . \tag{16}$$

where

$$T_I(t) = \exp(i\, \mathcal{H}_o t). \tag{17}$$

As before, the equation of motion can be obtained from the equation for ρ_R. Using Eqs. (17), (16), and (10) we have:

$$\frac{d\rho^*}{dt} = -i[\mathcal{H}^*(t),\, \rho^*] \,, \tag{18}$$

where

$$\mathcal{H}^*(t) = e^{i\mathcal{H}_o t}\, \mathcal{H}_{dx}^{AB}\, e^{-i\mathcal{H}_o t} \,.$$

Using

$$[\mathcal{H}_{SS},\, \mathcal{H}_e^B] = 0$$

and

$$e^{-i\alpha S_z}\, S_{xk}\, e^{+i\alpha S_z} = (S_{xk}\cos\alpha + S_{yk}\sin\alpha)$$

we can rewrite $\mathcal{H}^*(t)$ in the form:

$$\mathcal{H}^*(t) = -\sin\theta(\mathcal{H}_{lx}(t)\, \cos\omega_{eB} t + \mathcal{H}_{ly}(t)\, \sin\omega_{eB} t). \tag{19}$$

where

$$\mathcal{H}_{\substack{lx \\ (y)}}(t) = \sum_{i,k} A_{ik}^{AB}\, I_{zi}(t)\, S_{\substack{xk, \\ (y)}}$$

and

$$I_{zi}(t) = e^{i\mathcal{H}_{SS}t} I_{zi} e^{-i\mathcal{H}_{SS}t} .$$

As we see from Eq. (19), $\mathcal{H}^*(t)$ contains two kinds of time dependence: a coherent oscillation at frequency ω_{eB} associated with precession around H_{eB}, and an approximately random fluctuating field given by $I_{zi}(t)$. The quantity $\sum_i A_{ik}^{AB} I_{zi}(t)/\gamma_B$ can be thought of as a fluctuating local field at the kth B spin site caused by its A neighbors. If we imagine analyzing $I_{zi}(t)$ into its frequency components, the component at ω_{eB} will combine with the coherent oscillation at ω_{eB} to give a secular perturbation which changes $\rho^*(t)$ slowly; but the effects of the fluctuating components of $I_{zi}(t)$ at other frequencies than ω_{eB} will average to zero, even when combined with the coherent oscillation at ω_{eB}.

We can characterize the "slow" (slow compared to ω_{eB}^{-1} and the correlation time τ_c of $I_{zi}(t)$) time-development of $\rho^*(t)$ by plotting one of the temperatures which appears in it (see Fig. 8). Equation (18) can be used to calculate $\rho^*(t + \Delta)$ if $\rho^*(t)$ is known, and an equation for the diagonal part of $\frac{d\rho^*}{dt}$ to second order in $\mathcal{H}^*(t)$ can be found, which averages over the rapid fluctuations of $\mathcal{H}^*(t)$ to find the long-term effects on $\rho^*(t)$. In Appendix B a crude but hopefully understandable derivation of the approximate equation (the master equation) for the diagonal part of $\frac{d\rho^*}{dt}$ is given; for a more complete treatment of the derivation and examples of its use, many references can be given.[23,24,25,26]

The result of Appendix B is an equation of motion for any operator O which commutes with both zero order parts of the Hamiltonian ($\mathcal{H}_{SS}$, $\mathcal{H}_e^B$):

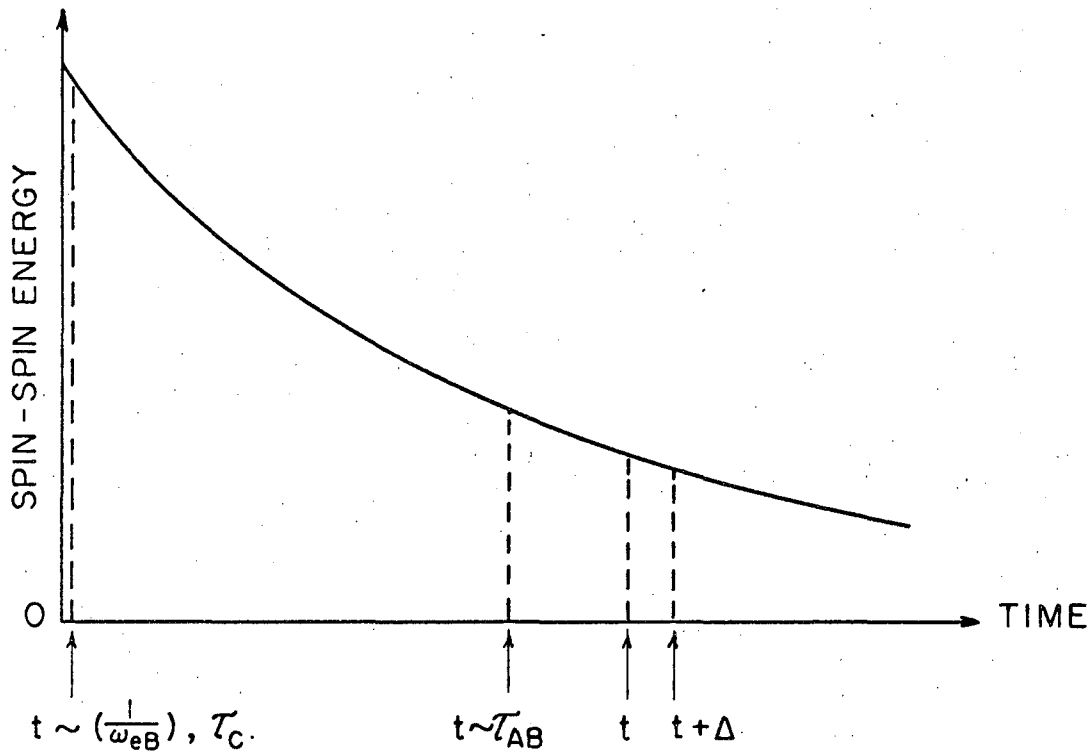

XBL 676-4155

Fig. 8 Diagram of various times involved in the cross-relaxation calculation

$$\frac{d}{dt}\langle 0\rangle \cong -\int_0^\infty d\tau \, \mathrm{Tr}\left\{0\left[\mathcal{H}^*(0),\left[\mathcal{H}^*(\tau),\rho^*(t)\right]\right]\right\}. \qquad (20)$$

Since we have assumed that ρ_R is given by assuming a spin temperature for $\mathcal{H}_{SS}$ and $\mathcal{H}_e^B$ during cross-relaxation, Eqs. (16) and (17) state that:

$$\rho^*(t) = \rho_R(t) = \exp\left\{-\frac{\hbar}{k}\left(\frac{\mathcal{H}_{SS}}{T_S} + \frac{\mathcal{H}_e^B}{T_B}\right)\right\}/\mathrm{Tr}\ \{1\}. \qquad (21)$$

Since $\hbar\omega_{LA}$, $\hbar\omega_{eB} \ll kT_A$, kT_B we can use the high temperature expansion for $\rho^*(t)$, so that Eq. (20) becomes (with $0 = \mathcal{H}_{SS}$)

$$\frac{d}{dt}\langle\mathcal{H}_{SS}\rangle \cong -\frac{1}{\alpha}\int_0^\infty d\tau \, \mathrm{Tr}\left\{\mathcal{H}_{SS}\left[\mathcal{H}^*(0),\left[\mathcal{H}^*(-\tau), -\frac{\hbar\mathcal{H}_{SS}}{kT_{SS}} - \frac{\hbar\mathcal{H}_e^B}{kT_B}\right]\right]\right\} \qquad (22)$$

where

$$\alpha = \mathrm{Tr}\ \{1\}.$$

But

$$\frac{\hbar\mathcal{H}_{SS}}{kT_{SS}} + \frac{\hbar\mathcal{H}_e^B}{kT_B} = \frac{\hbar\mathcal{H}_{SS}}{kT_{SS}} - \frac{\hbar\mathcal{H}_{SS}}{kT_B} + \frac{\hbar(\mathcal{H}_{SS}+\mathcal{H}_{eB})}{kT_B},$$

so that Eq. (22) becomes

$$\frac{d}{dt}\langle\mathcal{H}_{SS}\rangle \cong \frac{\hbar}{\alpha k}\left(\int_0^\infty d\tau \, \mathrm{Tr}\left\{\mathcal{H}_{SS}\left[\mathcal{H}^*(0),\left[\mathcal{H}^*(-\tau),\mathcal{H}_{SS}\right]\right]\right\}\right)\left(T_{SS}^{-1} - T_B^{-1}\right)$$

$$-\frac{\hbar}{\alpha k T_B}\int_0^\infty d\tau \, \mathrm{Tr}\left\{\mathcal{H}_{SS}\left[\mathcal{H}^*(0),\left[\mathcal{H}^*(-\tau),\mathcal{H}_0\right]\right]\right\}. \qquad (23)$$

But it can be shown[5] that the second term in Eq. (23) vanishes, since it is proportional to the correlation function of $\mathcal{H}^*(t)$ for $\tau \gg \tau_c$, the correlation time of the random function $\mathcal{H}^*(t)$. This result is to be expected on physical grounds because Eq. (23) then implies that cross-

relaxation stops when the spin-spin and Zeeman systems have reached the same spin temperature.

To relate the left side of Eq. (23) to a spin temperature we use Eq. (21) and the high temperature approximation to give

$$\langle \mathcal{H}_{SS} \rangle = \mathrm{Tr}\,\{\rho_R \mathcal{H}_{SS}\} = \mathrm{Tr}\,\{\rho^* \mathcal{H}_{SS}\}$$

$$\simeq \frac{\hbar}{\alpha k T_{SS}}\ \mathrm{Tr}\,\{\mathcal{H}_{SS}^2\}\ ,$$

so that

$$\frac{d}{dt}\langle \hbar \mathcal{H}_{SS}\rangle = -\frac{\hbar}{\alpha k}\ \mathrm{Tr}\,\{\mathcal{H}_{SS}^2\}\ \frac{d}{dt}\ (T_{SS}^{-1})\ . \tag{24}$$

Using Eq. (24), Eq. (23) becomes an equation for the rate of change of T_{SS}:[26]

$$\frac{d}{dt}\ (T_{SS}^{-1}) = -\left(\frac{\int_0^\infty d\tau\ \mathrm{Tr}\left\{\mathcal{H}_{SS}\left[\mathcal{H}^*(0),\left[\mathcal{H}^*(-\tau),\mathcal{H}_{SS}\right]\right]\right\}}{\mathrm{Tr}\,\mathcal{H}_{SS}^2}\right)\left(T_{SS}^{-1} - T_B^{-1}\right) \tag{25}$$

or,

$$\frac{d}{dt}\ (T_{SS}^{-1}) = -\frac{\epsilon}{\tau_{AB}}\ (T_{SS}^{-1} - T_B^{-1})\ . \tag{26}$$

When we put in expressions for $\mathcal{H}^*(t)$ from Eq. (19) we can write the trace in Eq. (25) as:

$$\mathrm{Tr}\left\{\mathcal{H}_{SS}\left[\mathcal{H}^*(0),\left[\mathcal{H}^*(-\tau)\ \mathcal{H}_{SS}\right]\right]\right\}$$

$$= \sin^2\theta \begin{pmatrix} \mathrm{Tr}\left\{\mathcal{H}_{SS}\left[\mathcal{H}_{1x},\left[\mathcal{H}_{1x}(-\tau)\ \mathcal{H}_{SS}\right]\right]\right\}\cos\omega_{eB}\tau \\ \mathrm{Tr}\left\{\mathcal{H}_{SS}\left[\mathcal{H}_{1x},\left[\mathcal{H}_{1y}(-\tau)\ \mathcal{H}_{SS}\right]\right]\right\}\sin\omega_{eB}\tau \end{pmatrix}\ . \tag{27}$$

The commutators appearing in the correlation functions above can be reduced to time derivatives of the correlation functions by noting the following relationship:

$$\frac{d}{d\tau}\left(\mathcal{H}_{1x}(-\tau)\right) = \frac{d}{d\tau}\left(e^{-i\mathcal{H}_{SS}\tau}\,\mathcal{H}_{1x}\,e^{+i\mathcal{H}_{SS}\tau}\right) \tag{28}$$

$$= -i\left[\mathcal{H}_{SS},\ \mathcal{H}_{1x}(-\tau)\right].$$

Using the relations

$$\mathrm{Tr}\,\{A\,[B,C]\} = \mathrm{Tr}\,\{[A,B]\,C\}\ , \tag{29}$$

and

$$[A,B] = -\,[B,A]\ , \tag{30}$$

we find

$$\mathrm{Tr}\left\{\mathcal{H}_{SS}\left[\mathcal{H}_{1x},\ \left[\mathcal{H}_{1x}(-\tau),\ \mathcal{H}_{SS}\right]\right]\right\}$$

$$= -\,\mathrm{Tr}\left\{\mathcal{H}_{1x}\left[\mathcal{H}_{SS},\ \left[\mathcal{H}_{SS},\ \mathcal{H}_{1x}(-\tau)\right]\right]\right\}.$$

Using Eq. (28) twice enables us to show finally

$$\mathrm{Tr}\left\{\mathcal{H}_{SS}\left[\mathcal{H}_{1x},\ \left[\mathcal{H}_{1x}(-\tau),\ \mathcal{H}_{SS}\right]\right]\right\} \tag{31}$$

$$= -\frac{d^2}{d\tau^2}\left(\mathrm{Tr}\left\{\mathcal{H}_{1x}\ \mathcal{H}_{1x}(-\tau)\right\}\right) \equiv -\frac{d^2 g_x(-\tau)}{d\tau^2}\ ,$$

and

$$\mathrm{Tr}\left\{\mathcal{H}_{SS}\left[\mathcal{H}_{1x},\ \left[\mathcal{H}_{1y}(-\tau),\ \mathcal{H}_{SS}\right]\right]\right\}$$

$$= -\frac{d^2}{d\tau^2}\left(\mathrm{Tr}\left\{\mathcal{H}_{1x}\,\mathcal{H}_{1y}(-\tau)\right\}\right) \equiv -\frac{d^2}{d\tau^2}\,g_{xy}(-\tau).$$

But it can be shown that $g_{xy}(-\tau)$ vanishes, by considering a rotation of the entire spin system by 180° around the x-axis:

$$I_x \rightarrow I_x \qquad S_x \rightarrow S_x$$

$$I_y \rightarrow -I_y \qquad S_y \rightarrow -S_y$$

$$I_z \rightarrow -I_z \qquad S_z \rightarrow -S_z$$

Under this rotation, $\mathcal{H}_d^A(s)$, $\mathcal{H}_{dz}^{AB}$, and $\mathcal{H}_{1y}$ are unchanged, but $\mathcal{H}_{1x}$ changes sign. Thus $g_{xy}(-\tau) = -g_{xy}(-\tau)$, so that $g_{xy}(-\tau) = 0$.

Before attempting to evaluate $g_x(-\tau)$, we first note that it is even in τ since:

$$g_x(-\tau) = \mathrm{Tr}\{\mathcal{H}_{1x}\mathcal{H}_{1x}(-\tau)\} = \mathrm{Tr}\{\mathcal{H}_{1x}(-\tau)\mathcal{H}_{1x}\}$$

$$= \mathrm{Tr}\{\mathcal{H}_{1x} e^{+i\mathcal{H}_{SS}\tau}\, \mathcal{H}_{1x}\, e^{-i\mathcal{H}_{SS}\tau}\}$$

$$= g_x(\tau).$$

We can also show that the cross-relaxation rate τ_{AB}^{-1} is proportional to the Fourier component of the fluctuating local field at ω_{eB}, the B spin Larmor frequency in the rotating frame. Using Eqs. (27), (25), and (31), we find:

$$\frac{\epsilon}{\tau_{AB}} = -\frac{\int_o^\infty d\tau \sin^2\theta \dfrac{d^2 g_x(\tau)}{d\tau^2} \cos\omega_{eB}\tau}{\mathrm{Tr}\{\mathcal{H}_{SS}^2\}} \tag{32}$$

If we integrate Eq. (32) twice by parts, using the results that $g_x(\tau)$ is even in τ and approaches zero asymptotically for $\tau \gg \tau_c \approx T_{2A}$, we find:

$$\frac{\epsilon}{\tau_{AB}} = \frac{\sin^2\theta\omega_{eB}^2}{\mathrm{Tr}\{\mathcal{H}_{SS}^2\}} \int_o^\infty d\tau \cos\omega_{eB}\tau\, g_x(\tau)\,. \tag{33}$$

Thus (ϵ/T_{AB}) is proportional to the spectral component of the fluctuating local field at frequency ω_{eB}.

In principle one can evaluate the correlation function $g_x(\tau)$ exactly, but in practice the Hamiltonian terms are so complicated that $g_x(\tau)$ can only be written down for small τ. It is thus necessary to assume a functional form for $g_x(\tau)$, and use the expansion for small τ to find the constants appearing in the functional form. Expansion of $g_x(\tau)$ to order τ^2 yields the following approximation:

$$g_x(\tau) \cong g(0) \left(1 - \frac{\tau^2}{\tau_c^2}\right)$$

In Appendix C the following expressions for $g(0)$ and τ_c^{-2} are derived, along with values of the lattice sums for the case of CaF_2:

$$\sin^2\theta g(0) = \mathrm{Tr}\{\mathcal{H}_{1z}^2\} \sin^2\theta \tag{34}$$

$$\tau_c(\theta)^{-2} = -\frac{1}{2} \mathrm{Tr}\left\{\left[\mathcal{H}_{SS}, \mathcal{H}_{1x}\right]^2\right\} \Big/ \mathrm{Tr}\left\{\mathcal{H}_{1z}^2\right\} .$$

Suppose we let the assumed functional form of $g_x(\tau)$ be given by

$$g_x(\tau) = g(0)\, f(\tau). \tag{35}$$

Usually the functional form assumed for $f(\tau)$ is a Gaussian in τ:[2,11,26]

$$f(\tau) = e^{-\tau^2/\tau_c^2}$$

If we insert this into Eq. (33), we find that the cross-relaxation rate should be a Gaussian in ω_{eB}:

$$\frac{\epsilon}{T_{AB}} \propto e^{-\omega_{eB}^2 \tau_c^2/4}$$

But the experimental data, as seen in Figs. 43 and 44, fit an exponential function of ω_{eB} much better. This implies that $f(\tau)$ is closer to a Lorentzian in time:

$$f(\tau) = (1 + \tau^2/\tau_c^2)^{-1}$$

If we assume that $f(\tau)$ has this form, and use Eqs. (34), (15), (11), and (6) and evaluate the traces explicitly we find as before

$$\epsilon = \frac{C_B H_{eB}^2}{C_A H_{LA}'^2} ,$$

but for τ_{AB}^{-1}:

$$\tau_{AB}^{-1} = \frac{\pi}{2} \sin^2\theta \, \langle \Delta\omega_B^2 \rangle_{BA} \, \tau_c(\theta) \, e^{-\omega_{eB}\tau_c(\theta)}$$

Here C_A and C_B are the nuclear Curie constants, H_{LA}' is an effective local field for the A spins given by

$$H_{LA}'^2 = \frac{1}{3} \langle \Delta\omega_A^2 \rangle_{AA} / \gamma_A^2 ,$$

and $\langle \Delta\omega_A^2 \rangle_{AA}$ and $\langle \Delta\omega_B^2{}_{BA} \rangle$ are the Van Vleck second moments.[19]

If we calculate $\langle \mathcal{H}_e^B \rangle$ in a similar manner from Eq. (20) we find an equation (36) analogous to Eq. (25) for $\frac{d}{dt}(1/T_B)$. Equations (36) and (37) can be used to calculate the behavior of the A dipolar and B Zeeman systems during cross-relaxation, when isolated from the lattice:

$$\frac{d}{dt}\left(\frac{1}{T_A}\right) = - \frac{\epsilon}{\tau_{AB}} \left(\frac{1}{T_A} - \frac{1}{T_B}\right) \qquad (36)$$

$$\frac{d}{dt}\left(\frac{1}{T_B}\right) = \frac{1}{\tau_{AB}}\left(\frac{1}{T_A} - \frac{1}{T_B}\right). \qquad (37)$$

Equations (36) and (37) are the foundation of the analysis of our double resonance data. Their solutions with audio saturation effects and A spin-lattice relaxation taken into account will be discussed in Sec. II.D.4 and II.E, and comparison with experiment will be made.

Equations (36) and (37) are a special case of the equations derived by Schumacher[27] to describe cross-relaxation between the Zeeman energies of two spin species in low laboratory magnetic field. The sets of equations are the same, because they both treat the cross-relaxation as a small perturbation on the main energy reservoirs of the two spin systems, and both assume spin temperatures for the energy reservoirs during relaxation. Although he gave theoretical expressions for τ_{AB}^{-1} and $\epsilon\,\tau_{AB}^{-1}$, Schumacher did not calculate them explicitly. In his work he was concerned with strong spin-lattice interaction, whereas we are interested in spin-lattice interaction only as a small perturbation on the simple equations (36) and (37).

We note here that for our purposes it has been necessary to make a more accurate calculation (to $< \frac{1}{2}$ % error) of the Van Vleck second moment formula for a simple cubic lattice. Van Vleck[28] finds

$$\langle \Delta\omega_A^2 \rangle_{VV} = \frac{\gamma^4 \hbar^2}{a^6}(12.3)\,(\alpha^4 + \beta^4 + \gamma^4 - .187)\,I(I+1),$$

while we find (using a computer to evaluate the sums in the [111] and [110] directions to $r \leq 5a$, and making an integral correction for farther neighbors):

$$M_2 = \frac{12.44\gamma^4\hbar^2 I(I+1)}{a^6}\left[(\alpha^4 + \beta^4 + \gamma^4) - .1948)\right].$$

This additional accuracy has been necessary because for large ω_{eB}, a small error in the value of τ_c (in the exponential) produces a large discrepancy in τ_{AB}^{-1}.

5. Relation of the A Dipolar Correlation Function to the B Spin Free Induction Decay

Instead of assuming a functional form for the trace obtained in the $\epsilon\tau_{AB}^{-1}$ calculation, we can apply a method first used by Clough to calculate the relaxation time between dipolar energy and rotating-frame Zeeman energy of an abundant spin species.[29] If quadrupole and H_o inhomogeneity effects are negligible, this method relates the unknown correlation function in the limit $\theta \to 0^\circ$, to the ordinary free induction decay of a transverse B magnetization in high field.

If we calculate $\frac{d}{dt}\langle S_z\rangle$ instead of $\frac{d}{dt}\langle \mathcal{H}_{ss}\rangle$ by the method of Sec. II.B.4, the same spin temperature and commutation assumptions lead to an expression for τ_{AB}^{-1}, instead of $\epsilon\tau_{AB}^{-1}$:

$$\tau_{AB}^{-1} = \sin^2\theta \int_0^\infty d\tau\, g_B(-\tau)\, \cos\omega_{eB}\tau, \tag{38}$$

where

$$g_B(-\tau) = \mathrm{Tr}\{S_z[\mathcal{H}_{1x};\, \mathcal{H}_{1x}(-\tau),\, S_z]\}\,/\mathrm{Tr}\{S_z^2\}$$

$$\mathcal{H}_{1x}(-\tau) = e^{i\mathcal{H}_{ss}\tau}\, \mathcal{H}_{1x} e^{+i\mathcal{H}_{ss}\tau},$$

and

$$\mathcal{H}_{ss} = \mathcal{H}_d^A(s) + \cos\theta\, \mathcal{H}_{1z}.$$

Clough pointed out that for $\theta \neq 90^\circ$ the zero order spin-spin Hamiltonian $\mathcal{H}_{ss}$ is related to the perturbation Hamiltonian $\mathcal{H}_{1x}$ through

$$\mathcal{H}_{1x} = i[\mathcal{H}_{ss}, S_y]/\cos\theta,$$

since

$$[\mathcal{H}_d^A(s), S_y] = 0 .$$

Using the invariance of the trace under cyclic permutation of the operators, and using

$$[\mathcal{H}_{ss}, S_z] = 0 ,$$

$g_B(-\tau)$ can be rewritten:

$$\mathrm{Tr}\{S_z^2\} g_B(-\tau) = \mathrm{Tr}\left\{[S_z, \mathcal{H}_{1x}]\, e^{-i\mathcal{H}_{ss}\tau}\, [\mathcal{H}_{1x}, S_z]\, e^{+i\mathcal{H}_{ss}\tau}\right\} . \quad (38a)$$

But

$$\left[S_x, [\mathcal{H}_{ss}, S_y]\right] = i\,[S_x, \mathcal{H}_{ss}] ,$$

so that Eq. (38a) becomes:

$$\mathrm{Tr}\{S_z^2\}\, g_B(-\tau) = \cos^{-2}\theta\ \mathrm{Tr}\,\{S_x[\mathcal{H}_{ss}; \mathcal{H}_{ss}, S_x(-\tau)]\},$$

where

$$S_x(-\tau) = e^{-i\mathcal{H}_{ss}\tau}\, S_{xe}\, e^{+i\mathcal{H}_{ss}\tau} .$$

Direct differentiation shows that

$$[\mathcal{H}_{ss}; \mathcal{H}_{ss}, S_x(-\tau)] = \frac{d^2}{d\tau^2}\ S_x(-\tau),$$

so that $g_B(-\tau)$ becomes:

$$g_B(-\tau) = -\frac{d^2 g_\theta(-\tau)}{d\tau^2} = -\frac{d^2}{d\tau^2}\ g_\theta(\tau) ,$$

where

$$g_\theta(\tau) = \mathrm{Tr}\left\{ S_x e^{i\mathcal{H}_{ss}\tau} S_x e^{-i\mathcal{H}_{ss}\tau} \right\} / \mathrm{Tr}\{S_z^2\} .$$

Integrating by parts twice in Eq. (38), and using the facts that $\frac{dg_\theta}{d\tau}(\tau) = 0$ at $\tau = 0$, and $g_\theta(\infty) = 0$ yield:

$$\tau_{AB}^{-1} = \omega_{eB}^2 \tan^2\theta \int_0^\infty d\tau \cos\omega_{eB}\tau \; g_\theta(\tau)$$

$$= \omega_{eB}^2 \tan^2\theta \, \mathcal{J}_\theta(\omega_{eB}).$$

At $\theta = 0^\circ$, the function $g_\theta(\tau)$ is just the dipolar-broadened free induction decay envelope of a transverse B magnetization,[19] and $\mathcal{J}_o(\omega_{eB})$ is the ordinary B line shape relative to ω_{Bo}. Since the B resonance line is motionally narrowed by mutual spin flips between A spins, and experimentally we know that for large ω_{eB}, $\tau_{AB}^{-1} \propto e^{-\omega_{eB}\tau_c}$, it is reasonable to use for $\mathcal{J}_o(\omega_{eB})$ a functional form similar to that of Anderson and Weiss,[30] but with an exponential instead of a Gaussian to cut off the wings of the Lorentzian:

$$\mathcal{J}_o(\omega_{eB}) = N(0)\, T_2(0)(1 + \omega_{eB}^2 T_2^2(0))^{-1} e^{-\omega_{eB}\tau_c}$$

where

$$T_2^{-1}(0) = \frac{\pi}{2} \langle \Delta\omega_B^2 \rangle_{BA} \tau_c,$$

and $N(0)$ is a normalization constant. If we generalize $\mathcal{J}_o(\omega_{eB})$ to include $\theta \neq 0^\circ$ by assuming τ_c is independent of θ, and thus replacing $T_2(0)$ by

$$T_2(\theta) = T_2(0)/\cos^2\theta,$$

we find

$$\tau_{AB}^{-1}(\theta, \omega_{eB}) = \frac{\sin^2\theta}{T_2(0)} \; e^{-\omega_{eB}\tau_c} \; \frac{N(\theta)\omega_{eB}^2 T_2^{\,2}(0)}{\cos^4\theta + \omega_{eB}^2 T_2^{\,2}(0)} \; .$$

But as in Sec. II.B.4, use of the Fourier integral theorem[31] on the general formula (38) for τ_{AB}^{-1} requires that

$$\sin^2\theta g_B(0) = \langle \Delta\omega_B^{\,2} \rangle_{BA} \sin^2\theta = \frac{2}{\pi} \int_0^\infty d\omega_{eB} \tau_{AB}^{-1}(\omega_{eB}) \quad (39)$$

$$= \frac{2}{\pi} \frac{N(\theta)\sin^2\theta}{T_2^{\,2}(0)} \int_0^\infty \frac{dx \; x^2 \; e^{-\mu x}}{(\beta^2 + x^2)} \; ,$$

where $\mu = \tau_c T_2^{-1}(0)$ and $\beta = \cos^2\theta$. Therefore, $N(\theta)$ is:[32]

$$N(\theta) = \left[1 - \zeta(ci(\zeta)\sin\zeta - si(\zeta)\cos\zeta)\right]^{-1},$$

where

$$\zeta = \cos^2\theta \; \tau_c \; T_2^{-1}(0) = \frac{\pi}{2} \cos^2\theta \; \tau_c^{\,2} \; \langle \Delta\omega_B^{\,2} \rangle_{BA} \; ,$$

$$ci(x) = -\int_x^\infty \frac{\cos t}{t} \; dt,$$

and

$$si(x) = -\int_x^\infty \frac{\sin t}{t} \; dt \; .$$

At $\theta = 90°$ τ_{AB}^{-1} reduces to the simple exponential, since $\zeta = 0$:

$$\tau_{AB}^{-1} = \frac{\pi}{2} \langle \Delta \omega_B^{\,2} \rangle_{BA} \; \tau_c \; e^{-\omega_{eB}\tau_c} \; , \quad (39a)$$

but for $\theta \neq 90°$ $\tau_{AB}^{-1}(\theta,0) = 0$. τ_{AB}^{-1} increases, proportional to ω_{eB}^2 to be within 10% of the exponential form Eq. (39a) if $\omega_{eB} \gtrsim 3 \cos^2\theta \; T_2^{-1}(0)$

(that is, $\omega_{eB} \gtrsim 2\pi(2\text{kHz})$ for $\theta = 30°$, parallel to H_o[111] in CaF_2). Even when $\omega_{eB} \gg 3\cos^2\theta\, T_2^{-1}(0)$, there is a deviation from the $\sin^2\theta$ law because of the normalization requirement on the τ_{AB}^{-1} spectrum, since for $0 \neq 90°$, $N(\theta) > 1$. Figure 49 shows this deviation from the $\sin^2\theta$ law for H_o parallel to [111] in CaF_2. If instead we use the calculated $\tau_c(\theta)$ when we define $T_2(\theta)$, the deviation from the $\sin^2\theta$ law is still large.

C. Transient Oscillations in the Rotating Frame

1. Qualitative Description

When no rf pulses are being applied to the sample, there is a coupling between the spin-spin energy of the F^{19}, $\mathcal{H}_d^A(s)$, and the spin-spin energy between F^{19} and Ca^{43}, $\mathcal{H}_d^{AB}(s)$, implied by $[\mathcal{H}_d^A, \mathcal{H}_d^{AB}] \neq 0$. This coupling brings these two parts of the Hamiltonian rapidly to a common spin temperature, in a time of order T_{2A}. This process can be viewed as follows: The Ca^{43} spins have a long spin-lattice relaxation time ($T_{1B} \approx 4 \times 10^6 T_{2A}$), and the Ca-Ca interaction is negligible ($T_2(\text{Ca-Ca}) \approx 10^7 T_{2A}$), so between BRF pulses the $\langle S_{zi} \rangle$ for each Ca^{43} spin is a constant, to a very good approximation. Thus for times of the order of T_{2A}, the Ca^{43} spins produce fixed, inhomogeneous magnetic fields for their F^{19} neighbors. But the F^{19} neighbors can adjust to these fixed magnetic fields in a time of order T_{2A}, through the F^{19}-F^{19} mutual spin slip process. Thus after a few T_{2A} we can say, approximately,

$$\rho \cong \exp\left\{-\hbar\left(\mathcal{H}_d^A(s) + \mathcal{H}_d^{AB}(s)\right)/kT_{ss}\right\}/\text{Tr}\{1\}$$

The order represented by this low spin temperature corresponds to a non-zero, time-averaged F^{19} local field in the direction of each Ca^{43} spin. This may not correspond to any F^{19} magnetization if the Ca^{43} spins are randomly oriented.

Therefore in doing ADRF double resonance, as long as no rf pulses are actually being applied to the sample, the secular spin-spin interactions between all spin species must be considered a single thermal reservoir.[20,18] The spin temperature T_{ss} of this whole spin-spin reservoir determines the size of the dipolar signal observed from a single spin species, when a resonant rf pulse is applied at its Larmor frequency.[6] Therefore a double resonance effect (i.e., a change in T_{ss}) will be observed whenever this spin-spin reservoir is disturbed in any way. The "scrambling" in an rf pulse of a part of this reservoir (the secular part of the dipole-dipole coupling between Ca and F spins) is responsible for the transient oscillations in the rotating frame.

The physical basis of this "scrambling" effect can be understood as follows: When an rf pulse near the Ca^{43} Larmor frequency is applied to the sample, the major transfer of energy takes place between the dipolar energy of the F^{19} nuclei, and the Ca^{43} Zeeman energy in the rotating frame. But initially there exists also the spin-spin energy of the Ca^{43} nuclei aligned in the local field from their F^{19} neighbors, and when the B rf pulse is applied, these Ca^{43} nuclei precess in the resultant field composed of H_{1B} and the non-zero-average fields from their F^{19} neighbors, (see Fig. 9). The magnetization components perpendicular to the plane of the paper cancel, for spins $\pm(H_{LB})$. This precession leads to an oscillating component of Ca^{43} magnetization along H_{1B}, which decays to a steady state value because the random fluctuations of H_{LB} dephase the different B spins as they precess.[17] Thus the spin-spin interaction of the F^{19} nuclei quickly restores internal thermal equilibrium within the F^{19} dipolar part of the spin-spin reservoir, when the nature of the spin-spin reservoir is perturbed by the action of the external field H_{1B}.

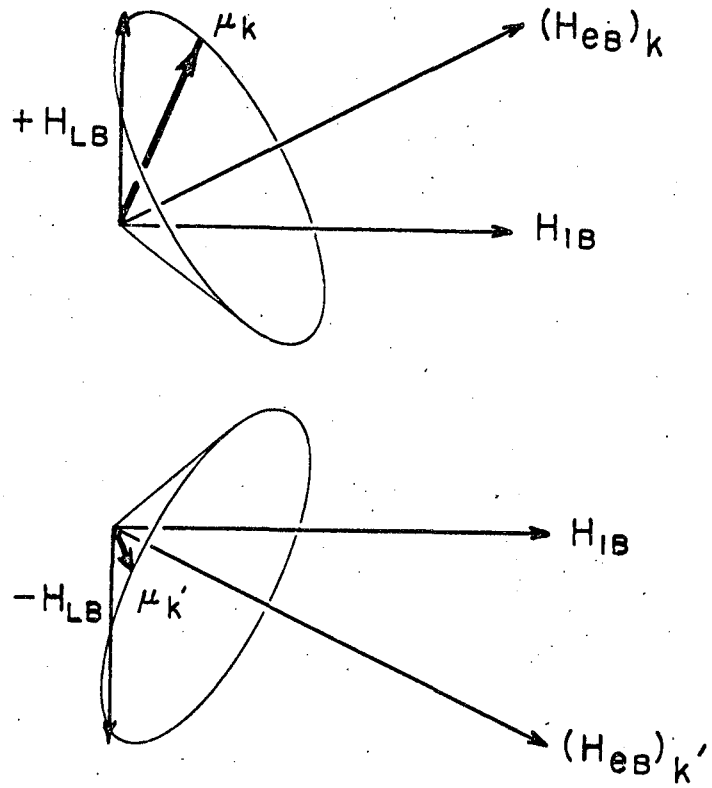

XBL 676-4156

Fig. 9 Precession of two different B spins in their instantaneous effective fields, at beginning of the B rf pulse ($\Delta\omega_B = 0$)

If $\omega_{1B} \gg \omega_{LB}$ and ω'_{LA}, the average field which the Ca^{43} spins produce at their F^{19} neighbors approaches zero because the F^{19} spins cannot follow the Ca^{43} local field, since $\omega_{1B} \gg 1/T_{2A}$. Thus for times long compared to T_{2A}, $\langle \mathcal{H}_d^{AB} \rangle \rightarrow 0$, and the energy which formerly resided in the Ca^{43}-F^{19} spin-spin interaction is required by conservation of total rotating frame energy to reside in the Ca^{43} Zeeman interaction in the rotating frame. But the transient oscillatory exchange between the Ca^{43} Zeeman energy and Ca^{43}-F^{19} spin-spin energy is very small because only a very small part of the initial spin-spin order can be destroyed.

The usual cross-relaxation energy exchange produces the major double-resonance effect, and this process can be made very weak for short times by making τ_{AB} very long. That is, the spin temperature corresponding to the F^{19} signal we observe is determined not only by $\mathcal{H}_d^A(s)$, but to a small extent $\left(\langle \mathcal{H}_d^{AB} \rangle / \langle \mathcal{H}_d^A \rangle \leq 10^{-3} \right)$ by $\mathcal{H}_d^{AB}(s)$, as well. For the case $H_{1B} \gg H_{LB}$, the destruction of order ocrresponding to these transient oscillations increases the observed $\langle E_{ss} \rangle \equiv \hbar \langle \mathcal{H}_d^A(s) + \mathcal{H}_d^{AB}(s) \rangle$ by an amount corresponding to $\mathcal{H}_d^{AB}(s) \rightarrow 0$. Since $\hbar \langle \mathcal{H}_d^{AB}(s) \rangle \; i \ll \hbar \langle \mathcal{H}_d^A(s) + \mathcal{H}_d^{AB}(s) \rangle \equiv E_{ss}$, only a <u>small heating</u> of the F^{19} dipolar reservoir is possible.

2. <u>Calculation of the Transient Oscillations</u>

This small effect can be made observable by applying <u>many</u> short B rf pulses to the sample after ADRF, and observing the resultant destruction of order in the spin-spin systems. Figure 10 shows one of these B rf pulses and the accompanying values of spin-spin and Zeeman energy. The time τ_o between the pulses is always $\gg T_{2A}$, T_{2B}, so just before a B rf pulse is applied ($t = -\delta t$), $\mathcal{H}_d^A(s)$ and $\mathcal{H}_d^{AB}(s)$ are in thermal equilibrium with each other at a spin temperature $(T_{ss})_i$, as discussed above. At $t = 0$ the B rf pulse begins and the rotating frame Hamiltonian changes from $\mathcal{H}_d^A(s) + \mathcal{H}_d^{AB}(s)$

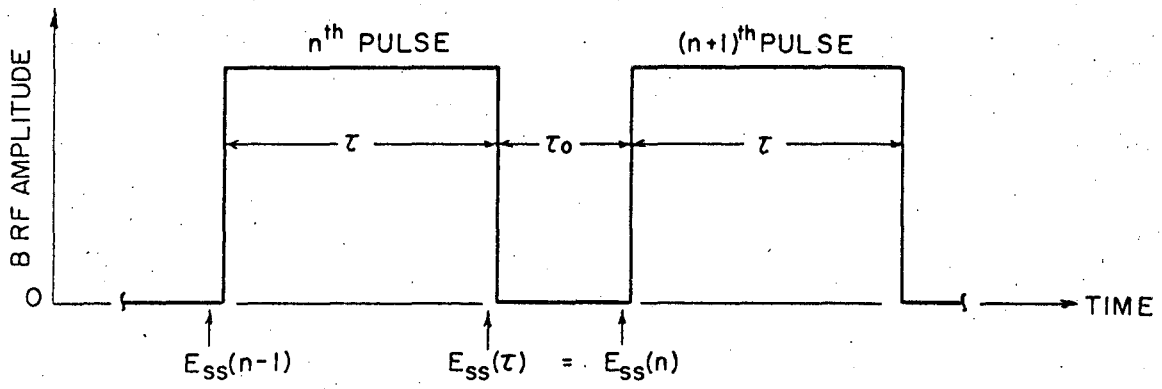

XBL 676-4157

Fig. 10 Properties of B rf pulses applied to observe transient oscillations in the B rotating frame; E_{ss} is the instantaneous spin-spin energy

to $\mathcal{H}_d^A(s) + \mathcal{H}_d^{AB}(s) + \mathcal{H}_e^B$ · $\langle\mathcal{H}_d^A(s)\rangle, \langle\mathcal{H}_d^{AB}(s)\rangle$, and $\langle\mathcal{H}_e^B\rangle$, evolve under this Hamiltonian until the end of the B rf pulse ($t = \tau - \delta t$), where $\tau \geq T_{2A}$; a density matrix treatment of this evolution valid for $H_{1B} \gg H_{LB}$ will be given below. When the B rf pulse is turned off suddenly, no change occurs in the expectation values, except that work is done on the B rf system so that the Ca^{43} Zeeman energy goes to zero:

$$t = \tau - \delta t: \quad (E_{tot})_{R^-} = \hbar\langle\mathcal{H}_d^A(s)\rangle_{\tau^-} + \hbar\langle\mathcal{H}_d^{AB}(s)\rangle_{\tau^-} + \hbar\langle\mathcal{H}_e^B\rangle_{\tau^-}$$

$$t = \tau + \delta t: \quad (E_{tot})_{R^+} = \hbar\langle\mathcal{H}_d^A(s)\rangle_{\tau^-} + \hbar\langle\mathcal{H}_d^{AB}(s)\rangle_{\tau^-}$$

But for times $t \sim T_{2A} \ll T_{1A}, T_{1B}$, the spin-spin interactions are isolated, and the total energy in the rotating frame is conserved. After a period of several T_{2A}, $\mathcal{H}_d^A(s)$ and $\mathcal{H}_d^{AB}(s)$ have again come to a common spin temperature $(T_{ss})_f$, so that

$$\rho_f \cong \exp\{-\hbar\left(\mathcal{H}_d^A(s) + \mathcal{H}_d^{AB}(s)\right)/k(T_{ss})_f\}/\mathrm{Tr}\{1\} . \tag{40}$$

T_{Af} determines the size of the F^{19} signal measured after the B rf pulse, and we can calculate T_{Af} by using the conservation of rotating frame energy during the thermal equilibration time just after the end of the B rf pulse:

$$E_{ss}(\tau^-) = (E_{ss})_n \tag{41}$$

or

$$\langle\mathcal{H}_d^A(s)\rangle_{\tau^-} + \langle\mathcal{H}_d^{AB}(s)\rangle_{\tau^-} = \langle\mathcal{H}_d^A(s) + \mathcal{H}_d^{AB}(s)\rangle_f$$

$$\cong \frac{1}{\alpha}\mathrm{Tr}\left\{\hbar\left(\mathcal{H}_d^A(s) + \mathcal{H}_d^{AB}(s)\right)\left(1 - \hbar\left(\mathcal{H}_d^A(s) + \mathcal{H}_d^{AB}(s)\right)/k(T_{ss})_f\right)\right\}$$

$$= -\frac{\hbar^2}{\alpha k(T_{ss})_f}\left(\mathrm{Tr}\{\mathcal{H}_d^A(s)^2\} + \mathrm{Tr}\{\mathcal{H}_d^{AB}(s)^2\}\right)$$

Thus to calculate the decrease of S_A by this process, it will suffice to calculate $\langle \mathcal{H}_d^A(s) \rangle_{\tau-}$ and $\langle \mathcal{H}_d^{AB}(s) \rangle_{\tau-}$ in terms of the initial spin temperature $(T_{SS})_i$ before the B rf pulse was applied.

Since the change in T_{SS} produced by this "scrambling" of the weak A-B interaction by the B rf pulse is small, we can define

$$\frac{S_A(f)}{S_A(i)} \equiv \frac{(T_{SS})_i}{(T_{SS})_f} = e^{-R_p};$$

then

$$\frac{S_A(f) - S_A(i)}{S_A(i)} \propto \frac{\left((1/T_{SS})_f - (1/T_{SS})_i\right)}{(1/T_{SS})_i}$$

$$= (e^{-R_p} - 1) \approx -R_p(\tau).$$

Calculation of $\langle \mathcal{H}_d^A(s) \rangle$ and $\langle \mathcal{H}_d^{AB}(s) \rangle$

During the B rf pulse the density matrix of the spin system changes according to the equation

$$\frac{d\rho_R}{dt} = i[\mathcal{H}_R, \rho_R]$$

where

$$\hbar \mathcal{H}_R = \hbar\left(\mathcal{H}_d^A(s) + \mathcal{H}_d^{AB}(s) + \mathcal{H}_e^B\right),$$

$\mathcal{H}_d^A(s)$ and $\mathcal{H}_d^{AB}(s)$ are given by Eqs. (6) and (7); and

$$\mathcal{H}_e^B = -\gamma_B H_{1B} \sum_k S_{xk}.$$

As mentioned above, we need to calculate

$$\langle \mathcal{H}_d^A(s)\rangle_{\tau-} + \langle \mathcal{H}_d^{AB}(s)\rangle_{\tau-} \equiv \mathrm{Tr}\left\{\rho_R(\tau)\left(\mathcal{H}_d^A(s) + \mathcal{H}_d^{AB}(s)\right)\right\}$$

Since in these experiments

$$H_{1B} \gtrsim 24_g \gg H_{LB} \approx 3.4_g, \text{ then } \mathcal{H}_e^B \gg \mathcal{H}_d^{AB}(s)$$

so it is useful to transform to the interaction representation to calculate $\rho_R(\tau)$. If ρ^* is the transformed density matrix, then

$$\rho^*(t) \equiv T(t)\,\rho_R(t)\,T^{-1}(t)$$

so that

$$\rho_R(t) = T^{-1}(t)\,\rho^*(t)\,T(t) \tag{42}$$

where

$$T(t) = \exp\left\{i\left(\mathcal{H}_d^A(s) + \mathcal{H}_e^B\right)t\right\}.$$

Then $\rho^*(t)$ obeys

$$\frac{d\rho^*}{dt} = -i[\mathcal{H}^*(t),\ \rho^*] \tag{43}$$

where

$$\mathcal{H}^*(t) = T(t)\,\mathcal{H}_d^{AB}(s)\,T^{-1}(t),$$

and using

$$e^{-i\theta Sx}\,S_z\,e^{+i\theta Sx} = S_z\cos\theta - S_y\sin\theta,$$

we find:

$$\mathcal{H}^*(t) = \sum_{i,k} A_{ik}^{AB}\,I_{zi}(t)\,(S_{zk}\cos\omega_{1B}t - S_{yk}\sin\omega_{1B}t)$$

$$\equiv \mathcal{H}_1(t)\cos\omega_{1B}t - \mathcal{H}_z(t)\sin\omega_{1B}t. \tag{44}$$

Here we define

$$I_{zi}(t) = \exp\left(i\,\mathcal{H}_d^A(s)t\right) I_{zi} \exp\left(-i\,\mathcal{H}_d^A(s)t\right) .$$

The sum $\sum_i A_{ik}^{AB} I_{zi}(t)$ can be regarded as a randomly varying local field at the kth B spin site. Now we can calculate $\langle\mathcal{H}_d^A(s)\rangle + \langle\mathcal{H}_d^{AB}(s)\rangle$, by Eqs. (42) and Tr {AB} = Tr {BA} :

$$\hbar\langle\mathcal{H}_d^A(s) + \mathcal{H}_d^{AB}(s)\rangle = \mathrm{Tr}\left\{\rho_R(t)\,\hbar\left(\mathcal{H}_d^A(s) + \mathcal{H}_d^{AB}(s)\right)\right\}$$

$$= \mathrm{Tr}\left\{\mathcal{H}_d^A\rho^*(t)\right\} + \cos\omega_{1B}t\ \mathrm{Tr}\left\{\mathcal{H}_1(t)\ \rho^*(t)\right\}$$

$$- \sin\omega_{1B}t\ \mathrm{Tr}\left\{\mathcal{H}_2(t)\ \rho^*(t)\right\} . \qquad (45)$$

Equation (45) is still exact, but we now need to solve approximately for $\rho^*(t)$ as a power series in the small perturbation $\mathcal{H}_d^{AB}(s)$, by iteration of Eq. (43):

$$\rho^*(t) \cong \rho^*(0) - i\int_0^t dt'\ [\mathcal{H}^*(t'),\ \rho^*(0)]$$

$$+ (-i)^2 \int_0^t dt' \int_0^{t'} dt''\ \left[\mathcal{H}^*(t'),\ [\mathcal{H}^*(t''),\ \rho^*(0)]\right] , \qquad (46)$$

where $\rho^*(\theta)$ is given by

$$^*(0) \cong \frac{1}{\mathrm{Tr}\{1\}}\left[1 - \frac{\hbar\left(\mathcal{H}_d^A(s) + \mathcal{H}_d^{AB}(s)\right)}{k(T_{ss})_i}\right] \qquad (47)$$

(An additional term $-\hbar\,\omega_{Bo}S_z/k\,T_{Bi}$ can be added to $\rho^*(0)$ to account for an initial B magnetization along the laboratory z-axis, but it does not change the results to second order in $\mathcal{H}_d^{AB}(s)$.) Putting Eqs. (46) and (47) into Eq. (45) and keeping only terms which are second order or lower in $\mathcal{H}_d^{AB}(s)$, the following expression for $\langle\hbar\left(\mathcal{H}_d^{A}(s) + \mathcal{H}_d^{AB}(s)\right)\rangle$ results from a calculation which does not involve any further approximations (an example of each of the features of the calculation will be given below):

$$E_{ss}(t) \equiv \langle\hbar\ \mathcal{H}_d^{A}(s) + \mathcal{H}_d^{AB}(s)\ \rangle t = C + A(t) + B(t) \qquad (48)$$

where

$$C = -\frac{\hbar^2}{\alpha k\,(T_{ss})_i}\ \mathrm{Tr}\left\{\mathcal{H}_d^{A^2}(s)\right\},$$

$$\alpha = \mathrm{Tr}\{1\},$$

$$A(t) = -\frac{\hbar^2}{\alpha k\,(T_{ss})_i}\ g(t)\cos\omega_{1B}t,$$

$$g(t) = \mathrm{Tr}\left\{\mathcal{H}_d^{AB}(s)\ e^{i\mathcal{H}_d^{A}(s)t}\ \mathcal{H}_d^{AB}(s)\ e^{-i\mathcal{H}_d^{A}(s)t}\right\},$$

and

$$B(t) = -\frac{\hbar^2}{\alpha k\,(T_{ss})_i}\int_o^t dt'\int_o^{t'} d\tau\ \cos\omega_{1B}\tau\ \frac{d^2g(\tau)}{d\tau^2}.$$

To demonstrate the calculational procedures involved, we will carry through the most complicated calculation in Eq. (48), that for the term B(t) above. It originates in the following term of Eq. (45) above:

$$-\hbar^2\int_o^t dt'\int_o^{t'} dt''\ \mathrm{Tr}\left\{\mathcal{H}_d^{A}\left[\mathcal{H}^*(t'),\left[\mathcal{H}^*(t''),\rho^*(0)\right]\right]\right\}. \qquad (49)$$

First we put in the explicit forms of $\mathcal{H}^*$ and $\rho^*(0)$ from Eqs. (44) and (47), and use the fact that some of the $\mathrm{Tr}_B\{\ \}$ vanish, to reduce Eq. (49) to the following form:

$$\frac{\hbar^2}{\alpha k (T_{ss})_i} \int_0^t dt' \int_0^{t'} dt'' \left[\mathrm{Tr} \left\{ \mathcal{H}_d^A(s) \left[\mathcal{H}_1(t'), [\mathcal{H}_1(t''), \mathcal{H}_d^A(s)] \right] \right\} \cos\omega_{1B} t' \cos\omega_{1B} t'' \right.$$

$$\left. + \mathrm{Tr} \left\{ \mathcal{H}_d^A(s) \left[\mathcal{H}_2(t'), [\mathcal{H}_2(t''), \mathcal{H}_d^A(s)] \right] \right\} \sin\omega_{1B} t' \sin\omega_{1B} t'' \right] \quad (50)$$

Next, using

$$\mathrm{Tr}\{BA\} = \mathrm{Tr}\{AB\} \quad (51)$$

and

$$\left[\mathcal{H}_d^A(s),\ e^{i\mathcal{H}_d^A(s)t} \right] = 0$$

we find, for i = 1, 2:

$$\mathrm{Tr} \left\{ \mathcal{H}_d^A(s) \left[\mathcal{H}_i(t'), [\mathcal{H}_i(t''), \mathcal{H}_d^A(s)] \right] \right\} = - \mathrm{Tr} \left\{ [\mathcal{H}_d^A(s), \mathcal{H}_i(t'-t'')] [\mathcal{H}_d^A(s),\ \mathcal{H}_i(0)] \right\} \quad (52)$$

Using the invariance of the trace (52) under a rotation of the B spins through 90° about the x-axis (so that $y \to z$ and $z \to -y$) and defining $\tau = t' - t''$ we see that

$$\mathrm{Tr} \left\{ \left[\mathcal{H}_d^A(s),\ \mathcal{H}_2(0) \right] \left[\mathcal{H}_d^A(s),\ \mathcal{H}_2(\tau) \right] \right\} = \mathrm{Tr} \left\{ \left[\mathcal{H}_d^A(s),\ \mathcal{H}_d(0) \right] \left[\mathcal{H}_d^A(s),\ \mathcal{H}_1(\tau) \right] \right\}, \quad (53)$$

so that the two correlation functions in Eq. (50) are actually identical. Taking account of Eq. (53), using a trigonometric identity, and changing the variable of integration in the second integral, we find that Eq. (50)

becomes:

$$-\frac{\hbar^2}{\alpha k (T_{ss})_i}\int_o^t dt' \int_o^{t'} d\tau \;\; \mathrm{Tr}\left\{\left[\mathcal{H}_d^A(s),\, \mathcal{H}_d^{AB}(s)\right]\left[\mathcal{H}_d^A(s), \mathcal{H}_1(\tau)\right]\right\} \cos\omega_{1B}\tau . \tag{54}$$

The trace in Eq. (54) can now be rewritten, using Eq. (51) and noting that

$$\frac{d}{dt}\mathcal{H}_1(t) = \frac{d}{dt}\mathcal{H}_d^{AB}(t) = i[\mathcal{H}_d^A, \mathcal{H}_1(t)]$$

we have

$$\mathrm{Tr}\left\{[\mathcal{H}_d^A(s),\mathcal{H}_d^{AB}(s)]\,[\mathcal{H}_d^A(s),\mathcal{H}_1(\tau)]\right\} = -i^2\mathrm{Tr}\left\{\mathcal{H}_d^{AB}(s)\,\frac{d^2}{d\tau^2}\mathcal{H}_1(\tau)\right\}$$

$$= \frac{d^2}{d\tau^2}\,\mathrm{Tr}\left\{\mathcal{H}_d^{AB}(s)\mathcal{H}_1(\tau)\right\} \equiv \frac{d^2 g(\tau)}{d\tau^2} .$$

Thus our final expression for Eq. (49) becomes:

$$-\frac{\hbar^2}{\alpha k (T_{ss})_i}\int_o^t dt' \int_o^{t'} d\tau \cos\omega_{1B}\tau \,\frac{d^2 g(\tau)}{d\tau^2} , \tag{55}$$

where

$$g(\tau) \equiv \mathrm{Tr}\left\{\mathcal{H}_d^{AB}\, e^{i\mathcal{H}_d\tau}\,\mathcal{H}_d^{AB}\, e^{-i\mathcal{H}_d^A\tau}\right\} = g_x(\tau)$$

This term in $\langle\hbar\left(\mathcal{H}_d^A(s) + \mathcal{H}_d^{AB}(s)\right)\rangle$ given by Eq. (55) resembles an earlier expression for τ_{AB}^{-1}, since it involves the same correlation function for the local field, $g_x(\tau)$. Since $g_x(\tau)$ eventually approaches zero as $\tau \gg \tau_c$ (the correlation time of $g_x(\tau)$), the $\int_o^t d\tau$ will approach a constant, and Eq. (55) will represent a constant rate of exchange of energy between the Ca^{43} Zeeman reservoir, and the F^{19} spin-spin reservoir. In

fact, for $t \gg \tau_c$, it can be shown that Eq.(55) is just the leading term in an expansion in powers of t, of the exponential approach of $\mathcal{H}_d^A(s) + \mathcal{H}_d^{AB}(s)$ and $\mathcal{H}_z^B$ to a common spin temperature: That is, for times t such that $\tau_c \ll t \ll \tau_{AB}$,

$$B(t) = -\frac{\hbar^2}{\alpha k (T_{ss})_i} \int_0^t dt' \int_0^{t'} d\tau \cos\omega_{1B}\tau \frac{d^2 g(\tau)}{d\tau^2} \cong -\frac{\epsilon t}{\tau_{AB}} .$$

Thus we see that the second-order expansion of $\langle \mathcal{H}_d^A(s) + \mathcal{H}_d^{AB}(s) \rangle$ must become inaccurate if $t \gtrsim \tau_{AB}$, since the exponential cross-relaxation function can no longer be represented by its linear term. Therefore the simple theory given by Eq. (48) will fail for $f_{1B} \lesssim$ 2kHz, where $\tau_{AB} \sim$ 1ms or less.

We now need to relate the calculated values of $E_{ss}(t)$ to the experimentally observed quantity, S_A (Npulses, length τ). As can be seen from Fig. 11, the initial condition for each pulse is specified completely by $(T_{ss})_i$, since $M_B = 0$. Thus the effect of a single B rf pulse on S_A can be represented by a factor $\xi (\xi \leq 1)$: $S_A(n) = \xi S_Z(n-1)$. The signal observed after N pulses will be given by $S_A(n) = \xi^N S_{A1}$.

Suppose we let $\xi = e^{-R_p}$. R_p is thus the logarithmic decrease of S_A caused by a single B rf pulse. Since $R_p \approx 10^{-3} \ll 1$, R_p can be calculated approximately (to accuracy $\approx$ 1/2%) by

$$\frac{S_A(n)}{S_A(n-1)} = \xi = e^{-R_p} \cong 1 - R_p ,$$

or

$$R_p \cong \frac{S_A(n-1) - S_A(n)}{S_A(n-1)} = \frac{E_{ss}(n-1) - E_{ss}(n)}{E_{ss}(n-1)}$$

Using the equality between $E_{ss}(n)$ and $E_{ss}(\tau-)$ from Eq. (41), the value of $\rho^*(0)$ from Eq. (47) to calculate $E_{ss}(n-1)$, and the expression for $g(\tau)$

given by experiment as explained above, we find for $R_p(\tau)$:

$$R_p(\tau) \cong \left(\frac{\delta}{1+\delta}\right)\left(1 - f(\tau)\cos\omega_{1B}\tau\right) - \frac{\delta}{1+\delta}\int_o^t dt' \int_o^{t'} d\tau \cos\omega_{1B}\tau \frac{d^2 f(\tau)}{d\tau^2} \quad (56)$$

where

$$f(\tau) = (1 + \tau^2/\tau_c^2)^{-1},$$

$$\delta = C_B H_{LB}^2 / C_A L_{LA}^2, \qquad H_{LB}^2 = \langle \Delta\omega_B^2 \rangle_{BA} / \gamma_B^2,$$

and $\omega_{1B} = \gamma_B H_{1B}$. For H_o parallel to the [111] direction in CaF_2, $\delta = 1.07 \times 10^{-3}$.

D. Theory of Audio Saturation Double Resonance

1. Applications of Audio Saturation Double Resonance

Audio saturation double resonance is very useful because it can reveal much information about the rare spin resonance being studied:

(1) Audio saturation double resonance locates the center of the rare spin resonance line as a function of ω_B very accurately, by making use of the symmetrically-placed resonances which occur on either side of the line center ($\omega_B = \omega_{Bo}$) for certain special conditions.

(2) When the B rf frequency ω_B is at the center of the B resonance line ($\omega_B = \omega_{Bo}$), an audio resonance measures the magnitude of the B rf field in the rotating frame if the B spin gyromagnetic ratio γ_B is known.

(3) If ω_{Bo} is known, then $\Delta H_B = \Delta\omega_B/\gamma_B$ can be used together with the measured value of $H_{eB} = \omega_{eB}/\gamma_B$ from an audio resonance, to determine the angle θ between the effective field in the rotating frame (H_{eB}) and the laboratory magnetic field direction.

(4) The width of the audio resonance line gives information about the broadening of the rare spin resonance line, which is useful because this width is not easily found from the double resonance line width as a function of ω_B.

(5) For the case of rare spin double resonances which involve quadrupole splittings, the audio resonance in the rotating frame (or the F-M resonance)[5] can help to identify the species of rare spin under study.

In this section we shall develop the equations describing the audio saturation double resonance process, solve them for simple special cases, and give the exact solutions to these equations for corrections to be made to the simpler solutions, for the cases of short A spin relaxation time T_{1A}, and large rare-spin heat capacity.

2. Symmetrically-Located Resonances

We first consider the origin of the two resonances symmetrically located on either side of the rare spin resonance center (ω_{B0}), which help to locate it more accurately.[7] For the case of double resonance following adiabatic demagnetization in the rotating frame (ADRF), the double resonance cross-relaxation rate τ_{AB}^{-1} is large only if energy can be conserved in the cross-relaxation process: that is,

$$\omega_{eB} = \gamma_B H_{eB} \leq \gamma_A H'_{LA} \tag{57}$$

where H'_{LA} is a magnetic field characterizing the width of the A dipolar spectrum. But for the case of Ca^{43} in CaF_2, $\gamma_B \cong (\gamma_A/14)$, so large effective fields H_{eB} still satisfy (57). Thus for almost all our measurements H_{eB} is much larger than any other local magnetic fields seen by the Ca^{43} nuclei, and the energy levels in the rotating frame are given to a good approximation by

$$E_m = -\gamma_B \hbar H_{eB} m_S .$$

Figure 7 shows the effective field H_{eB} for a particular value of ω_B. If ω_{aud} is held constant while ω_B is swept through the rare spin resonance at ω_{Bo}, the effective field decreases to its minimum value of H_{1B} at $\omega_B = \omega_{Bo}$, and increases again on the other side of the resonance center. Two cases may then be distinguished, depending on the relative sizes of ω_{aud} and $\gamma_B H_{1B}$:

$$\text{case I:} \quad \omega_{aud} \leq \gamma_B H_{1B}$$

$$\text{case II:} \quad \omega_{aud} > \gamma_B H_{1B}.$$

As ω_B is swept for case I the audio resonance condition in the rotating frame,

$$\omega_{aud} = \gamma_B H_{eB}, \tag{59}$$

is never satisfied or is satisfied only at resonance ($\omega_B = \omega_{Bo}$). Both these conditions give rise to only a single double resonance line.

But for case II, the audio resonance condition (58) is satisfied twice during the sweep of ω_B, at equal effective fields $H^o_{eB} = \omega_{aud}/\gamma_B$ on either side of the minimum value $H_{eB} = H_{1B}$. The open circles in Fig. 1 show such a pair of symmetrical resonances. The case II mode of operation is very useful when making searches for rare spin resonances, for two reasons: (1) it doubles the chance that a weak resonance will be seen, and (2) since the audio resonance condition will not be satisfied perfectly during a search, and since the audio resonance near $\theta = 90°$ can be quite narrow, it is possible that almost no resonance line at all will be seen even though $\omega_{aud} \cong \omega_{1B}$, if case I searches are attempted. (For the case of Ca^{43} in CaF_2, the double resonance appears only when ω_{aud} is <u>very</u> close to ω_{1B}, when ω_{aud} approaches ω_{1B} from below.)

These symmetrical resonances can be used to locate the center of a rare spin resonance by the following procedure: choose a small, fixed value of $\omega_{1B} = \gamma_B H_{1B}$. Make audio resonances for this fixed value of ω_{1B}, but with two slightly different values of B rf frequency, $\omega_B^{(1)}$ and $\omega_B^{(2)}$. Then the following equations may be solved for the unknowns ω_{1B}, ω_{Bo}:

$$\omega_{aud}^{(1)2} = \omega_{1B}^2 + (\omega_B^{(1)} - \omega_{Bo})^2,$$

$$\omega_{aud}^{(2)2} = \omega_{1B}^2 + (\omega_B^{(2)} - \omega_{Bo})^2.$$

The solution for ω_{Bo} is:

$$\omega_{Bo} = \frac{1}{2}\left(\omega_B^{(1)} + \omega_B^{(2)}\right) - \frac{1}{2}\,\frac{\left(\omega_{aud}^{(1)2} - \omega_{aud}^{(2)2}\right)}{\left(\omega_B^{(1)} - \omega_B^{(2)}\right)}$$

This value of ω_{Bo} may be checked by making audio resonances at $\omega_{Bo} = \omega_{Bo} \pm \Delta\omega_B$, and checking that the audio resonance centers are at the same frequency.

The improved accuracy of this method comes from the high accuracy with which the aduio resonance frequencies can be measured, because the audio resonances near $\theta = 90°$ are narrow.

3. Equations for Audio Saturation Double Resonance

The conditions meantioned above for the validity of Eqs. (36) and (37) are well satisfied for Ca^{43} in CaF_2, because the experiments described in Sec. V.C, performed using pulsed double resonance, agree with the form of these equations to within the experimental error of a few percent. (As noted in Sec. II.B.4, Eqs. (36) and (37) neglect the transient oscillations which die out in a time of order T_{2A} after the B rf pulse is

turned on; these oscillations die away as soon as the A system has come to internal thermal equilbrium following the turn-on of the A-B perturbation.)

By inspection of Eqs. (36) and (37) it can be seen that the cross-relaxation proceeds until the A and B spin systems reach a common spin temperature, since their steady-state solution is given by $T_A = T_B$. Another important property of these equations is that the "total energy" is conserved during the cross-relaxation process. This can be seen by re-expressing the equations in terms of the A dipolar energy E_A, and the B Zeeman energy E_B:

$$E_A = - \frac{C_A H_{LA}'^2}{T_A} ,$$

$$E_B = - \frac{C_B H_{eB}^2}{T_B} .$$

Then Eqs. (36) and (37) become:

$$\frac{dE_A}{dt} = - \frac{1}{\tau_{AB}} (\epsilon E_A - E_B) , \qquad (58a)$$

and

$$\frac{dE_B}{dt} = \frac{1}{\tau_{AB}} (\epsilon E_A - E_B) . \qquad (58b)$$

By inspection it can be seen that

$$\frac{d}{dt} (E_A + E_B) = 0$$

which expresses the conservation of rotating frame energy if one neglects A and B spin lattice interactions, and if no audio frequency fields are applied to the sample.

The effect of the audio field applied parallel to the laboratory magnetic field H_o during audio saturation double resonance is to saturate the B spin magnetization parallel to H_{eB} in the rotating frame, without affecting the A spin dipolar order directly. The audio field component parallel to H_o will be unchanged by the transformation to the rotating frame, and if a finite B rf field H_{1B} is also being applied to the sample, the audio field will have a component perpendicular to H_{eB}. If $\omega_{aud} \cong \omega_{eB}$ this component can induce transitions between the equally spaced B Zeeman levels in the rotating frame, tending to saturate any B spin magnetization along H_{eB}.

The fact that the audio field does not directly destroy the A dipolar order can be seen by noting that the A dipolar Hamiltonian $\mathcal{H}_{ss}(\theta)$ contains only the secular terms or those which commute with the operator $\exp(i\omega_{Ao}I_z t)$ for the transformation to the rotating frame. Since the audio perturbation on the A spins is of the form:

$$\hbar\mathcal{H}^A_{aud} = -2\gamma_A \hbar H_{1aud} \cos(\omega_{aud} t) I^A_z ,$$

and this perturbation commutes with the A dipolar Hamiltonian, the z-component of the audio field cannot affect the A dipolar order directly. The accidental components of audio perpendicular to H_o can be neglected, since they are at a frequency ω_{aud} which is far off the A resonance frequency $\omega_{Ao} \cong 2\pi(11\text{MHz})$. The audio saturation method of double resonance cannot be used with spin-locked double resonance (SLDR) because the z-component of audio would tend to destroy the locked component of A magnetization as well as the B magnetization.

The effect of the audio perturbation on the B magnetization may be calculated by noting the analogy between audio saturation in the rotating-

frame effective field H_{eB}, and saturation of a magnetization in a laboratory field H_o by an rf field near the resonance frequency.[16,1] The audio field tends to destroy the B magnetization according to the equation:

$$\left(\frac{dE_B}{dt}\right)_{aud} = \frac{d}{dt}\ (-M_B H_{eB}) = -\left(\frac{1}{\tau_{aud}}\right) E_B,$$

where

$$\tau_{aud}^{-1} = \left(\frac{\omega_{aud}}{\omega_{eB}}\right)\pi\gamma_B^2\ H_1^2\ _{aud}\ f(\omega_{aud})$$

is the audio saturation rate. This expression for τ_{aud}^{-1} assumes a spin temperature for the B Zeeman levels even during audio irradiation, and assumes that the audio field is a small perturbation on the B Zeeman system (this requirement may be violated in the case of extreme saturation). Since the audio saturation linewidth is not always much smaller than the audio resonance center frequency ω_{eB}, it is necessary to retain the $(\omega_{aud}/\omega_{eB})$ factor in front of the usual τ_{aud}^{-1}. Here we implicitly assume that the correlation time of the broadening mechanism giving rise to the lineshape function $f(\omega_{eB})$ is much shorter than τ_{AB}. Since τ_{AB} determines the rate of change of the spin temperature $T_B(t)$, even though the energy difference between the m^{th} and $(m-1)^{th}$ B Zeeman levels fluctuates, the population of the m^{th} level will be determined by the average position $E(m) = -\hbar\omega_{eB}m$ of the m^{th} level, rather than the instantaneous position caused by the broadening. This means $\tau_{aud}^{-1} \propto (\omega_{aud}/\omega_{eB})$ rather than $\tau_{aud}^{-1} \propto (\omega_{aud}/\omega_{eB})^2$.

The effects of A and B spin-lattice interactions may be included by adding terms to Eqs. (36) and (37), since these processes are independent of the cross-relaxation process. Strictly speaking, the terms to be added are:

$$\left(\frac{dE_A}{dt}\right)_{S.L.} = - \frac{1}{T_{1A}(dip)} (E_A - E_{Ao}), \qquad (59)$$

and

$$\left(\frac{dE_B}{dt}\right)_{S.L.} = - \frac{1}{T_{1B}} (E_B - E_{Bo}) . \qquad (60)$$

But because of the very low initial spin temperature of the A dipolar system after ADRF, the A dipolar energies which produce observable signals are much larger than the thermal equilibrium A dipolar energy ($E_A(\text{initial}) \sim 1000E_{Ao}$). This means that the B magnetizations are also very large, so it is a good approximation to neglect E_{Ao}, E_{Bo} in Eqs. (59) and (60). Finally, in our experiments in CaF_2 it is found that $T_{1B} \cong 200$ sec, which can be completely neglected in comparison with the other, shorter time constants in these equations ($\tau_{AB} \leq T_{1A}(dip) = 4.3$ sec).

Thus the set of equations expected to describe the audio saturation data for Ca^{43} in CaF_2 is:

$$\frac{dE_A}{dt} = - \frac{1}{\tau_{AB}} (\epsilon E_A - E_B) - \frac{E_A}{T_{1A}} , \qquad (61)$$

and

$$\frac{dE_B}{dt} = \frac{1}{\tau_{AB}} (\epsilon E_A - E_B) - \frac{E_B}{\tau_{aud}} . \qquad (62)$$

4. Solution of the Audio Saturation Equations

Initial Conditions. The initial conditions $E_A(0)$ and $E_B(0)$ to be inserted in Eqs. (61) and (62) are clear for the case $\theta = 90°$. Because $E_B(0)$ represents the Zeeman energy of the initial B magnetization aligned along H_{eB} when the B rf pulse is first turned on, there is no such component if

H_{eB} is perpendicular to the laboratory magnetic field H_o (we assume that there exist no initial B magnetization components perpendicular to H_o, since a time much greater than T_{2B} will have elapsed since the end of any preceding B rf pulse). Furthermore $E_A(0)$ will always have the same value E_{Ao} for each experimental point, since we allow the A spin system to come completely to thermal equilibrium with the lattice between experiments, and then apply a constant ADRF pulse sequence which results in the same initial A dipolar energy. Therefore for $\theta = 90°$ the initial conditions are clearly:

$$E_A(0) = E_{Ao}, \qquad E_B(0) = 0. \tag{63}$$

If $0 \neq 90°$, $E_B(0)$ may be non-zero, if there remains a component of B magnetization M_{Bi} along the laboratory magnetic field after the last double resonance sequence. This remaining component also depends on the value of T_{1B}: If T_{1B} is short compared to T_{1A}, then M_{Bi} will always be given by the thermal equilibrium value M_{Bo}, and the equations may be solved for this case; but if $T_{1B} \gg T_{1A}$, as is the case for Ca^{43} in CaF_2, M_{Bi} depends on the details of the preceding experiment. If there were no audio saturation, M_{Bi} could be as large as $(\epsilon/1+\epsilon)E_{Ao}\cos\theta$. For the audio resonance experiments to be described here, this effect is probably small because of the smallness of ϵ, and because audio saturation begins to reduce M_{Bi} sharply just when ϵ begins to increase it. Therefore we shall solve Eqs. (61) and (62) using the initial conditions of Eq. (63), even for $\theta \neq 90°$.

Solutions for T_{1A}, $T_{1B} = \infty$. If T_{1A} is much longer than $t_{B\ rf}$ or τ_{AB}, we can neglect it in Eqs. (61) and (62), which then become

$$\dot{E}_A = -C_1 E_A + C_2 E_B \tag{64}$$

$$\dot{E}_B = C_3 E_A - C_4 E_B \tag{65}$$

where

$$C_1 = \epsilon/\tau_{AB} = C_3$$

$$C_2 = \tau_{AB}^{-1}$$

and

$$C_4 = \tau_{AB}^{-1} + \tau_{aud}^{-1}$$

The two coupled first order equations involving both E_A and E_B are equivalent to two uncoupled second-order equations for $E_A(t)$ or $E_B(t)$ separately. For example:

$$\ddot{E}_A + (C_1 + C_4)\dot{E}_A + (C_1 C_4 - C_2 C_3) = 0.$$

Thus the time constants involved in $E_A(t)$ and $E_B(t)$ are given by:

$$\lambda_{\pm} = \tfrac{1}{2}(C_1 + C_4)\left(1 \pm \sqrt{1 - \frac{4(C_1 C_4 - C_2 C_3)}{(C_1 + C_4)^2}}\right), \tag{66}$$

where

$$E_A(t) = E_A(+)\, e^{-\lambda_+ t} + E_A(-)\, e^{-\lambda - t}, \tag{67}$$

and

$$E_B(t) = E_B(+)\, e^{-\lambda_+ t} + E_A(-)\, e^{-\lambda - t}. \tag{68}$$

To simplify working with Eqs. (64) and (65) it is useful to introduce the parameter z, which is an "audio saturation parameter" in the sense that it is zero if there is no audio, and is large if the audio saturation is large:

$$z = \left(\frac{\tau_{AB}}{\tau_{aud}}\right) = \pi \omega_{1\ aud}^2 \tau_{AB} f(\omega_{aud}), \tag{69}$$

where

$$\omega_{1\ aud} = \gamma_B H_{1\ aud},$$

and $f(\omega_{aud})$ is an audio resonance lineshape function which depends on the broadening mechanisms important for the audio resonance. A Lorentzian lineshape is appropriate if the two main sources of audio resonance broadening are (1) lifetime broadening by the A-B interaction itself, and (2) motionally-narrowed dipolar broadening by the A-B dipolar interaction, if $\theta \neq 90°$. For a Lorentzian lineshape z becomes:

$$z = \frac{(\omega_{1\ aud})^2 \tau_{AB} T_2^{aud}}{1 + (\omega_{aud} - \omega_{eB})^2 (T_2^{aud})^2}$$

At the center of the audio resonance ($\omega_{aud} = \omega_{eB}$) z is exactly analogous to the usual saturation parameter for magnetic resonance, if τ_{AB} is regarded as an "effective T_1" for the audio resonance in the rotating frame. The results about to be derived do not depend on the details of the audio resonance lineshape, so it can be left unspecified.

Using the initial conditions (63), Eqs. (64) and (65) yield the initial values of $\dot{E}_A$ and $\dot{E}_B$. These conditions together with Eq. (63) determine the constants $E_A(\pm)$ and $E_B(\pm)$ in Eqs. (67) and (68). Thus the exact solution (for $T_{1A} = \infty$, and $T_{1B} = \infty$) for $E_A(t)$ is given by:

$$E_A(t_{B\ rf}) = \frac{E_{Ao}\left(1 - (C_1/\lambda_+)\right)}{\left(1 - (\lambda_-/\lambda_+)\right)} e^{-\lambda_- t_{B\ rf}} \left[1 + \frac{C_1 - \lambda_-}{(\lambda_+ - C_1)} e^{-(\lambda_+ - \lambda_-)t_{B\ rf}}\right] \tag{70}$$

The second term in Eq. (70) which involves $e^{-(\lambda_+-\lambda_-)t_{Brf}}$ may be neglected if $t_{B\,rf} \gg \tau_{AB}$. Since in our experiments

$$\left(\frac{C_1 - \lambda_-}{\lambda_+ - C_1}\right) \cong \quad \epsilon \leq .2$$

then if

$$t_{B\,rf} \geq 3\tau_{AB}/(1 + \epsilon), \tag{71}$$

then

$$\frac{(C_1 - \lambda_-)}{(\lambda_+ - C_1)} \; e^{-(\lambda_+-\lambda_-)t_{B\,rf}} \leq .01. \tag{72}$$

This second term is the decrease in A dipolar energy caused by thermal equilibration between the A and B reservoirs. If $t_{B\,rf} \gg \tau_{AB}$, this equilibration will have proceeded to completion, and its effects are then contained in the factor

$$C_e = \frac{(\lambda_+ - C_1)}{(\lambda_+ - \lambda_-)} .$$

Condition (71) is satisfied in all our audio saturation experiments on Ca^{43} in CaF_2, so we can neglect the second term in what follows.

For the case of rare spin double resonance, ϵ is usually a small quantity because the heat capacity of the rare spin species is lowered by its small natural abundance. Thus it is possible to expand the solution (70) in powers of the small quantity ϵ. Such an expansion for the quantities C_e and λ_- yields:

$$C_e \cong 1 - \frac{\epsilon}{(1 + z)^2} .$$

and

$$\lambda_- \cong \left(\frac{\epsilon}{\tau_{AB}}\right)\left(\frac{z}{1+z}\right)\left[1 - \frac{\epsilon}{(1+z)^2}\right] .$$

C_e differs appreciably from unity only if ϵ is large while $z \propto (H_{1\ aud})^2 \tau_{AB}$ is small. But since $\epsilon \propto H_{eB}^2$, and experimentally it is known that $\tau_{AB} \propto \exp(+\alpha H_{eB})$, this criterion is not easily satisfied unless T_{1A} is very long so that observable double resonance signals can be seen even with very small audio fields, or unless we are far in the wings of the audio resonance. If the audio field is large so that M_B never grows to a large value, then $E_B = 0$, so that the simple solution of Eq. (64) should apply:

$$E_A(t) = E_{Ao}\, e^{-\left(\frac{\epsilon\, t_{B\ rf}}{\tau_{AB}}\right)} .$$

The correction term $\epsilon/(1+z)^2$ is less than five percent for all $\theta = 45°$ audio saturation data in CaF_2, which is less than the experimental noise.

If the audio saturation data are normalized by dividing by the A dipolar signal for no double resonance effect,

$$S_{A,N} = \frac{S_A(\text{B rf, audio})}{S_A(\text{no B rf, no audio})} ,$$

then if C_e is approximately unity it is reasonable to define a double resonance time constant T_{AB} by the equation:

$$T_{AB} = \frac{t_{B\ rf}}{-\ln (S_{A,N})} \cong \frac{(\tau_{AB} + \tau_{aud})}{\epsilon} . \qquad (73)$$

If the correction terms are important, an expansion of Eq. (73) to second order in ϵ, making use of the relation

$$\ell n(1 + X) \cong X - \frac{1}{2}X^2 ,$$

yields an approximate expression for the effective double resonance time constant T_{AB}:

$$T_{AB} \equiv \frac{t_{B\,rf}}{-\ell n(S_{A,N})} \cong \frac{(\tau_{AB} + \tau_{aud})}{\epsilon} \quad v^{-1} \qquad (74)$$

where

$$v = 1 + \left(\frac{\tau_{AB}}{t_{B\,rf}}\right) \frac{1}{z(1 + z)} - \frac{\epsilon}{(1 + z)^2}$$

Equation (74) is the basis of interpretation of the audio saturation data to be discussed in Sec. IV.A. Since both ϵ and τ_{AB} are small for small H_{eB}, the equation reduces to

$$T_{AB} \cong \frac{(\tau_{AB} + \tau_{aud})}{\epsilon} = \frac{\tau_{AB}}{\epsilon} \quad \frac{(1 + z)}{z} \qquad (75)$$

for small H_{eB}. This equation has a simple interpretation in terms of the thermal reservoir model of the double resonance process. As can be seen from Fig. 6 the audio energy feeds continuously through the B reservoir into the A reservoir, raising its temperature. If either τ_{aud} or τ_{AB} is long there is a corresponding decrease in the double resonance rate T_{AB}^{-1}, since in such a series chain of energy flow, one bottleneck can block the flow.

If the simple Eq. (75) is valid, it is possible to measure the double resonance parameter (ϵ/τ_{AB}) by plotting $z\,T_{AB}$ versus z. The slope of the resulting straight line will give the minimum double resonance time constant τ_{AB}/ϵ. As will be seen in Sec. IV.A.1, if $(H_{1\,aud})^2\,T_{AB}$ is plotted versus $(H_{1\,aud})^2$ instead, the intercept at $H_{1\,aud} = 0$ will give the audio resonance line width.

Solutions for $\tau_{AB} \ll T_{1A} < \infty$, $T_{1B} = \infty$. If T_{1A} is not infinite, the equations (64) and (65) remain almost unchanged with the exception of the coefficient C_1, which now becomes

$$C_1 = \epsilon\, \tau_{AB}^{-1} + T_{1A}^{-1} \equiv (\epsilon + \eta)\, \tau_{AB}^{-1}$$

where $\eta = \tau_{AB}\, T_{1A}^{-1}$ is assumed to be a small quantity. The definitions of $\lambda_{\pm}$, z, $E_A(\pm)$ and $E_A(t_{B\ rf})$ in Eqs. (66), (69), (67), (68), and (70) remain unchanged, and the condition (71) for neglecting the second term also remains valid. It is only necessary to expand the expressions for C_e and λ_- to second order in the three small quantities $(\tau_{AB}/t_{B\ rf})$, ϵ, and η, in order to obtain the first order corrections to the audio saturation double resonance rates. But if $T_{1A} < \infty$ it is necessary to change the definition of the normalized signal by including the decay of the ordered A dipolar state:

$$S_{A,N} = \frac{S_A(\text{B rf, audio})}{S_A(\text{no B rf, no audio})}$$

$$\cong \frac{E_A(0) C_e\, e^{-\lambda_- t_{B\ rf}}}{E_A(0)\, e^{-t_{B\ rf}/T_{1A}}}$$

$$= C_e\, e^{-(\lambda_- - T_{1A}^{-1}) t_{B\ rf}} .$$

The approximate expressions (correct to first order in the small quantities above) for C_e, $(\lambda_- - T_{1A}^{-1})$, and T_{AB} are given by:

$$C_e \cong 1 - (\epsilon/(1 + z)^2),$$

$$(\lambda_- - T_{1A}^{-1}) \cong \frac{\epsilon z}{(1+z)\tau_{AB}} \left[1 - \frac{\epsilon}{(1+z)^2} - \frac{\eta}{z(1+z)} \right],$$

and

$$T_{AB} = \frac{t_{B\,rf}}{-\ell n(S_{A,N})} \cong \frac{t_{B\,rf}}{-\ell n\, C_e} + (\lambda_- - T_{1A}^{-1})^{-1}$$

$$\cong \frac{(1+z)\tau_{AB}}{\epsilon z} (v')^{-1}, \qquad (76)$$

where

$$v' \cong \left[1 + \left(\frac{\tau_{AB}}{t_{B\,rf}} \right) \frac{1}{z(1+z)} - \frac{\epsilon}{(1+z)^2} - \frac{\eta}{z(1+z)} \right].$$

It will be noted from Eq. (76) that even for $z \to 0$, that is in the wings of the audio resonance line, there exists an effective double resonance rate

$$T_{AB}^{-1}(\text{eff}) \cong \frac{\epsilon}{t_{B\,rf}} - \frac{\epsilon}{T_{1A}} .$$

This double resonance rate represents a competition between two processes: On the one hand, the decrease of the A signal through thermal equilibration between the A and B systems leads to a normalized A signal (if $T_{1A} = \infty$ and $t_{B\,rf} \gg \tau_{AB}$)

$$S_{A,N} = \left(\frac{1}{1+\epsilon} \right),$$

which yields a double resonance "rate" (if ϵ is small):

$$T_{AB}^{-1} \cong \frac{\epsilon}{t_{B\,rf}} .$$

On the other hand, when $z = 0$ and $\tau_{AB} \ll T_{1A}$, the A and B systems are coupled closely into one total system, which is being relaxed primarily by the A spin-lattice interaction if T_{1B} is very long compared to T_{1A}. Then $T_A \cong T_B$, so that $E_B \cong \epsilon E_A$, and Eqs. (61) and (62) (including T_{1A}) predict:

$$(1 + \epsilon)\dot{E}_A \cong \dot{E}_A + \dot{E}_B = -T_{1A}^{-1} E_A,$$

so that a reduced relaxation rate $[(1 + \epsilon)T_{1A}]^{-1}$ holds for the A system when a B rf field is applied near the B resonance. Normalizing this signal to the A signal at $t = t_{B\ rf}$ without any B rf pulses results in a normalized signal

$$S_{A,N} \cong e^{-t_{B\ rf}\left(1/(1+\epsilon)T_{1A} - 1/T_{1A}\right)} = e^{+\epsilon\, t_{B\ rf}/(1+\epsilon)T_{1A}}$$

or a "double resonance" rate which is negative:

$$T_{AB}^{-1} = -\frac{\epsilon}{(1+\epsilon)T_{1A}} \cong -\frac{\epsilon}{T_{1A}}$$

The approximate form (Eq. (76)) of the exact solution to the coupled Eqs. (61) and (62) exhibits these two effects clearly in the limit $z \to 0$.

5. Audio Resonance Lineshapes

Measurement of H_{eB}. As mentioned in the introduction to Sec. III.D if H_{1B} and f_B are kept constant and only ω_{aud} is swept, the only quantity in the equations describing $E_A(t_{B\ rf})$ which changes is the audio saturation parameter z. The center of the audio resonance line is given by the minimum of $S_A(\omega_{aud})$, which in turn is given by

$$\frac{\partial S_A}{\partial \omega_{aud}} = \left(\frac{\partial S_A}{\partial z}\right)\left(\frac{\partial_z}{\partial \omega_{aud}}\right) = 0$$

Since $\frac{\partial S_A}{\partial z}$ is necessarily not zero, the center of the audio resonance line is then given by

$$\frac{\partial_z}{\partial \omega_{aud}} = 0$$

For most of our data the observed lineshapes are approximately Lorentzian. At small f_{eB} the $(\omega_{aud}/\omega_{eB})$ factor in the definition of z can shift the resonance slightly toward a higher frequency than f_{eB}. Including the $(\omega_{aud}/\omega_{eB})$ factor in z and using the Lorentzian form of $f(\omega_{aud})$, we find the center of the resonance line to be

$$f_a^o = f_{eB}\sqrt{1 + (\delta f/f_{eB})^2}$$

where δf is the audio resonance finewidth. The apparent line center is shifted because the line is not quite symmetric about f_{eB}: the absorption of energy on the high side of f_{eB} is greater than on the low side, since the quanta $\hbar\omega_{aud}$ being absorbed are larger. This effict is negligible unless δf is large and f_{eB} is low. It results in a correction of a few percent to some audio resonances at $f_{eB} \cong 2$ kHz, for $\theta = 45°$ and $\theta = 30°$.

Audio Resonance Linewidths. There are four possible mechanisms of broadening of the audio resonance lines: broadening by inhomogeneity of the B rf field applied to the sample, lifetime broadening from the finite lifetime τ_{AB} of a B spin in a given state caused by the A-B cross-relaxation process, broadening by the secular part of the A-B dipolar interaction if $\theta \neq 90°$, and broadening of the resonance line by random quadrupole splittings around crystalline imperfections.

Broadening by inhomogeneity of the B rf field over the sample was reduced by using a solenoidal B rf coil about three times as long as the cylindrical sample. The B rf inhomogeneity should be a fixed fraction of the B rf amplitude, since it is determined by the dimensions of the B rf coil. This would give rise to a contribution to the audio resonance linewidth which is proportional to the audio resonance frequency f_{eB}. This component is expected to be less than one percent of f_{eB}, since the static gauss per ampere over the sample volume is measured to be constant within one percent. Inhomogeneous broadening should be largest at $\theta = 90°$ since ΔH_B contributes no inhomogeneous broadening to H_{eB}:

$$H_{eB} = \Delta H_B \sqrt{1 + (H_{1B}^2/\Delta H_B^2)} .$$

The lifetime broadening given by the uncertainty-principle relation adds a linewidth:

$$(\delta f)_{\text{lifetime}} = (2\pi \tau_{AB})^{-1} .$$

This component of broadening therefore decreases exponentially with effective field magnitude:

$$(\delta f)_{\text{lifetime}} = \frac{\langle \Delta\omega_B^2 \rangle_{BA} \tau_c}{4} e^{-\omega_{eB}\tau_c}$$

For the [111] direction and $\theta = 90°$ this component varies from 270 Hz at $f_{1B} = 2$kHz to 1.7 Hz at $f_{1B} = 12$ kHz.

One of the most important sources of broadening for the audio resonances at $\theta \neq 90°$ is caused by A-B dipolar coupling. The secular component of the local field produced at a B spin site by its near A neighbors is always parallel to the laboratory magnetic field because of the difference in the A and B spin Larmor frequencies. If $\theta \neq 90°$, this local field has

a component proportional to $\cos\theta$ parallel to H_{eB} in the rotating frame, which broadens the audio resonance. This local field fluctuates with a correlation time τ_c because of the mutual spin flips between A neighbors, so it is less effective in broadening than indicated by its rms value. This fluctuation results in a motionally narrowed Lorentzian lineshape of width[33]

$$T_2^{-1}(\theta) \cong \langle \Delta\omega_B^2 \rangle \cos^2\theta\tau_c .$$

Another approach to the calculation of the secular A-B dipolar contribution to the linewidth indicates a motionally-narrowed Lorentzian line by studying the ratio of the second moment to the fourth moment of the audio resonance line. The total Hamiltonian of the A and B spin systems in the rotating frame is (with the B-spin quantization axis rotated parallel to H_{eB}):

$$\mathcal{H}_{tot} = \mathcal{H}_d^A(s) - \omega_{eB}S_z - \sin\theta\mathcal{H}_d^{AB}(x) + \cos\theta\mathcal{H}_d^{AB}(z).$$

The linewidth of the B Zeeman resonance is determined by that part of the Hamiltonian which commutes with S_z, the zero order Hamiltonian for the B spins:

$$\mathcal{H}_1^* = \mathcal{H}_d^A(s) + \cos\theta\ \mathcal{H}_d^{AB}(z).$$

Because of the low natural abundance of the B spins, $\mathcal{H}_d^A(s) \gg \cos\theta\ \mathcal{H}_d^{AB}(z)$, but $\mathcal{H}_d^A(s)$ does not contribute to the second moment M_2 of the B spins because it commutes with S_x.[19] But because $[\mathcal{H}_d^A(s), \mathcal{H}_d^{AB}(z)] \neq 0$, $\mathcal{H}_d^A(s)$ contributes to the fourth moment M_4, making $M_4 \gg M_2$, and indicating a Lorentzian, motionally narrowed lineshape. A more exact treatment of this problem[30] results in approximately a Lorentzian line of width:

$$\Delta\omega = T_2^{-1}(\theta) = \frac{\pi}{2} \langle \Delta\omega_B^2 \rangle_{BA} \tau_c \cos^2\theta$$

if the correlation time τ_c is independent of θ.

This is an important mechanism for $\theta \neq 90°$ since it is independent of f_{eB} and is large. For H_o parallel to the [111] direction in CaF_2,

$$\frac{\pi}{2} \langle \Delta\omega_B^2 \rangle_{BA} \tau_c \cong 737 \text{ Hz} .$$

In fact, for Ca^{43} in CaF_2, this is the major contribution to the audio resonance linewidth for $\theta \neq 90°$.

In cubic crystals, crystalline imperfections are an important broadening mechanism for nuclear spins with large quadrupole moments, because of the randomly-varying electric field gradients around each imperfection. Because quadrupole splitting effects on the Ca^{43} resonance in CaF_2 are observed to be small, we shall assume that the first-order quadrupole splitting of the Ca^{43} resonance is small compared with the audio resonance frequency f_{eB}. Then the quadrupole effects are a small perturbation on the B Zeeman levels in the rotating frame and can be calculated by perturbation theory.

We shall calculate the quadrupolar-split energy levels of a Ca^{43} spin with a given quadrupole splitting parameter ν_{Qk}, and then average the results over a Gaussian random distribution of ν_{Qk}. Because the quadrupole splitting is a small perturbation in the rotating frame, it is certainly a small perturbation on the Zeeman states in the laboratory field H_o, so only the "secular" part of the quadrupolar Hamiltonian (that part which commutes with S_z) is retained in the rotating frame Hamiltonian:

$$\mathcal{H}_{Qk}^B = \frac{2\pi \nu_{Qk}}{2} \left[S_{zk}^2 - \frac{S(S+1)}{3} \right] .$$

The parameter ν_{Qk} is here defined so that quadrupole satellites are observed in the laboratory magnetic field H_o at ν_L, $\nu_L \pm \nu_{Qk}$, $\nu_L \pm 2\nu_{Qk}$, etc., where $\nu_L = (\gamma_B H_o/2\pi)$. We further specialize to the case of $\theta = 90°$ because at this angle the A-B dipolar coupling is absent, and quadrupole broadening effects would be most easily measured. We then rotate the axis of quantization through 90° to lie along H_{1B}, so the quadrupolar perturbation becomes ($S_z \rightarrow - S_x$):

$$\tilde{\mathcal{H}}_{Qk} = \frac{2\pi \nu_{Qk}}{2} \left[S_x^2 - \frac{S(S+1)}{3} \right] .$$

The diagonal part of this perturbation yields in first order perturbation theory:[34]

$$(E_{m-1} - E_m)_{\text{rot.frame}} = h(f_{1B} + \frac{\nu_{Qk}}{2} (m - \tfrac{1}{2})) .$$

Thus in the rotating frame $\theta = 90°$ audio resonance the quadrupole satellites of a given spin k are spaced at one-half the distance of the satellites in the laboratory frame. This means that appreciable quadrupolar broadening should be detectable in the audio resonances, if it is present.

To calculate the observed audio resonance lineshape for a random distribution of ν_{Qk}, we assume each satellite has a Lorentzian lineshape with a width T_2 independent of m, and average over the contributions from the range of ν_{Qk}:

$$f(\omega_{aud}) = \int_{-\infty}^{\infty} d\nu_{Qk} \, P(\nu_{Qk}) \sum_{m=+I}^{-I+1} \frac{a(m) T_2}{(1 + \Delta\omega^2(m,k) T_2^2} , \quad (77)$$

where

$$\Delta\omega(m,k) = 2\pi \left(f_{aud} - f_{1B} - \frac{\nu_{Qk}}{2} \left(m - \frac{1}{2} \right) \right)^2 ,$$

$$a(m) \propto |\langle m-1 \mid S_x \mid m \rangle|^2 = (S+m)\,(S-m+1),$$

and

$$P(\nu_{Qk}) = N_B \exp(-\nu_{Qk}^2/2\nu_Q^{-2}) \sqrt{2\pi}\, \bar{\nu}_Q .$$

The function (77) has been evaluated numerically on an IBM 1620II computer for several values of $\bar{\nu}_Q$ and T_2. If $(2\pi T_2)^{-1} \ll \bar{\nu}_{Q/2}$, Eq. (77) consists of a sharp central peak (since the $\pm\frac{1}{2}$ line is not split) with broad wings containing most of the area of the line. But if $(2\pi T_2)^{-1} \gtrsim \frac{2}{3} \left(\bar{\nu}_Q/2 \right)$, the line is very close to Lorentzian in shape, being only a little narrower at the top and having slightly broader wings. Also, the half width at half maximum is about 15% less than the sum of the quadrupolar and homogeneous linewidths. If appreciable quadrupolar broadening is present, it should manifest itself in the audio resonances as a non-Lorentzian lineshape or a smaller double resonance effect at the audio resonance center because only the $\pm\frac{1}{2}$ transition is being saturated. The audio resonance quadrupolar linewidth is one-half the laboratory resonance quadrupolar linewidth.

It is interesting to note that for $\theta \neq 90°$, the quadrupole satellites in the rotating frame are given by

$$E_{m-1} - E_m = h\nu_{eB} - h \frac{\nu_{Qk}}{2} (3\cos^2\theta - 1) \left(m - \frac{1}{2} \right)$$

This means that at $\theta \cong 55°$ quadrupole broadening of the audio resonance line is absent in first order. This fact may be useful in cases of extreme quadrupole broadening, as a means of narrowing the audio resonance

line to measure H_{eB} more accurately. Unfortunately, for the case of Ca^{43} in CaF_2, the A-B dipolar coupling at $\theta = 55°$ contributes about 250 Hz to the linewidth. Since the audio resonance linewidths at $\theta = 90°$ are about 100 Hz, if this linewidth were caused entirely by quadrupole splittings, its disappearance at $\theta = 55°$ would probably be masked by the A-B dipolar contribution to the linewidth.

Audio Resonance Line Shape at Large Audio Amplitude. The Ca^{43} audio resonance was studied as a function of the peak audio amplitude H_z to check whether large audio amplitudes would introduce any error into the H_{eB} measured by audio resonances. Here the audio Hamiltonian is given by

$$\mathcal{H}^B_{aud}(t) = -\gamma_B \hbar H_z \cos(\omega_{aud} t) S_z .$$

No shift of the first order audio transition at $\omega_{aud} = \gamma_B H_{eB}$ was observed as the audio amplitude was increased, until the resonance peak became poorly defined through audio broadening and complete destruction of the F^{19} dipolar order. No lines were observed at $\frac{3}{2}\omega_{eB}$ or $2\omega_{eB}$ as reported by Franz and Slichter,[21] probably because of the simplicity of the secular A-B dipolar Hamiltonian $\mathcal{H}^{AB}_d(s)$ and its small size compared with the H_{eB} Zeeman interaction. Therefore the audio resonance shape is not distorted by audio fields much larger than necessary to observe strong lines in CaF_2, so no error is introduced into the measured H_{eB}.

At $\theta = 45°$, for $H_z \geq 2.03$ gauss and $H_{eB} = 40.7$ gauss or 29 gauss, small audio resonance lines about half as wide as the unsaturated main transition were observed at about $\omega_{aud} = \omega_{eB}/2$. These can be interpreted either as caused by about 1% second harmonic audio distortion, or as audio double quantum transitions which are analogous to the proton multiple quantum

transitions studied by Wilking[35] and by Dederichs and Leibfried.[36] These authors have shown that for a spin = 1/2 system the double quantum transition occurs at a frequency

$$\omega_{aud} = \frac{\omega_{eB}}{2}\left[1 + \left(\frac{H_z}{2H_{eB}}\right)\sin^2\theta\right], \qquad (78)$$

and has an amplitude proportional to

$$H_z^4\, H_{eB}^{-2} \sin^2\theta \cos^2\theta .$$

At H_{eB} = 29 gauss and the maximum H_z = 3.0 gauss, the frequency shift in Eq. (78) is negligible ($\sim 10^{-3}$), so it cannot be used to distinguish between audio harmonic distortion and audio double quantum transitions. The observed lines are at least partly caused by harmonic distortion, since even at $\theta = 90°$ small lines are observed at $\omega = \omega_{eB}/2$. But the slightly stronger lines observed at $\theta = 45°$ obey the H_z^4 and H_{eB}^{-2} dependence approximately, so there is probably some contribution from double quantum transitions. This investigation has not been pursued because it is difficult to eliminate the harmonic distortion over a wide frequency range.

E. Theory of Pulsed ADRF-DR Measurements

1. $\theta = 90°$ Case

The spin-temperature density matrix calculation of the cross-relaxation rate τ_{AB}^{-1} neglects A and B spin lattice interactions. If these are now included, Eqs. (36) and (37) for the F^{19} dipolar energy (E_A), and Ca^{43} Zeeman energy in the field $H_{1B}(E_B)$ become:

$$\frac{dE_A}{dt} = -\frac{1}{\tau_{AB}}(\epsilon E_A - E_B) - \frac{E_A}{T_{1A}} \tag{79}$$

$$\frac{dE_B}{dt} = \frac{1}{\tau_{AB}}(\epsilon E_A - E_B) - T_{1B}^{-1} E_B \,. \tag{80}$$

Since $T_L = 300°K \gg T_{ss}(i) \sim .1°K$, we can assume that the A and B energies effectively approach zero for CaF_2. Since the measured value of $T_1(Ca^{43}) \sim 230$ sec $\gg T_1(F^{19}) = 4.3$ sec $\gg \tau_{AB}$, we can neglect T_{1B} completely in what follows for CaF_2, but not necessarily T_{1A}.

A study of the parameters ϵ and τ_{AB} of Eqs. (79) and (80) as a function of θ and ω_{eB}, will enable us to trace out the spectrum of the local field correlation function $g_x(\tau)$, and to check whether the thermodynamic model of the cross relaxation process describes our results even when the spin diffusion time constant $\tau_{SD} \gtrsim \tau_{AB}$.

The $\theta = 90°$ case is simpler than the $\theta \neq 90°$ cases because the initial value of E_B for each B rf pulse is always zero, if $\tau_o \gg T_{2B}$ (see Section VI for the $\tau_o \lesssim T_{2B}$ case); the components of B magnetization parallel to H_{1B} from the preceding pulse will have decayed to zero in a time of order T_{2B}.

The $\theta \neq 90°$ case is more complicated because (1) the initial Ca^{43} Zeeman

energy along $H_{eB}(E_{Bi})$ varies from pulse to pulse so a matrix must be used to relate $(E_A(\tau), E_B(\tau))$ to (E_{Ai}, E_{Bi}) for each pulse; (2) for $\theta \neq 90°$ the B system in principle cannot be described by a spin temperature during cross-relaxation, because the transition probabilities are no longer given by matrix elements of S_x alone; and (3) Clough[29] has shown that a shape change in the spectrum of the dipolar system occurs for $\theta \neq 90°$.

For simplicity we begin by neglecting T_{1A} in Eqs. (79) and (80) and finding the solution for $E_A(\tau)$, $E_B(\tau)$ at the end of a B rf pulse of length τ by multiplying (79) by ϵ and subtracting (80) from it:

$$\epsilon E_A(\tau) - E_B(\tau) = (\epsilon E_A(0) - E_B(0))\, e^{-(1+\epsilon)\tau/\tau_{AB}}$$

Using the conservation of rotating frame energy

$$E_A(\tau) + E_B(\tau) = E_A(0) + E_B(0) \quad ,$$

we can solve for $E_A(\tau)$, $E_B(\tau)$ in terms of $E_A(0)$, $E_B(0)$:

$$E_A(\tau) = C_1(\tau)\, E_A(0) + C_2(\tau)\, E_B(0) \tag{81}$$

$$E_B(\tau) = C_3(\tau)\, E_A(0) + C_4(\tau)\, E_B(0) \, . \tag{82}$$

Here

$$C_1(\tau) = (1 + \epsilon\, E(\tau))/(1 + \epsilon) \tag{83}$$

$$C_2(\tau) = [1 - E(\tau)]/(1 + \epsilon)$$

$$C_3(\tau) = \epsilon[1 - E(\tau)]/(1+\epsilon)$$

$$C_4(\tau) = [\epsilon + E(\tau)]/(1 + \epsilon)$$

and

$$E(\tau) = \exp(-(1 + \epsilon)\tau/\tau_{AB}) \, .$$

Using our initial condition $E_B(0) = 0$ for $\theta = 90°$, we can write the value of E_A (nth pulse) in terms of E_A((n-1)th pulse):

$$E_A(n) = \{[1 + \epsilon E(\tau)]/(1 + \epsilon)\}\, E_A(n-1) ,$$

so the effect of a sequence of N B rf pulses is ($\theta = 90°$ and neglecting T_{1A}, T_{1B}):

$$E_A(N) = \left[\frac{1 + \epsilon\, E(\tau)}{(1+\epsilon)}\right]^N E_A(0) .$$

A crude account of T_{1A} can be made by assuming cross-relaxation and A spin-lattice interaction are independent, so that

$$E_A(N) \simeq \left[\frac{1+\epsilon E(\tau)}{1+\epsilon}\right]^N e^{-N(\tau+\tau_o)/T_{1A}} E_A(0)$$

We can normalize the signals we obtain by dividing by $(S_A)_{NBrf}$ to take account of T_{1A} relaxation. $(S_A)_{NBrf}$ is the value of the F^{19} dipolar signal if the sequence in Fig. 1 is repeated, but without B rf pulses applied. Then we can fit the normalized data to the following functional form, in the least squares sense:

$$\frac{S_A(N)}{(S_A)_{NBrf}} = \frac{E_A(N)}{E_A(0)e^{\frac{-N(\tau+\tau_o)}{T_{1A}}}} = \left[\frac{1 + \epsilon\, E\,(\tau)}{1 + \epsilon}\right]^N \qquad (83')$$

Since N is known, the least squares fit[37] gives us experimental values of ϵ and τ_{AB} for the particular value of H_{1B} chosen.

The effect of T_{1A} in Eq. (79) can be included, but this results in a much more complicated functional form for the normalized A signal than Eq. (83'). The derivation of this functional form (valid for all T_{1A}) is described in Appendix E, but for small τ_{AB} ($\ll T_{1A}$) and small ϵ, the normalized A signal change caused by one B rf pulse is given approximately by:

$$\frac{E_A(1)}{E_A(0)e^{-\tau/T_{1A}}} \cong A_1 e^{+a_1\tau} + A_2 e^{-a_2\tau} \qquad (84)$$

where

$$A_1 \cong (1+\epsilon)^{-1}\left[1 - \frac{2\epsilon x}{1+\epsilon}\right]$$

$$A_2 \cong \epsilon(1+\epsilon)^{-1}\left[1 + 2x(1+\epsilon)^{-1}\right]$$

$$a_1 \cong \epsilon(1+\epsilon)^{-1} T_{1A}^{-1}$$

$$a_2 \cong (1+\epsilon)\,\tau_{AB}^{-1}\left[1 - x(1+\epsilon)^{-1}\right]$$

and

$$x = \tau_{AB}(1+\epsilon)^{-1} T_{1A}^{-1} .$$

The form (84) is very close to (83), since $x/1+\epsilon \leq 1/40$ for all our $\theta = 90^\circ$ measurements.

The effects of T_{1A} can be interpreted as follows: Normalization of the A signal compares spin lattice relaxation of the combined A and B spin systems during the B rf pulse, to the spin lattice relaxation of the A system alone. Thus a_1 in Eq. (84) is positive because the slightly larger ($\sim(1+\epsilon)$) heat capacity of the combined A and B systems makes the combination relax more slowly toward the lattice temperature than the A system alone would. The thermal equilibration rate a_2 is smaller because of the additional heating from the relatively hot lattice. As can be seen from Eq. (80), for $T_{1A} \ll \tau_{AB}$, the thermal equilibration rate for E_B should be given by the smaller value $1/\tau_{AB}$ rather than $(1+\epsilon)/\tau_{AB}$ as for isolated A and B systems, since E_A will rapidly approach zero. The small negative correction in a_2 represents the beginning of this effect.

To make certain all T_{1A} effects were included in the data analysis,

a computer program using the exact $\theta = 90°$ equations of Appendix E was used to obtain the $\theta = 90°$ data in Figs. 43 to 45. For this particular set of data ϵ was affected less than 1% by the T_{1A} correlation, while τ_{AB} was changed less than the experimental error.

2. $\theta \neq 90°$ Case

As mentioned in the introduction in Section II.B.3, there exists the possibility that the A-B cross-relaxation for $\theta \neq 90°$ might not be described by a spin temperature, thermal reservoir model. To investigate this effect and see whether it is important, it is useful to try interpreting the $\theta \neq 90°$ data in terms of the thermal reservoir model. If we do this, deriving "experimental" ϵ, τ_{AB} from the $S_A(N)$ data we are assuming that Eqs. (79), (80) hold. It is possible that even the form of these equations may be wrong, but in the absence of a detailed theory of this result of higher-order perturbation theory we can still check the importance of this modification by studying the magnitude and sign of the discrepancies with the simple theory. The probable error derived from the least squares fit of the data to Eq. (1) will indicate whether a drastic modification of the form of the equations is necessary.

If $\theta \neq 90°$, the general formalism of Section II.B can be used to calculate τ_{AB} and ϵ, assuming that the secular part $\mathcal{H}_{1z} \cos\theta$ of the Ca-F coupling can be lumped with $\mathcal{H}_d^A$ to form a total "spin-spin" reservoir. The form of Eqs. (E.1) and (E.2) of Appendix E remains unchanged, so the expressions for $E_A(\tau)$ and $E_B(\tau)$ at the end of a B rf pulse of length τ should be calculable from Appendix E, if the initial values E_{Ao}, E_{Bo} are known.

Once these relatively small changes of $\epsilon(\theta)$ and $\tau_{AB}(\theta)$ are made,

the major modification of the $\theta \neq 90°$ theory then consists of taking into account the component of Ca^{43} magnetization from the preceding pulse, which remains along H_o after the transverse component of Ca^{43} magnetization has decayed between B rf pulses. Suppose $E_B(n-1)$ gives the B energy just before the end of the preceding pulse; then the value of the magnetization aligned along H_{eB} is given by:

$$M_B(\tau, n-1) = \frac{-E_B(n-1)}{H_{eB}} .$$

If the B spin populations along H_{eB} are given by a high-temperature Boltzmann distribution, the cos θ projection law is obeyed,[38] so the component of M_B remaining along H_o after several T_{2B} is $M_z^B = M_B(\tau, n-1) \cos\theta$, and when H_{eB} is turned on again at the beginning of the next B rf pulse the initial value of E_B is given by

$$-H_{eB} M_B(\tau, n-1) \cos^2\theta = E_B(n-1) \cos^2\theta .$$

If we neglect T_{1A}, $E_A(\tau, n-1)$ is unchanged during τ_o, so using Eqs. (81) and (82), we find the following set of equations which describes the effects of one B rf pulse "cycle" on the A and B spin energies (see Fig. 11).

$$E_A(n) = C_1(\tau)\, E_A(n-1) - C_2(\tau) \cos\theta\, H_{eB}\, M_z^B(n-1) \qquad (85)$$

$$M_z^B(n) = \frac{-\cos\theta}{H_{eB}} C_3(\tau)\, E_A(n-1) + \cos^2\theta\, C_4(\tau)\, M_z^B(n-1) . \qquad (86)$$

Equations (85) and (86) can be written as a matrix which relates the "vector" $(E_A(n-1), M_z^B(n-1))$ at the beginning of a B rf pulse cycle to the value at the end:

$$\begin{pmatrix} E_A(n) \\ M_z^B(n) \end{pmatrix} = M \begin{pmatrix} E_A(n-1) \\ M_z^B(n-1) \end{pmatrix} .$$

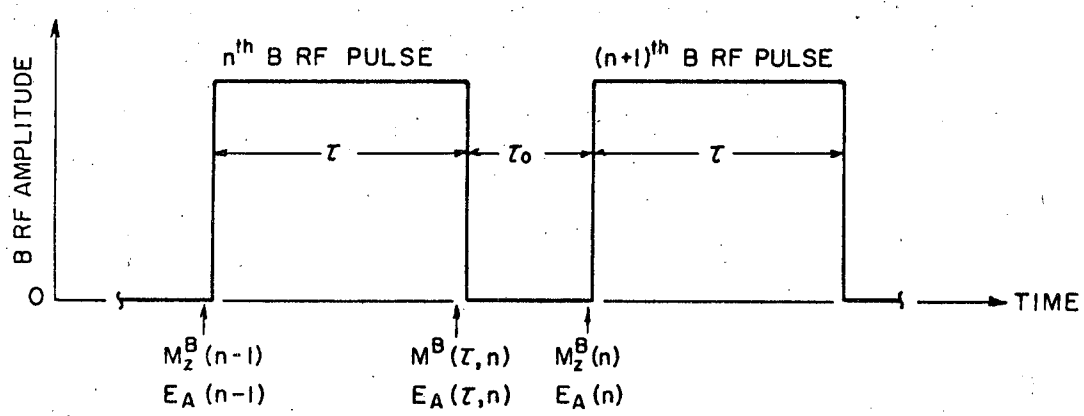

XBL 676-4158

Fig. 11 Properties of B rf pulses used in pulsed ADRF double resonance

The final value of E_A after N B rf pulses can be easily written in terms of a power of the matrix M:

$$\begin{pmatrix} E_A(n) \\ M_z^B(n) \end{pmatrix} = M^N \begin{pmatrix} E_A(0) \\ M_z^B(0) \end{pmatrix} .$$

Here

$$M \equiv \begin{bmatrix} C_1' & C_2' \\ C_3' & C_4' \end{bmatrix} ,$$

and the C_i' can be found by inspection from (85) and (86). The values of the elements of M^N can be written down easily using the fact that a matrix satisfies its characteristic equation. As a result a 2×2 matrix such as M^N can be written as a linear combination of M and the identity matrix I:

$$M^N \equiv \alpha\, I + \beta\, M$$

α and β can easily be determined from two equations satisfied by the eigenvalues λ_+, λ_- of M.[39] Explicit expressions for α and β for the case of neglect of T_{1A} are given in Appendix E. These expressions indicate that for $\tau \geq \tau_{AB}$, the initial value of M_z^B affects the results appreciably, so care must be taken that M_z^B has the same initial value for each sequence of B rf pulses during a run. The easiest initial condition to maintain is $M_z^B(0) = 0$. This large dependence on $M_z^B(0)$ comes from the unusually large amount of energy transferred between the A and B spin systems during the first B rf pulse, if $M_z^B(0) = 0$. The $\theta = 30°$ have been analyzed with a computer program written to include this effect, T_{1A}, and the effects of M_z^B remaining between B rf pulses.

III. EXPERIMENTAL APPARATUS

A. Arrangement of Coils and Sample

Figure 12 is a schematic diagram of the arrangement of the A rf coil, the B rf-Receiver coil, and the audio coil. A B rf coil with large gauss per ampere is required because of the small Ca^{43} gyromagnetic ratio, but H_{1B} also must be very homogeneous over the sample volume if details of the audio resonance lineshapes are not to be obscured by large inhomogeneous broadening. For this reason a solenoid about three times as long as the sample was chosen for the B rf coil, and oriented perpendicular to the laboratory magnetic field H_o. A portion of this solenoid about as long as the sample is switched to the input to the receiver during part of the experimental cycle, and acts as a receiver coil at the 11 MHz A rf frequency. This arrangement was possible because the B spin frequency is much lower than the A rf frequency. Perpendicular to both H_o and the B rf-Receiver coil is the axis of the A rf coil, chosen to be a Helmholtz pair to give good A rf homogeneity over the sample for good spin locking and sharp pulse conditions. The audio field parallel to H_o is provided by the outer set of coils, forming approximately a Helmholtz pair for good audio homogeneity over the relatively small sample volume.

The axis of the B rf-Receiver coilwas vertical, and a rod was glued to the cylindrical CaF_2 sample, which fit snugly into the B rf-receiver coil. The rod passed through a hole in the table over the magnet, and a pointer and a piece of circular graph paper, calibrated in degrees, were used to set the angle of the sample. Since the cylinder axis of the cubic cylinder axis of the cubic crystal was approximately parallel to the [110] direction, rotation about this axis could bring H_o along the [111],

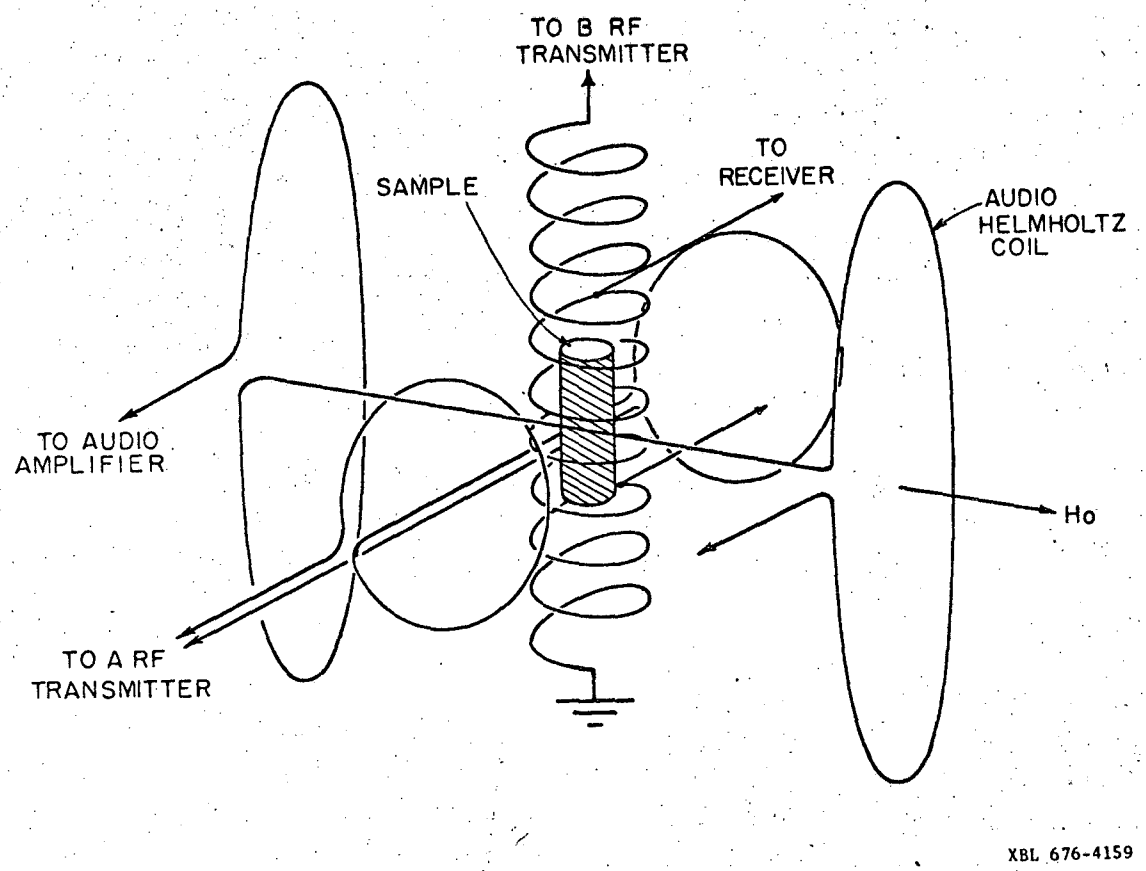

Fig. 12 Arrangement of sample, audio Helmholtz coil, A rf Helmholtz coil, and solenoidal B rf - receiver coil; the small section of the B rf coil between the two taps serves as a receiver coil

[110], or [100] directions. The angle of rotation of the crystal (Ω) was resettable with this arrangement to less than ± 0.5 degree. The rotation rod was parallel to the magnet pole faces within $\pm .5$ degree.

The angle Ω corresponding to a particular crystalline direction was measured by measuring the angular variation of $T_2(F^{19})$. The [111], [110] and [100] directions are all extrema of $T_2(F^{19})$ as the crystal is rotated around the [110] direction, with $T_2(F^{19})$ decreasing in the order [111], [110], and [100].[19] The angles corresponding to the [111] and [110] extrema of T_2 were measured to ± 1 degree by recording the amplitude of the F^{19} free induction decay as a function of Ω. The direction of the cylinder axis of the crystal was measured with x-rays to be rotated from the [110] axis about five degrees toward the [100] axis and three degrees toward the [111] direction. This agrees with the $T_2(\Omega)$ measurements since this small crystalline axis misorientation changes primarily the magnitude of $T_2(F^{19})$, and not the angle Ω at which the extremum occurs.

During the measurement of the temperature dependence of $T_1(Ca^{43})$ the A rf, B rf-receiver, and audio coils were enclosed in an insulating box made of styrofoam and masonite, and the temperature of the sample was regulated by passing hot air into the bottom of the box. A copper-constantan thermocouple junction was glued to a slot cut in the side of the sample, and the temperature of the sample was measured by recording the thermocouple voltage between an ice bath reference and the sample, with a Moseley 680 recorder. The input air was heated by passing over a resistance, the current through which was controlled by a resistance bridge. The bridge controlled a relay which changed the phase of about ten percent of the current through the resistance, so that it added to or subtracted from the main current. The main current was set with a Variac, and the one arm of the resistance

bridge contained a thermistor which was glued to the sample near the thermocouple junction. Because of severe heat leaks down the various rf inputs to the box, this arrangement was only able to hold the temperature steady within ±2 degrees at 355°K, but this was adequate to check the temperature dependence of $T_1(Ca^{43})$.

To measure the audio amplitude a small sensing coil with its axis parallel to H_o was inserted into the audio Helmholtz coil, and the voltage induced in the sensing coil was observed with a sensitive Tektronix 53/54D Plug-In. The minimum sensing coil voltage observable was about 1 mv peak, so that an audio amplitude $H_z \geq .03$ gauss peak at $f_{aud} = 1$ kHz could be measured.

B. Electronics

1. Magnetic Field Regulation

Figure 13 is a block diagram of the magnetic regulator system. The F^{19} NMR frequency is fixed by an 11 MHz crystal reference oscillator, so the laboratory magnetic field must be set to a fixed value H_o at the CaF_2 sample. For this purpose the probe of a Varian F-8 A Fluxmeter containing a proton sample is placed at another point in the magnet gap. A very stable but adjustable frequency source is necessary to set H_o via the proton resonance, because in general the magnetic field inhomogeneity in the gap makes the required proton frequency f_3 vary with the F-8A probe position. The Gertsch FM-6 Frequency Meter produces a frequency in the 20-40 MHz range which is stable to a few parts in 10^6 per day when it is properly locked. The FM-6 frequency is divided by 10 in the Gerstsch FM-5 Frequency Divider and multiplied by 3 in the Varian F-8A Fluxmeter to produce the required $f_3 \approx 11.6$ MHz.

The magnetic field H_o was set by first adjusting the phase sensitive

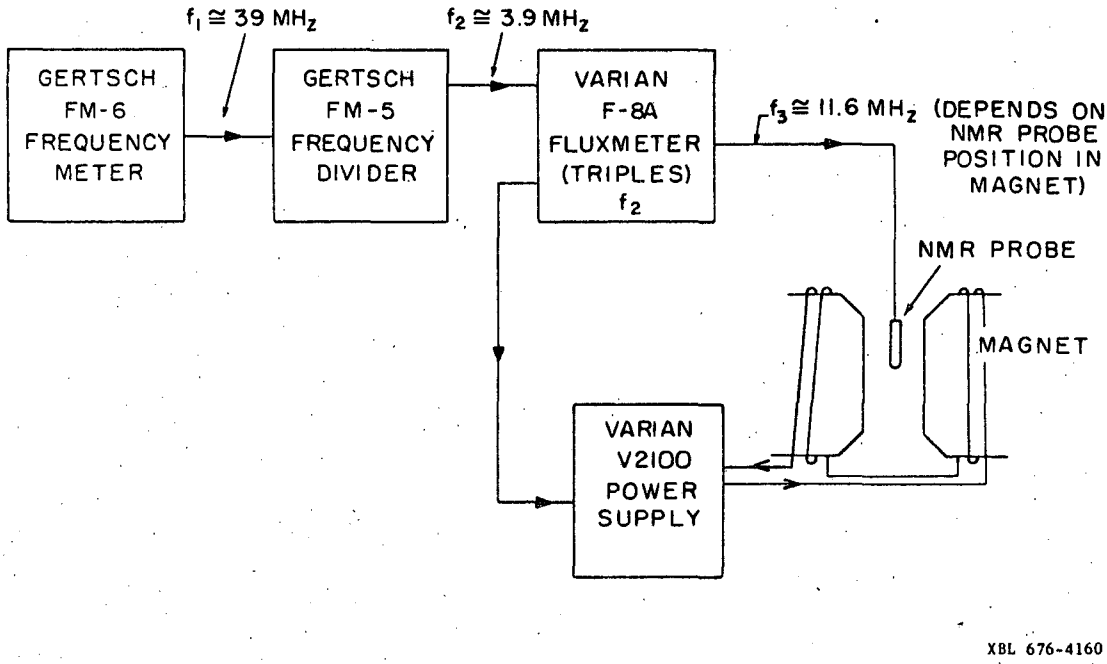

Fig. 13 Block diagram of magnetic field (H_o) regulating system

dectector so that zero signal was obtained at the beginning of the F^{19} free induction decay. If $(\gamma_A Ho)=2\pi$ · (11 MHz) exactly, there will be no phase drift between the nuclear signal at $\gamma_A Ho$, and the reference oscillator at $\omega_r = 2\pi$ (11 MHz). But if the resonance condition is not satisfied, the resulting phase drift yields a signal which is proportional to time:

$$S_A(t) \cong S_{Ao}\, e^{-\left(t^2/2T_2^2\right)} \sin\left[(\omega_r - \gamma_A Ho)t\right].$$

Thus the correct value of H_o is that which yields zero Zeeman signal for all time, if initially the phase is adjusted to give zero signal. By this method f_3 (and thus H_o) could be set with an error of less than ±300 Hz out of ~11.6MHz. This results in an error of setting f_{Bo} of $\left(\frac{\gamma_B}{\gamma_A}\right)(\Delta f_3) \cong$ ±20 Hz. Once $f_3 = .3f_1$ was set by this method, only mechanical displacement of the rf head or the Varian F-8A NMR probe could change H_o, so long as f_3 was monitored occasionally. Because $f_3 \cong \gamma_A H_o$, some 11.6MHz rf is picked up by the receiver coil to produce ~ 600 kHz beats at the phase sensitive detector output, but these beats are integrated out in the gated integrator.

During accurate measurements of double resonance rates it was found advisable not to use the automatic regulation feature of the F-8A, because the FM-6 would sometimes "jump" into another stable state separated from the desired one by 1-2 kHz (this is probably caused by instability in one of the frequency dividers in the FM-6). If the F-8A were automatically regulating it would pull Ho to the new value of f_3, but if this system is used as a monitor alone, such a "sudden jump in field" could be easily recognized as a sudden jump in f_3 instead, and corrected on this basis. Some noise might also be contributed by the automatic regulation because

of the constant, relatively slow "hunting" of H_o around its mean value, and because of drift in the zero setting of the F-8A discriminator.

2. A RF System

Figure 14 is a block diagram of the entire double resonance apparatus with the exceptions of the magnet regulator system and the Tektronix pulse generators which produce the controlling gates shown on the diagram. There are four main subsystems: the A rf system, the receiver system, the B rf system, and the audio system.

The A rf system supplies to the A rf coils the ADRF waveform, the saturating pulse for signal-zero measurement, and the θ° sensing pulse to read out the remaining A dipolar energy. The f_A = 11MHz crystal oscillator provides cw rf to the phase sensitive detector and the A rf system. The A rf gate (Fig. 15) circuit uses a 7077 tube with grounded grid, the plate of which is pulsed positive to turn on the A rf. When a +100 V pulse is applied to the A RF GATE input the FD 200 diode is back-biased and the DC voltage at the 7077 plate rises to 125 volts, allowing the f_A = 11MHz rf to be amplified and appear at the output tank circuit. Unless the output DC level of the amplifier providing the A RF GATE is less than about -10 V, this circuit will allow some 11MHz to leak through.

If zero voltage is applied to the A RF PHASE SHIFT input, the capacitor C_{ps} is effectively not in the 7077 tank circuit because the diode D2 is back-biased. The other capacitors in the 7077 tank circuit are then adjusted so that $(f)_{tank}$ is higher than f_A by about f_A/Q_{tank}. This detuning of $(f)_{tank}$ provides a 45 degree phase shift across this circuit if D2 is back-biased. When a +100V pulse is applied to the A RF PHASE SHIFT input D2 is forward-biased, putting C_{ps} into the tank circuit

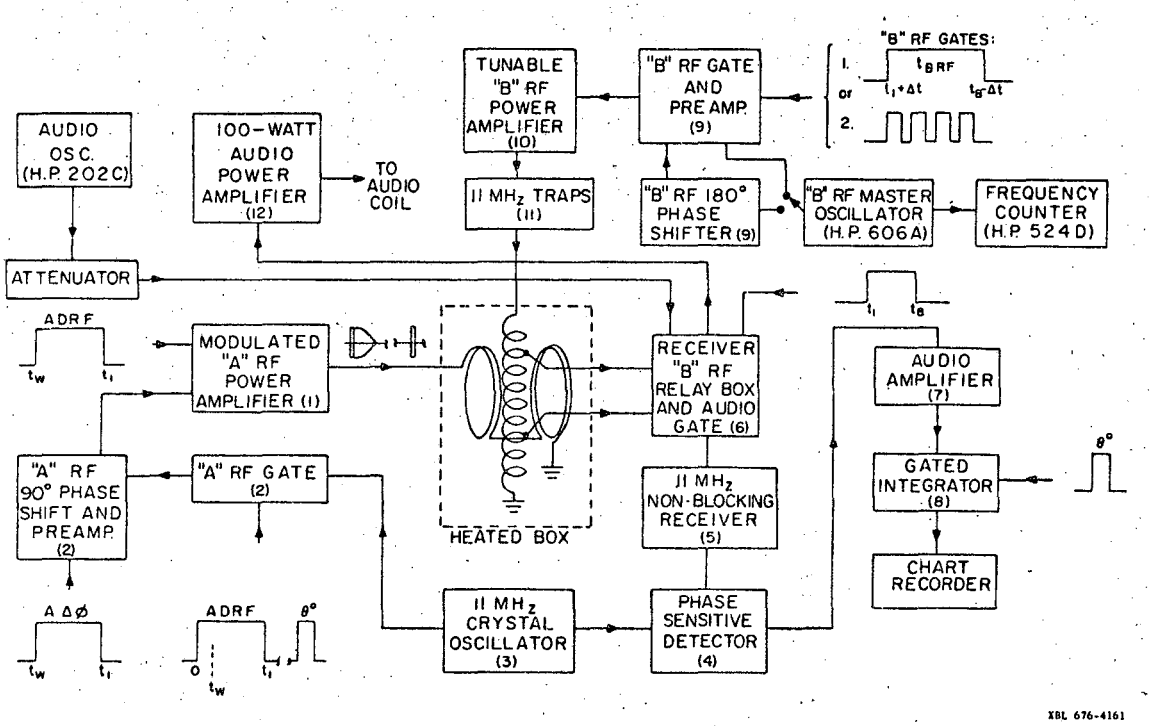

Fig. 14 Block diagram of the ADRF double resonance apparatus; audio coil and sample not shown; rf gating pulses provided by Tektronix pulse generators

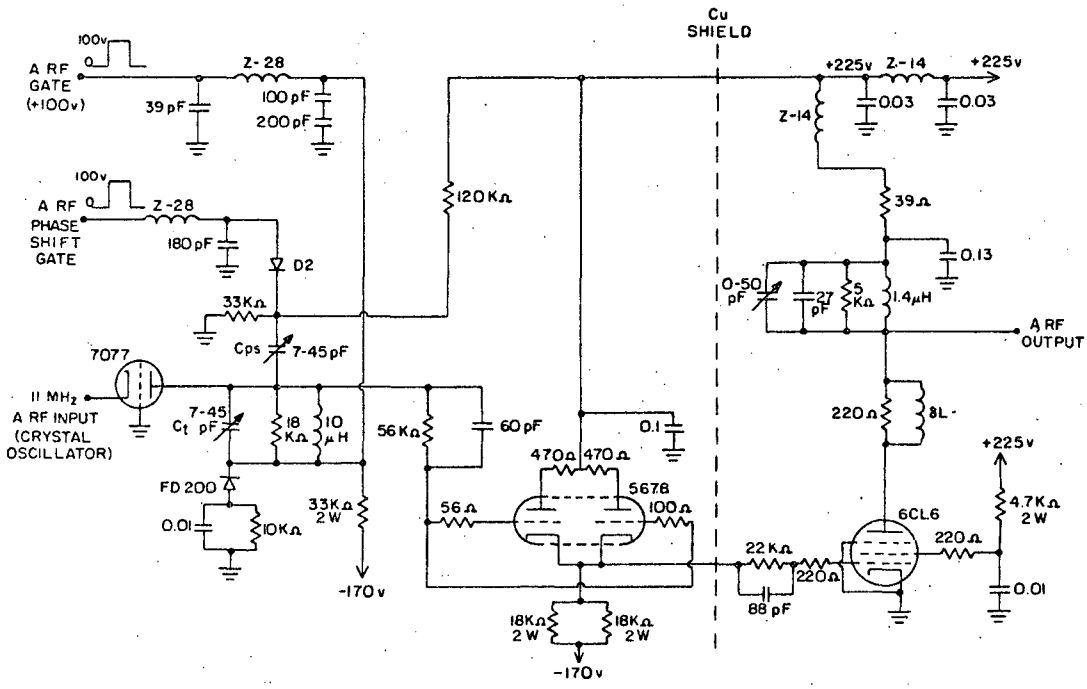

Fig. 15 A rf gate and 90° phase shift circuit (chassis 2)

and lowering $(f)_{tank}$ below f_A by about $-f_A/Q_{tank}$, which introduces a -45 degree phase shift into the A rf. The application of the A phase shift pulse thus causes a total phase shift of 90 degrees in the A rf appearing at the input to the 5678 cathode follower. Following the cathode follower is a standard 6CL6 amplifier stage. The small resistors and the inductor in the grid and plate leads of some of the stages are to stop parasitic oscillations.

The best method of adjusting C_t and C_{ps} to provide exactly a 90° phase shift but no amplitude change of the A rf was to use leakage into the phase sensitive detector (PSD). All stages following the 6CL6 amplifier were turned off, and the PSD phase was adjusted to give maximum signal with no phase shift pulse. Then the phase shift was turned on and C_{ps} adjusted to give zero signal at the PSD output just after the beginning of the phase shift pulse, since a 90° phase shift implies orthogonality to the PSD reference rf. To adjust the equality of the A rf before and after the 90° phase shift, the PSD phase was changed by 45 degrees to give equal weight to the unshifted and shifted A rf, and then C_t and C_{ps} were adjusted for equal signals at the PSD output. Since these two adjustments interact they must be repeated several times.

The gated and phase shifted A rf now passes into the MODULATED A RF POWER AMPLIFIER (Fig. 16, Fig. 17, Chassis 1), which generates the power needed for the A rf pulses and decreases the A rf smoothly to zero during the ADRF pulse. There are first two stages of class C power amplification (tubes 6CL6 and 5726), the screens of which are brought exponentially to a slightly negative voltage by the ADRF pulse from the cathode follower 6DJ8. The grids of the 6DJ8 are normally held at +225V, so the capacitor C1 is fully charged. Then the ADRF PULSE AMPLIFIER (Fig. 18, Chassis 13)

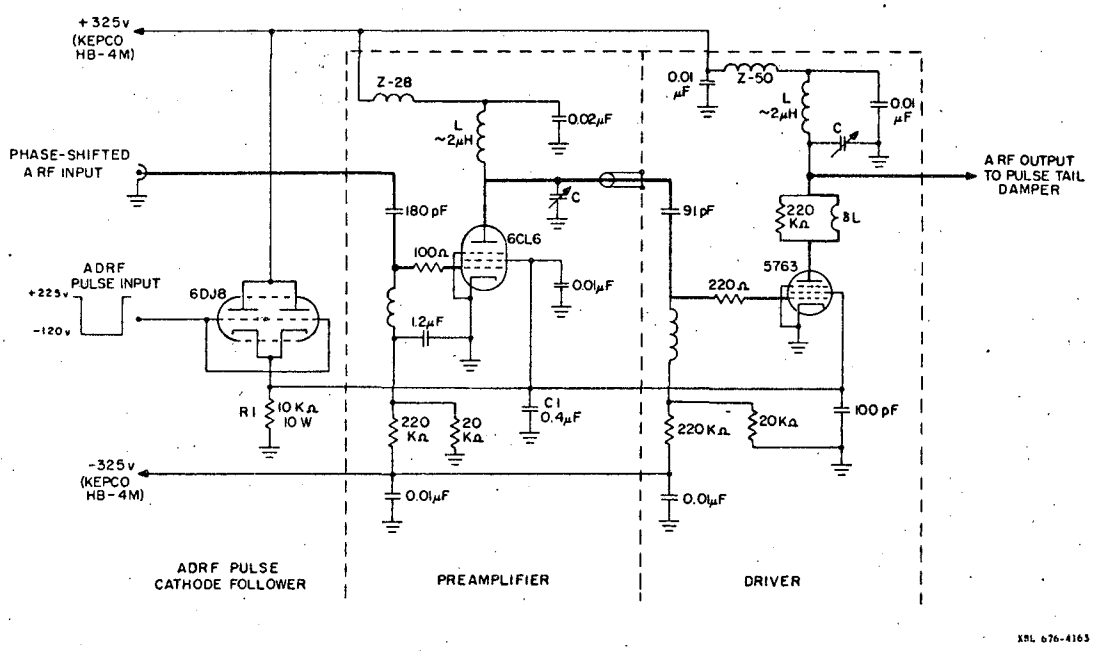

Fig. 16 Modulated A rf power amplifier (chassis 1)

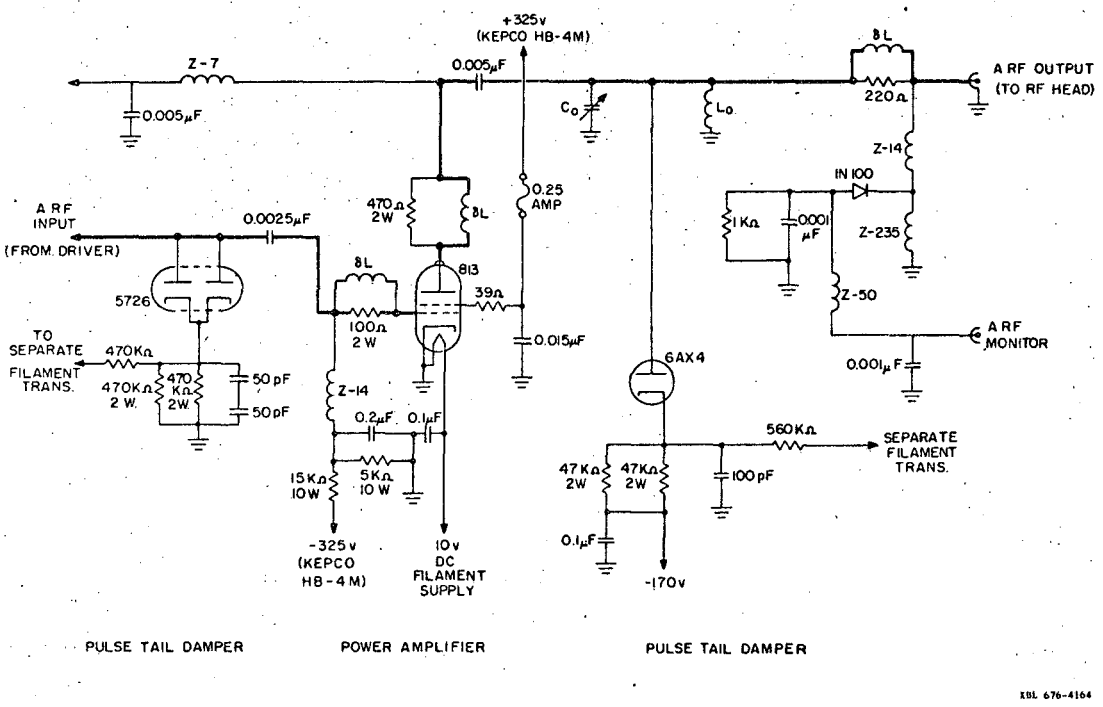

Fig. 17 Modulated A rf power amplifier (chassis 1)

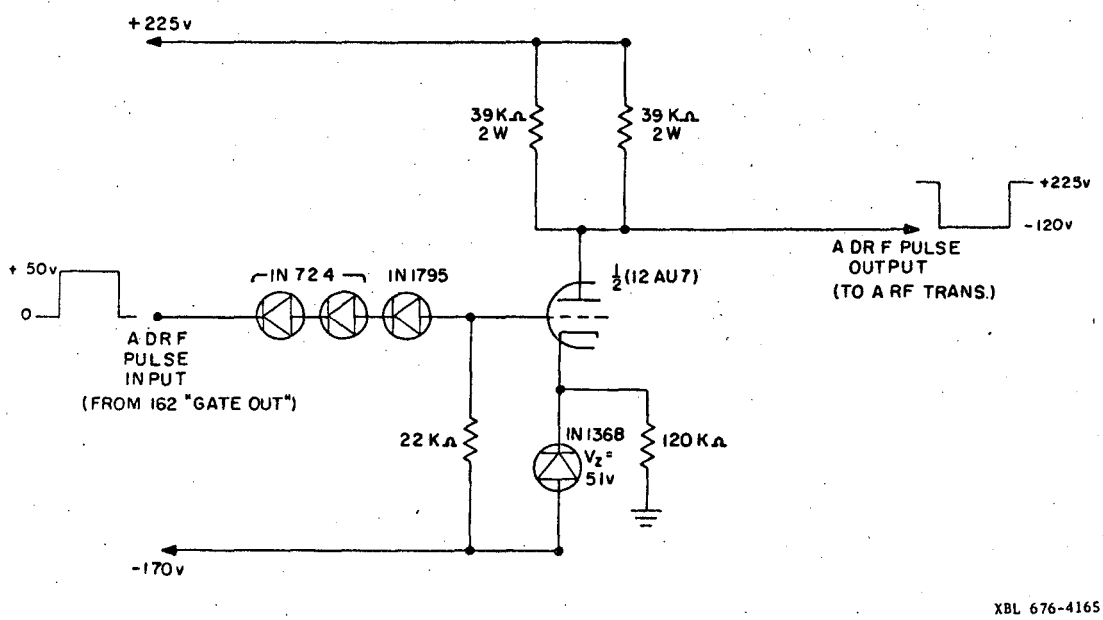

Fig. 18 ADRF pulse amplifier (chassis 13)

provides a negative pulse to the cathode follower, which allows C1 to discharge with a time constant $\tau \sim$ 2msec determined by C1, and R1 and the power requirements of the screens. The modulated A rf waveform then drives the grid of the 813 class C final amplifier to produce the ADRF pulse train. The variable air capacitor C_o tunes the A rf output together with L_o and L(A rf coil). The A rf system could produce a rotating component $H_{1A} \cong 7.5$ gauss peak.

If leakage from the ADRF waveform is observed at the PSD output, there is a large apparent phase shift of the A rf near the point where the A rf is finally cut off. This may be a real phase shift occurring in the modulated amplifier stages when the screens go slightly negative, or it may be only an apparent phase shift caused by the phase of the leakage from the 813 circuits is finally cut off. This sudden "phase shift" does not appear to affect the dipolar signal to noise..

The two diodes (5726 and 6AX4) are designed to damp the ringing of the 11 MHz tuned circuits after the θ° pulse by acting as loads on these circuits as long as no rf power is driving them. The time constant τ of the RC network in the cathode circuit is chosen to be much longer than an A rf period but shorter than the ringing time constant $\tau_r = (Q/2\pi f_A)$ of the tuned circuit. If no rf is applied to the tuned circuit the capacitor C remains charged to the DC voltage at the diode plate. When rf power is applied C charges rapidly to the peak rf voltage, and draws little power from the A rf waveform since $\tau \gg f_A^{-1}$. Then when the A rf drive to the tuned circuit ceases, the average voltage on C falls more rapidly than the ringing rf voltage because $\tau < \frac{Q}{2\pi f_A}$. When V_C falls below the peak rf voltage, power is drawn from the ringing tuned circuit to recharge C. It is necessary to have separate filament supplies for these diodes because

of the large positive voltages reached by the cathodes during A rf pulses.

3. Receiver System

The purpose of the Receiver system is to amplify and detect the 11MHz signals proportional to the F^{19} dipolar energy and display them in a graphical form on a chart recorder. It consists of the RECEIVER-B RF RELAY BOX, the 11MHz NON BLOCKING RECEIVER, the 11MHz CRYSTAL OSCILLATOR, the PHASE SENSITIVE DETECTOR, the LOW FREQUENCY AMPLIFIER, the GATED INTEGRATOR, and the CHART RECORDER.

The RECEIVER-B RF RELAY BOX (Fig. 19, Chassis 6) opens the receiver coil connections in the middle of the B rf coil during the B rf pulses, and gates the audio field H_z on at the same time if desired. During the B rf pulse both sides of the input to the receiver were grounded by the relay to prevent harmonic generation in the IN95 shorting diodes by B rf leaking across the relay contacts. If f_B is near a subharmonic of f_A, a very small amount of harmonic generated in these diodes can feed back across the relay contacts and destroy some of the A dipolar order, giving rise to a false "double resonance" signal. This was a serious problem in the gypsum double resonance studies. The capacitors in series with the leads from the relay to the B RF - RECEIVER coil are to prevent burning out the shorting diodes if B rf should accidentally be gated on without also switching the relay. Since $f_B \ll f_A$, these capacitors are a short for f_A, but a relatively large impedance for f_B. The capacitor C tunes the input to the receiver when the relay is in its normal position shown in the schematic. The TEST LEAKAGE INPUT is used to leak some 11MHz rf into the receiver for tuning C.

The relay power circuit shown is barely adequate to operate the relay

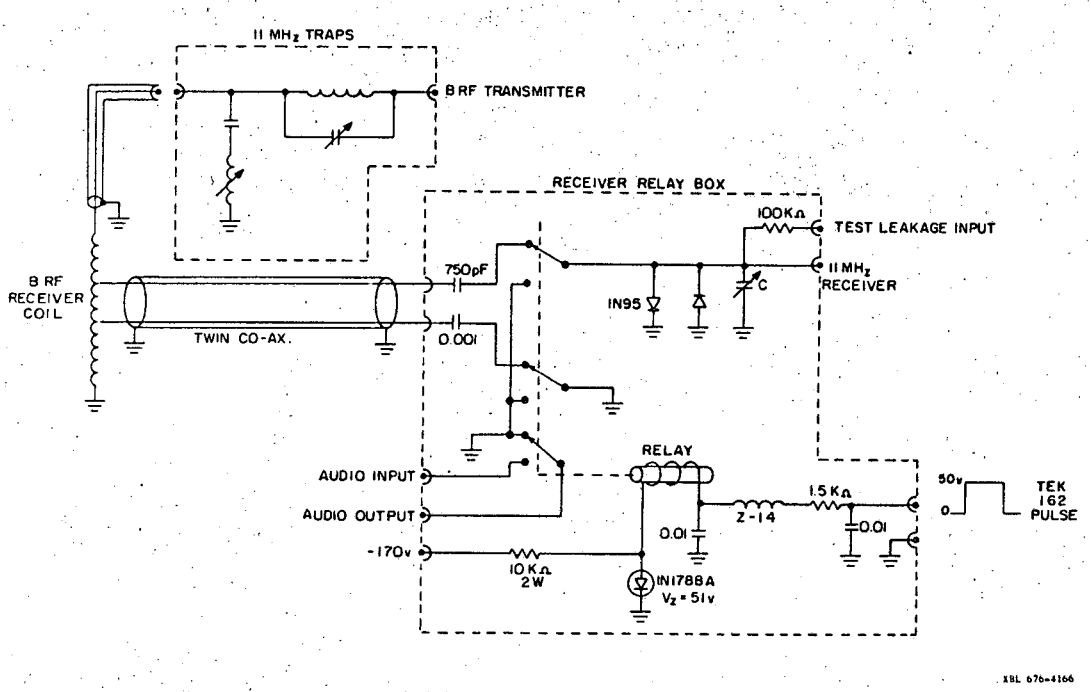

Fig. 19 Receiver - B rf relay box (chassis 6)

when only a 50 V pulse from a 162 is applied. For some of the later experiments involving short B rf saturating pulses another relay power circuit was used which gave more positive operation (chassis 15 and 16, Fig. 20). In these later experiments the audio gate was separated from the B rf - Receiver relay because 11MHz rf leaked into the 100 WATT AUDIO AMPLIFIER, causing it to pulse the laboratory magnetic field away from the resonance value H_o during the long ADRF pulse.

The 11MHz NON-BLOCKING RECEIVER (chassis 5) consists of a cascode input stage followed by four similar "long-tail pair" stages, designed by Blume. The gain of the receiver was about 10^4 and the recovery time was about 15 microseconds after the end of short (< 100μsec) A rf pulses. Unfortunately the receiver blocked for ~200μsec, after A rf pulses lasting longer than 100μsec, so it could not be used to study spin-locked double resonance.

The balanced output of the receiver feeds directly into the PHASE SENSITIVE DETECTOR (Fig. 21, Chassis 4). The reference rf at f_A = 11MHz from the crystal oscillator can be shifted in phase by slightly more than 360 degrees in the AD-YU delay line. The reference rf is then amplified, limited to provide a stable reference level, and amplified again in the cathode follower circuit which drives the detector circuit. The detector consists of the 6AL5 diode and associated circuitry. The 1k Ω potentiometer is adjusted to give zero DC level at the output. The reference rf at the input to the detector is about 30 volts peak, much larger than the rf signals coming out of the RECEIVER, so the reference rf controls the flow of current through the 50 pF capacitors leading to the RECEIVER. This current flow charges the 50 pF capacitors to DC levels determined by the reference rf amplitude, and the time constant for the change of

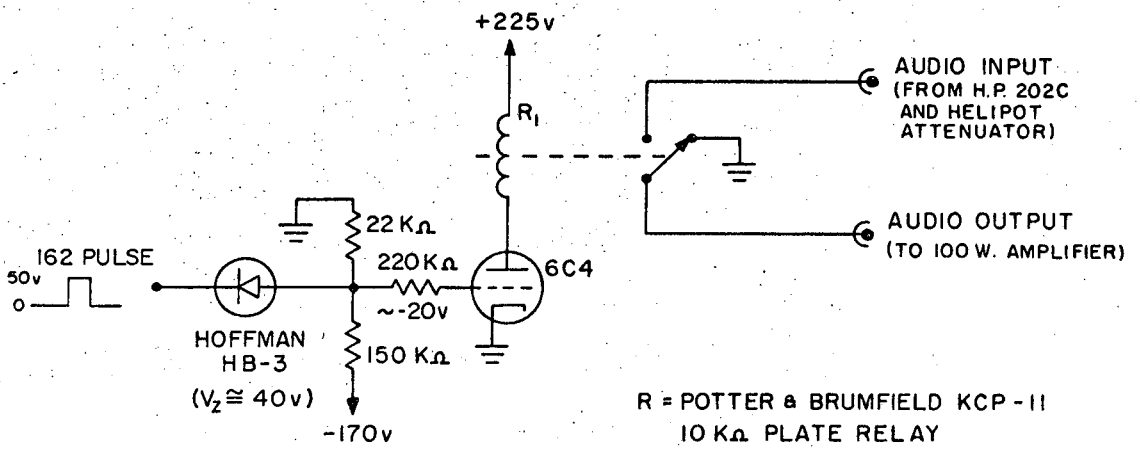

Fig. 20 Improved relay power circuit for gating audio, and switching B rf - receiver coil (chassis 15 and 16)

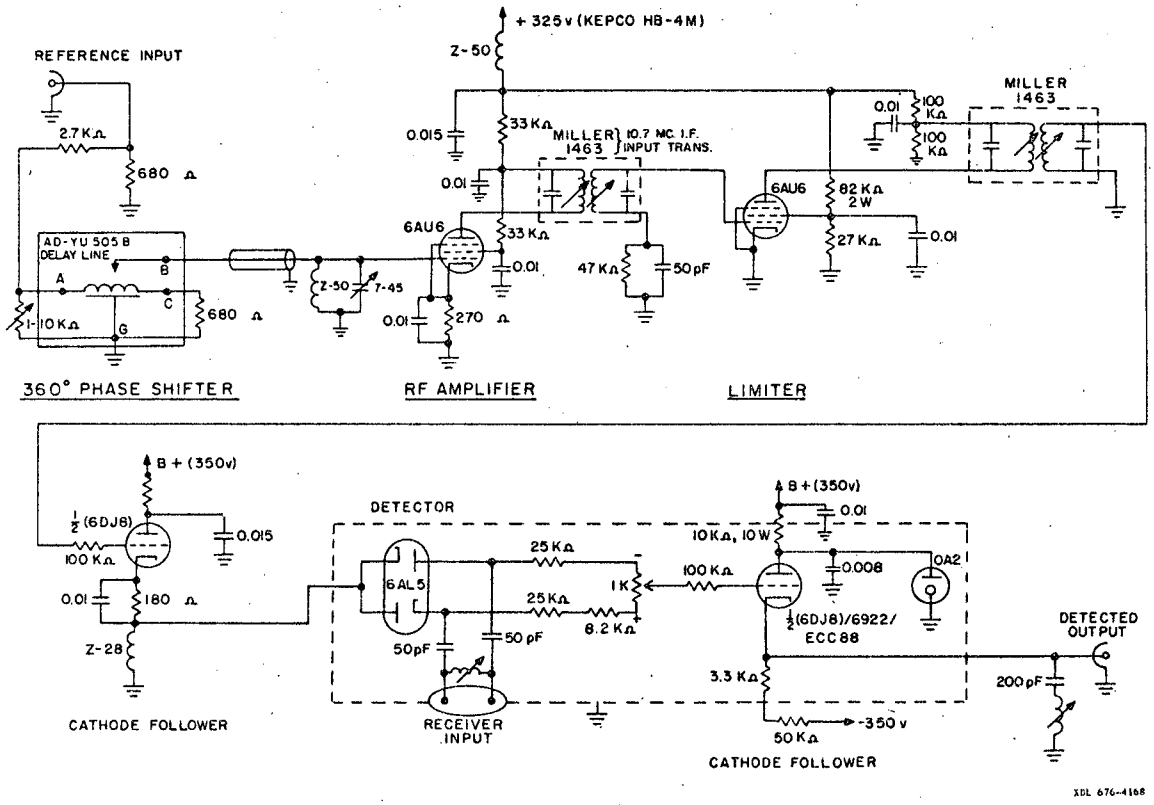

Fig. 21 Phase sensitive detector (chassis 4)

charge on the capacitors is given by $(50\ pF/2)(59\ k\ \Omega) \cong 1.25\ \mu sec \gg \frac{1}{f_A}$. If a small signal is present at the RECEIVER output it will add its small contribution to the current in the capacitors produced by the reference rf, shifting the voltage read by the second cathode follower from the potentiometer tap. The PHASE SENSITIVE DETECTOR and RECEIVER combination is linear within two percent for signals up to about 8 volts peak at the PSD output.

The LOW FREQUENCY AMPLIFIER (Fig. 22, chassis 7) has a gain of about seven with feedback, and is linear within 2% for output pulses up to 50 V. This amplifier was used to drive the GATED INTEGRATOR (or box car) when observing very small A dipolar signals. When $T_1(Ca^{43})$ was being studied the audio amplifier gain was increased to 30. Because the GATED INTEGRATOR was designed to sample large (~ 50 V) signals it was very helpful to amplify the input signals to make drifts in the integrator as negligible as possible.

The GATED INTEGRATOR (chassis 8) is a Reichert-Townsend type using operational amplifiers.[40] The integrator was used in the sampling mode, in which a single F^{19} dipolar free induction decay charges a capacitor to a fraction of the signal voltage during the time $T_2(F^{19})$. This charge is then held constant by bucking out leakage currents, and is sampled with an operational amplifier. Between $\theta°$ pulses in successive double resonance cycles the sampling capacitor is shorted out by a relay, which is opened just before the next $\theta°$ sampling pulse. The sampling capacitor holds the charge only long enough for the Mosely 680 chart recorder to deflect, (~ 5 seconds) so very long holding times are not necessary. The boxcar is linear within one percent for positive input signals less than 17 volts.

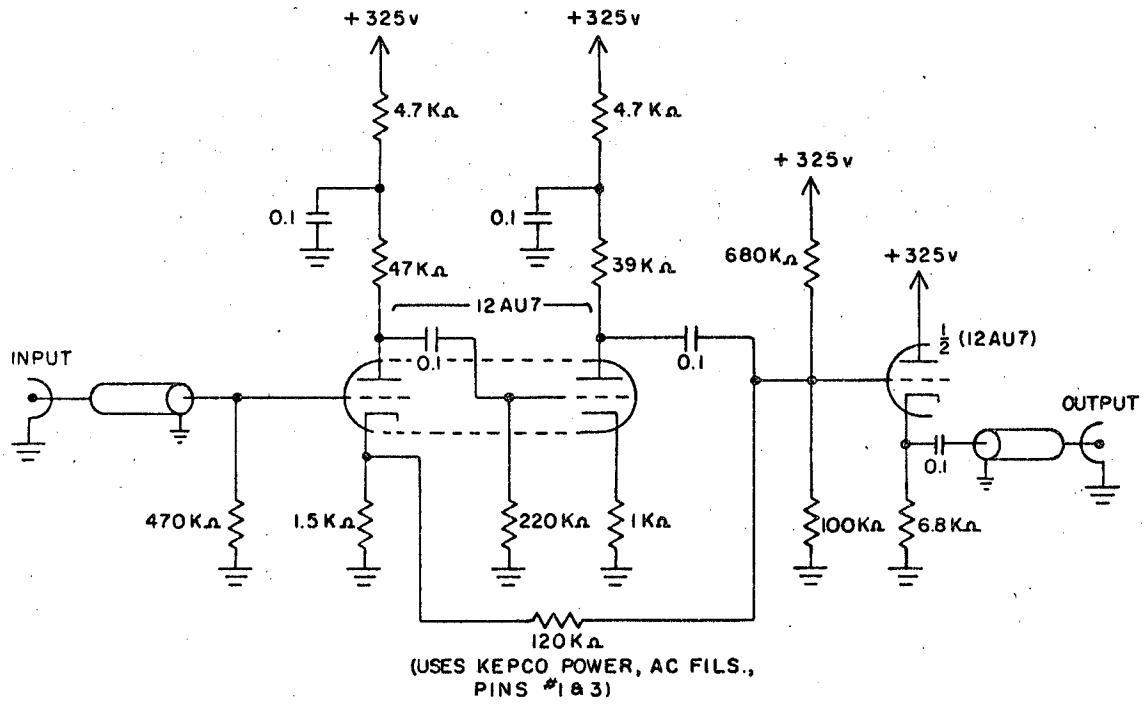

Fig. 22 Low frequency amplifier (chassis 7)

4. B RF System

The B rf system gates, phase shifts, and amplifies the cw output of the Hewlett-Packard 606A oscillator to provide the B rf pulses. The B rf PHASE SHIFTER (Fig. 23, chassis 9) shifts the phase of the B rf from the oscillator by 180° when a + 25 V pulse is applied to the SQUARE WAVE INPUT. Because of the common cathode connection in the phase splitter stage the rf voltages at the two plates are 180° out of phase with each other. The 250k Ω potentiometer provides a variable negative bias which allows only the rf from the second plate to reach the cathode follower stage, unless a positive pulse is applied to the SQUARE WAVE INPUT. Adjustment of the square wave amplitude V and the bias potentiometer allows some control over the sharpness of the 180 degree phase change, which may be useful to eliminate some of the sidebands from the phase-shifted B rf waveform and narrow the observed double resonance spectra.

Phase-shifted or cw B rf is then gated and amplified in the B RF GATE AND PREAMPLIFIER (Fig. 24, chassis 9). The B rf gate can be either a sequence of short pulses or a single long pulse and the gating circuit is analogous to the 11MHz one. The B rf driver stage is a class C amplifier with one tuning capacitor and a selection of coils which can be switched in to cover the range from 265kHz to 3.15MHz. The combination of 8L and the 47 Ω resistor in the 6CL6 plate circuit is a parasitic oscillation suppressor.

The TUNABLE B RF POWER AMPLIFIER (Fig. 25, chassis 10) consists of an 829B class C power amplifier stage with variable capacitor C which tunes the B rf-Receiver coil when the relay has opened the receiver connections. The screen voltage may be varied by the 10k Ω potentiometer to

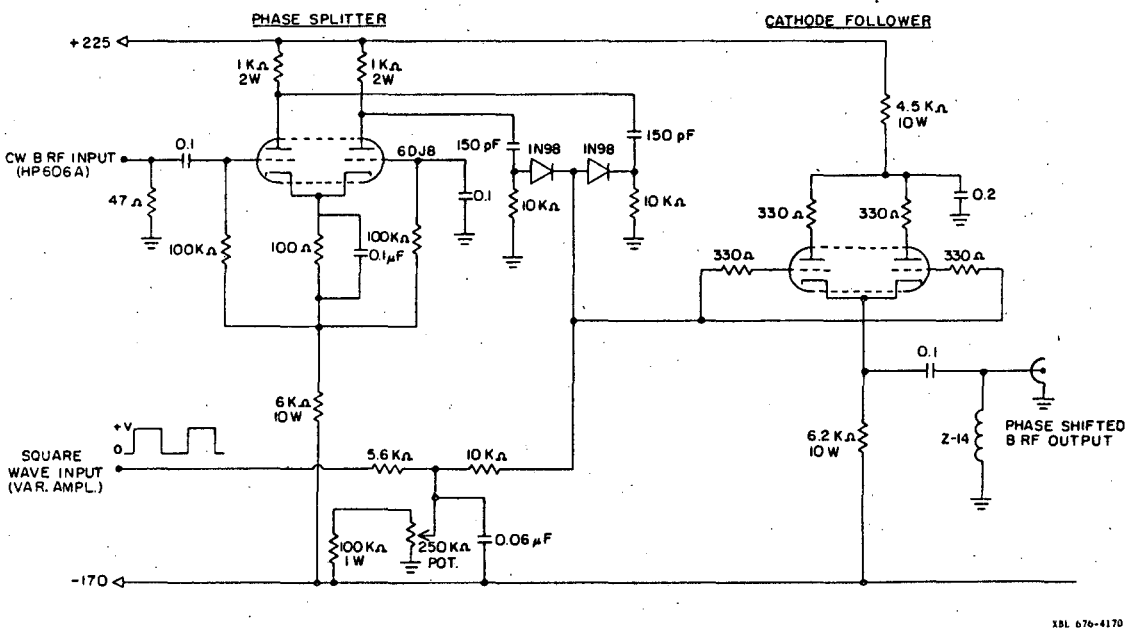

Fig. 23 B rf 180° phase shifter (chassis 9).

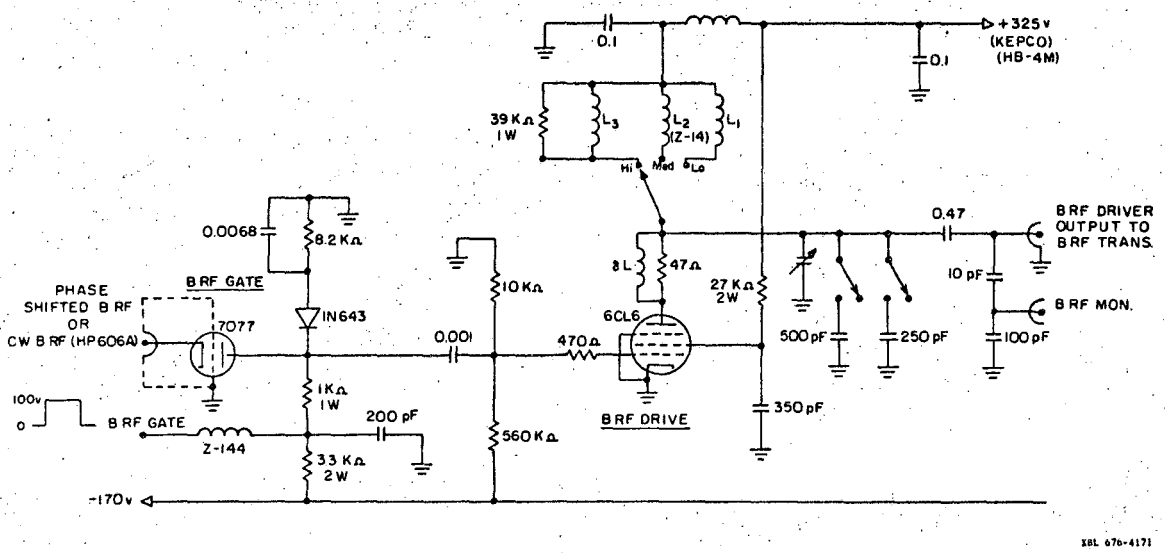

Fig. 24 B rf gate and preamplifier (chassis 9)

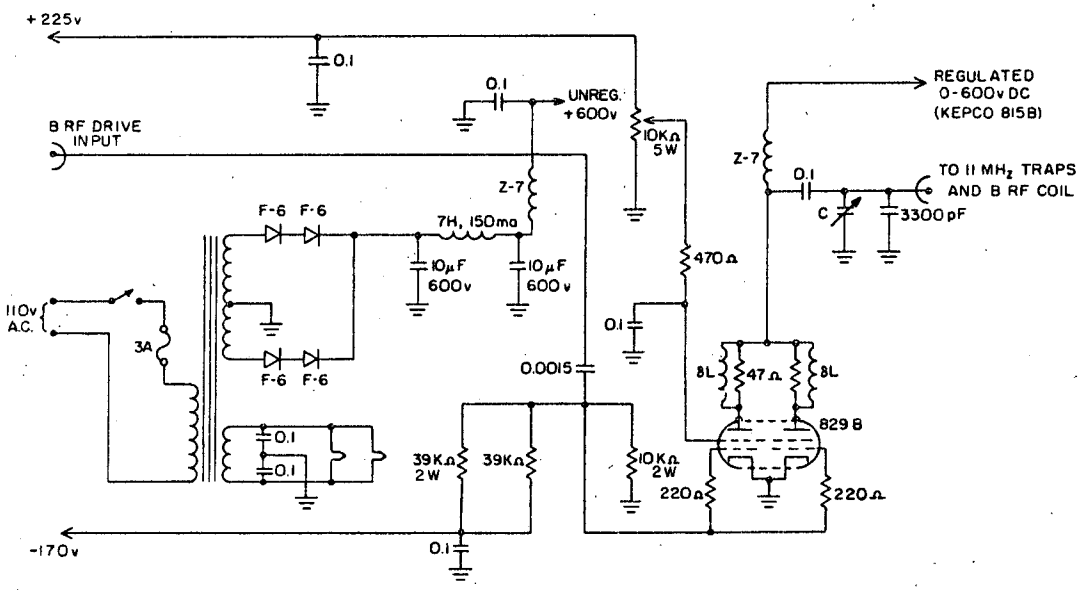

Fig. 25 Tunable B rf power amplifier (chassis 10)

regulate the B rf amplitude. For most of the measurements described here, separate, regulated plate and screen supplies were used because the unregulated ones shown in the diagram resulted in 5-10% droop on the B rf wave form for long B rf pulses. The internal supplies are adequate for searches using pulsed or 180° phase shifted B rf, since the B rf amplitude is not so critical. Tuning the B rf 829B stage during a search is difficult, and the best arrangement so far has been to use a variable speed motor, such as the Electrocraft Series E-150-4 motor with the 1800:1 gearhead, to drive the tuning capacitor C in step with the tuning of the 606A oscillator.

To reduce the harmonic content near f_A of the B rf as much as possible, traps tuned at f_A were inserted between the B rf amplifier and the B rf-Receiver coil (chassis 11). Figure 26 shows these traps and the associated monitor point for the B rf amplitude. The B rf amplitude for long CW pulses was monitored at this point with a Hewlett-Packard 410B vacuum tube voltmeter. The B rf amplitude was stable within less than ±1 percent when the regulated plate and screen supplies for the 829B were used, so only a single audio resonance was necessary to determined H_{1B}. No evidence of desctruction of S_A by B rf harmonics was observed, even though $f_B \cong \left(\frac{1}{14}\right) f_A$ for Ca^{43} in CaF_2.

To generate triggers for the ten B rf saturating pulses of length τ (sp) the TRIGGER GENERATOR (Fig. 27, chassis 14) was gated on at the end of each long B rf pulse, to produce the desired number of pulses. The time between trigger pulses can be adjusted around the value 1 msec with the 25k Ω potentiometer. The train of trigger pulses triggers a Tektronix 163 pulse generator which controls τ (sp).

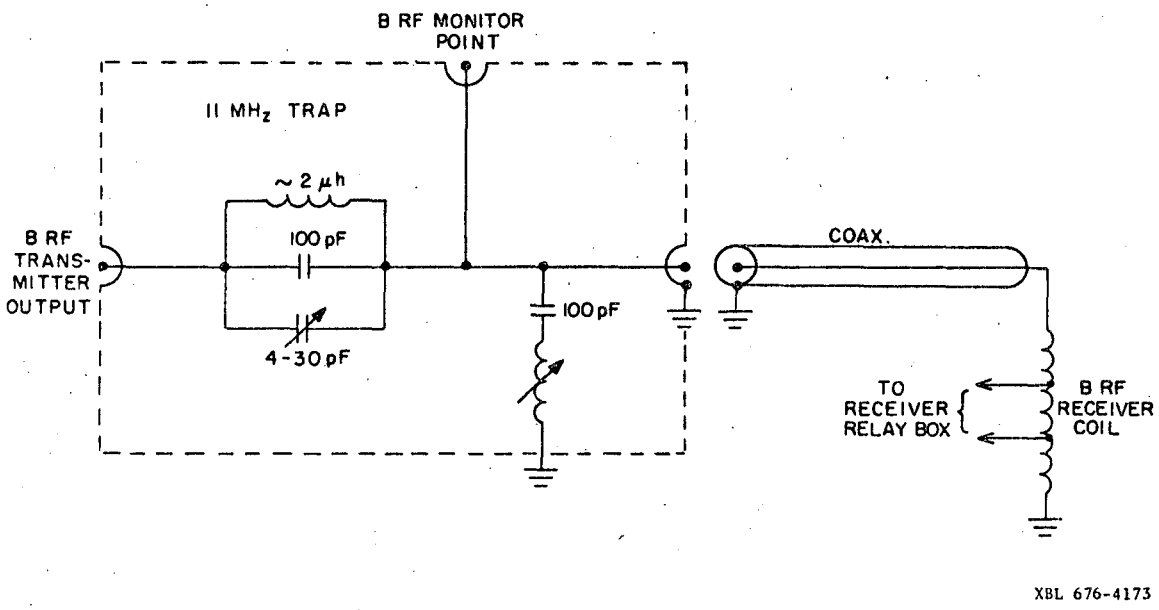

Fig. 26 11 MHz traps and B rf monitor point (chassis 11)

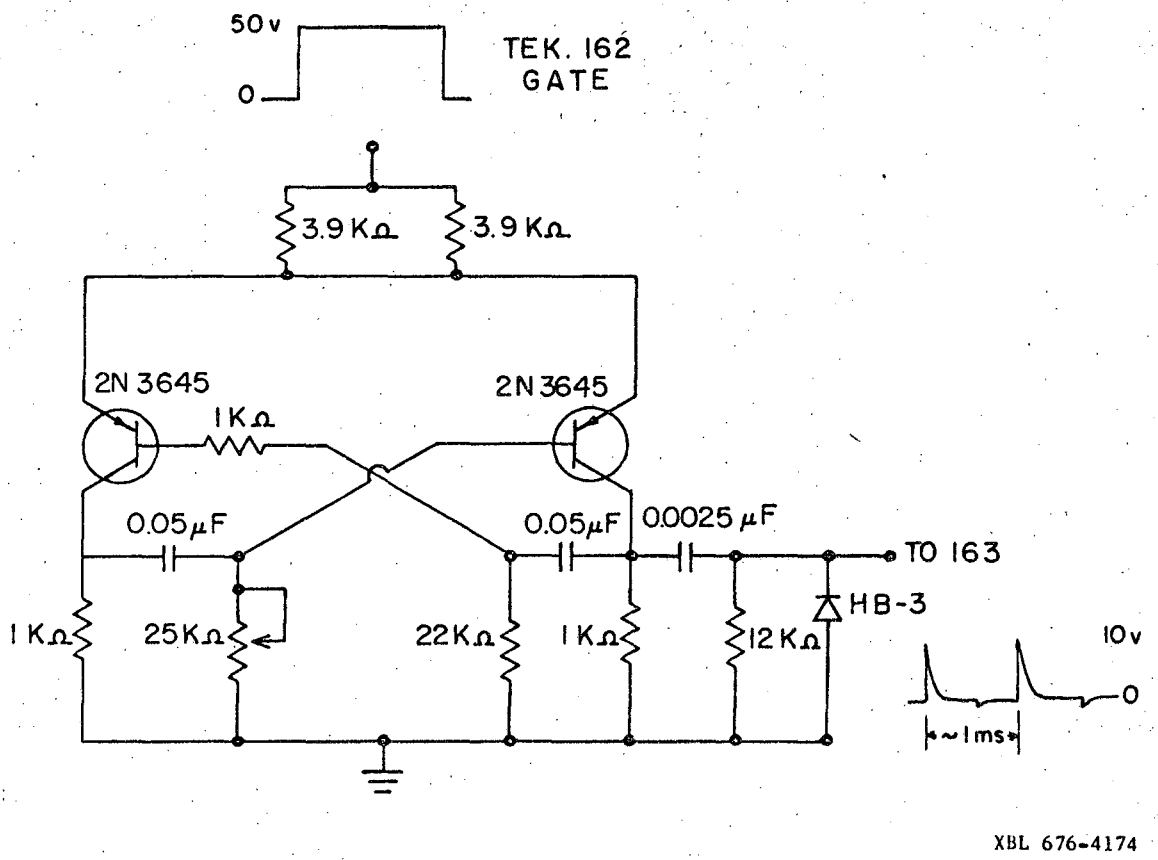

Fig. 27 Trigger generator circuit for B rf saturating pulses (chassis 14)

5. Audio System

The audio system consists of the AUDIO OSCILLATOR, ATTENUATOR, AUDIO GATE, 100-WATT AUDIO POWER AMPLIFIER, and the AUDIO MONITORING SYSTEM. The audio oscillator was a Hewlett-Packard 202C, the output of which was attenuated with a ten-turn Helipot for ease of setting audio amplitudes. The AUDIO GATE portion of the RECEIVER-B RF RELAY BOX is shown in Fig. 19, and the 100-WATT AUDIO POWER AMPLIFIER was used on its feedback mode for less distortion at low and high audio frequencies. The audio monitoring system consisted of the sensing coil inside the audio Helmholtz coil, a Helipot attenuator, and a Tektronix 531 oscilloscope with 53/54 D 1 millivolt plug-in. The Heliport was set at each f_{aud} to attenuate V (sensing coil) by an amount proportional to (f_{aud}^{-1}), so during an audio resonance it was only necessary to keep the attenuated sensing coil voltage at the oscilloscope constant, to maintain H_z constant.

Figure 20 shows the more reliable relay gating circuit used to control the audio separately from the B rf when ten short B rf saturating pulses were applied between the longer B rf pulses for the $\theta \neq 90°$ measurements.

IV. EXPERIMENTAL RESULTS OF AUDIO SATURATION DOUBLE RESONANCE IN CaF_2

A. Measurement of the Maximum Double Resonance Rate, $T_{AB}^{-1}(min)$

1. Experimental Method

As mentioned above in Section II.D.4., a study of the effective double resonance time constant T_{AB} as a function of the audio saturation parameter z enables us to measure the maximum possible audio saturation double resonance rate

$$T_{AB}(min)^{-1} = \frac{\epsilon}{\tau_{AB}}$$

If ω_B and H_{1B} are held constant, the effective field H_{eB} has a fixed magnitude and makes a fixed angle θ with the laboratory magnetic field. This means that the ratio of heat capacities ϵ, the A-B cross-relaxation time constant τ_{AB}, and the audio resonance linewidth $(T_2^{aud})^{-1}$ are all constant. To vary the saturation parameter z it is only necessary to change H_{1aud} since $z \alpha (H_{1aud})^2$. To obtain the greatest range of z for a given maximum value of H_{1aud} it is useful to work at the center of the audio resonance, where

$$z = z_o = (\omega_{1aud})^2 T_2^{aud} \tau_{AB} .$$

Working near $\omega_{aud} \cong \omega_{eB}$ also has two other advantages: it allows us to check that H_{eB} is at its proper value, and it reduces noise caused by fluctuations of H_{eB} and ω_{aud}, since we are at a stationary point of $S_A(\omega_{aud})$.

Because the audio resonances are so narrow at $\theta = 90°$, it is useful to do audio saturation double resonance near $\theta = 45°$, where the A-B dipolar coupling broadens the audio resonance, but where $\tau_{AB} \alpha (\sin^2\theta)^{-1}$ is still reasonably small.

One of the major experimental problems of audio saturation double resonance is the measurement of H_{laud}, since the measured double resonance rates depend on $(H_{laud})^2$. This calibration of H_{laud} is complicated by the presence of the metal close by in the magnet pole faces. The metal makes the effective gauss per ampere of the audio coil depend strongly on the audio frequency, and to some extent on the audio amplitude. To measure the audio amplitude a small sensing coil was placed inside the larger audio coil, with its axis parallel to the axis of the audio Helmholtz coil. The voltage induced in this sensing coil was measured as a function of audio frequency, with a sensitive oscilloscope, while the rf head and audio coil were outside the magnet gap. For constant audio amplitude the sensing coil voltage was proportional to the audio frequency within 2%. Using the measured static gauss per ampere of the audio coil, and the A-C current through the audio coil measured through a resistor in series with the coil, a relation between sensing coil voltage and peak audio field and frequency could be derived. This relation remains valid even when the audio coil is in the magnet gap, since the audio field is just sampled by the sensing coil, and not distorted by the very small amount of current flowing in the sensing coil. To characterize the audio amplitude a parameter V_{sc} was introduced, which is the sensing coil voltage divided by the audio frequency, normalized to a standard frequency. Therefore for any audio frequency V_{sc} is proportional to the audio field, so that

$$z_o = \gamma_B^2 (H_{laud})^2 T_2^{aud} \tau_{AB}$$

$$= \gamma_B^2 \mathcal{K}^2 T_2^{aud} \tau_{AB} V_{sc}^2 = \eta V_{sc}^2$$

where $\mathcal{K}$ is independent of audio frequency.

The zero of the F^{19} dipolar signal was determined by turning off the 90° phase shift of the A rf during the ADRF pulse sequence, so that the initial F^{19} dipolar signal was negligible (that is, less than or equal to the small thermal equilibrium value).

To measure the effective double resonance time constant T_{AB}, the experimental procedure shown in Fig. 28 was used. First, the effect of spin-lattice relaxation of the F^{19} dipolar energy was allowed for, by performing the procedure of Fig. 30 exactly as in the double resonance experiments, except that no audio or B rf fields were applied to the sample after the ADRF pulse sequence. The F^{19} dipolar signal so obtained was used to normalize the double resonance data:

$$S_A \text{ (no audio, no B rf)} = S_{Ao} .$$

Then at a given value of H_{1aud} (or V_{sc}), a sequence of measurements using the procedure of Fig. 28 was made, while sweeping ω_{aud} through a small range near the audio resonance center, ω_{eB}. The minimum F^{19} signal from this sweep (averaging over noise) was taken as the audio saturation double resonance signal for this value of H_{1aud}. The double resonance time constant T_{AB} was calculated according to:

$$T_{AB} = \frac{-t_{B\ RF}}{\ell n \left(\frac{S_A(\text{audio, Brf})}{S_{Ao}} \right)}$$

As discussed in Section II.D.4., if $\tau_{AB} \ll t_{BRF}$ and $\epsilon \ll 1$, T_{AB} can be expressed in terms of the saturation parameter z by:

$$T_{AB} = \frac{\tau_{AB}}{\epsilon} \frac{(1+z)}{z} = \frac{1}{V_{sc}^2} \left[\frac{\tau_{AB}}{\eta\epsilon} + \frac{\tau_{AB}}{\epsilon} V_{sc}^2 \right]$$

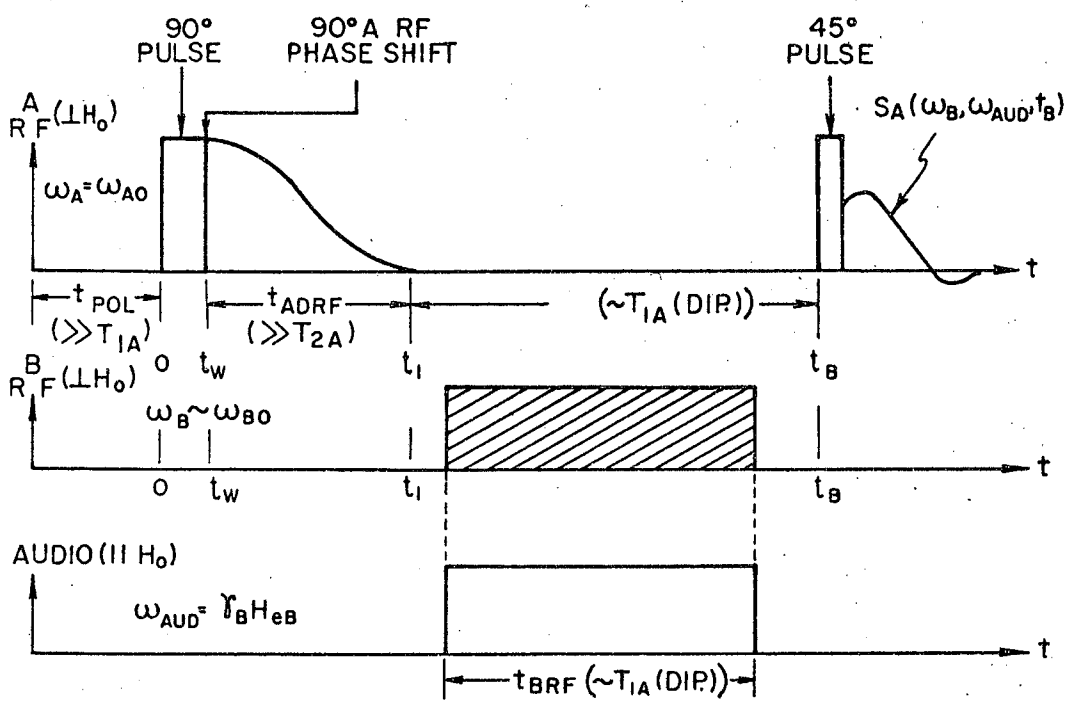

Fig. 28 Experimental procedure for audio saturation double resonance following ADRF (times not to scale); $0 \leq t \leq t_1$: formation of ordered A spin dipolar state; $t_1 < t < t_B$: double resonance occurs; at $t = t_B$, remaining A dipolar order is sampled

Thus the plot of $V_{sc}^2 T_{AB}$ versus V_{sc}^2 will be approximately a straight line (for sufficiently small τ_{AB} and ϵ). The slope S_g of this straight line yields directly the minimum audio saturation double resonance time constant $T_{AB}(\min)$ for this value of H_{eB} and θ:

$$T_{AB}(\min) = \frac{\tau_{AB}}{\epsilon} = S_g .$$

The intercept I_g of this straight line is related to the audio resonance line width $(T_2^{aud})^{-1}$:

$$\frac{\tau_{AB}}{\epsilon\eta} = (\epsilon\gamma_B^2 \; ^2 \; T_2^{aud})^{-1} = I_g$$

2. Results and Discussion

Figure 29 shows such a $V_{sc}^2 T_{AB}$ plot for the case of Ca^{43} in CaF_2. The calculated saturation parameter z_o is based on a value of T_2^{aud} assuming only motionally narrowed dipolar broadening of the audio resonance, since $\tau_{AB} \cong 60 T_2^{aud}$ at this value of H_{eB}. These calculated z_o could be in error by 20% because of the large angular dependence of z_o ($\alpha \sin^{-4}\theta \cos\theta$), and error in measurement of H_{laud}. This assumption does not affect the measured values of $T_{AB}(\min)$. The values of the intercept I_g might be affected by the presence of inhomogeneous broadening, however.

Figure 30 shows the values of $W_{AB} = \tau_{AB}^{-1}$ obtained from the audio saturation data by measuring $T_{AB}(\min)$ at several values of H_{eB}, for several different angles θ. Since the audio saturation method does not give ϵ directly, we have used the value of ϵ measured by the pulsed double resonance technique (Figs. 45 and 46):

$$\epsilon = 1.09\times10^{-3} f_{eB}^2 \text{ (kHz)};$$

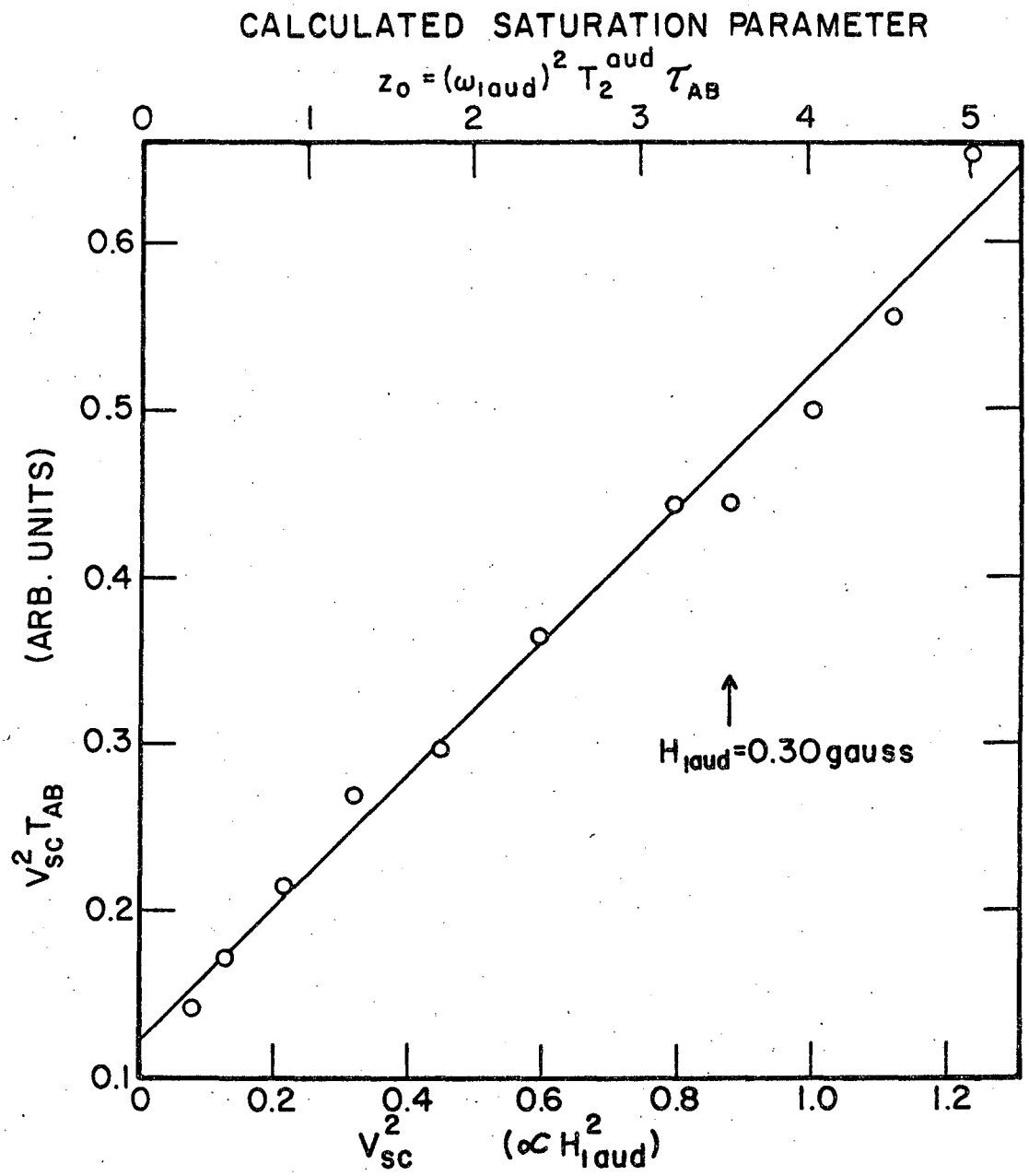

XBL 676-4176

Fig. 29 Measurement of T_{AB}(min) by audio saturation double resonance; $H_o \parallel [111]$ in CaF_2, H_{eB} = 28 gauss, $\theta = 45°$, T_{AB}(min) = 0.4 sec

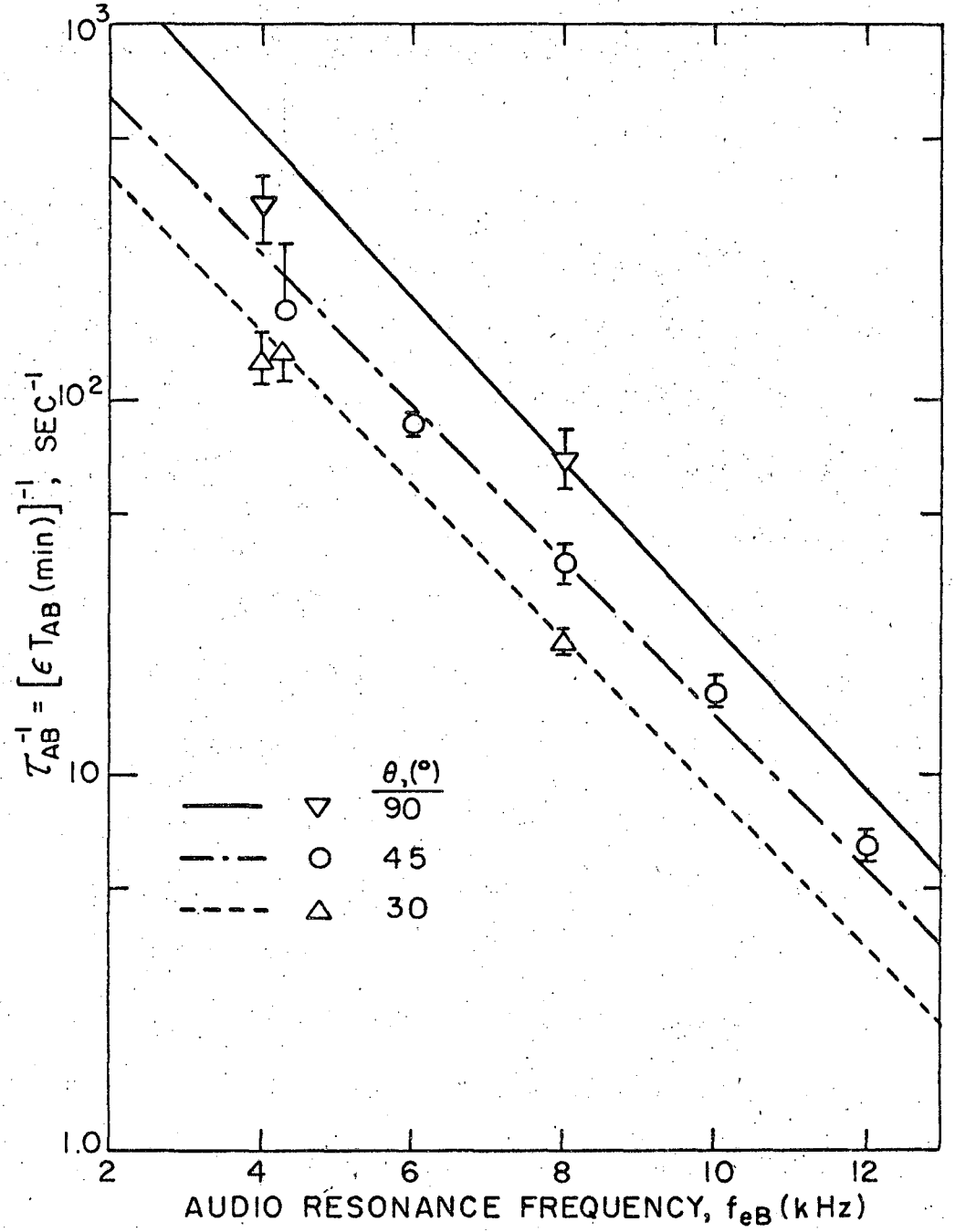

XBL 676-4177

Fig. 30 A dipolar-B Zeeman cross-relaxation spectrum; uses audio saturation measurement of $T_{AB}(\min)$ and pulsed measurement of $\epsilon(\omega_{eB})$; $H_o \parallel [111]$ in CaF_2, $\theta = 45°$; straight lines are least-squares W_{AB} at $\theta = 90°$, 45° and 30° from pulsed ADRF-DR measurements

τ_{AB}^{-1} is then given by:

$$\tau_{AB}^{-1} = [\epsilon\ T_{AB}(\min)]^{-1}$$

For comparison with the pulsed τ_{AB}^{-1} data, the lines obtained from the least squares fits to the $\theta = 90°$, $45°$, and $30°$ pulsed data are shown in Fig. 30. It is seen that, within the experimental error, the audio saturation method yields the same magnitude and functional form for τ_{AB}^{-1} as found by the more accurate pulsed double resonance method.

The error in $T_{AB}(\min)$ becomes very large at small f_{eB}, because the slope of the $V_{sc}^2 T_{AB}$ curve becomes smaller than the experimental scatter. Although T_{AB} data were taken at $f_{eB} = 2$kc for $\theta = 45°$, the slope was so small that no useful value of T_{AB} (min) could be measured.

At low H_{eB} large audio fields are required to produce appreciable saturation of the audio resonance, since τ_{AB} (the analog of T_1) is exponentially becoming smaller. But these large audio fields begin to approach H_{eB} in size near $f_{eB} = 2$kHz, and since H_{laud} is no longer a perturbation on the B Zeeman system in the rotating frame, another approach must be used to calculate the double resonance effect. It might be more appropriate to take the vector sum of H_{eB} and $H_{laud}(t)$ as a zero-order Hamiltonian, and consider the modulation that this total magnetic field produces on the A-B dipolar coupling. Such a modulation of the A-B coupling would effectively "bypass" the resonant nature of the B Zeeman system, because it would result in absorption of audio energy by the A dipolar system at any audio frequency, so long as the audio frequency is within the A dipolar spectrum. The strength of this non-resonant audio absorption should be proportional to the angle through which the total magnetic field $H_{tot} = H_{eB} + H_{laud(t)}$ varies during one audio cycle.

For the τ_{AB}^{-1} data shown in Fig. 30, the Bloch-Siegert[41] shift of the audio resonance center is not important, since the maximum audio fields used were $\approx .3$ gauss, while at $f_{eB} = 4$kHz, $H_{eB} \cong 14$ gauss. Then the maximum Bloch-Siegert shift for this data is given by:

$$\omega \cong \omega_{eB} \left(1 + \left(\frac{.3}{28}\right)^2\right) \cong \omega_{eB} (1.0001)$$

Figure 31 shows a quantity proportional to the unsaturated effective audio resonance line width $(T_2^{aud})^{-1}$ for various values of H_{eB} at $\theta = 45°$. The intercept J_g must be multiplied by f_{eB}^2 to remove the frequency dependence of ϵ. Since at $\theta = 45°$ the major contribution to the audio resonance line width comes from motionally narrowed A-B dipolar coupling, $(T_2^{aud})^{-1}$ should be a constant because the H_{eB}-dependent contribution τ_{AB}^{-1} is negligible at $f_{eB} = 4$kHz, and quadrupole broadening would be constant (a contribution from B rf inhomogeneity would probably be proportional to H_{eB}, but the observed B rf inhomogeneity is small). As can be seen from Fig. 31, the audio resonance line seems to broaden suddenly for $f_{eB} \gtrsim 10$kHz. Since this broadening sets in just at the point where the audio resonance is completely saturated, even for the smallest audio fields used, this broadening may be related to doubly-rotating frame effects, or caused by the presence of some inhomogeneous broadening of the audio resonance, as noted in Section II.D.5.

The audio saturation double resonance method gives results in agreement with the pulsed double resonance method, but is less useful for measuring double resonance rates for three reasons: (1) The audio method does not measure ϵ and τ_{AB} independently, but only gives the ratio ϵ/τ_{AB}, unless the unsaturated audio resonance line width $(T_2^{aud})^{-1}$ is accurately

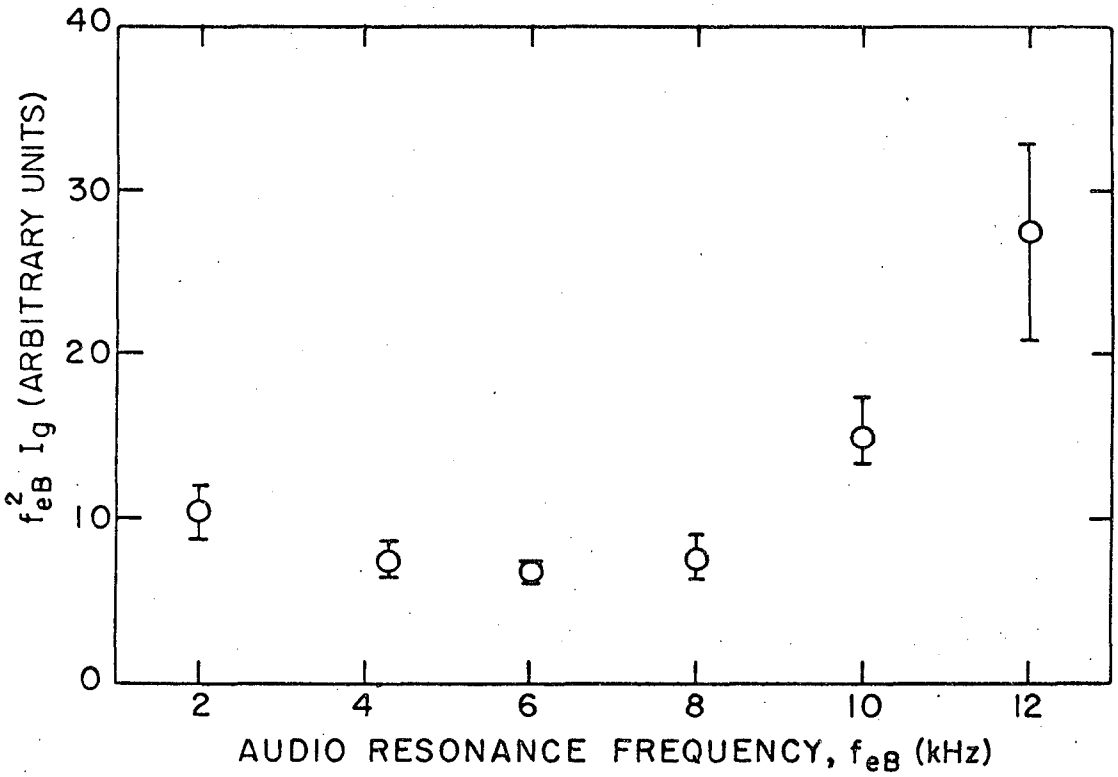

XBL 676-4178

Fig. 31 Effective unsaturated audio linewidth (proportional to $f_{eB}^2 I_g$); $H_o \parallel [111]$ in CaF_2, $\theta = 45°$

known. (2) At small H_{eB} it is difficult to simultaneously satisfy the requirements that H_{laud} produce appreciable saturation, and yet remain a small perturbation on H_{eB}; this makes it difficult to interpret the data, since the correspondence between the saturation parameter and the observed double resonance signal is complicated by the possible presence of non-resonant absorption. (3) Experimentally, it is difficult to measure the audio field H_{laud}, so the $(H_{laud})^2$ dependence of Z introduces appreciable error into the $V_{sc}^2 T_{AB}$ versus V_{sc}^2 curves, causing more scatter in the audio saturation data. But audio saturation double resonance is a very accurate means of measuring H_{eB}, since the center of the resonance curve is not affected by these complications, so long as H_{laud} is constant over the small frequency region near the audio resonance center, and t_{BRF} is long so that very small audio fields can be used.

B. Audio Resonance Linewidths

1. Experimental Method

If we neglect the small corrections to $T_{AB}^{-1}(\omega_{aud})$ caused by large B spin heat capacity and finite A spin-lattice relaxation, the observed double resonance rate is given by

$$T_{AB}^{-1}(\omega_{aud}) \cong \frac{\epsilon}{\tau_{AB}} \left(\frac{z}{1+z}\right) , \qquad (87)$$

where $$z = (\omega_{aud}/\omega_{eB})\pi\omega_{1aud}^2 \tau_{AB} f(\omega_{aud}) ,$$

and $$z_o = z(\omega_{eB}) = \pi\omega_{1aud}^2 \tau_{AB} f(\omega_{eB}) .$$

Since all observed audio resonance lineshapes are approximately Lorentzian, we assume this form for $f(\omega_{aud})$. If ω_{1aud} is chosen so that $z_o \ll 1$, then for all ω_{aud}, $z(\omega_{aud}) \ll 1$, and Eq. (87) shows that T_{AB}^{-1} is proportional to $f(\omega_{aud})$, so the audio resonance lineshape can be read directly from the

T_{AB}^{-1} data. Since the double resonance rate $T_{AB}^{-1}(\omega_{eB})$ at the center of the audio resonance line must be much larger than the minimum observable double resonance rate R_{min}, we have the requirement:

$$R_{min} \ll T_{AB}^{-1}(\omega_{eB}) = \epsilon\, z_o/(1+z_o)\,\tau_{AB}$$

$$\tilde{=} \frac{\epsilon z_o}{\tau_{AB}} = \epsilon\omega_{laud}^2\, T_2^{aud} \quad , \tag{88}$$

but in order to read T_2^{aud} directly from the $T_{AB}^{-1}(\omega_{aud})$ data we require $z_o \ll 1$:

$$z_o = \omega_{laud}^2\, \tau_{AB}\, T_2^{aud} \ll 1 \quad . \tag{89}$$

The opposing requirements (88) and (89) result in the reasonable requirement that the minimum observable double resonance rate R_{min} be much less than the maximum possible double resonance rate ϵ/τ_{AB}:

$$R_{min} \ll \epsilon/\tau_{AB} \tag{90}$$

Since $\epsilon \propto H_{eB}^2$ while $\tau_{AB}^{-1} \propto \exp(-\gamma_B H_{eB} \tau_c)$, ϵ/τ_{AB} has a peak at $\omega_{eB} = (2/\tau_c)$. For Ca^{43} in CaF_2, this condition (90) means that only near $f_{eB} \tilde{=} 4$kHz will it be possible to deduce the unsaturated audio resonance linewidth $(T_2^{aud})^{-1}$ directly from the $T_{AB}^{-1}(\omega_{aud})$ data. In the general case it is better to use the measured maximum double resonance rate (ϵ/τ_{AB}) obtained from pulsed double resonance data, and solve Eq. (87) for $z(\omega_{aud})$, which then yields T_2^{aud} directly:

$$z(\omega_{aud}) \tilde{=} \eta/(1+\eta)$$

where

$$\eta = T_{AB}^{-1}(\omega_{aud})/(\epsilon\,\tau_{AB}^{-1})$$

For large ϵ it is also necessary to include the corrections mentioned in Section II.D.4, resulting in a more complicated expression for $z(\omega_{aud})$. A computer program has been written which solves for $z(\omega_{aud})$ including these corrections, and fits the resulting $z(\omega_{aud})$ to a Lorentzian form. The audio saturation equation for $z(\omega_{aud})$ (correct to first order in the small quantities ϵ, τ_{AB}/t_{BRF}, and τ_{AB}/T_{1A} can be written:

$$(1+z)^2\eta = (1+z)z + q - \frac{\epsilon z\lambda}{(1+z)} \quad , \tag{91}$$

where

$$q = \tau_{AB}(t_{BRF}^{-1} - T_{1A}^{-1})$$

and $$\lambda = 1$$

The term $-\lambda\epsilon z\ (1+z)^{-1}$ is not important in the wings of the line, as is the correction q, so we first solve Eq. (91) neglecting the term proportional to λ. The approximate solution z_+ satisfies (91) (to second order in q):

$$(1+z_+)^2\ \eta \cong (1+z_+)z_+ + q$$

where $$z_+ \cong \eta(1-\eta)^{-1} - q - q^2(1-\eta).$$

The effects of the remaining small term in Eq. (91) are found by solving (91) to first order in the perturbation parameter λ, after setting:

$$z = z_+ + \lambda\ z_1 \quad .$$

The approximate solution to (91) is (to first order in λ):

$$z \cong z_+ + \epsilon z_+\ (1+z_+)^{-1}\ (1+2z_+ - 2\eta(1+z_+))^{-1} \quad . \tag{92}$$

This last correction increases the observed linewidths by less than two

percent, so all higher corrections are probably negligible.

The computer gives least-squares values for both the amplitude of the audio resonance line and its linewidth. For the case of appreciable inhomogeneous broadening of the audio resonance line the theory of the calculation of τ_{aud}^{-1} must be modified since it implicitly assumes a homogeneously broadened audio resonance line. That is, the expression for τ_{aud}^{-1} (ω_{aud}) is the same one that would be obtained by assuming the B spins obey Bloch's equations, in which τ_{AB} replaces T_1 and T_2^{aud} replaces T_2, and one calculates the rate of change of $E_B = -M_B H_{eB}$. Bloch's equations are appropriate for a liquid, in which the spins are isolated from each other but see randomly varying local fields which relax them. The case of rare B spins in a solid being influenced by the A-B dipolar coupling satisfies exactly these requirements if we consider a single B spin "isochromat" in the inhomogeneously broadened audio resonance line.

If there is significant inhomogeneous broadening of the audio resonance line (by quadrupole splittings or B rf inhomogeneity), we can still solve Bloch's equations for each B isochromat and then average over the inhomogeneous distribution h(x) of width $(T_2^+)^{-1}$. But the "amplitude" of the audio resonance line and its observed linewidth[1] $(T_2^*)^{-1}$ are now no longer related by the simple normalized Lorentzian curve because the "amplitude" and width are measured in physically different ways. The "amplitude" z_o (l.sq.) is determined by the amount of energy per unit time being fed into the A spin system by the audio field, while the width $(T_2^{aud})^{-1}$(l.sq.)is determined by h(x) if inhomogeneous broadening is dominant. It is possible that z_o(l.sq.) can be small if the saturation-broadened homogeneous linewidth $(T_2')^{-1}$ is much smaller than $(T_2'^*)^{-1}$. To see this we note that in a

homogeneously broadened line of width $(T_2')^{-1}$ all the spins eventually pass through the frequency ω_{aud}. But for inhomogeneous broadening the audio field affects only those spins within $(T_2')^{-1}$ of ω_{aud} rather than all the spins spread out over $(T_2'^*)^{-1}$, so the saturation effectiveness should be reduced by about $(T_2'^*/T_2^r)$. Explicit calculation[1] for a Lorentzian distribution of inhomogeneity h(x) shows that the actual reduction factor at the line center is $(T_2^+/T_2')^{1/2}$. But the measured linewidth $(T_2'^*)^{-1}$ still gives the inhomogeneous distribution linewidth $(T_2^+)^{-1}$, since the homogeneous linewidth does not change from isochromat to isochromat.

For best signal to noise and least distortion of the audio resonance lineshape by excessive saturation, t_{BRF} was set to $\sim .6T_{1A}$, and a value of H_1 and chosen which reduced S_A at the center of the audio resonance to about e^{-1} of its initial value. This value of H_{1aud} was less than 0.4 gauss peak in all resonances studied. The B rf amplitude was monitored with a VTVM and f_B was checked with a Hewlett-Packard 524D electronic counter before and after the audio resonance sweep. During the sweep the audio frequency at each point was set and monitored with the electronic counter and f_{aud} is accurate to $\pm .01$ kHz. The time t_{BRF} was measured with the electronic counter, using a Hewlett-Packard 526B Time Interval Plug-In, so t_{BRF} is accurate to $\pm .01$ sec. The value of H_{1aud} was calibrated by measuring the sensing coil voltage at f_{aud} when a known audio current was passing through the audio coil (outside the magnet gap). The static gauss per ampere of the audio coil then relates sensing coil voltage to peak audio amplitude. The $S_A(\omega_{aud})$ data were converted to $T_{AB}^{-1}(\omega_{aud})$ rates using the measured t_{BRF}, and the resulting $z(\omega_{aud})$ calculated from Eq. (92) were fitted to a Lorentzian functional form with variable

amplitude, width and center frequency. The rms deviation between the least-squares curve and the data points was usually less than two percent of z_o (l.sq.) for the given audio resonance.

2. Results and Discussion

To separate the contributions to the audio resonance linewidths in CaF_2 it is useful to analyze the $\theta = 90^\circ$ audio resonances first. As noted in Section II.D.5, at $\theta = 90^\circ$ the secular A-B dipolar contribution to the linewidth vanishes, while the inhomogeneous broadening from H_{1B} is largest and the quadrupolar broadening is at a local maximum. The maximum experimental error of setting θ near $\theta = 90^\circ$ resulted in an AB coupling linewidth of less than 8 Hz. Figures 32 and 33 show such narrow audio resonance lines at $\theta = 90^\circ$. As Fig. 34 shows for Ca^{43} in CaF_2 the audio resonance linewidth $(2\pi T_2^{aud})^{-1}$ over the range from $f_{1B} = 2.44$ kHz to $f_{1B} = 12.65$ kHz is constant at 125±15 Hz, within the experimental error. The rms deviation between the least-squares Lorentzian and the data was less than 2% and the curves seem Lorentzian within the experimental error as seen in Fig. 35. The sum of $(2\pi\tau_{AB})^{-1}$ and one percent inhomogeneity broadening shows considerable curvature over this region, while the data are constant within the experimental error. Thus there is no evidence of a significant component proportional to f_{1B}, so we may conclude that the magnetic inhomogeneous broadening is less than one percent of f_{1B}. The constancy of the linewidth suggests that it may be caused mainly by quadrupolar broadening. If so, the rms quadrupole splitting in the laboratory frame would then be $\bar{\nu}_Q = 240$ Hz. It is puzzling that the linewidth at $f_{1B} \approx 2.44$ kHz is less than the linewidth caused by τ_{AB} lifetime broadening alone, but there is considerable experimental scatter, and the computer program does not

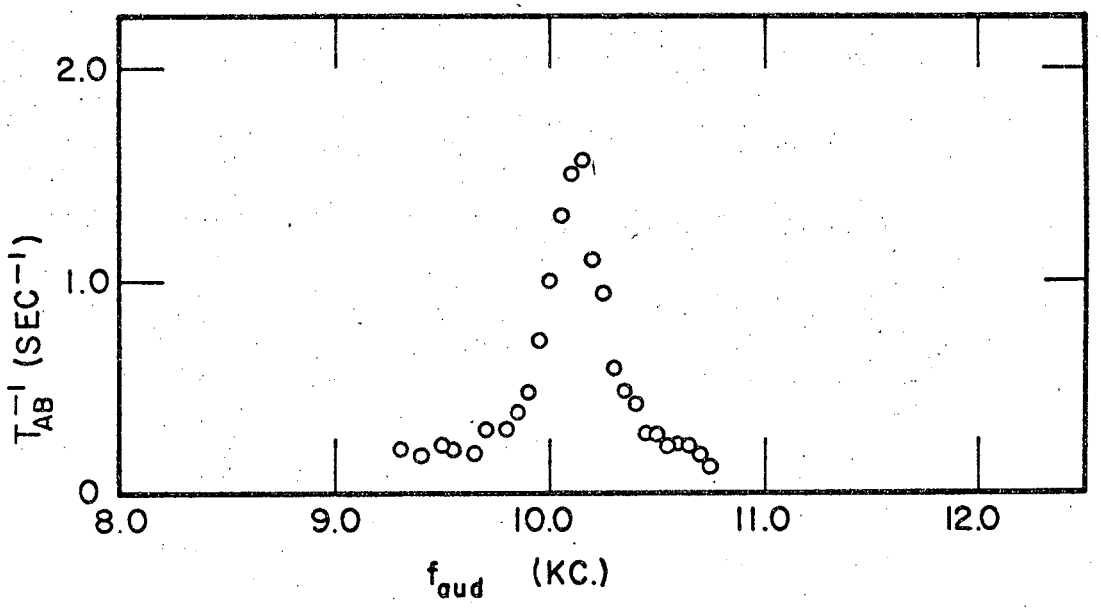

XBL 676-4179

Fig. 32 Typical raw audio resonance data, showing narrow line at $\theta = 90°$, and long τ_{AB}

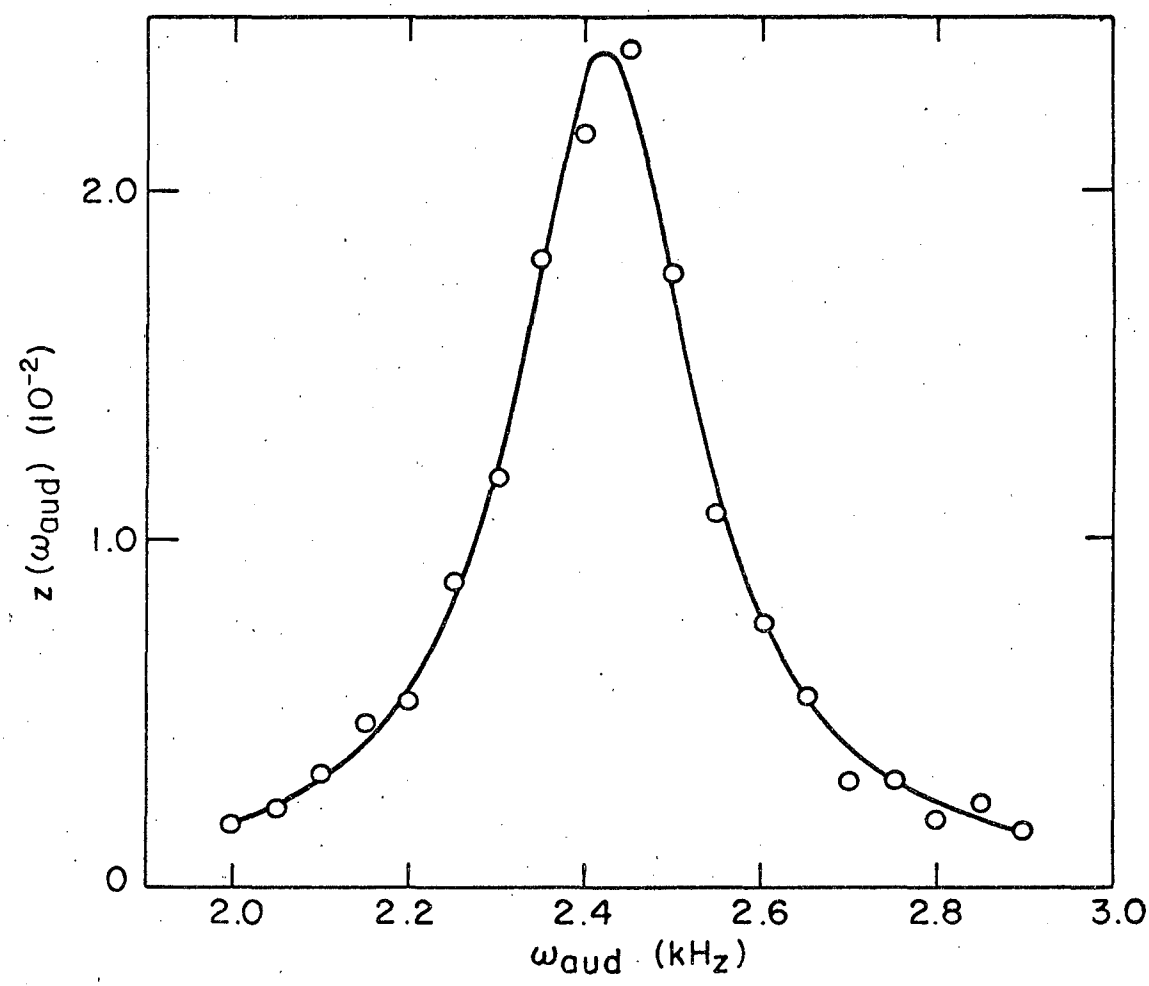

XBL 676-4180

Fig. 33 Fit of Lorentzian line to derived audio resonance lineshape $z(f_{aud})$; $H_o \parallel [111]$ in CaF_2, $\theta = 90°$, and $H_{laud} = 0.085$ gauss

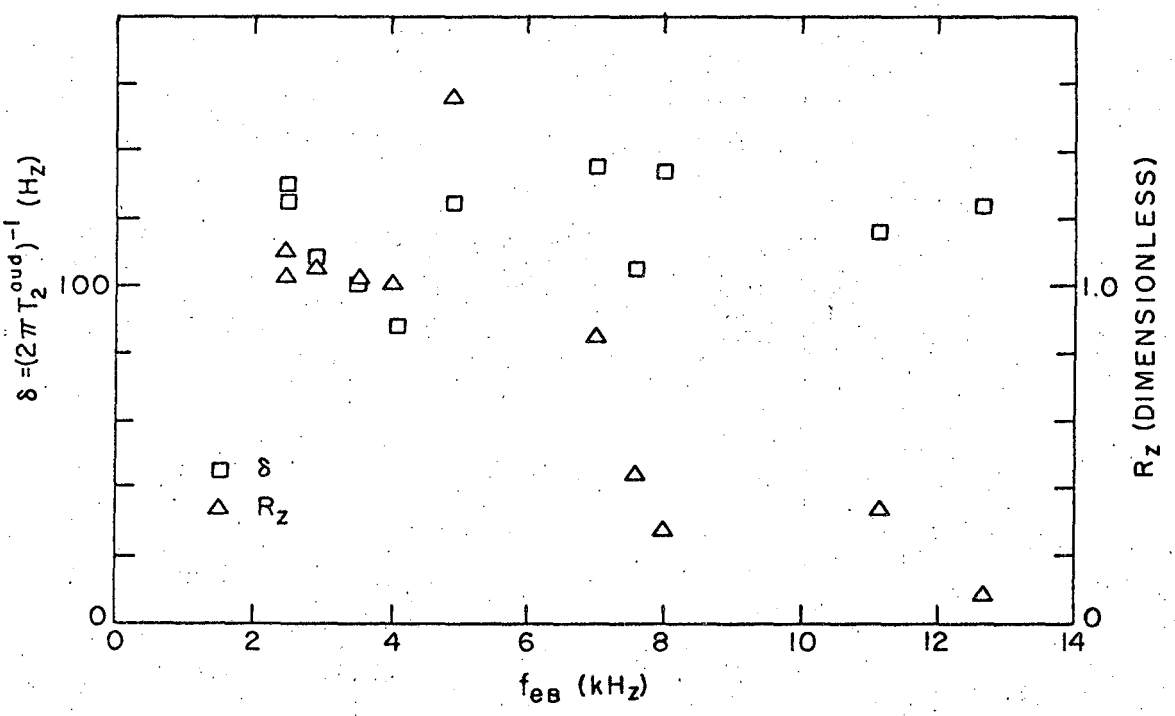

XBL 676-4181

Fig. 34 Derived audio resonance linewidth, δ, and fraction of theoretical saturation parameter, R_z; $H_o \parallel [111]$ in CaF_2, $\theta = 90°$

properly take account of inhomogeneous broadening.

The least-squares τ_{AB} and T_2^{aud} together with the measured value of H_{1aud} yield a theoretical value of z_o, $(z_o(th))$, which may be compared with the least squares z_o (l.sq.) obtained from the data. As the homogeneous linewidth $(2\pi\tau_{AB})^{-1}$ becomes much less than $(2\pi T_2'^*)^{-1}$, Fig. 34 shows that $R_z = (z_o(\text{l.sq.})/z_o(th))$ becomes much less than 1, as would be expected from an inhomogeneously broadened line.

Since the $\theta = 90°$ data show linewidths of the order of 120Hz, but the $\theta \neq 90°$ data have much larger linewidths (see Fig. 35), we may attribute the $\theta \neq 90°$ linewidths largely to secular A-B dipolar coupling. At $\theta = 45°$ for the [111] direction, the calculated value of the linewidth based on the τ_{AB}^{-1} least squares data is 310 Hz. The measured values of the linewidth in Fig. 36 are 330±20 Hz, in reasonable agreement with theory. The measured values of z_o are approximately constant and the ratio $R_z \tilde{=} 1.4$. Since the error in measuring H_{1aud} could be about 20%, this is reasonable agreement between theory and experiment. It is possible that better agreement could be obtained by doing the audio resonance theory to include slight inhomogeneous broadening, but it would be very complicated because a single homogeneous spin temperature cannot be used to describe the B spins, and a new E_B would have to be calculated by averaging over h(x), in order to define

$$\tau_{aud}^{-1} = \frac{-1}{\langle E_B \rangle} \left\langle \frac{dE_B}{dt} \right\rangle_{audio} .$$

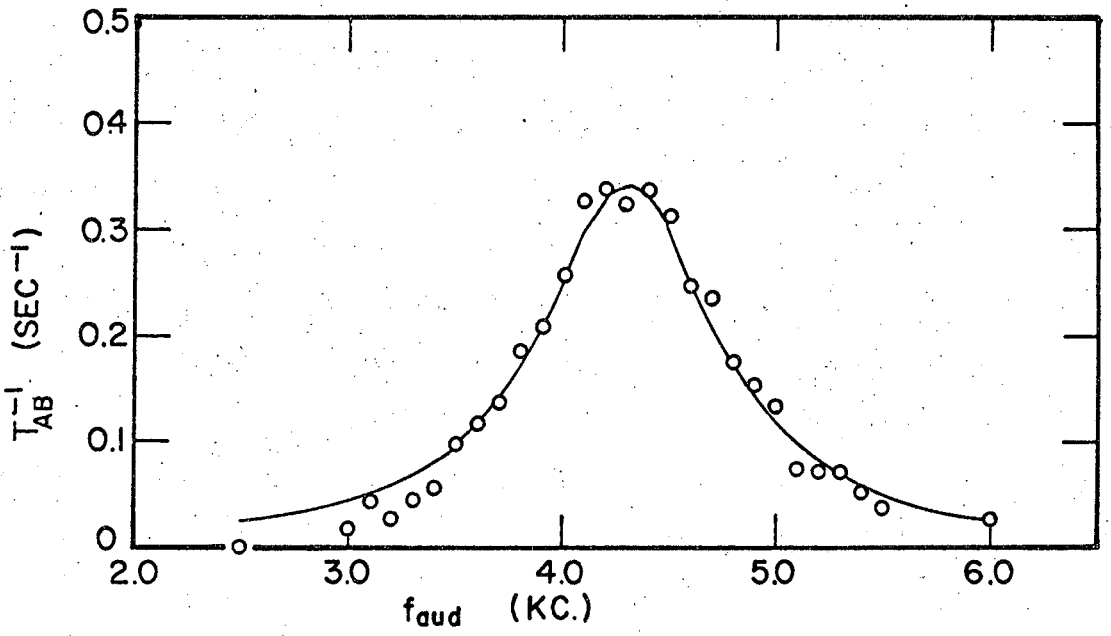

XBL 676-4182

Fig. 35 Raw audio resonance data at $\theta = 30°$, showing motionally-narrowed dipolar broadening; solid curve is Lorentzian; $H_o \parallel [111]$ in CaF_2

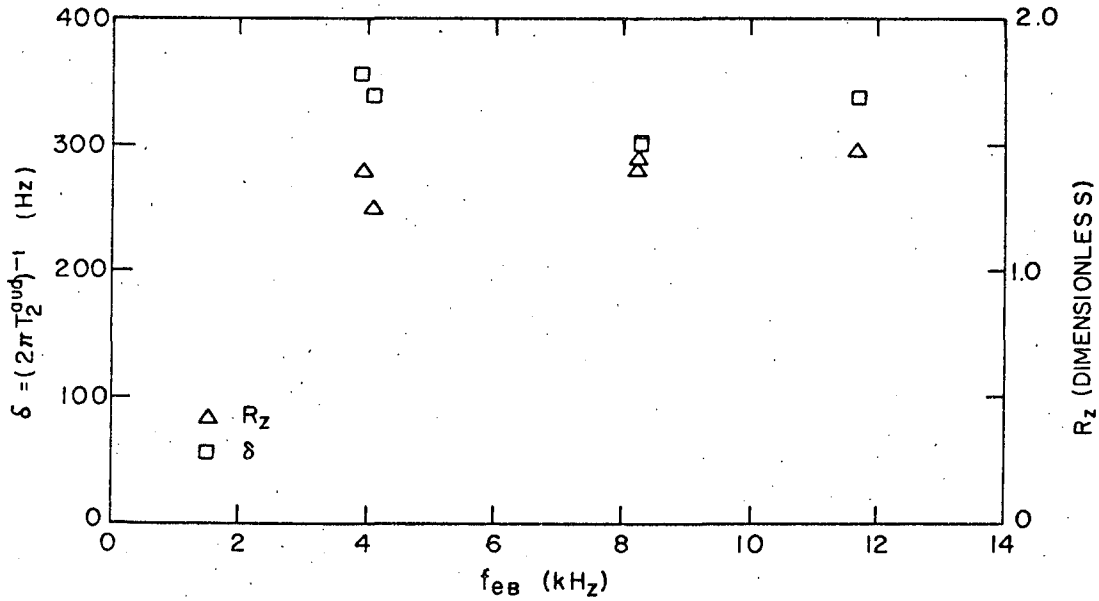

Fig. 36 Derived audio resonance linewidth, δ, and fraction of theoretical saturation parameter, R_z; $H_o \parallel [111]$ in CaF_2, $\theta = 45°$

V. EXPERIMENTAL RESULTS OF PULSED DOUBLE RESONANCE IN CaF_2

A. Transient Oscillations in the Rotating Frame

We consider the transient oscillations first because for low f_{eB} ϵ is of the order of δ, and the presence of the oscillations might distort our least-squares values of ϵ and τ_{AB} if we do not take account of the oscillations in the functional form which we fit to the data. Figure 37 shows the curve calculated from Eq. (56) of Section II.C.2 as a function of the pulse length τ, using the Lorentzian correlation function, which agrees with the Clough function for $\theta = 90°$. Here $H_{1B} = 44$ gauss and $H_{LB} = 3.5$ gauss, so the condition $H_{1B} \gg H_{LB}$ is well satisfied. The data agree with the theory as far as the period of the oscillations, order of magnitude of the decay time constant, and the added term $\epsilon t/\tau_{AB}$ are concerned. The magnitude of the oscillations is not as large as it should be, and this is not understood.

Figure 38 shows the shape of the oscillations in a region where H_{1B} is not much greater than H_{LB}, since $H_{1B} = 8.5$ gauss. Therefore the simple theory does not apply, and it can be seen that the small oscillations present fluctuate around a function of roughly the form

$$\epsilon(1 - e^{-t/\tau_{AB}}).$$

Therefore the oscillations should not seriously affect the measurement of ϵ and τ_{AB} by the least squares fit method.

B. Measurement of ϵ and τ_{AB} at $\theta = 90°$

1. Experimental Procedure

The sample was a Harshaw single crystal of CaF_2 in the form of a cylinder with the cylinder axis approximately parallel to the [110] axis.

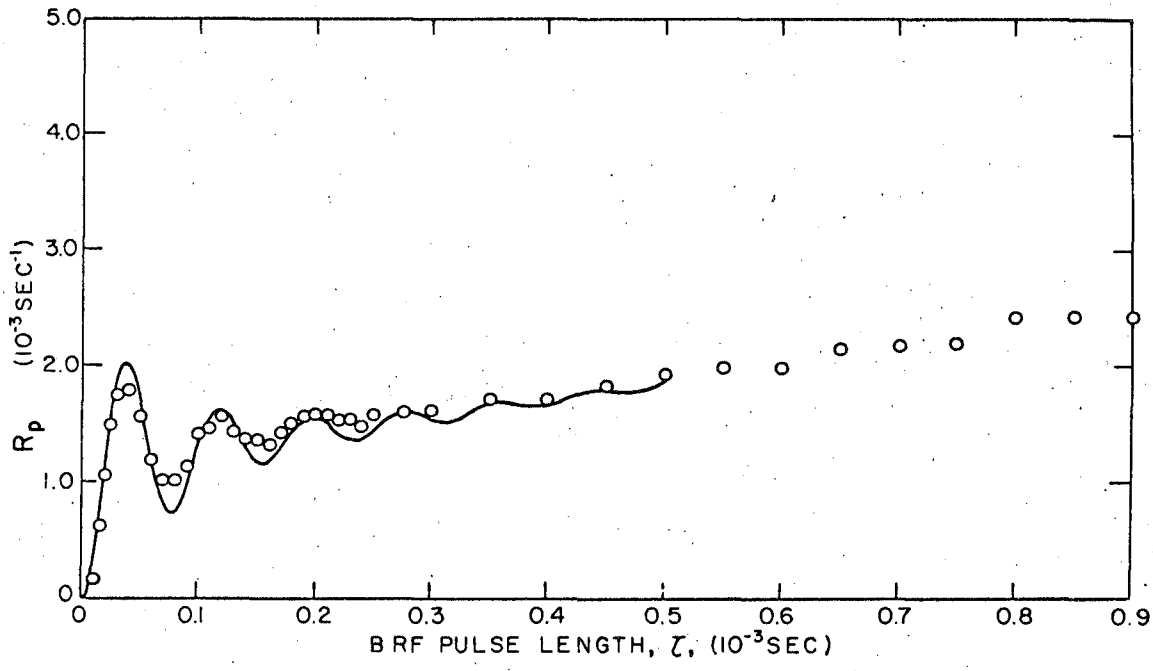

XBL 676-4184

Fig. 37 Transient oscillations in the B rotating frame; $\theta = 90°$, $f_{1B} \cong 12.6$ kHz, $H_o \parallel [111]$ in CaF_2; solid curve is theoretical $R_p(\tau)$

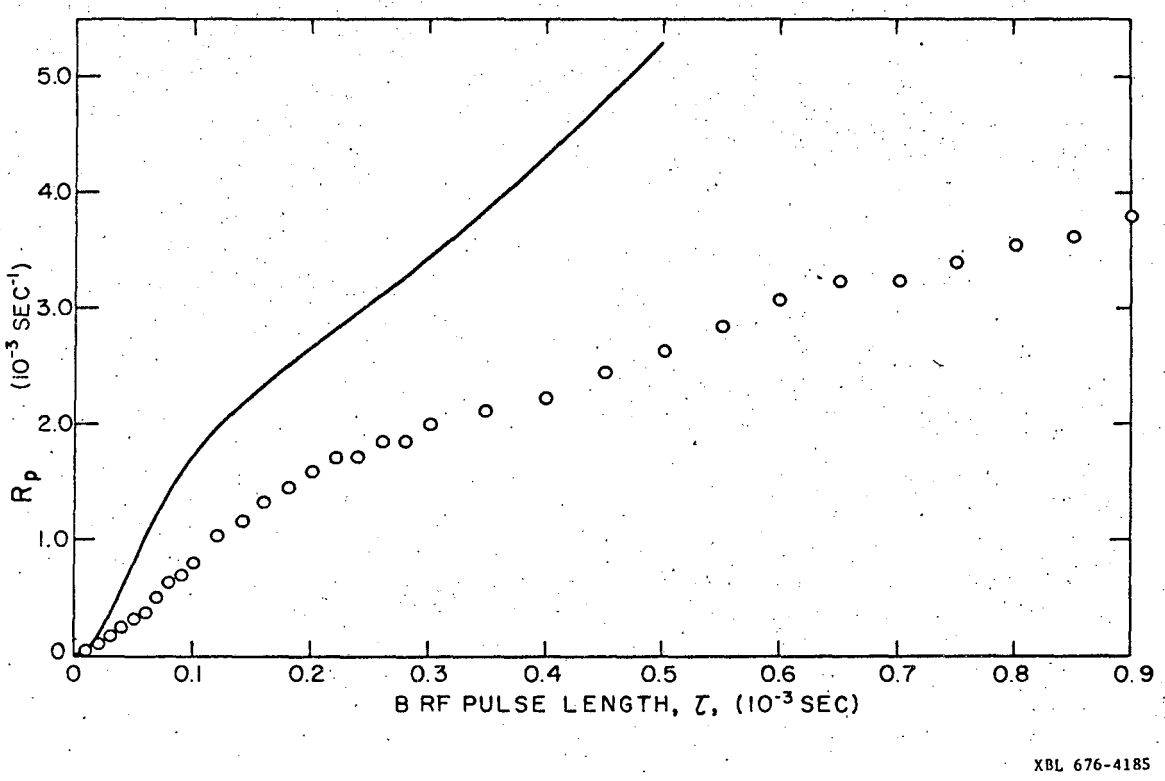

Fig. 38 Transient oscillations in the B rotating frame; $\theta = 90°$, $f_{1B} = 2.43$ kHz, $H_o \parallel [111]$ in CaF_2; solid curve is theoretical $R_\rho(\tau)$

The sample was rotated with this axis perpendicular to the laboratory magnetic field.

Before a measurement of $S_A(\tau)$ was made, the frequencies of the Gertsch oscillator regulating the Laboratory magnetic field, and the B rf oscillator were checked with an electronic counter. Then the amplitude of the B rf pulse was set to approximately the desired value with the oscilloscope monitor or VTVM, and an audio saturation double resonance plot at this value of B rf was made, to measure H_{1B} in the rotating frame (Fig. 28). The value of the minimum of the audio resonance curve (S_A vs. ω_{aud}) was taken as the measured value of f_{1B} in all cases, and the audio frequency was monitored with an electronic counter. Another audio resonance was taken as a check after each run at a given H_{1B}, and the two values usually agreed to less than ±.05 kHz.

Then the sequence of rf pulses of Fig. 39 was applied to the sample, keeping the cycle time $(\tau_o + \tau) = t_c$, the number of B rf pulses N, and the amplitude of the B rf constant during the entire run. Only the pulse length τ was varied, between the limits $\tau = 0$ and $\tau = t_c$-2ms, since it was necessary to allow all transverse components of M_B to decay completely between pulses. The pulse lengths τ were measured with an electronic counter and are accurate to ±.2%, the main error coming from pulse length instability of the Tektronix pulse generators. At each value of τ, two $S_A(\tau)$ points were taken, plus one value of S_A with no B rf pulses applied to the sample (S_A(NBRF)), and two zero points of S_A, with and without B rf pulses. The zero points were obtained by applying a large CW pulse of A rf lasting about 5 ms to saturate the F^{19} dipolar and Zeeman reservoirs, and then recording the resulting signal after the 45° A pulse, in its usual position in the sequence. These zero-signal points were

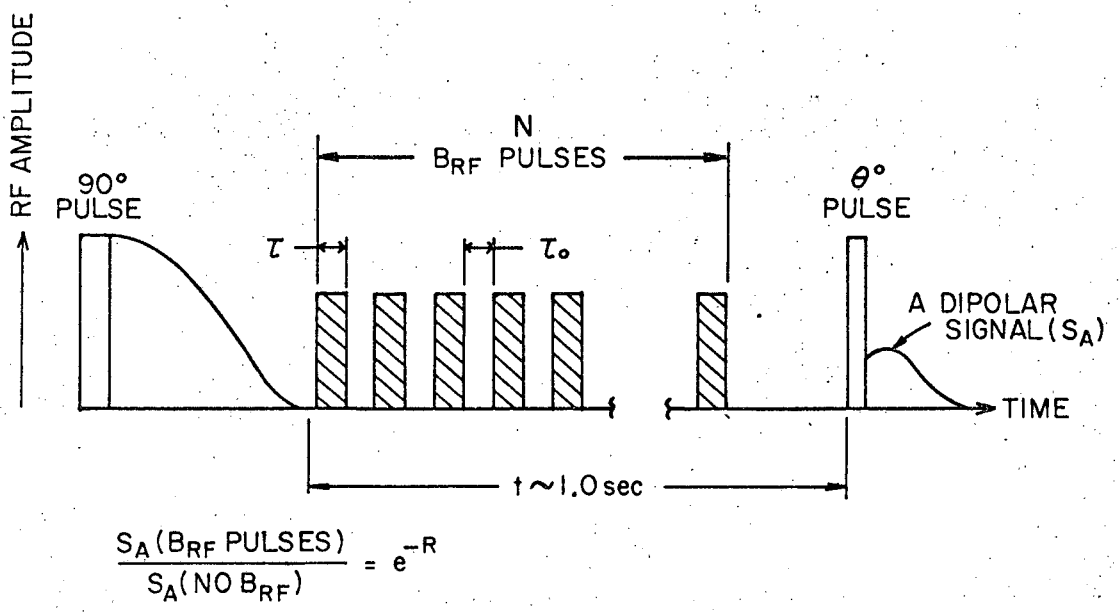

Fig. 39 Experimental procedure for pulsed double resonance following ADRF (times not to scale); unshaded pulses at frequency ω_{Ao}, shaded pulses at frequency ω_B

averaged and subtracted from the $S_A(\tau)$ and $(S_A)_{NBRF}$ signals. Without these zero-signal points a false (S_A) signal-zero might have been caused by small amounts of F^{19} Zeeman signal adding to the dipolar signal, if the phase of the phase sensitive detector were set improperly, or drifted from the correct setting. It was not sufficient to delete the 90° A rf phase shift from the ADRF wave form to obtain the zero points, probably because a small off-resonance component of magnetic field ΔH_A could allow some order to be transferred from a small spin-locked magnetization $\delta M_A \sim M_{oA} \cos(\pi/2 + \delta\theta)$ to the F^{19} dipolar system during the rest of the ADRF wave form. This would yield a small dipolar signal, again giving a false zero for S_A. The phase of the phase sensitive detector was adjusted by applying one of the saturating A rf pulses above and adjusting for zero signal after the $\theta°$ A sensing pulse.

The normalized F^{19} dipolar signals as a function of τ were obtained by subtracting the average "zero" signal from the signal at τ, and dividing the result by the averaged F^{19} dipolar signal with no B rf pulses:

$$\frac{S_A(\tau)}{S_A(NBRF)} = \frac{M(\tau)-\langle 0\rangle}{M(0)-\langle 0\rangle}$$

These normalized signals were fitted to the theoretical expression in Appendix E using an IBM 1620II computer (see Fig. 40).

In order that these least-squares ϵ and τ_{AB} be meaningful, they should be independent of τ_{max}, the length of the longest B rf pulse applied during a measurement at fixed H_{1B}. For example, if τ_{max} is too short for a particular value of H_{1B}, the least squares fit will yield ϵ and τ_{AB} values which are too small because the A and B spin systems have not come completely to thermal equilibrium. For these experiments, at each value

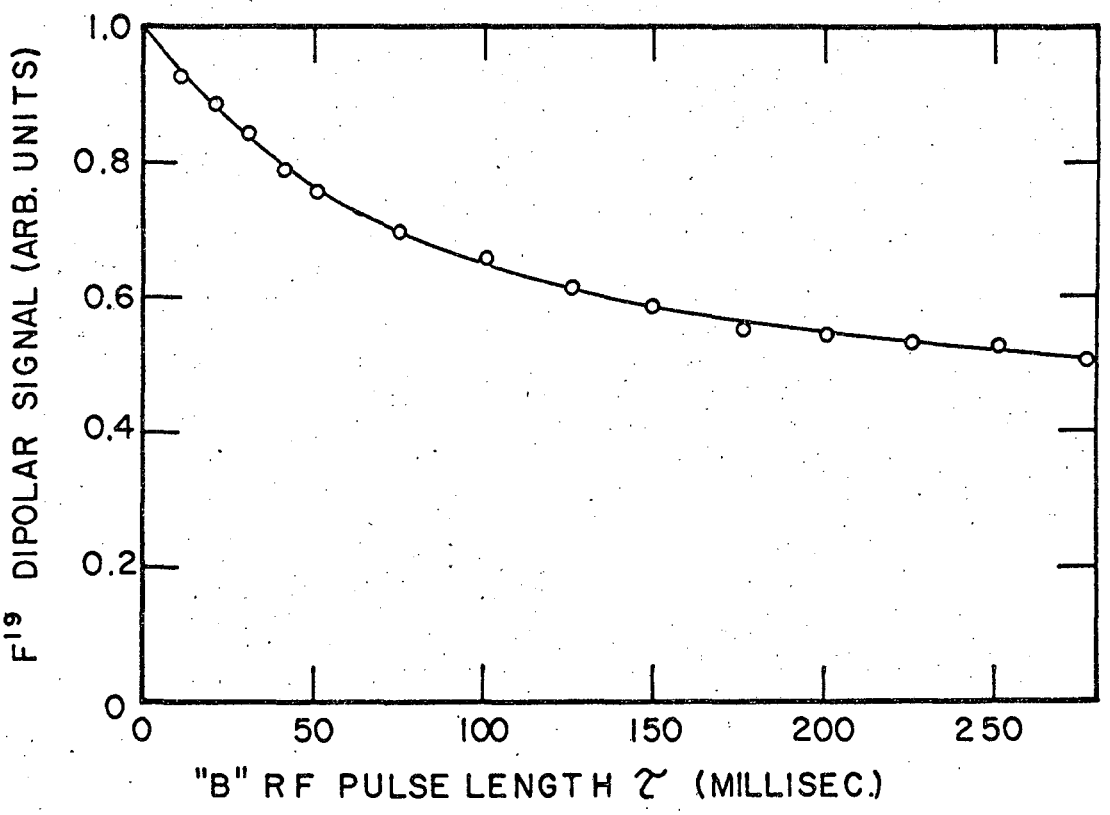

Fig. 40 Typical least-squares fit to $S_A(\tau)$ data ; $\theta = 45°$, $f_{eB} = 11.95$ kHz, seven B rf pulses

of H_{1B}, τ_{max} was set at 3.5 τ_{AB} and $S_A(\tau)$ was measured at fifteen equally-spaced points within the interval $0 < \tau \leq \tau_{max}$. Figure 41 shows the derived least-squares ϵ and τ_{AB} for several experiments at constant H_{1B}, using this procedure but with varying τ_{max}. It can be seen that if $\tau_{max} \gtrsim 3 \cdot \tau_{AB}$, the values of ϵ and τ_{AB} are found to be independent of τ_{max}. Figure 42 shows that the least-squares ϵ and τ_{AB} are independent of the number N of B rf pulses applied to the sample.

2. Experimental Results

The above procedure for measuring ϵ and τ_{AB} was repeated at many values of H_{1B} for H_o approximately parallel to the [111] and [110] directions of the CaF_2 crystal. Plots of the $\tau_{AB}^{-1}(f_{1B})$ and $\epsilon(f_{1B})$ data (Figs. 43-45) showed that they obeyed the following functional forms within the experimental error:

$$\tau_{AB}^{-1}(f_{1B}) = A \exp(-2\pi \tau_c f_{1B}) \qquad (93)$$

$$\epsilon(f_{1B}) = C f_{1B}^2 \text{ (kHz)}$$

To determine the values of A, τ_c, and C, the ϵ and τ_{AB}^{-1} data were fitted to these functional forms, and the least squares values of these parameters are shown in Tables II and III.

Table II: $H_o \parallel$ [110]

	$A(10^3 \text{ sec}^{-1})$	$\tau_c(10^{-6} \text{ sec})$	$C(10^{-3} \text{ kHz}^{-2})$
Theory	2.646	60.5	.5286
Experiment (no sat. pulses)	2.17(±.04)	57.2(±.4)	.484(±.008)

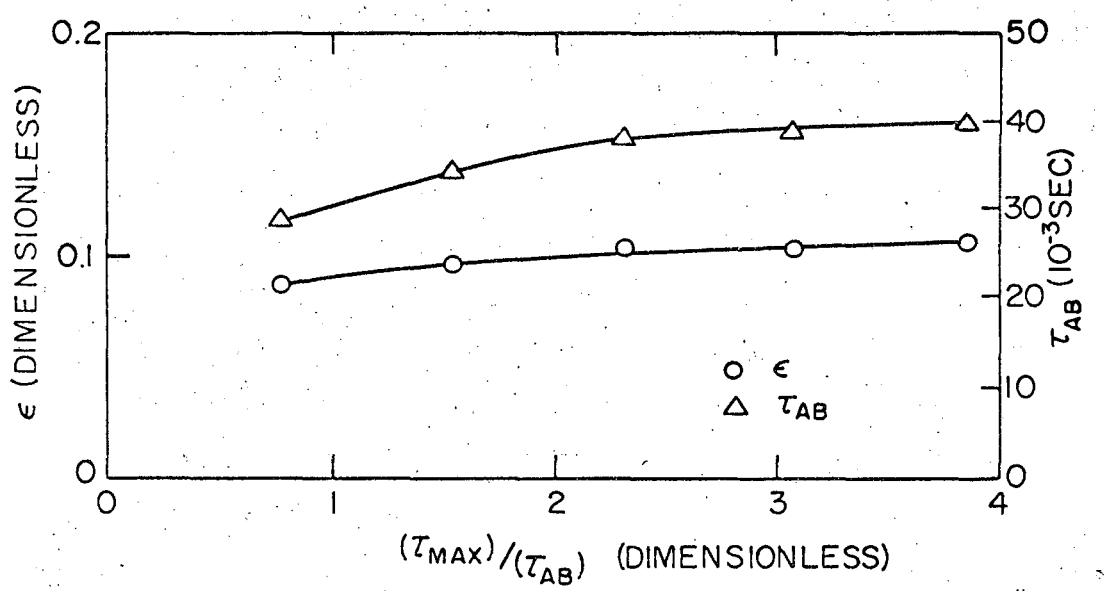

Fig. 41 Effect of τ_{max} on least-squares ϵ and τ_{AB}; $H_o \parallel [111]$ in CaF_2, $\theta = 90°$, $f_{1B} = 10.4$ kHz

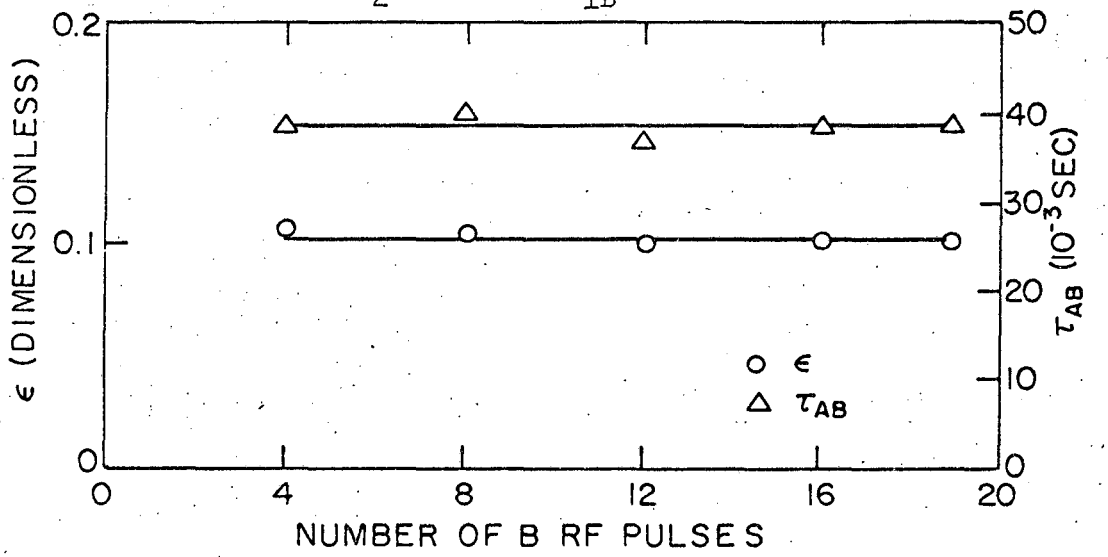

Fig. 42 Effect of number of B rf pulses on least-squares ϵ and τ_{AB}; $H_o \| [111]$ in CaF_2, $\theta = 90°$, $f_{1B} = 10.4$ kHz

XBL 676-4188

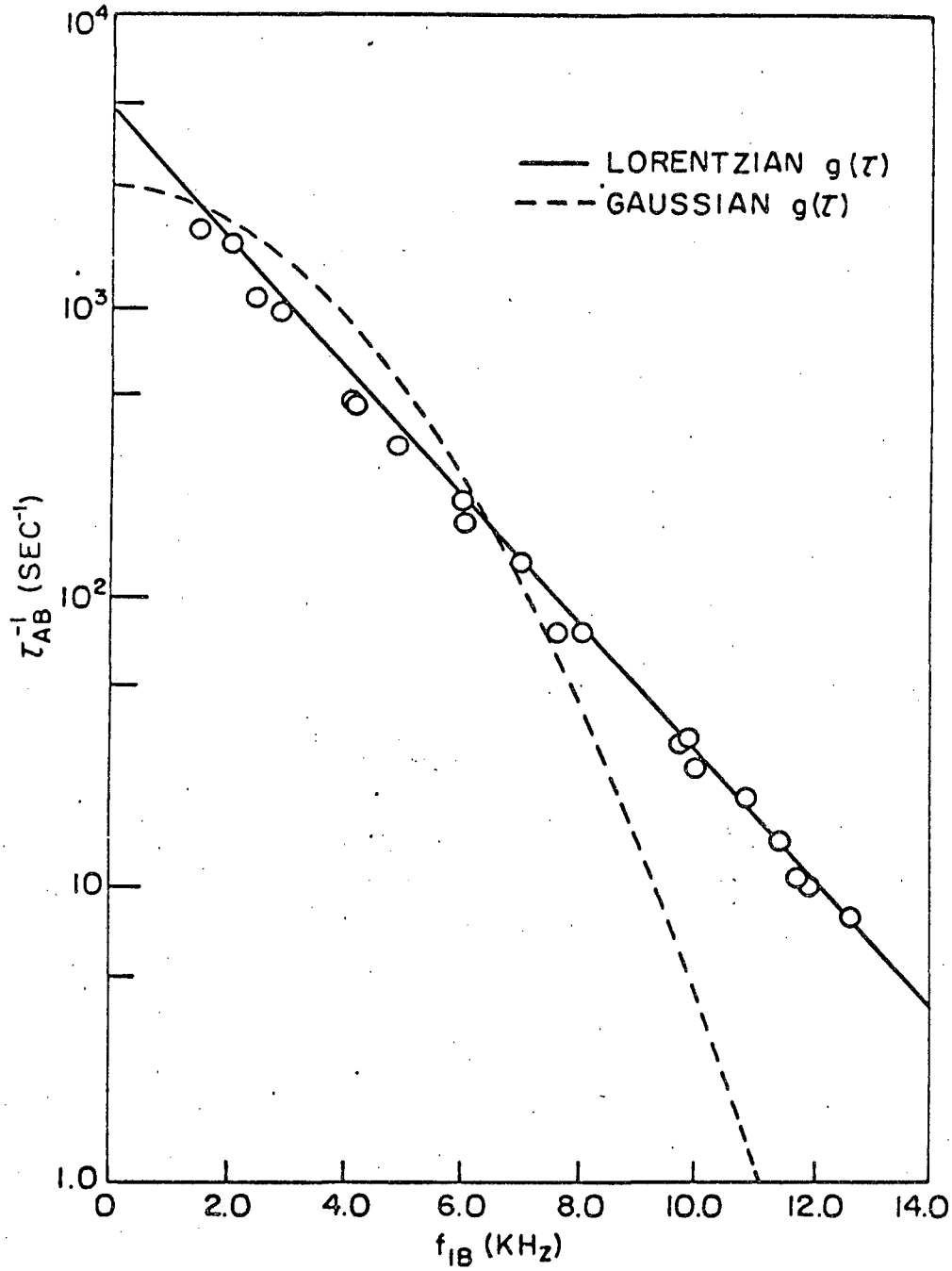

XBL 676-4189

Fig. 43 A dipolar-B Zeeman cross-relaxation spectrum, measured by pulsed ADRF double resonance; curves are theoretical spectra for H_o exactly $\parallel$ [111] in CaF_2, $\theta = 90°$

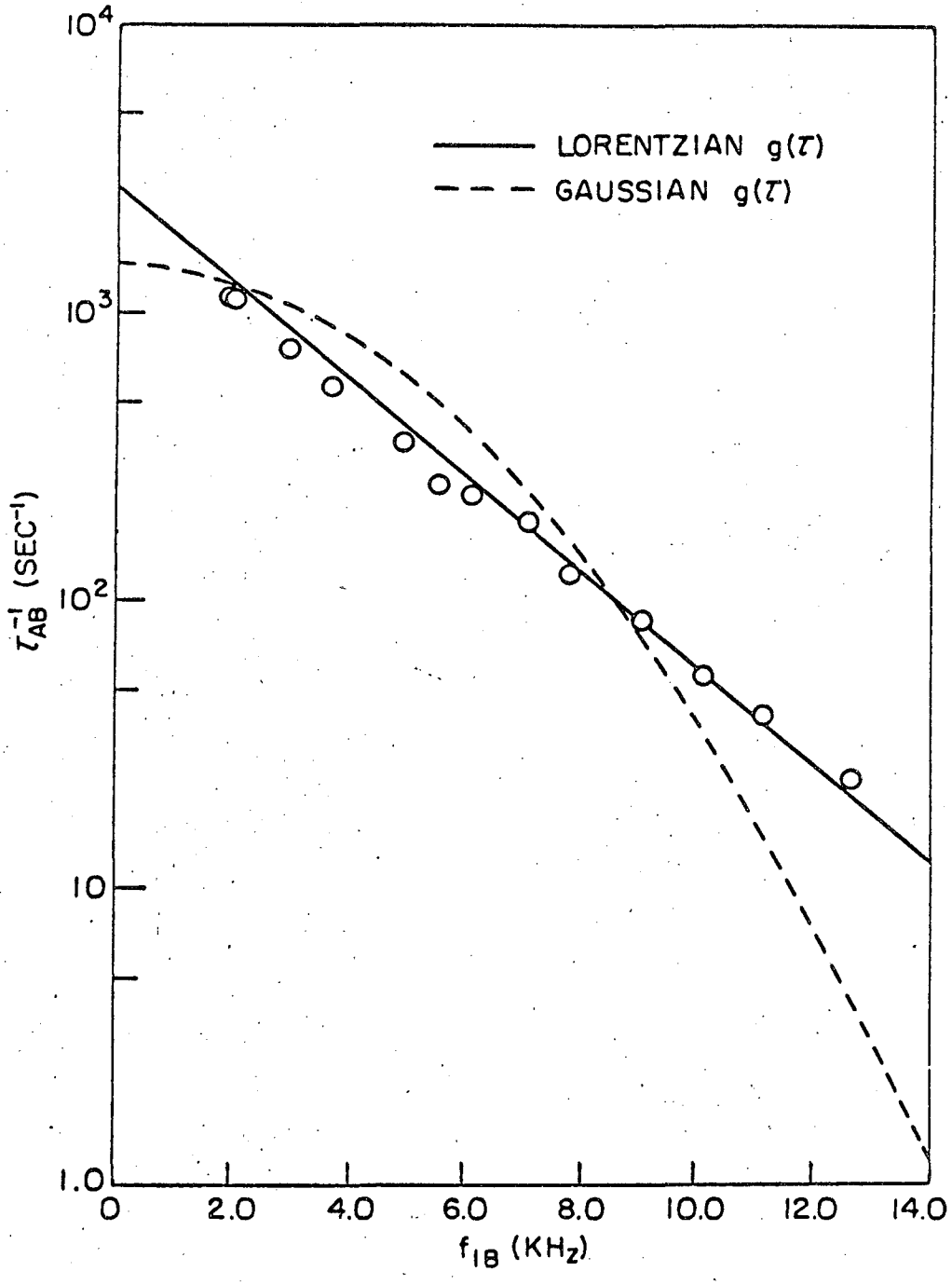

XBL 676-4190

Fig. 44 A dipolar-B Zeeman cross-relaxation spectrum, measured by pulsed ADRF double resonance; curves are theoretical spectra for H_o exactly $\|$ [110] in CaF_2, $\theta = 90°$

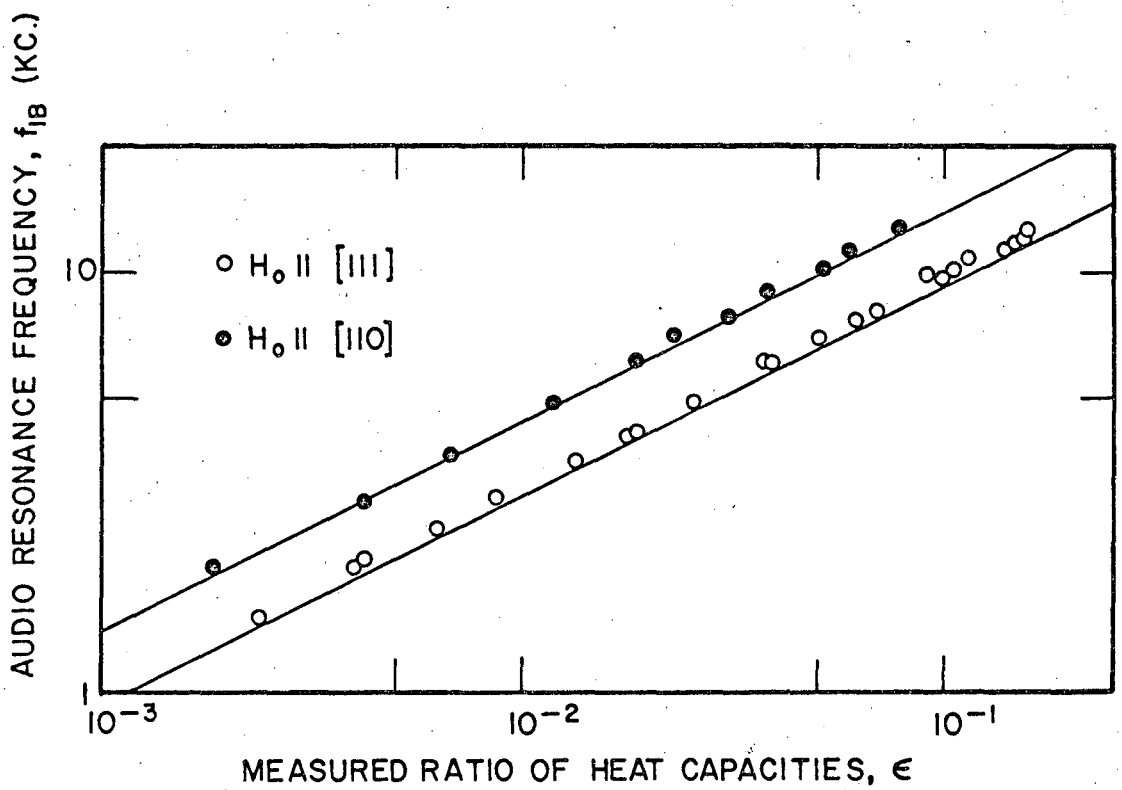

XBL 676-4191

Fig. 45 Ratio of heat capacities, ϵ, measured by pulsed ADRF double resonance in CaF_2; solid lines are theoretical dependence of ϵ, assuming the relative abundance of Ca^{43} is 0.13%

Table III: $H_o \parallel [111]$

	$A(10^3\ sec^{-1})$	$\tau_c(10^{-6}\ sec)$	$C(10^{-3}\ kHz^{-2})$
Theory	4.636	80.6	1.165
Experiment (no sat. pulses)	3.89(±.09)	78.4(±.5)	1.03(±.03)
Experiment (sat. pulses)	3.77(±.12)	80.0(±.6)	1.10(±.05)

Table IV shows the relation between the experimental and theoretical values of A, τ_c and C.

Table IV: Ratio of experimental to theoretical values

	A/A_{th}	$\tau_c/(\tau_c)_{th}$	C/C_{th}	$Area/(Area)_{th}$
[110] (no saturating pulses)	.82	.94	.92	.87
[111] (no saturating pulses)	.84	.97	.88	.87
[111] (saturating pulses)	.81	.99	.94	.82

3. Discussion

a. Effects of crystalline misorientation. Table IV shows that the experimental values of A, τ_c and C are all somewhat smaller than the theoretical values. But Table IV shows that the [111] data taken at $\theta = 90°$ with 10 saturating pulses (explained in detail in section V.C.) agrees within experimental error with the data without saturating pulses. This is to be expected since for $\theta = 90°$ there should be no remaining component of B magnetization parallel to H_o for the saturating pulses to destroy.

The discrepancies between the theoretical and experimental values of A, τ_c and C are outside the experimental error if H_o is exactly parallel to the [111] and [110] axes. The axis of the cylindrical sample has been measured on one end by a back-reflection Laue photograph, and it was found that the cylinder axis is displaced from the [110] axis about five degrees toward the [100] axis, and about three degrees toward the [111] axis. The axis about which the cylindrical sample was rotated in the laboratory magnetic field was measured to be parallel to the magnet pole faces within ±.5 degrees. Because the [110] and [111] directions of the CaF_2 crystal are both stationary points in the A-A and A-B dipolar interaction, this measured angular disorientation produces only small changes in $\langle \Delta\omega_B^2 \rangle_{BA}$, τ_c, and C, as can be seen in Table V. This is still not enough to bring the experimental values into agreement with theory, unless the average orientation of the bulk of the crystal deviates from the orientation of the end face measured. Adding only one degree to the angular errors quoted above increases the error quoted in Table V by about 50 percent, so we are just on the edge of rapid variation of A, τ_c and C with angle. Since the Laue photographs did show some evidence of lineage,[42] it is perhaps possible that the crystal orientation is the primary cause of the discrepancies in ϵ and τ_{AB}^{-1}.

Table V: Effect of crystal misorientation

	$A/(A)_{th}$	$\tau_c/(\tau_c)_{th}$	$C/(C)_{th}$	$Area/(Area)_{th}$
$[111]_1$	.935	.953	.915	.982
$[111]_2$	.986	.991	.983	.995
[110]	.887	.910	.955	.974

b. Magnitude of ϵ. The fact that the measured ϵ values are about 10% low means that the double resonance process is not as efficient as it should be on the basis of the simple theory, because $(1 + \epsilon)^{-1} \alpha \left[\frac{S_A(N)}{S_A(O)}\right]^{1/N}$. The curves of Fig. 45 use the more recent value for the natural abundance of Ca^{43}, that is, .13%[43] rather than the .145% measured in 1938.[44] The experimental error in the measurement of the Ca^{43} relative abundance is about 15%,[43] which brings the experimental value of ϵ into agreement with theory within the experimental error.

A small quadrupole perturbation would be expected to increase the B spin heat capacity slightly, but this increase is less than the experimental error for high f_{1B}, and probably could not be detected except at $f_{1B} \lesssim 2$kHz. The perturbed ϵ is given by

$$\epsilon_Q = \epsilon_o \left[1 + (\bar{\nu}_Q/f_{1B})^2\right] ,$$

where $\bar{\nu}_Q$ is the rms quadrupole splitting of the Ca^{43} resonance line. There is no evidence for this contribution at these low values of f_{1B} (Fig. 45).

An analysis of the sensitivity of ϵ to the signal zero of S_A shows that for large total destruction of A signal, there could be sizeable amount of error in ϵ, if the A signal zero is inaccurate. In the limit

$\tau \gg \tau_{AB}$, and neglecting T_{1A}, the erroneous measured heat capacity ratio ϵ_m is defined by:

$$\frac{(S_A(N) + \Delta S_0)}{(S_A(0) + \Delta S_0)} = \frac{(X + \Delta_0)}{(1 + \Delta_0)} = (1 + \epsilon_m)^{-N} ,$$

where ΔS_0 is the A dipolar signal-zero error, $X = S_A(N)/S_A(0)$, and $\Delta_0 = \Delta S_0/S_A(0)$. If $\Delta S_0 = 0$, the true ϵ is given by

$$X = (1 + \epsilon)^{-N} ,$$

where usually $.2 \lesssim X < 1$. Since Δ_0 and ϵ are small, $\epsilon \approx (1-X)/N$, and we find the relative errors in ϵ_m is:

$$\frac{(\epsilon_m - \epsilon)}{\epsilon} \approx \Delta_0/X .$$

Since X varied from run to run, this source of error should produce scatter in the values of ϵ, rather than a consistant error in ϵ. About a 3% error Δ_0 would be required to explain the 10% discrepancy in ϵ, but the variation of the zero of S_A when slightly different methods were used to measure it was usually about 1 to 2%, so this source of error is probably insufficient to explain the observed discrepancy.

c. Magnitude of τ_{AB}^{-1}. Since the correlation function $g_x(\tau)$ cannot be evaluated explicitly, the form $Ae^{-B} f_{1B}$ assumed for τ_{AB}^{-1} is justified only by its agreement with experiment. To determine whether other functional forms for $g_x(\tau)$ would fit the data better, the following functions were tried (each has the expansion $(1 + \lambda \tau^2)$ for small τ):

$$\tau_{AB}^{-1} = \langle \Delta\omega_B^2 \rangle_{BA} \int_0^\infty \frac{\cos \omega_{1B}\tau d\tau}{[1+(\tau/\tau_c')^2]^2}, \quad \tau_c' = \sqrt{2}\,\tau_c, \tag{94}$$

$$\tau_{AB}^{-1} = \langle \Delta\omega_B^2 \rangle_{BA} \int_0^\infty \frac{\cos\omega_{1B}\tau}{\cosh\left(\frac{\tau}{\tau_c'}\right)}\, d\tau, \quad \tau_c' = (\tau_c/\sqrt{2}) \tag{95}$$

and

$$\tau_{AB}^{-1} = \langle \Delta\omega_B^2 \rangle_{BA} \int_0^\infty \frac{\cos\omega_{1B}\tau\, d\tau}{\sqrt{1+(\tau/\tau_c')^2}}, \quad \tau_c' = (\tau_c/\sqrt{2}). \tag{96}$$

Forms (94) and (95) yield τ_{AB}^{-1} spectra which are concave downward on a semilog plot versus f_{1B}, while (96) is concave upward but approaches infinity as f_{1B} approaches zero. The data do not show any evidence of being concave within the experimental error, and using the theoretical values of τ_c and $\langle \Delta\omega_B^2 \rangle_{BA}$ in (94), (95) and (96), yields τ_{AB}^{-1} curves which deviate significantly from the data at intermediate and high f_{1B}. The usual assumption of a gaussian correlation function $g_x(\tau)$ yields a τ_{AB}^{-1} spectrum which does not agree at all with experiment, as shown in Figs. 43 and 44:

$$\tau_{AB}^{-1} = \frac{\sqrt{\pi}}{2} \langle \Delta\omega_B^2 \rangle_{BA}\, \tau_c\, e^{\frac{-\omega_{1B}^2 \tau_c^2}{4}}.$$

The exponential spectrum (39') and spectrum (96) both are physically unsatisfying because they have a "cusp" at $f_{1B} = 0$, while spectra (94) and (95) do not. It is possible to remove the cusp from the exponential spectrum by adding more parameters to the functional form. For example, if

$$\tau_{AB}^{-1} \propto \frac{A(f_{1B} + f_o)\, e^{-Bf_{1B}}}{(f_{1B} + f_o\, e^{-Bf_{1B}})} \tag{97}$$

it is readily seen that the cusp is removed since $d/df_{1B}(\tau_{AB}^{-1}) = 0$ at $f_{1B} = 0$. To determine the third parameter f_o theoretically it would be necessary to expand $g_x(\tau)$ to order τ^4. If f_o were much less than 1kHz, (97) would still agree with the form of the observed τ_{AB}^{-1}.

It should be noted that the Fourier transform relation between $g_x(\tau)$ and $\mathcal{G}(\omega) = \tau_{AB}^{-1}$ [Eq. (38)] requires that the total area under $\mathcal{G}(\omega)$ be a constant, independent of the shape of $\mathcal{G}(\omega)$. This means that it will be difficult to fit the experimentally measured points with any form of correlation function since the area under the measured $\mathcal{G}(\omega)$ seems definitely smaller than the theoretical value, unless one assumes a very long tail to the $\mathcal{G}(\omega)$ function, which does not show up at $f_{1B} \leq 12$kHz. This seems unlikely because our data fit the assumed exponential functional form very well in this region.

The decrease of τ_{AB}^{-1} at low f_{1B} might be caused by inhomogeneity in H_o, which should change the direction of H_{eB} away from H_{1B} if the inhomogeneity were large enough. The τ_{AB}^{-1} data for the [111] direction can be fitted at low f_{1B} (though not very well at high f_{1B}) by assuming a Lorentzian distribution of inhomogeneity with a width of about 500 Hz. But the magnetic field inhomogeneity is given also by the shape of a free induction decay of a liquid proton sample, which has a $(T_2)_p \gtrsim 2$ms. Thus

$$(\Delta f)_{B,inh} = \frac{\gamma_B (\Delta H)_{inh}}{2\pi} \leq \left(\frac{1}{2\pi}\right)\left(\frac{\gamma_B}{\gamma_A}\right) (T_2)_p^{-1} = 6 \text{ Hz}.$$

Thus, the measured inhomogeneity of H_o is far too small to account for the decrease of τ_{AB}^{-1} at low f_{1B}.

The B rf field H_{1B} should be very homogeneous over the sample ($\leq 1\%$ inhomogeneity over the sample volume has been measured for the case of a

static field in the B rf coil). The relative amount of inhomogeneity should be constant as the size of H_{1B} is changed, so B rf inhomogeneity should result in an overall decrease of τ_{AB}^{-1}. A particular average value of H_{1B} is measured by the audio resonance and this average should not differ greatly from the average represented by τ_{AB}^{-1}, particularly since the distribution of H_{1B} is so narrow. The $\theta = 90°$ audio resonances indicate that the B rf inhomogeneity is less than one percent of f_{1B}. If we assume a Gaussian B rf inhomogeneity distribution of width $\omega_i = f_i\omega_{1B}$, so that

$$P(\omega) = e^{-(\omega-\omega_{1B})^2/2\omega_i^2},$$

and average the exponential form of τ_{AB}^{-1} over this distribution, the new value of τ_{AB}^{-1} is given by:

$$(\tau_{AB}^{-1})_i = \tau_{AB}^{-1}\left[\exp(f_i^2\,\omega_{1B}^2\,\tau_c^2/2)\right]\left[\int_{-1/f_i + f_i\omega_{1B}\tau_c}^{\infty} dt \left(e^{-t^2/2}\right)\left(\frac{1}{\sqrt{2\pi}}\right)\right]$$

Since the measured value of f_i is $\leq .01$, it is clear that $(\tau_{AB}^{-1})_i$ should equal (τ_{AB}^{-1}) within $\sim(f_i^2\,\omega_{1B}^2\,\tau_c^2/2) = 2\times10^{-3}$ for our experiments, because the integral above is very nearly unity. The effects of B rf inhomogeneity also seem to have the wrong sign to explain our results.

Another more likely explanation of the discrepancy at low f_{1B} would be small, random quadrupole splittings of the Ca^{43} resonance line by impurities, dislocations, and other lattice defects in the CaF_2 crystal. These quadrupole splittings would influence τ_{AB}^{-1} most strongly for small H_{1B}, since the eigenstates of the new total Hamiltonian $\hbar(\mathcal{H}_e^B + \mathcal{H}_Q^{B'})$ in the rotating

frame would deviate significantly from the simple Zeeman eigenstates assumed for the theory in Section II.B. Thus at low H_{1B} the matrix elements of S_x would be very different from those of the simpler theory, and the transition probabilities between the new Ca^{43} eigenstates $|\tilde{m}>$ in the rotating frame might change sufficiently to lead to a non-Boltzmann population distribution as well.

It has been shown in Appendix D that the matrix elements of the dipolar perturbation between states $|\tilde{m}>$ (with quadrupole perturbation) do change to first order in (ν_{QK}/f_{1B}), and a first order splitting of the audio resonance in the rotating frame does occur. But when the rate of change of the total B spin energy is calculated, the first order changes cancel out, leaving only a second order change in τ_{AB}^{-1}. This is in agreement with part of the results of the density matrix calculation of the quadrupole splitting effect in Appendix D. This calculation shows that an rms quadrupole splitting $\bar{\nu}_Q \cong .6$kHz. is necessary to fit the data, but a quadrupole splitting as large as $\bar{\nu}_Q/2 = 300$Hz is not seen in the audio resonances. However, as explained in Appendix D, the density matrix calculation is probably seriously in error so conclusions from it cannot be trusted.

The finite spin diffusion rate between F^{19} spins should in principle affect the theoretical value of the Ca^{43}-F^{19} cross-relaxation rate τ_{AB}^{-1}. The simple theory of Section II.B. assumes that spin diffusion among F^{19} spins is much faster than τ_{AB}^{-1}, because the effective heat capacity of the F^{19} spin system is chosen as though any energy flowing from the Ca^{43} spin into the F^{19} spin system were shared immediately by all the F^{19} nuclei. In fact, those nearest F^{19} spins must rise to a higher spin temperature, thus inhibiting the energy flow into the A spin system. If

we define a spin diffusion time constant τ_{SD} as a time which allows all 1540 F^{19} nuclei to communicate with each other (see Appendix A), we would thus expect a decrease in the coupling rate when $\tau_{AB} < \tau_{SD}$. For the [111] τ_{AB}^{-1} data we do not observe a lowering of the cross relaxation rates for $\tau_{AB} \lesssim \tau_{SD} \cong 3$ msec, so we conclude that τ_{AB} is possibly more closely related to immediate communication of each B spin with its nearest A neighbors, and it is perhaps only necessary for each B spin to share energy immediately with a few A spins, without literally having to share it with its average number.

C. Measurement of ϵ and τ_{AB} at $\theta \neq 90°$

1. Experimental Procedure

Measurements of ϵ and τ_{AB} for angles θ other than 90° were undertaken in spite of the added complication of M_Z^B remaining between B rf pulses, for several reasons:

(1) Clough has shown that the dipolar spectrum vanishes at $\omega_{eB} = 0$ if $\theta \neq 90°$, possibly leading to an observable change of $\tau_{AB}^{-1}(\omega_{eB})$.

(2) Interference between the A-B dipolar perturbations $\mathcal{H}_{1x}$ and $\mathcal{H}_{1z}$ in second order time-dependent perturbation theory could lead to changes in τ_{AB}^{-1} (see Section II.B.3.) because the B Zeeman eigenstates with large $|m_B|$ would tend to come to thermal equilibrium with the A spin system faster then the eigenstates with low $|m_B|$. This might result in a cross-relaxation bottleneck, and would mean that a thermal-reservoir model of the B spin system during cross-relaxation would lead to incorrect predictions for τ_{AB}^{-1}.

(3) If the B Zeeman populations deviate significantly from a high-temperature Boltzmann distribution as a result of higher order contributions to τ_{AB}^{-1}, the cos θ law for the projection of a B magnetization onto the

laboratory z-axis would no longer hold.[38]

(4) It is of interest to check the thermal reservoir model of the cross-relaxation process by measuring whether $\tau_{AB}^{-1} \propto \sin^2\theta$, and whether $\epsilon \propto f_{eB}^2$, even for $\theta \neq 90°$.

As discussed in Section II.E.2., it is possible to measure ϵ and τ_{AB} by assuming the cos θ projection law, the thermal-reservoir equations (79) and (80) for the change of E_A, E_B, and putting the B system in a definite state (say $M_z^B = 0$) before applying the sequence of B rf pulses to the sample. A computer program could then be used to take account of the B magnetization projection between B rf pulses and of the initial condition on M_B. But it is theoretically easier to interpret the $S_A(\tau)$ data in terms of ϵ and τ_{AB}, if the Ca^{43} magnetization remaining along H_o is destroyed following each B rf pulse, so each B rf pulse sees the initial condition $E_B(0) = 0$. Saturating the B magnetization has several advantages: (1) For a given number of B rf pulses the double resonance signal is much larger for small $|\sin\theta|$, since each B rf pulse does the maximum amount of heating of the A dipolar system; (2) neglecting the projection complication greatly simplifies the function to which the $S_A(\tau)$ data for $\theta = 90°$ are fitted, which makes it more believable that the least squares ϵ and τ_{AB} have the meaning they have in the simple thermal-reservoir equations; and finally, (3) the questionable assumption that the cos θ projection law for a magnetization holds is removed.

To saturate any B magnetization before each B rf pulse, a sequence of 10 B rf pulses of length $\tau(sp)$ spaced $\tau_{op} \tilde{=} .9$ msec $\gg T_{2B} \tilde{=} .2$ msec apart were applied to the sample. The first set of 10 pulses was applied before ADRF on the F^{19} spins, and thereafter the saturating pulses followed each B rf pulse. At each angle θ and each f_{eB}, $\tau(sp)$ was chosen so that

rotation of the magnetization M_B around H_{eB} through an angle $\phi_o(\theta) = \omega_{eB}\tau(sp)$ would bring M_B into the x-y plane perpendicular to H_o. During the time $\tau_{op} \gg T_{2B}$, M_B would decay to zero. This was repeated ten times to ensure complete saturation, because of possible errors in ω_{eB}, θ, and $\tau(sp)$. For $\theta \geq 45°$ it is always possible to bring M_B perpendicular to H_o, but for $\theta = 30°$ the same process as above with $\omega_{eB}\tau(sp) = \pi$ resulted in reducing M_B only by a factor $(\cos(60°))^{10} \cong .001$. To take account of this small remaining magnetization, the computer program mentioned earlier in Section II.E.2 was used to interpret the data, but $\cos^2\theta$ was replaced by $(\cos 2\theta)^{10}$.

The saturating pulses also destroyed some A signal because they changed the local field at neighboring A spin sites as in the case of the transient oscillations (Section II.C.) To subtract out this effect from the double resonance effect of the long B rf pulses, the $S_A(\tau)$ data were normalized to the value of the A signal when only the saturating pulses were applied, $S_A(sp)$:

$$S_{A,norm.} = \frac{S_A(sp,\tau)}{S_A(sp)}$$

For small f_{eB} (and thus small ϵ), the number of B rf pulses required to observe a large double resonance signal was over 100. But the effect of the saturating pulses alone on S_A also increases for small f_{eB}, because $\tau(sp)$ $(\alpha \frac{1}{\omega_{eB}})$ approaches τ_{AB} $(\alpha \exp(\omega_{eB}\tau_c))$. Thus $S_A(sp)$ becomes much smaller, so the ϵ and τ_{AB} data for $\theta \neq 90°$ and small f_{eB} are much noisier than the $\theta = 90°$ data taken without saturating pulses.

2. Experimental Results

Figures 46 and 47 show the experimental ϵ and τ_{AB}^{-1}, respectively, for θ approximately equal to 90°, 60°, 45°, and 30°. The ϵ data are proportional to f_{eB}^{n}, where n = 2.08, or within 4% of the theoretical value of n. The values of ϵ for all four values of θ are equal, within the experimental error. This can be seen in Fig. 48 where the ϵ data at each value of θ have been fitted to the form $\epsilon = Cf_{eB}^{2}$. Figure 47 shows that within the experimental error the form of $\tau_{AB}^{-1}(f_{eB})$ does not change with θ. The least-squares values of A and τ_c are shown in Figs. 49 and 50, respectively. The value of τ_c seems to decrease slightly as θ decreases, which is in qualitative (but not quantitative) agreement with the calculation of Appendix C. The values of τ_c for $\theta = 90°$ with and without saturating pulses do not quite agree within the experimental error derived from the least-squares fit. However, it is not clear whether the slight decrease of τ_c with decreasing θ is real or just experimental scatter. Figure 49 shows that the least-squares values of A as a function of θ obeys the $\sin^2\theta$ law valid for constant τ_c within the experimental error, and that the values of A at $\theta = 90°$ with and without saturating pulses agree within experimental error. But if we use the calculated $\tau_c(\theta)$, $A(\theta)$ should be proportional to $\sin^2\theta\ \tau_c(\theta)$, which is slightly smaller than $\sin^2\theta$. The normalized Clough θ-dependence for constant τ_c is the upper curve shown in Fig. 49.

3. Discussion

These experimental results indicate that the thermal reservoir model of the cross-relaxation process is obeyed very well, the main discrepancy being that the correlation time τ_c does not become as small

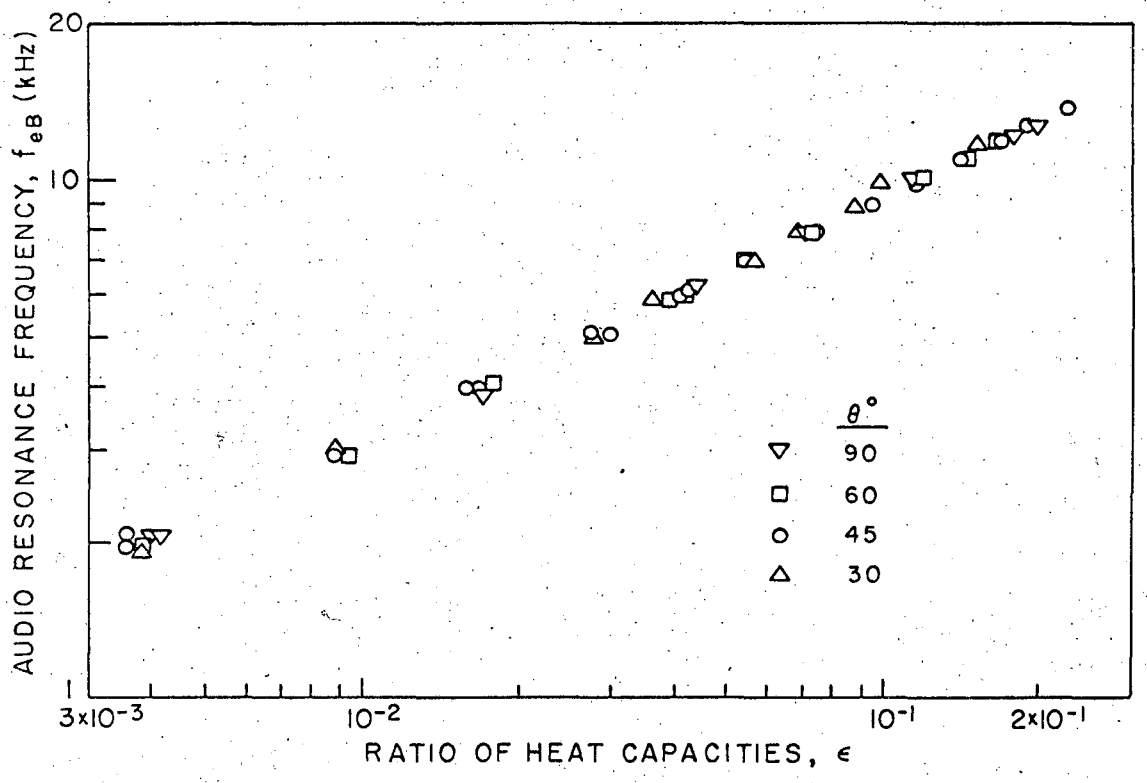

Fig. 46 Ratio of heat capacities, ϵ, measured by pulsed ADRF double resonance, using ten saturating pulses before each B rf pulse; $H_o \parallel [111]$ in CaF_2.

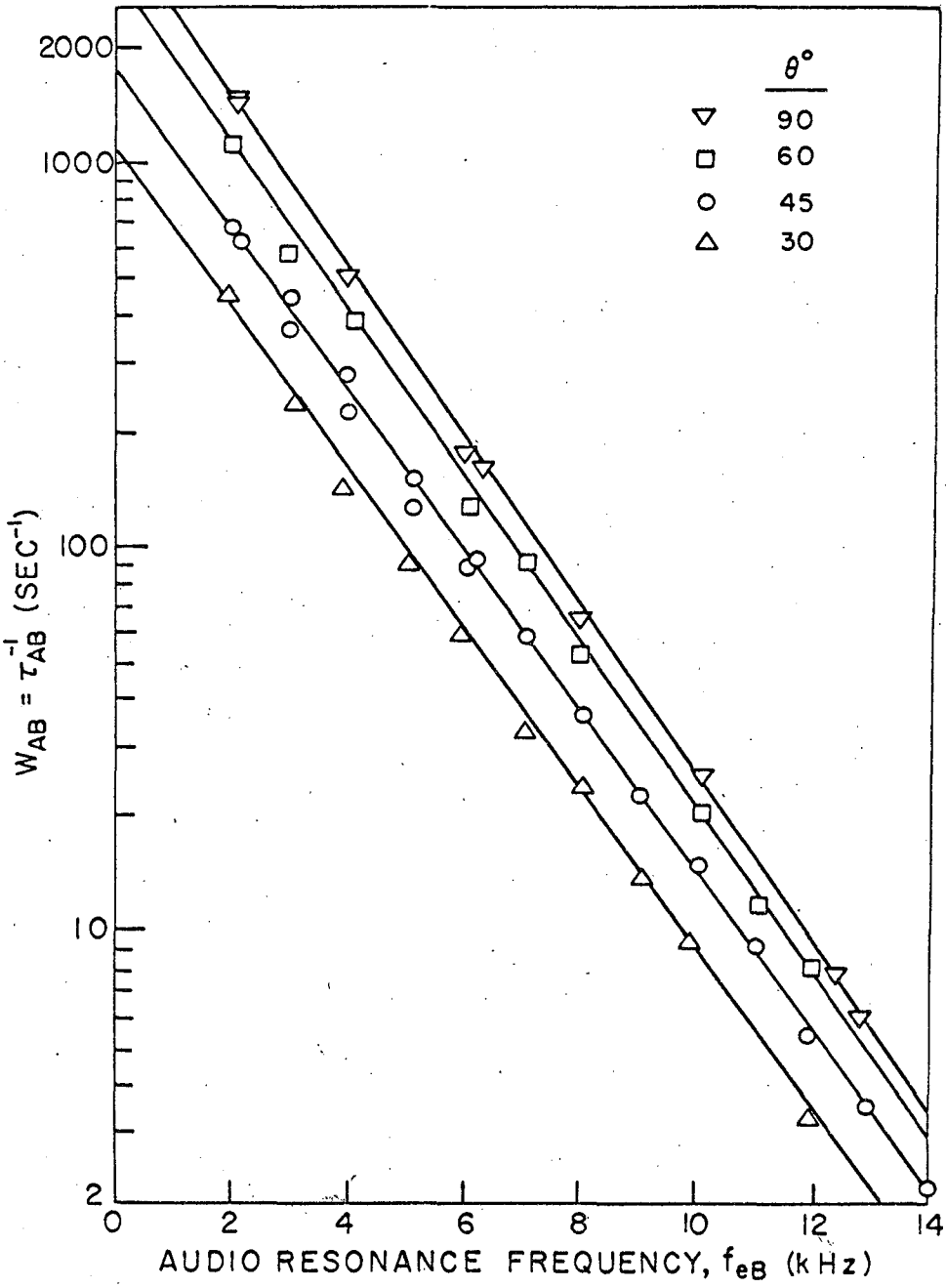

XBL 676-4193

Fig. 47 A dipolar-B Zeeman cross-relaxation spectrum, measured by pulsed ADRF double resonance, with ten saturating pulses before each B rf pulse; $H_o \parallel [111]$ in CaF_2; solid lines are the least-squares curves

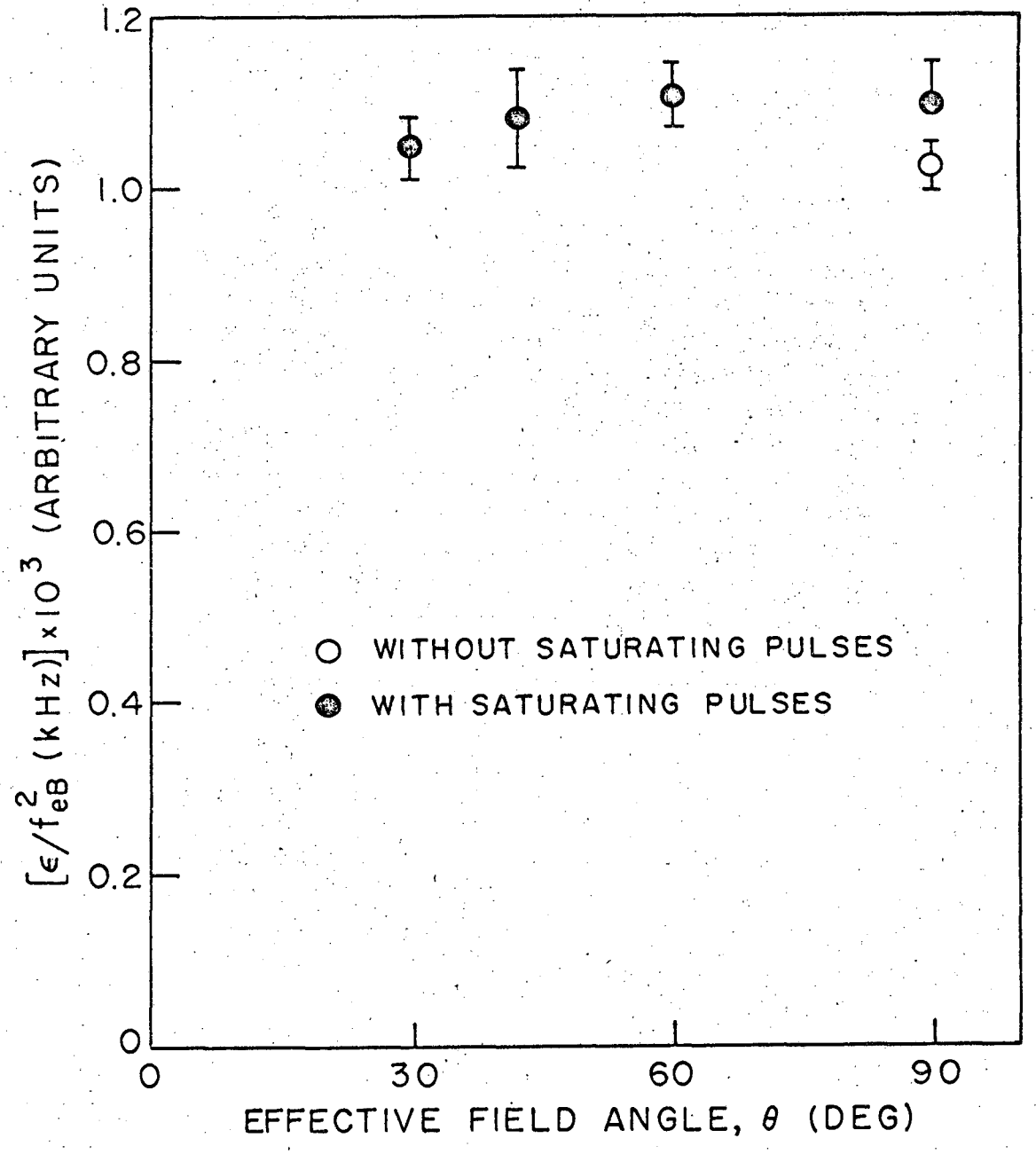

XBL 676-4194

Fig. 48 Dependence of the parameter C on θ, measured by pulsed ADRF double resonance; $H_o \parallel [111]$ in CaF_2

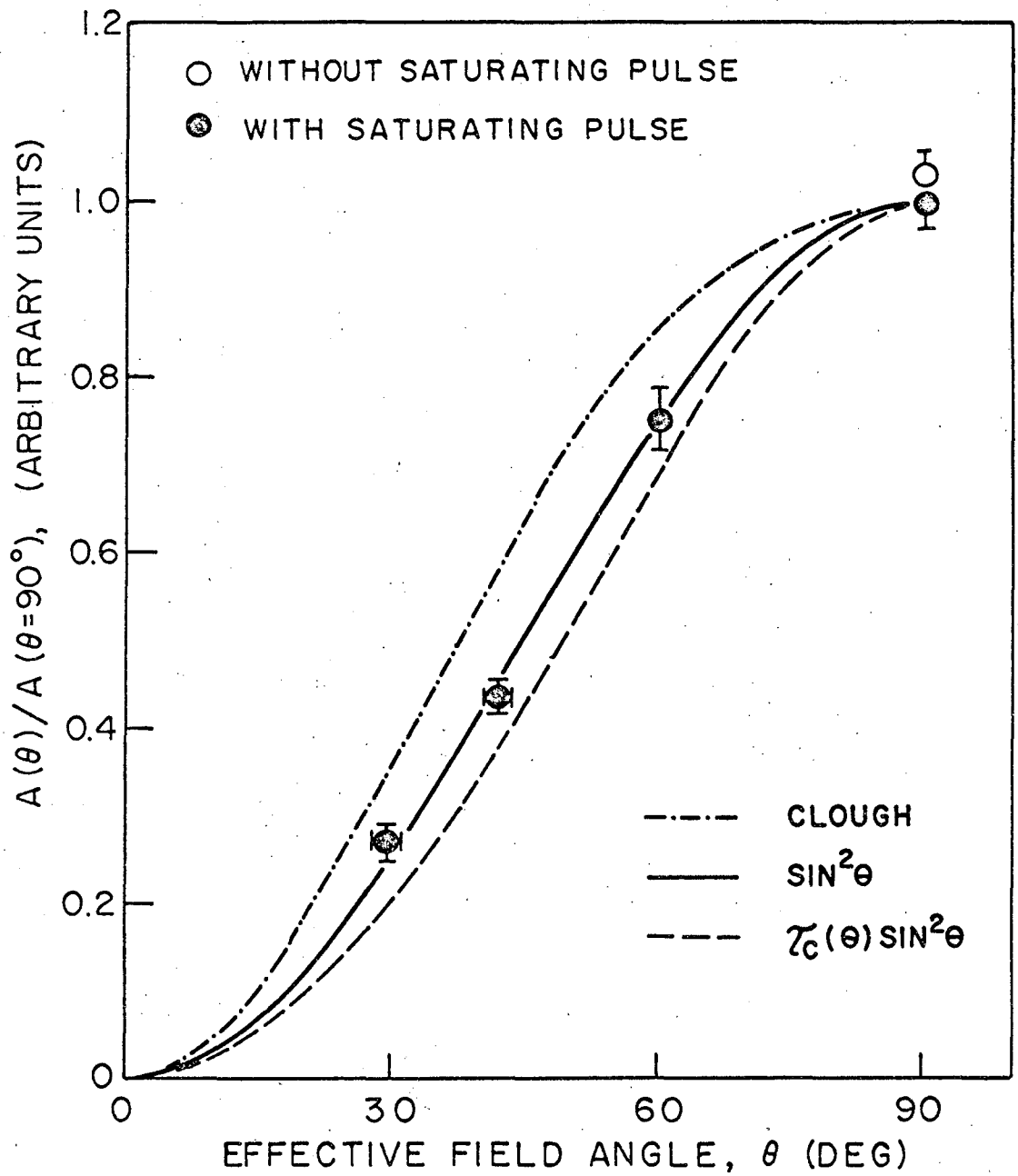

XBL 676-4195

Fig. 49 Dependence of the parameter A on θ, measured by pulsed ADRF double resonance; $H_o \| [111]$ in CaF_2;
Clough curve = $N(\theta)\ \sin^2\theta$
$\sin^2\theta$ curve = $\sin^2\theta$
$\tau_c(\theta)$ curve = $\tau_c(\theta)\ \sin^2\theta$

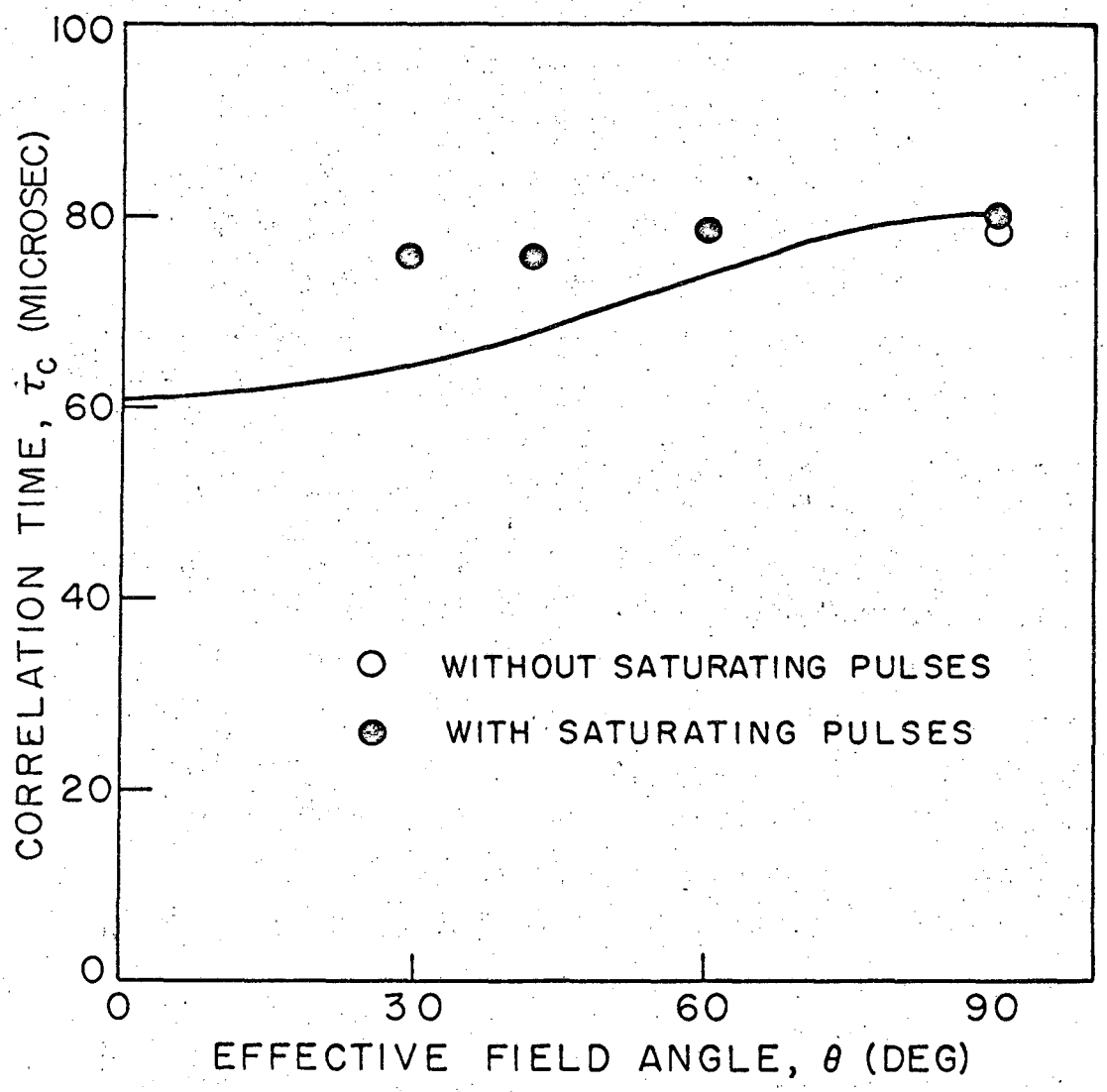

XBL 676-4196

Fig. 50 Dependence of τ_c on θ, measured by pulsed ADRF double resonance; $H_o \| [111]$ in CaF_2; solid line is angular dependence calculated in Appendix C

as the theory indicates for small θ. If we assume that the small variation of τ_c we measure is the result of experimental scatter, then it is consistent for the $\sin^2\theta$ law to be obeyed.

But if we believe the calculation of $\tau_c(\theta)$ for the exponential spectrum, then the lower curve, which is almost within the experimental error, should be obeyed. The measured variation of $\tau_c(\theta)$ is then not in agreement with experiment.

If we use the Clough method of evaluating $g_B(\tau)$, assuming τ_c is practically constant (as experiment indicates), and requiring the area under the $\tau_{AB}^{-1}(\omega_{eB})$ curve to be proportional to $\sin^2\theta$, we obtain the upper curve for $N(\theta)\sin^2\theta$. The disagreement between the data and the Clough function θ-dependence seems to be outside the experimental error. There should be little error in using the least-squares $A(\theta)$ from the exponential spectrum fit to compare directly with the quantity $N(\theta)\sin^2\theta$ of the Clough theory, because for all the data points in the least-squares fits (except for $f_{eB} \approx 2$kHz), the Clough function is equal to the exponential within $\leq 3\%$.

This disagreement is not understood. Perhaps we should find the correlation function corresponding to the Clough spectrum for $\theta \neq 90^\circ$, and expand this function to order τ^2, to evaluate the constants appearing in the spectrum. It should be noted that a combination of smaller τ_c as $\theta \to 0^\circ$, and the loss of area near $\omega_{eB} = 0$ would tend to compensate each other, but this does not restore the $\sin^2\theta$ dependence, and such a large $\tau_c(\theta)$ dependence is not observed either. In conclusion, to within about 5%, the $\theta \neq 90^\circ$ data show that the spectrum obeys the $\sin^2\theta$ law, and τ_c is constant.

VI. MEASUREMENT OF Ca^{43} FREE INDUCTION DECAY IN CaF_2

A. Physical Basis of the Method

The double resonance lineshape as a function of ω_B is in general very complicated, since θ and ω_{eB} change as ω_B is swept through the resonance value ω_{Bo}. The double resonance parameters ϵ, τ_{AB}, and τ_c are complicated functions of θ and ω_{eB}; in addition, no matter which method of saturation of the B resonance is used (B rf pulses, audio saturation, or FM), the effectiveness of the saturation mechanism also depends on θ.

A more easily intepreted method of measuring the B lineshape makes use of the Fourier transform relationship between the B lineshape in frequency space, and the transient decay of a B magnetization transverse to the laboratory magnetic field.[19] This "free induction decay" shape for the rare spin can be measured indirectly using the pulsed double resonance method, by simply placing the B rf pulses "too close together". The strength of the pulsed double resonance process depends on a complete decay of the B magnetization between B rf pulses, or a complete heating of the B spin reservoir back to infinite spin temperature. Suppose a train of a fixed number N of B rf pulses is applied to the sample after ADRF, each pulse having a constant length τ, but separated from its neighbors by a variable time $\tau_o \sim T_{2B}$. A B rf master oscillator is used, so the B rf phase is coherent from pulse to pulse, and for $\tau_o \lesssim T_{2B}$ the B rf field at the beginning of a pulse "catches" the remaining B magnetization from the preceding pulse. This means that the B spin reservoir begins the cross-relaxation process in a somewhat "colder" state than would occur if the B magnetization were allowed to decay completely between B rf pulses. If $\tau_o \lesssim T_{2B}$, S_A will rise toward a maximum (or minimum double resonance effect), but for $\tau_o \gg T_{2B}$,

S_A will approach a minimum (maximum double resonance effect). A study of $S_A(\tau_o)$, for constant τ and N, will yield the free induction decay of the transverse B magnetization.

This method will be applicable to any situation in which a fairly large double resonance effect is observable. To make interpretation of the experimental data easier it is convenient to choose $\tau \gg \tau_{AB}$, so that τ_{AB} drops out of the thermodynamic equations. This entails a certain loss of double resonance sensitivity, which could be regained by letting $\tau \approx \tau_{AB}$, but using more complicated equations to calculate the free induction decay shape. A further advantage of letting $\tau \gg \tau_{AB}$ is that more time is allowed for spin diffusion between the abundant spins, so spin diffusion effects are minimized.

B. Contributions to the Ca^{43} Linewidth in CaF_2

Three possible mechanisms of broadening of the Ca^{43} resonance in CaF_2 are: (1) magnetic field inhomogeneity, (2) dipole-dipole broadening caused by the F^{19} neighbors of the Ca^{43} spin, and (3) quadrupolar broadening caused by lattice strains around impurities or dislocations, since S = 7/2 for Ca^{43}. The magnetic field inhomogeneity is small, because the T_2 of protons in a liquid sample is about 2 ms. This implies that $(T_{2B})_{inh} = (\gamma_p/\gamma_{Ca^{43}})(T_{2p})_{inh} \approx 30$ ms.

The dipolar broadening by F^{19} neighbors is expected to be large because the F^{19} neighbors are so close ($r_{ik} \sim \frac{\sqrt{3}a}{2}$) and have large magnetic moments, and because the angle between H_o and the crystalline axes has been chosen to maximize the Ca-F dipolar coupling for maximum double resonance rates. But the correlation time of the F^{19} local field ($\tau_c \leq 80_{\mu s}$) is shorter than the time constant characterizing the Ca-F dipolar coupling

$\left((\langle \Delta\omega_B^2 \rangle_{BA})^{-1/2} \gtrsim 170\mu s \right)$, so most of the Ca^{43} spins precess less than one cycle in the local field from their F^{19} neighbors before this local field changes its value. This random walk of the phase of a Ca^{43} spin means that the Ca-F broadening mechanism is less effective because it is motionally narrowed.

The extent of the motional narrowing can be changed by rotating the crystal with respect to the laboratory magnetic field, since the requirement for motional narrowing is $p = \sqrt{\langle \Delta\omega_B^2 \rangle}\, \tau_c \ll 1$. For H_o parallel to the [111] direction this parameter is $\approx .49$, but for the [110] it is $\approx .32$. Since p is not $\ll 1$ for our case, we should expect to see incipient rather than complete motional narrowing. The completely narrowed resonance has a Lorentzian lineshape,[30,33] corresponding to an exponential free inducation decay. If the Ca-F dipolar coupling is the dominant broadening mechanism, we should observe a free-induction decay with zero slope for $t = 0$, which becomes an exponential for times long compared with the local field correlation time τ_c.

The third mechanism is quadrupolar broadening caused by random strains in the CaF_2 lattice, which destroy the cubic symmetry near a Ca^{43} spin site and result in random quadrupole splitting of the Ca^{43} resonance line. This broadening should be independent of the angle between the magnetic field and the crystalline axes if the strains are random, so the amount of this contribution to the Ca^{43} line width should be derivable from the anisotropy of the linewidth. This broadening would be difficult to estimate because the quadrupole moment of Ca^{43} and the antishielding factor of Ca are difficult to estimate.[45]

C. Theory of the Method

As mentioned above, we want to apply many B rf pulses of length $\tau \gg \tau_{AB}$ to the sample. H_{1B} must be large enough so that the major double resonance effect comes from the buildup of a Ca^{43} magnetization along H_{1B}: that is,

$$\epsilon = \frac{C_B H_{1B}^2}{C_A H_{LA}'^2} \gg \delta = \frac{C_B H_{LB}^2}{C_A H_{LA}'^2} .$$

Then we can neglect the transient oscillations and use Eqs. (81) and (82) to relate the values of E_A and E_B at the end of the B rf pulse to their initial values.

We will also neglect T_{1A} in these equations, because $\tau \ll T_{1A}$ and $\epsilon \ll 1$. The effect of the strong Ca^{43}-F^{19} coupling during cross-relaxation on the F^{19} spin-lattice interaction is to cause the combined Ca-F system to relax at a slightly slower rate $\frac{1}{(1+\epsilon)T_{1A}}$ toward the lattice temperature. For short times τ_{AB} and small ϵ, this effect is characterized by:

$$\frac{\exp\left(-\frac{\tau}{(1+\epsilon)T_{1A}}\right)}{\exp\left(-\frac{\tau}{T_{1A}}\right)} = \exp\left(\frac{\epsilon\tau}{(1+\epsilon)T_{1A}}\right)$$

We are justified in using τ rather than $N\tau$ here because we are studying a parameter of a single B rf pulse, so all observed signals will be taken to the $\left(\frac{1}{N}\right)$ power. The denominator arises because we divide $S_A(N,\tau)$ by $S_A(0)$. For H_o parallel to [111], $\epsilon\tau/(1+\epsilon)T_{1A} \tilde{=} 1.5\times10^{-4} \ll 1$, so the effects of T_{1A} are negligible.

Figure 51 shows the F^{19} and Ca^{43} energies in the rotating frame while

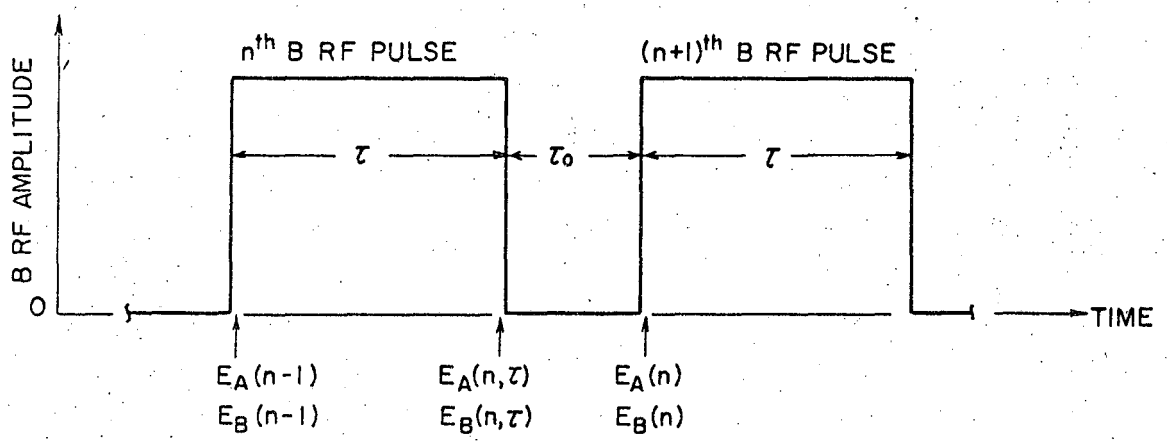

Fig. 51 Properties of B rf pulses used to measure $T_2(Ca^{43})$ in CaF_2; $\tau_o \lesssim T_2(Ca^{43})$, $\tau \gg \tau_{AB}$

B rf is on, but at the beginning and end of B rf pulses. The simplified equations (58') and (58") are used, which have the solutions for $\tau \gg \tau_{AB}$:

$$E_A(\tau,N) \cong \frac{E_A(n-1)}{(1+\epsilon)} + \frac{E_B(n-1)}{(1+\epsilon)}$$

$$E_B(\tau,n) \cong \frac{\epsilon E_A(n-1)}{(1+\epsilon)} + \frac{\epsilon}{(1+\epsilon)} E_B(n-1)$$

Since we neglect T_{1A}, we can account for the values of E_A, E_B at the beginning of the next pulse by assuming E_A remains constant, and M_B decays according to some arbitrary function of τ_o, which approaches zero for large τ_o:

$$M_B(\tau_o) \equiv M_B(\tau)\, f(\tau_o) .$$

Then $$E_B(n) = -M_B(\tau+\tau_o)H_{1B} = -M_B(\tau_o)H_{1B}\, f(\tau_o) = E_B(\tau,n)\, f(\tau_o).$$

Thus the relation between $E_A(n)$, $E_B(n)$, and $E_A(n-1)$, $E_B(n-1)$ can be represented by a matrix M, and the effect of N B rf pulses by a power of M:

$$\begin{pmatrix} E_A(N) \\ E_B(N) \end{pmatrix} = \begin{pmatrix} \left(\frac{1}{1+\epsilon}\right) & \left(\frac{1}{1+\epsilon}\right) \\ \frac{\epsilon f(\tau_o)}{(1+\epsilon)} & \frac{\epsilon f(\tau_o)}{(1+\epsilon)} \end{pmatrix}^N \begin{pmatrix} E_A(0) \\ E_B(0) \end{pmatrix} \equiv M^N \begin{pmatrix} E_A(0) \\ E_B(0) \end{pmatrix}$$

As with the case of the Ca-F cross relaxation calculation for $\theta \neq 90°$, M^N can be written as a polynomial in I and M using the eigenvalues of M. In this case

$$M^N = \left[\frac{1+\epsilon f(\tau_o)}{1+\epsilon}\right]^{N-1} M,$$

and since for $\theta = 90°$, $E_B(0) = 0$, we have

$$E_A(N) = \left[\frac{1+\epsilon f(\tau_o)}{1+\epsilon}\right]^N \frac{E_A(0)}{[1+\epsilon f(\tau_o)]} \qquad (97')$$

To solve for $f(\tau_o)$ we take the Nth root of Eq. (97') and use the fact that $\frac{\epsilon f(\tau_o)}{N} \leq \frac{2.5\times10^{-2}}{32} \ll 1$ for our experiments:

$$\eta(\tau_o) = \left[\frac{S_A(N,\tau_o)}{S_A(0)}\right]^{1/N} = \left[\frac{E_A(N,\tau_o)}{E_A(0)}\right]^{1/N}$$
$$\cong \left[\frac{1+\epsilon f(\tau_o)}{1+\epsilon}\right] \frac{1}{\left[1+\frac{\epsilon f(\tau_o)}{N}\right]} . \qquad (98)$$

Since $f(\tau_o \to \infty) = 0$, $\eta(\infty) = \frac{1}{(1+\epsilon)}$, so we can find $f(\tau_o)$ to a very good approximation by expanding the denominator in Eq. (98)

$$f(\tau_o) \cong (\tfrac{1}{\epsilon}) \frac{\left[\left(\eta(\tau_o)/\eta(\infty)\right)-1\right]}{\left[1-\frac{\eta(\tau_o)}{\eta(\infty)}\right]} \qquad (99)$$

To derive Eq. (99) for $f(\tau_o)$, the only assumption we have made about its properties is the very reasonable one that $f(\infty) = 0$.

A theoretical expression for $f(\tau_o)$ can be found from the Anderson-Weiss model of a motionally-narrowed broadening mechanism, by using the information we already possess about the correlation function of the local field at a Ca^{43} spin site. The best fit to our τ_{AB}^{-1} measurements at $\theta = 90°$ indicates that this correlation function is given by:

$$g(\tau) = \frac{\langle\Delta\omega_B^2\rangle_{BA}}{(1+\tau^2/\tau_c^2)}$$

The Anderson-Weiss model finds the free induction decay shape by calculating the slow accumulation of phase using the correlation function of the broadening mechanism, $\omega_p^2\,\phi_{\Delta\omega}(\tau)$. Suppose the kth Ca^{43} spin undergoes a transition from state m to state n and we let $\Delta\omega_{mn}^{(k)}$ be the change

in the diagonal matrix elements of the broadening mechanism (Ca-F dipolar coupling). Then

$$\Delta\omega_{mn}^{(k)} \propto \left(\sum_i A_{ik}^{AB} I_{zi} \right) (m-n) \propto (H_{LB})_k$$

But $\Delta\omega_{mn}^{(k)}$ is the analogue of Anderson's $\Delta\omega_{ij}$, so we have the result that the correlation function $\phi_{\Delta\omega}(\tau)$ appearing in Eq. (31) of reference 46 is just the correlation function of the local field at a Ca^{43} spin site. This is a reasonable result because it is physically obvious that the same fluctuating local field both causes cross-relaxation and contributes to the decay of a transverse Ca^{43} magnetization.

The theoretical curves in Fig. 52 are calculated using the Anderson-Weiss theoretical expression for $\phi(\tau)$, the free induction decay envelope:

$$\phi(\tau) = \exp\left(-\omega_p^2 \int_0^\tau dx\ (\tau - x)\phi_{\Delta\omega}(\tau) \right)$$

where $\omega_p^2 = g(0) = \langle \Delta\omega_B^2 \rangle_{BA}$, and

$$\phi_{\Delta\omega}(\tau)\Big|_{\text{Lorentzian}} = \frac{1}{\left(1 + \tau^2/\tau_c^2\right)}$$

and

$$\phi_{\Delta\omega}(\tau)\Big|_{\text{Gaussian}} = e^{-\tau^2/\tau_c^2} \qquad (99')$$

The asymptotic exponential decay is determined mainly by the spectral density of the correlation function near zero frequency in the rotating frame. Since the gaussian $\phi_{\Delta\omega}(\tau)$ in (99') spreads the spectral density over a wider range near low frequencies, it produces a slower decay of M_B. For our case, the asymptotic decay rates are

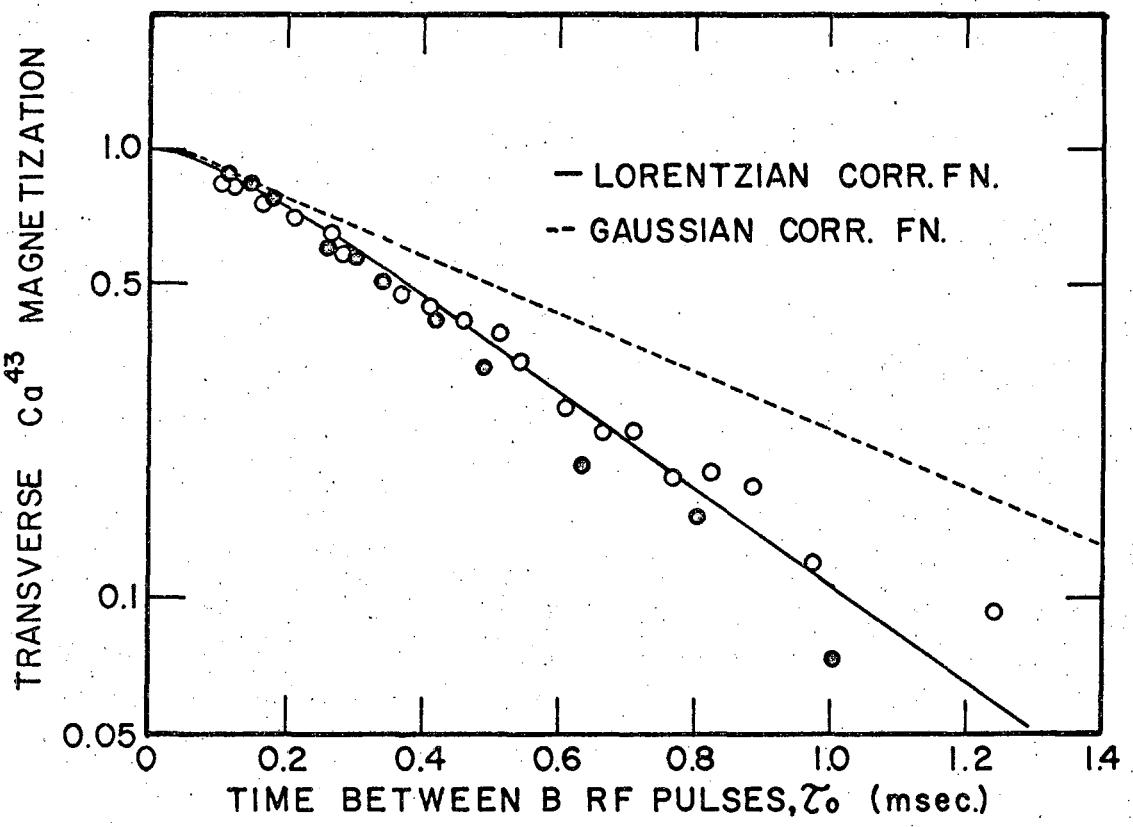

XBL 676-4198

Fig. 52 Free induction decay of Ca^{43} in CaF_2 for $H_o \parallel [110]$; $f_{1B} = 5.5$ kHz, $\tau = 25$ msec, N = 32 B rf pulses; theoretical curves calculated from Anderson-Weiss model using correlation function of local field at Ca^{43} site.

$$\left(\frac{1}{T_2}\right)_{\text{Lorentzian}} = \frac{\pi}{2} \langle \Delta\omega_B^2 \rangle_{BA} \tau_c$$

$$\left(\frac{1}{T_2}\right)_{\text{Gaussian}} = \frac{\sqrt{\pi}}{2} \langle \Delta\omega_B^2 \rangle_{BA} \tau_c$$

D. Experimental Results and Discussion

This experiment requires very good stabilization of the B rf frequency and the laboratory magnetic field, because a small $\Delta\omega_B$ during the time τ_o between pulses can give a spurious contribution to the observed relaxation rate. That is, if during τ_o the B magnetization precesses an angle $\Delta\phi_B = \Delta\omega_B \tau_o$ in the x-y plane, the initial B energy for the succeeding B rf pulse will be multiplied by $\cos \Delta\phi_B$:

$$E_B(n+1) = \cos \Delta\phi_B \; f(\tau_o) \; E_B(\tau, n)$$

Then what is measured using Eq. (99) is $f_{true}(\tau_o) \cos \Delta\phi_B$. The largest drift of f_B during a T_{2B} run was $\Delta f_B \sim 25$ cycles, so $\cos(\Delta\phi_B)$ for $\tau_o = 1$ ms is approximately

$$\cos(\Delta\phi_B) \cong 1 - \frac{(\Delta\phi_B)^2}{2} = 1 - .012$$

(Here we neglect the drift of H_o since it is locked to the Gertsch oscillator which drifts only 1-2 cycles during a run. We assume that larger but short-term fluctuations of H_o average out over the many experimental points taken on each curve.)

This source of experimental error always tends to make T_{2B} look too short. It cannot account for the agreement with a Lorentzian correlation function instead of a Gaussian, because $\Delta\phi_B$ would have to be ~60°, or $\Delta f_B = \text{const} \sim 170$ cps, which is larger than the observed drift, or

error of setting, of f_B. This is probably the source of much of the experimental scatter, however.

The times τ_o were measured with an electronic counter to .1μs, but are actually accurate only to ~± 10μs because of the finite rise and fall time of the B rf pulses at the B rf coil.

η (∞) and ϵ in Eq. (99) were found by averaging 3 values of η for τ_o = 2.0, 2.5, and 3.0 ms $\gg T_{2B}$. The accuracy of setting the laboratory magnetic field parallel to [111] and [110] was $\lesssim \pm 5^\circ$, including the error of the crystal axis.

The slope of the asymptotic exponential decay of M_B defines an effective $T_2(Ca^{43})$. In CaF_2, these measured T_2 values are:

$$T_2([111])\big|_m = (217\pm18)\ \mu\text{sec} ;$$
$$T_2([110])\big|_m = (421\pm47)\ \mu\text{sec}.$$

The calculated values are $T_2([111]) = 216$ μsec, $T_2([110]) = 378$ μsec.

The angular dependence and magnitude of (T_{2B}^{-1}) (slope of the asymptotic part of $f(\tau_o)$) are approximately given by assuming the Anderson-Weiss model with a Lorentzian correlation function for H_{LB}. To see this, suppose we assume that the Gaussian correlation function is actually correct, but add a term caused by random quadrupole splittings:

$$\left(\frac{1}{T_{2B}}\right)_{obs} = \left(\frac{1}{T_{2B}}\right)_{Gauss} + \left(\frac{1}{T_{2B}}\right)_{Q} \qquad (100)$$

Then if we attempt to fit the data in the [111] and [110] directions with Eq. (100), we derive two different values of $(T_{2B}^{-1})_Q$ differing by ~50%:

$$(T_{2B}^{-1})_{Q,[111]} = 1.69\times10^3$$
$$(T_{2B}^{-1})_{Q,[110]} = .95\times10^3 .$$

On the other hand, we could assume that we have an anisotropic contribution to T_{2B}^{-1} from Ca-F coupling, with the theoretical angular dependance but arbitrary magnitude, and add a constant quadrupole contribution. We then find from the [111] and [110] data that $(T_{2B}^{-1})_Q$ is very small but negative, and the magnitude of $(T_{2B}^{-1})_{AB}$ is approximately equal to the Lorentzian contribution. Thus it seems that the quadrupole broadening of the Ca^{43} resonance is very small, especially since we also observe very little quadrupole broadening of the audio resonances.

As mentioned above, spin diffusion should not affect these results, because the time constant τ_{SD} calculated in Appendix A is much shorter than τ. Therefore during the B rf pulse of length τ the entire average number of A spins can communicate with each other and the B spin.

VII. SPIN-LATTICE RELAXATION OF Ca^{43} IN CaF_2

A. Introduction

The neighborhood of a nuclear spin in a cubic crystal is cubic only if all ions of the crystal occupy their equilibrium positions. But thermal vibrations destroy the instantaneous cubic symmetry, giving rise to an interaction between the instantaneous electric field gradient and the nuclear quadrupole moment. Since the time-average field gradient vanishes, the effect of the fluctuating field gradients is to produce relaxation of the nuclear spins toward the lattice temperature. Van Kranendonk has calculated the transition probabilities caused by this process between the Zeeman eigenstates of the nuclear spin in the laboratory magnetic field.[47] Van Kranendonk finds that there exist both $|\Delta m| = 1$ and $|\Delta m| = 2$ processes, which would not conserve a Boltzmann population distribution during relaxation; he also finds that the transition probabilities depend on the angle the laboratory magnetic field makes with the crystalline axes.[47]

The spin-lattice relaxation process of a rare spin species with a quadrupole moment is of particular interest, because it is possible that the relaxation might have to be described by more than one time constant, and because the relaxation time constants might depend on the angle the laboratory magnetic field makes with the crystalline axes. For the case of an abundant spin species with a quadrupole moment in a cubic environment, the equal spacing of the Zeeman energy levels allows mutual spin flips to take place between neighboring abundant spins, because in this process the Zeeman energy in the laboratory magnetic field is conserved. The quadrupolar spin-lattice transition probabilities are anisotropic and tend to set up a non-Boltzmann distribution, but this strong coupling

between neighboring spins tends to restore a Boltzmann population distribution. Thus in the case of an abundant spin species, it is a good approximation to calculate the spin-lattice relaxation by assuming that the population distribution is always Boltzmann during relaxation; this assumption causes the anisotropy and non-exponential behavior of the relaxation to cancel out, leaving a single, isotropic T_1.[48]

In the case of Ca^{43} in CaF_2, the Ca^{++} sites have cubic symmetry and the quadrupole interaction vanishes, so the Ca^{43} eigenstates in the laboratory magnetic field are the equally-spaced Zeeman levels. But the low natural abundance of Ca^{43} means that the average distance between Ca^{43} spins is large, so the rate of mutual spin flips between Ca^{43} neighbors is much lower than for neighboring F^{19} nuclei ($T(\text{flip})^{-1} \propto r_B^{-6}$). Not only is the dipolar coupling between Ca^{43} neighbors very weak, but two Ca^{43} neighbors may be "detuned" from each other considerably at any instant of time by the large local fields produced at each Ca^{43} site by its close F^{19} neighbors. The weak dipolar coupling between Ca^{43} spins is modulated rapidly with a time constant $\tau_c \sim T_{2A}$, so the resulting mutual-spin-flip time for two Ca^{43} spins is given approximately by[33]

$$\frac{1}{T(\text{flip})} \sim \left[\frac{\gamma_B^4 (1-3\cos^2\theta)^2 \hbar^2}{\bar{r}_B^{\,6}} \right] T_{2A} \gtrsim \frac{1}{500 \text{ sec}} .$$

Since the measured spin-lattice relaxation times of Ca^{43} in CaF_2 are $T_1(300°K) \sim 240$ sec and $T_1(355°K) \sim 170$ sec, $T(\text{flip}) \gtrsim T_1(Ca^{43})$, and during the spin-lattice relaxation the Ca^{43} spins may be treated as isolated from each other. Thus Van Kranendonk's transition probabilities should describe the relaxation process of naturally-abundant Ca^{43} in CaF_2, possibly leading to a non-exponential decay and an anisotropic $T_1(Ca^{43})$.

B. Theory of the Method

In the following, we will use T_{1B} to represent a characteristic time of the Ca^{43} spin-lattice interaction. The measurement of $T_1(Ca^{43})$ in CaF_2 observes the spin-lattice relaxation of Ca^{43} indirectly, using the abundant F^{19} nuclei of the sample twice: (1) to polarize the Ca^{43} spins in H_o to a magnetization $M_{Bi} \gg M_{Bo} = \frac{C_B H_o}{T_L}$, and (2) to sample the Ca^{43} magnetization remaining along H_o after it has been allowed to relax toward the lattice temperature for a suitable time. As will be seen below, this method makes use of the facts that for Ca^{43} in CaF_2, we can simultaneously satisfy the requirements:

$$H'_{LA} \ll H_{eB}, \tag{101}$$

$$\tau_{AB} \ll T_{1A}, T_{1B} \tag{102}$$

and

$$\frac{\epsilon \cos^2\theta}{(1+\epsilon)^2} > \left(\frac{1}{\psi_A}\right), \tag{103}$$

where ψ_A is the signal to noise of the F^{19} dipolar signal. Requirement (103) simply states that the F^{19} signal characteristic of the remaining Ca^{43} magnetization must be greater than the noise.

Figure 53 shows the sequence of operations performed to obtain one point on a curve of $M(Ca^{43})$ versus t. First the F^{19} dipolar reservoir is placed in a state of low spin temperature ($(T_{SS})_i \ll T_L$) by the ADRF process. Then a long off-resonance B rf pulse ($\theta = 45°$) with large H_{eB} is applied to the sample. Since $\tau \gg \tau_{AB}$ (H_{eB}), the F^{19} and Ca^{43} spins come to a common spin temperature in the rotating frame. Since ϵ is still relatively small, this common spin temperature is nearly equal to the initial, very low, A dipolar spin temperature. Thus the Ca^{43} magnetization in the rotating frame is much greater than the Ca^{43} magnetization obtained

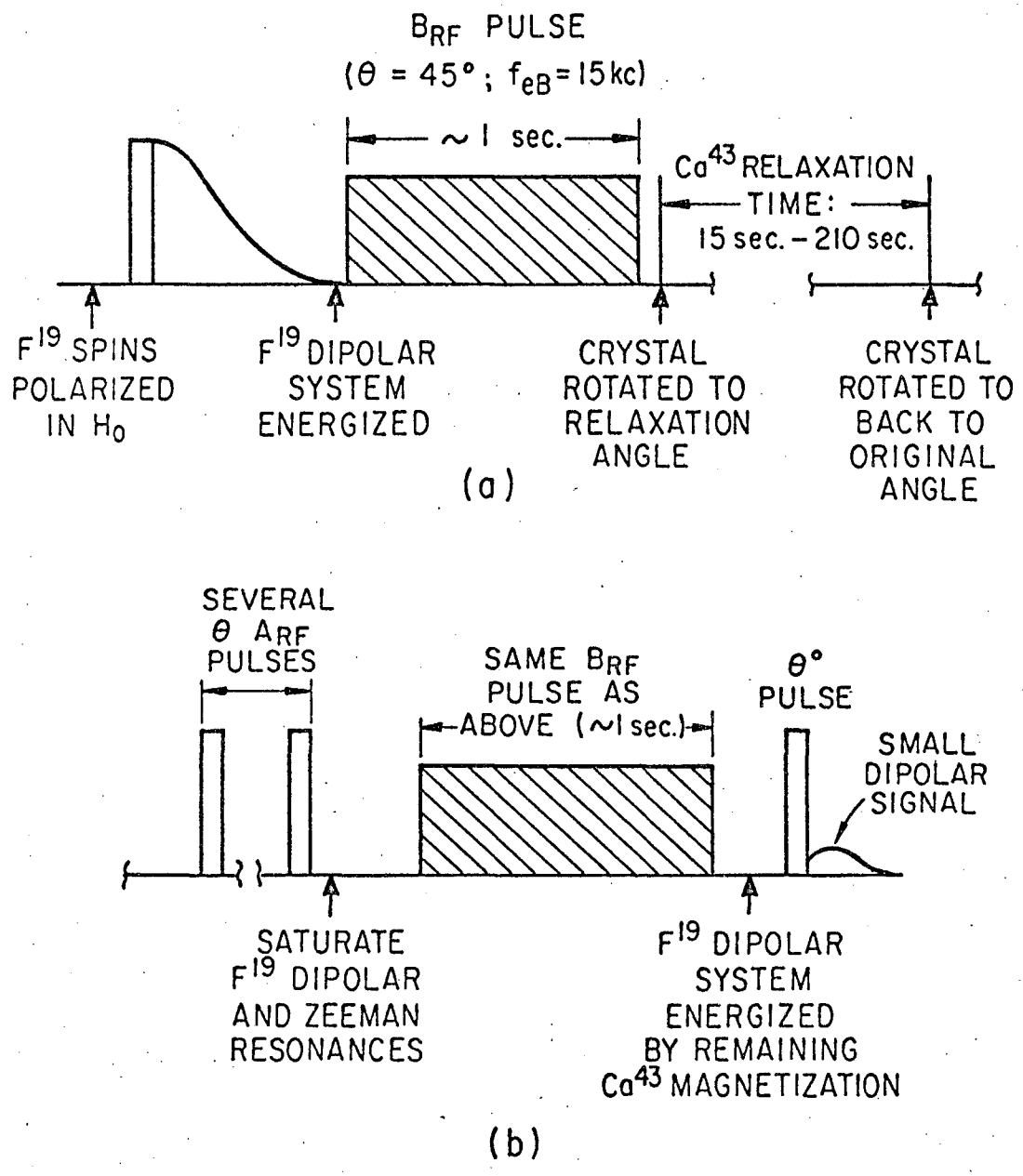

XBL 676-4199

Fig. 53 Experimental procedure for measuring spin-lattice relaxation time $T_1(Ca^{43})$; Fig. 53a shows B spin polarization process, and relaxation period; Fig. 53b shows procedure for sampling remaining B magnetization, $M_B(t_r)$

by allowing the Ca^{43} spins to come into thermal equilibrium in H_o at room temperature. Assuming (102) (which does not quite hold for Ca^{43} in CaF_2), and assuming that the thermal-reservoir model of the cross-relaxation process holds, the initial B magnetization M_{Bi} parallel to H_o after the B rf pulse of length $\tau \gg \tau_{AB}$ is given by:

$$M_{Bi} = \frac{-\cos\theta}{H_{eB}} \left(\frac{\epsilon}{1+\epsilon}\right) E_A(0) = \cos\theta \frac{C_B H_{eB}}{(1+\epsilon)(T_{SS})_i} \tilde{=} \frac{C_B H_o}{T_L} \frac{\cos\theta H_{eB}}{(1+\epsilon)H'_{LA}},$$

since $(T_{SS})_i \tilde{=} T_L(H'_{LA}/H_o)$.

For these measurements, $H_{eB} \approx 52g$, $H'_{LA} \approx .855g$, and $\epsilon \tilde{=} .25$, so that $M_{Bi} \sim 35\ M_{Bo}$, so the Ca^{43} magnetization corresponding to thermal equilibrium with the lattice would give $\sim \frac{1}{30}$ of the F^{19} signal corresponding to the maximum $M_B = M_{Bi}$. We can then say that the Ca^{43} magnetization relaxes essentially toward zero, because our F^{19} signal to noise is not large enough to see this small thermal equilibrium magnetization.

Once the initial Ca^{43} magnetization M_{Bi} is formed by the first B rf pulse, it is allowed to relax toward the lattice temperature for a variable time t_R. The long Ca^{43} relaxation time makes it possible to work with the longest T_2 of the F^{19} (H_o parallel to the [111] direction), but still measure T_{1B} for other angles. It is possible to rotate the crystal quickly to another angle in the laboratory magnetic field for the relaxation time t_R, and then rotate it back to the reference angle just before sampling the remaining Ca^{43} magnetization.

After the relaxation time t_R, the remaining Ca^{43} magnetization is sampled by using the Ca-F double resonance process again. Just before the second long B rf pulse the dipolar and Zeeman reservoirs of the F^{19} system are saturated by applying several 45° A rf pulses to the sample.

These pulses do not affect the Ca^{43} magnetization, but ensure that $E_A(0) = 0$ for the second B rf pulse, and make the errors caused by small amounts of F^{19} Zeeman signal as small as possible. Since the F^{19} dipolar reservoir is now hot, the remaining Ca^{43} magnetization cools it, resulting in a small F^{19} dipolar signal proportional to $M_B(t_R)$. This dipolar signal can be calculated from Eqs. (81) and (82), assuming that $\tau_{AB} \ll \tau$, $E_A(0) = 0$, and

$$E_B(0) = - (M_{Bi} \mathcal{R}(t_R) \cos\theta) H_{eB},$$

where $\mathcal{R}(t_R)$ gives the spin-lattice relaxation of the Ca^{43} magnetization. The small dipolar signal is then (using $S_A \propto E_A$)

$$\frac{S_A(t_R)}{S_{Ai}} = \frac{E_A(t_R)}{E_{Ai}} = \frac{\epsilon \cos^2\theta}{(1+\epsilon)^2} \mathcal{R}(t_R) \quad . \qquad (103')$$

Equation (103') shows that this method of measuring T_{1B} is useful only if the rare spin species is sufficiently abundant, since the signal proportional to $M_B(t_R)$ is of order $\epsilon \cos^2\theta$ times the maximum signal from the A spin species. In general, one cannot arbitrarily increase H_{eB}, since then τ_{AB} becomes very long because the cross-relaxation quantum falls in the wings of the A dipolar spectrum. The competition between requirements (102) and (103) above leads to an optimum H_{eB}.

In the CaF_2 case, where $\tau_{AB} \lesssim T_{1A}$ so that assumption (102) does not hold, and $\tau \gtrsim \tau_{AB}$, we must use the exact solutions of the thermodynamic equations in Appendix E. Assuming $E_B(0) = 0$ for the first B rf pulse, Eq. (E.10) yields $E_B(\tau)$, so that

$$M_{Bi} = \frac{-\cos\theta}{H_{eB}} E_B(\tau) = \frac{-\cos\theta}{H_{eB}} Z_3(\tau)\, E_A(0)$$

$$= \left[\frac{-\cos\theta}{H_{eB}} \left(\frac{\epsilon}{1+\epsilon}\right) E_A(0)\right] \left[e^{-\lambda_- \tau} \frac{}{(1+x)Q} (1-e^{-R_o Q(1+x)\tau})\right]$$

Equation (E.9) also yields the value of $E_A(\tau)$ caused by the remaining Ca^{43} magnetization after time t_R:

$$E_A(\tau, t_R) = \mathcal{R}(t_R) \frac{\epsilon \cos^2\theta}{(1+\epsilon)^2} E_A(0) \left[\frac{e^{-\lambda_- \tau}}{(1+x)Q} (1-e^{-R_o Q(1+x)\tau}\right]^2$$

$$\equiv \mathcal{R}(t_R) \frac{\epsilon\cos^2\theta}{(1+\epsilon)^2} E_A(0)\, K^2(\tau) \qquad (104)$$

The correction factor $K(\tau)$ is given exactly by the following parameters appearing in it, to the extent that the thermodynamic model is correct for $\theta = 45°$. Approximate expressions (accurate to about 3% for $x \leq .2$) are also given ($\epsilon \cong .25$ here):

$$R_o = \frac{(1+\epsilon)}{\tau_{AB}}$$

$$x = \frac{\tau_{AB}}{(1+\epsilon)T_{1A}}$$

$$Q = \sqrt{1-(4x/[(1+\epsilon)(1+x)^2]}$$

$$\lambda_- = R_o(1+x)\frac{(1-Q)}{2} \cong \left(\frac{1}{T_{1A}}\right)\left(1 - \frac{\epsilon x}{(1+\epsilon)}\right)$$

$$R_o Q(1+x) \cong \frac{(1+\epsilon)}{\tau_{AB}} \left(1 - \frac{x(1-\epsilon)}{1+\epsilon}\right)$$

$$\frac{1}{(1+x)Q} \cong \left(1 + \frac{x(1-\epsilon)}{(1+\epsilon)}\right)$$

For this experiment (τ = 1 sec, $\tau_{AB} \approx .5$ sec, $\epsilon \cong .25$, $x \approx .2$, $T_{1A} = 4.3$ sec), $K^2(\tau) \cong 65\%$.

C. Experimental Procedure

The ADRF wave form in Fig. 53a was the same one employed for all other double resonance measurements. The angle θ was set by choosing $\Delta f_B = f_{eB}/\cos\theta$, and adjusting the B rf amplitude to give an audio resonance centered at 15 kHz. The values of θ and f_{eB} are not critical as long as they are constant, since they determine the overall amplitude of the small dipolar signal, not its behavior as a function of t_R. The relaxation time t_R was varied in 30 sec steps from 30 sec to 210 sec for each run, and was timed with a watch. The crystal was rotated by hand at the beginning and end of the time t_R, requiring less than one second for each rotation. The second part of the process, Fig. 53b, was initiated by hand following the rotation back to the reference angle ([111] - direction). Six 45° pulses spaced by ~160 msec were applied to saturate the F^{19} Zeeman and dipolar reservoirs before sampling the remaining Ca^{43} magnetization. The small dipolar signals were amplified in a gain of 30 AC amplifier and sampled with a gated integrator of the Reichert-Townsend type.[40] The DC level from the integrator was displayed on a recorder, the output of which was shorted between sampling events to prevent excessive drift. The largest dipolar signals $S_A(t_R \sim 15$ sec) had a signal to noise of 3 or 4 to 1, in rough agreement with the values expected from Eq. (104).

At each value t_R two zero-signal points were obtained by bringing the B spin system into thermal contact with the relatively hot (room temperature) F^{19} dipolar reservoir three times to destroy any remaining Ca^{43} magnetization, and then using the signal obtained from the sampling

sequence (Fig. 53b) as the zero of signal. Three one-second B rf pulses separated by a time 5 sec ~ T_{1A} (dip.) were applied, which reduced M_B(remaining) by a factor $\lesssim (\frac{\epsilon}{1+\epsilon}) \cos^6\theta = \frac{1}{40}$.

The sequence of operations in Fig. (53) was repeated five times for each value of t_R and the results averaged to yield one point on a graph of $M_B(t_R)$ such as Fig. 54. The error bars in Fig. 54 are the rms error calculated from the deviations from the average of the five measurements. The error in t_R caused by rotation of the crystal and variations of the starting time of the sampling sequence (Fig. 53b) was ±2 sec. The average $M_B(t_R)$ values for each angle and temperature were fitted to an exponential decay law

$$M_B(t_R) = M_B(0)_e^{-t_R/T_{1B}}$$

with an IBM 1620II computer, since the data did not show any repeatable deviations from a single exponential. Figure 55 shows the temperature dependence, anisotropy, and rms error of the Ca^{43} T_1 derived from these least squares fits.

The error of resetting the angle Ω between the crystalline axes and H_o was ±1°. The [111] and [110] directions were determined by measuring the maxima and minima of $T_2(F^{19})$ to ±1°, by looking at the F^{19} Zeeman free induction decay with a constant integrator sampling pulse for a range of Ω. One junction of a copper constantan thermocouple was cemented to the CaF_2 single crystal and the thermocouple voltage between the ice point and the sample temperature was measured with a Moseley recorder. The sample temperature was regulated by heating a stream of inflowing air, the heating current being controlled by a resistance bridge connected to a thermistor on the sample. The temperature was accurate to ±2°C at 82°C, and to ±1°C at 27°C.

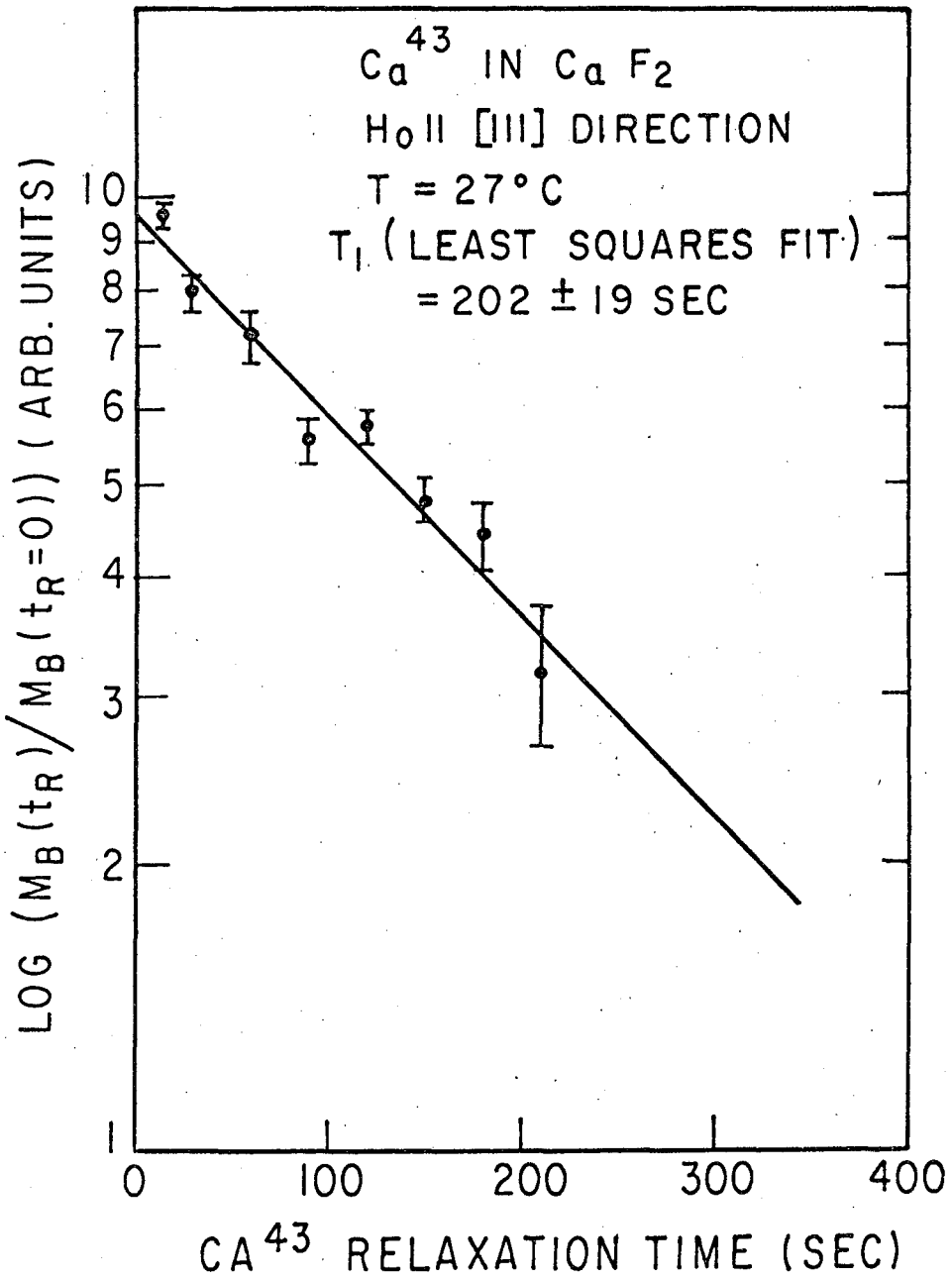

XBL 676-4200

Fig. 54 Typical spin-lattice relaxation of Ca^{43} magnetization in CaF_2; $H_o \parallel [111]$, $T_L = 300°K$, T_{1B} (l.sq.) = 202±19 sec; rms error of the average of five measurements is shown

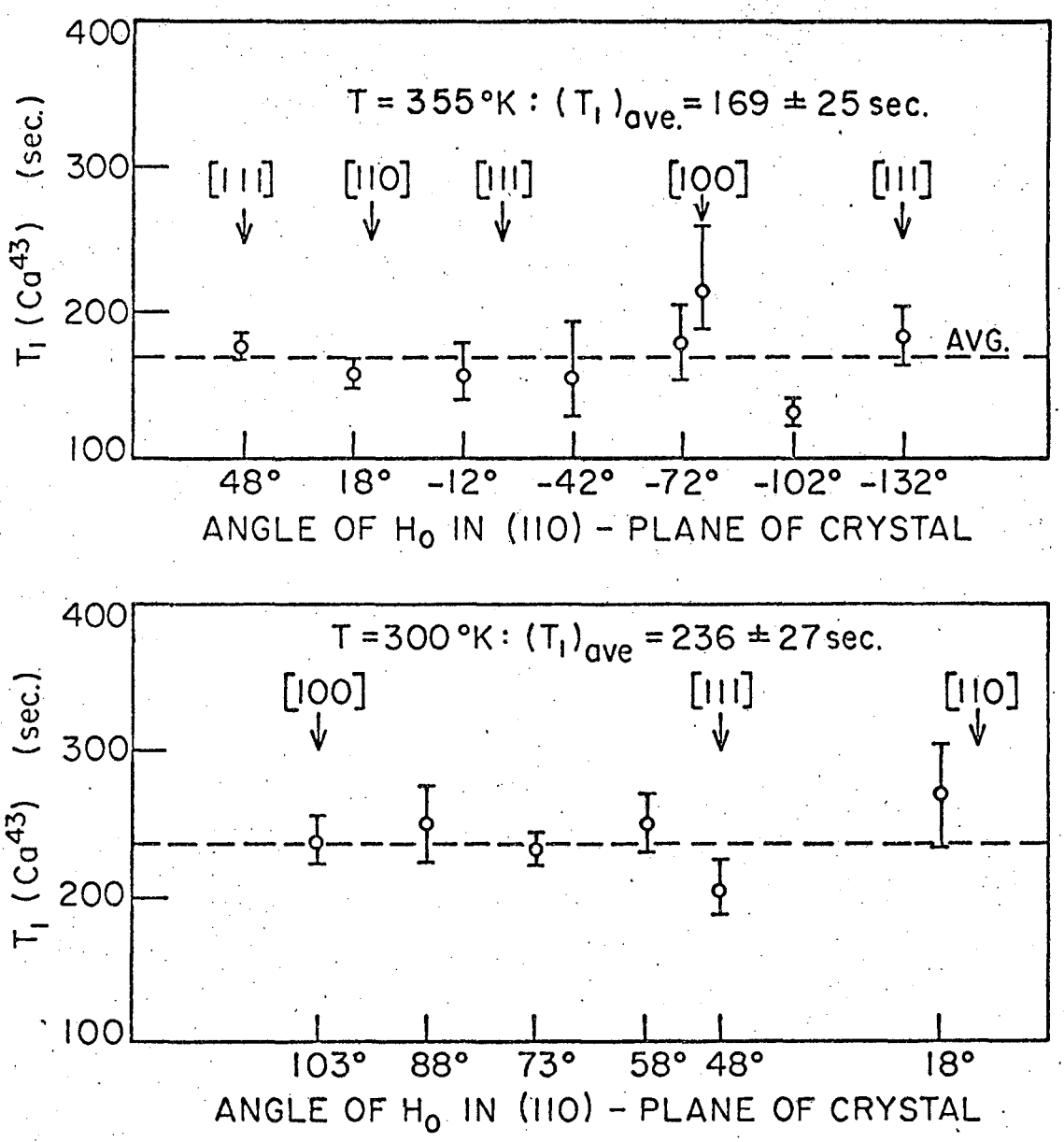

XBL 676-4201

Fig. 55 Angular dependence of spin-lattice relaxation time $T_1(Ca^{43})$ in CaF_2, at two different temperatures; rms error from the least-squares fit is shown

D. Experimental Results and Discussion

As can be seen from Fig. 54, the poor signal to noise ratio may mask a small non-exponential behavior, especially since two nearly equal time constants would be very hard to detect.[10] But as mentioned in Section II.B.3., for $\theta \neq 90°$ there exist small $|\Delta m| = 1$ transition probabilities proportional to $m_B^2 (S + m_B)(S - m_B+1)$, which could lead to a non-Boltzmann initial population distribution for the Ca^{43} spins (corresponding to M_{Bi}). This non-Boltzmann initial distribution would also lead to a non-exponential spin lattice relaxation, and would confuse the interpretation of the relaxation data. But our $\theta \neq 90°$ cross-relaxation measurements confirm that these higher order processes are unimportant. Within the experimental signal to noise, non-exponentiality from both these effects appears to be unobservable.

It has been shown[49] that the nuclear spin-lattice relaxation can be described by a single, isotropic time constant (that is, the Bloch equations apply), even for the case of the quadrupolar relaxation mechanism, under the following set of assumptions:

(1) The ensemble of relaxing nuclei can be considered to interact separately with their molecular environment so the behavior of the whole sample can be found by summing the contributions from the independent relaxing spins.

(2) The Larmor frequency ω_{Bo} of the nuclear spin in the laboratory magnetic field, and the characteristic fluctuation time $1/\omega^*$ of the perturbations on the isolated nuclear spin satisfy the relations:

$$(\omega^*, \omega_{Bo}) \gg \left(\frac{1}{T_{2B}}, \frac{1}{T_{1B}}\right),$$

(3) The high temperature approximation holds,

$$\hbar\omega_{Bo} \ll k\, T_L$$

and (4) The molecular surroundings are isotropic and have a characteristic frequency $\omega^* \gg \omega_{Bo}$.

The theory of reference 5 does not allow us to calculate the effects of both the Ca-F dipolar coupling and the quadrupolar spin-lattice relaxation because the characteristic frequency ω^* of the F^{19} dipolar interactions does not satisfy the criterion $\omega^* \gg \omega_{Bo}$ stated in assumption (4), and also may not satisfy $\omega^* \gg T_{2B}^{-1}$, since $\omega^* \simeq T_{2A}^{-1} \simeq 4\, T_{2B}^{-1} \gg 1$. But since we do not expect any interference to occur between the dipolar broadening and the quadrupolar spin-lattice relaxation, we can use the Wangsness-Bloch theory to calculate the quadrupolar contribution to the T_2 and T_1 of the Ca^{43} resonance, but use the Anderson-Weiss exchange narrowing theory of Section VI.B. to find the magnetic contribution to T_2 of Ca^{43}. The Wangsness-Bloch theory[49] results in $(\frac{1}{T_2})_Q = (\frac{1}{T_1})_Q$, but the quadrupole line width $(\frac{1}{T_2})_Q \simeq (\frac{1}{200})$ sec^{-1} will be completely masked by the much larger nuclear dipole-dipole broadening

$$(T_{2B}^{-1})_{magnetic} \sim 2\times10^3 \text{ sec}^{-1} .$$

If we treat these two perturbations independently as above, the crucial assumption to obtain a single, isotropic T_1 is that the molecular surroundings be isotropic. Although this has not been proved, it seems to be a reasonable assumption and could yield the isotropic single exponential T_1 we seem to observe.

Figure 55 shows the temperature dependence and anisotropy of the Ca^{43} T_1 derived from the least squares fit for each angle and temperature. The data do not show any repeatable anisotropy of the Ca^{43} T_1's although again

we cannot exclude a small anisotropy (10 to 20%), of the order of the experimental noise. The dotted lines represent the average of all data points weighted equally. The expected anisotropy of the Ca^{43} transition probabilities has not been calculated explicitly, although the calculations for the CsCl structure[50] should apply to the CaF_2 case since only the nearest neighbors of the relaxing ion appear in the Van Kranendonk calculation. But it has been shown[51] that for positive ions in alkali halide crystals, an important contribution to the quadrupolar spin-lattice relaxation comes from electric dipole moments induced on neighboring negative ions by long-wavelength optical phonons. Calculation of this mechanism requires knowledge of the optical phonon densities of states, the dipolar polarizibilities of the F^{19} ions, and requires modification of the van Kranendonk theory to include non-equivalent ions.[50] No calculation of the anisotropy of T_1 caused by the induced-dipole mechanism has been made, so even if the anisotropy of the simpler ionic displacement model of Van Kranendonk were known for this crystal structure, the theoretical anisotropy would still neglect the anisotropy of the important induced-dipole mechanism.

For a rough estimate of the expected anisotropy of the Van Kranendonk ionic model we note that for the NaCl lattice Van Kranendonk[47] found that the $\Delta m = \pm 1$ transition probability in the [111] direction was about 50% larger than in the [100], while the $\Delta m = \pm 2$ transition probability was 10% smaller in the [111] than in the [100]. Mieher found for the zincblende lattice a smaller anisotropy: for $\Delta m = \pm 1$ the transition probabilities were 15% smaller for [111] than for [100], while the $\Delta m = \pm 2$ transition probabilities were 4% smaller in [111] than in [100].[48]

Since we observe an exponential spin-lattice relaxation of M_z^B, and anisotropic T_1 for Ca^{43} within experimental error, it is reasonable to

calculate the temperature dependence of the average T_1 of Ca^{43} using the single-exponential, isotropic value for T_1 calculated by Mieher.[48] There is a small difference between the temperature dependence calculated for the Van Kranendonk model, and that for the optical mode relaxation mechanism, which we neglect. The temperature dependence of T_1 is given by the function $1/T_1 = T^{*2}E(T^*)$, where $T^* = (T/\Theta_D)$, and Θ_D is the Debye temperature. For calcium fluoride $\Theta_D = 510°K$, so the calculated ratio of T_1 is given by

$$\frac{T_1(355°K)}{T_1(300°K)} = \frac{(.589)^2}{(.696)^2}\frac{E(.589)}{E(.696)} = .685$$

The experimental value of this ratio, based on the average T_1's of Fig. 55 is in agreement within the experimental error:

$$\frac{T_1(355°K)}{T_1(300°K)} = .72 \pm .13 .$$

The contribution to T_1 of the Ca^{43} from magnetic spin-lattice relaxation through paramagnetic impurities should be very small because of the small magnetic moment and the low abundance of the Ca^{43} spins. The low abundance prevents spin diffusion from carrying the spin energy from the Ca^{43} spin to the paramagnetic impurity. The same paramagnetic impurities will relax both the F^{19} and the Ca^{43} spins, so a rough calculation of the ratios of T_1's of Ca^{43} and F^{19} due to the same paramagnetic impurity is given by (assuming the spin-diffusion-limit case, and assuming the diffusion concept is valid for the widely-separated Ca^{43} spins[52](:

$$\frac{\left(\frac{1}{T_{1B}}\right)}{\left(\frac{1}{T_{1A}}\right)} = \left(\frac{\bar{C}_B}{\bar{C}_A}\right)^{1/4}\left(\frac{D_B}{D_A}\right)^{3/4} = \left(\frac{\gamma_B^2}{\gamma_B^2}\right)^{1/4}\left(\frac{1+\tau^2\omega_A^2}{1+\omega_B^2\tau^2}\right)^{1/4}$$

$$\left[\left(\frac{11.4\ \bar{r}_B}{a}\right)^2 \quad \frac{T_{2F}}{T_2^h(Ca)}\right]^{3/4}$$

$$\leq 4.73\times10^{-5}\left(\frac{1+\omega_A^2\tau^2}{1+\omega_B^2\tau^2}\right)^{1/4},$$

using $T_2^h(Ca) \gtrsim 500$ sec.

Since the observed ratio $\left.\dfrac{\frac{1}{T_{1B}}}{(T_{1A}^{-1})}\right|_{300°K} = 1.8\times10^{-2}$

this would imply:

$$\left(\frac{1+\omega_A^2\tau^2}{1+\omega_B^2\tau^2}\right) = (385)^4 \cong \frac{1+(196)\omega_B^2\tau^2}{1+\omega_B^2\tau^2} \leq 196.$$

Thus it is impossible to find an electronic relaxation time τ which will give agreement between the Ca^{43} and F^{19} relaxation times, if we assume both species of spin are relaxed to the lattice by the same kind of paramagnetic impurity with a Lorentzian spectrum.

VIII. RARE SPIN DOUBLE RESONANCE IN GYPSUM

A. Introduction

A search for rare spin double resonances was made in gypsum ($CaSO_4 \cdot 2H_2O$), using the protons in the waters of hydration as the abundant A spins, and using the ADRF double resonance method. Gypsum has a monoclinic lattice of symmetry C_{2h}^6,[53] so electric field gradients at the nuclear spin sites will not in general vanish. Thus we may expect quadrupole splitting of the Larmor resonance lines of spin species with spin $S > 1/2$. A search was made for possible quadrupolar-split double resonance lines from the following rare spins: deuterium (D), O^{17}, Ca^{43}, and S^{33}.

In gypsum, lengthy searches for the resonances of O^{17} and D in waters of hydration are not necessary, since the waters of hydration are not greatly distorted on going into the gypsum lattice. We can thus infer the approximate D and O^{17} quadrupole splittings from previous measurements on deuterated waters of hydration or free water molecules.[54,55] A study of the quadrupole splittings of naturally-occurring deuterium and O^{17} would be of interest for four reasons: (1) It would demonstrate the ability of the double resonance technique to detect the resonances of spin species about an order of magnitude less abundant than Ca^{43}: D (.0156% abundant) and O^{17} (.037%). (2) It would check the influence of quadrupole splittings on double resonance intensities, A-B cross-relaxation, and audio resonance frequencies. (3) It would allow us to check the validity of the thermal reservoir model of the double resonance process for the case of A spins grouped into strongly interacting pairs. It is possible that spin diffusion rates and A-B cross relaxation might be modified by this strong interaction. (4) It would investigate the ability of audio saturation double resonance

to identify resonance lines observed, and to separate overlapping resonance lines with widely differing effective gyromagnetic ratios γ_{eff} in the rotating frame.

B. Experimental Procedure

The arrangement of A rf and B rf-receiver coils in Fig. 12 was wound on a machined Teflon form and placed in the tip of a glass dewar, unsilvered near the tip. The dewar walls oriented the coils approximately with respect to the magnet pole faces. The audio saturation coil (approximately a Helmholtz pair) was slipped over the outside of the dewar tail, between the dewar wall and the magnet pole faces.

The gypsum sample was a cylindrical single crystal from Ward's of California which was ground to fit snugly inside the B rf-receiver coil. The cylinder axis, measured by cleavage planes of the crystal,[53] was parallel to the (010) plane (Wooster's axes), making an angle of about 99° with Wooster's [100] axis, and about 52.5° with Wooster's [001] axis. A rod was attached to the sample so it could be rotated about its axis in the vertical B rf-receiver coil, perpendicular to H_o. The sample, B rf-receiver coils, and A rf coil were immersed in liquid nitrogen.

The gypsum crystal was irradiated with γ-rays in a Co^{60} bomb to reduce the proton Zeeman T_1 to (59 ± 6) seconds at 77°K. The proton dipolar T_1 was (8 ± 1) seconds at 77°K, probably determined by hindered rotation of the waters of hydration.[56] Rotation about the cylinder axis varies the splitting between the two components of the proton line in gypsum, which is split by the close nuclear dipole-dipole coupling between protons on the same water molecule.[57] Figure 56 shows a proton dipolar free induction decay for the orientation which produces maximum splitting of the proton line. The beats on the signal decrease the signal to noise at the gated

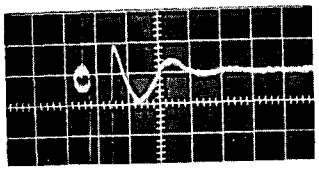

Fig. 56a Proton Zeeman signal at detector; horizontal: 20μsec/div.; vertical: 1 volt/div.; H_o approximately ∥(010) in gypsum

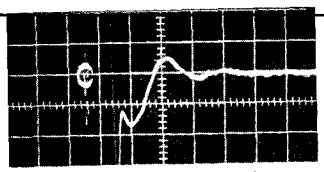

XBB 677-3644

Fig. 56b Proton dipolar signal at detector; horizontal: 20μsec/div.; vertical: 1 volt/div.; H_o approximately ∥(010) in gypsum

integrator output, because it is necessary to use a small sampling capacitor (which increases boxcar drift) and a short sampling time (which decreases the signal size).

Several audio resonance studies were made to determine the effective gyromagnetic ratio in the rotating frame, γ_{eff}. γ_{eff} is defined by

$$\gamma_{eff} = 2\pi f^{o}_{aud}/H_{1B}$$

where f^{o}_{aud} is the center of the audio resonance, and H_{1B} is the rotating component of rf field calculated from the peak B rf amplitude V_B, the inductance of the B rf coil L_B, and the gauss per ampere of the B rf coil $(g/a)_B$:

$$H_{1B} = \left(\frac{V_B}{\omega_B L_B} \right) (g/a)_B .$$

There is at least 10% uncertainty in H_{1B}, and the audio resonances are broadened by the large audio fields necessary to observe an appreciable double resonance effect. Without detailed knowledge of the B spin states between which the transition is taking place, there is no way to calculate γ_{eff} and thus check the value of H_{1B}. (In practice it might be useful to have a test sample of CaF_2 to calibrate the gauss per B rf volt of the B rf coil, using the Ca^{43} double resonance.) Much of the scatter in the γ_{eff} reported here may be caused by not being able to set f_B during each audio resonance exactly at the center of the B resonance line because of the broad resonance lines. Thus

$$f^{o}_{aud} = \frac{1}{2\pi} \sqrt{\gamma^2_{eff} H^2_{1B} + \Delta\omega^2_B} \qquad (105)$$

where $\Delta\omega_B$ is unknown, or Eq. (105) has to be averaged over an inhomogeneous distribution, yielding an asymmetric audio resonance line with a meaningless

center frequency. In the case of an inhomogeneously broadened B resonance, it is probably best to keep $\gamma_B H_{1B}$ large compared to the inhomogeneous line width when measuring γ_{eff}, if possible.

The audio saturation double resonance technique may be useful if the phase-shifted double resonance method yields two overlapping lines. If the γ_{eff} of the two lines are sufficiently different and the audio resonances sufficiently narrow, it may be possible to satisfy the condition (106) for optimum double resonance intensity for species (1),

$$\omega_{aud} = \gamma_{eff}(1)\, H_{1B} \cong \gamma_A H'_{LA} \qquad (106)$$

but have for species (2):

$$\omega_{aud} \ll \gamma_{eff}(2)\, H_{1B} \gg \gamma_A H'_{LA} \qquad (107)$$

or

$$\omega_{aud} \gg \gamma_{eff}(2)\, H_{1B} \ll \gamma_A H'_{LA}\,.$$

Then the double resonance intensity for spin species 2 should be decreased, especially if condition (107) holds, since the audio resonance condition is never satisfied for species 2 at any $\Delta\omega_B(2)$.

C. Results and Discussion

Figure 57 shows the rotation spectra obtained in gypsum at 77°K, in the region 500 kHz to 2.2 MHz. The B rf amplitude was adjusted to be proportional to f_B so $H_{1B} \cong 22$ gauss for all f_B, and the B rf was shifted in phase by 180° every millisecond. These spectra are not simple quadrupole splittings of Zeeman resonance lines, and $\gamma H_o \sim 2\pi\nu_Q$, so calculation of the resonance frequencies must be done exactly. The linewidths vary from 5 kHz to about 50 kHz, and the double resonance time constants from $T_{AB} \cong 9$ sec. to $T_{AB} \cong 80$ sec. Some of the resonances seem to be inhomogeneously

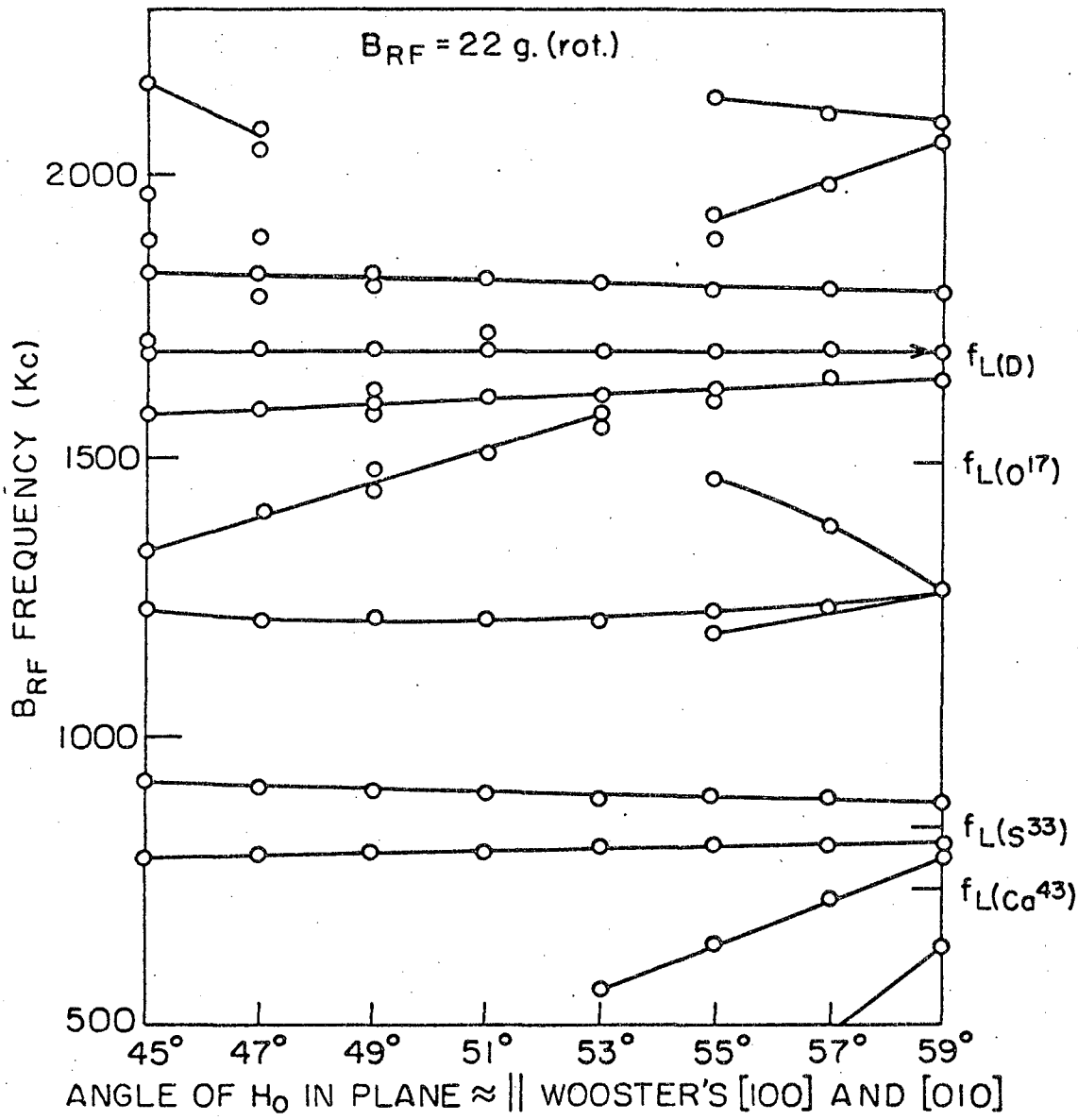

XBL 676-4203

Fig. 57 Orientation dependence of ADRF double resonance spectra in gypsum; Larmor frequencies of rare spin species D, O^{17}, Ca^{43}, and S^{33} are shown

broadened because they have relatively narrow audio resonance lines, but broad resonances as a function of f_B are obtained if a sweep is made, satisfying the audio resonance condition at the line center:

$$(f_{aud})_{sweep} = (f^o_{aud})_{f_b} = f_{Bo} .$$

The most striking feature of the data is the weak resonance line at about 1692 kHz, approximately equal to the Larmor frequency of deuterium ($f_L(D) = 1688.5$ kHz). The signal to noise of this line is about four to one, and at some angles a small splitting (~ 1 - 3 kHz) of this line into two components is observed. This line is interpreted as a double quantum transition between the $m_B = \pm 1$ levels of naturally-occurring deuterium (.0156% abundant). The quadrupole splitting parameters for deuterium in ~~$BaClO_3 \cdot D_2O$ at 77°K have been measured to be~~ $(e^2qQ/h) = 247.17 \pm .05$ kHz and $\eta = .103 \pm .006$,[58] so that $\nu_Q \cong 371$ kHz. Since the D_2O deuterium quadrupole interaction should be close to the HDO deuterium quadrupole interaction in gypsum, we see that the second order frequency shift $\nu_m^{(2)} \sim \nu_Q^2/12\, f_L(D) = .7$ kHz is negligible, and first order perturbation theory should give the deuterium quadrupole splittings accurately. Then the $m_B = \pm 1$ levels of D are displaced equally by the quadrupole interaction, and to first order the energy difference $(E_{-1} - E_{+1}) = 2hf_L(D)$. Thus in a double quantum transition the two quanta absorbed will have frequency $\nu = f_L(D)$ to first order. The signal corresponding to the double quantum transition is large because all four inequivalent deuterium sites in the gypsum unit cell may contribute to it equally in spite of variations in quadrupole splitting from site to site. An exact diagonalization of the deuterium Hamiltonian shows a small upward shift of the $(E_{-1} - E_{+1})$ energy difference for reasonable ν_Q, and the observed splitting is probably caused by magnetic interaction with the

neighboring protons on the DHO molecule, which causes a splitting varying with orientation between 0 and 8.74 kHz. The D^2 transition could not be observed when the proton line splitting was largest, probably because of poor signal to noise.

The intensity of this kind of double quantum transition has been calculated by Hughes and Grabner.[59] They find that the intensity of the double quantum transition is as large as the ordinary first order transitions ($\Delta m = \pm 1$) if

$$[-\hbar\omega + (E_o - E_{+1})] \approx \langle -1|V_o|\ 0\rangle\ , \qquad (107')$$

where

$$V_o = -\gamma_B \hbar\, H_{1B}\, S_x\ .$$

Since the observed transitions are always near $\omega = 2\pi f_L(D)$, then condition (107') becomes (assuming $\eta = 0$, $H_{1B} = 26$ gauss, and $\gamma(D)/2\pi = .654$ kHz/g).

$$(\Delta f)_s = \frac{\nu_Q}{2}\left(\frac{3\mu^2-1}{2}\right) \sim \frac{\gamma_D}{2\pi}\ \frac{H_{1B}}{\sqrt{2}} \cong 12 \text{ kHz},$$

where μ is the cosine of the angle between H_o and the z principal axis of the field gradient tensor. The double quantum transition intensities are also larger because they are half as wide as the first order transitions.

The first-order quadrupole satellites corresponding to this double-quantum transition have not been observed, probably because of poor experimental signal to noise. There are four physically inequivalent deuterium sites in the gypsum unit cell, and all the deuterium sites may contribute to the double quantum transition. Then if each of the first-order transitions has a different frequency and is at least twice as broad as the double-quantum transition, it is reasonable to divide the signal to noise of the

first order transitions. This factor would reduce the experimental signal to noise to 1/2 to 1, making these lines unobservable. The first-order satellites might also be much broader because of the crystalline imperfections, which do not affect the double-quantum transitions.

Other prominent features of the spectra in Fig. 57 are the sets of narrow lines (H.W.H.M. ~ 5 to 10 kHz) symmetrically located around $f_B \cong 1715$ kHz and $f_B \cong 858$ kHz. An attempt was made to attribute the upper set of lines to deuterium or O^{17} in water molecules of gypsum, but the large "second order shift" of these lines from $f_L(D)$ or $f_L(O^{17})$ required us to assume ν_Q was were several times as large as previously measured values.[54,55,58] An exact diagonalization (using an IBM 7094 computer) of the S = 1 and S = 5/2 Hamiltonians for arbitrary quadrupole frequency and principal axes as measured earlier yielded lines whose shape did not agree with these lines. The four inequivalent deuterium sites and the two inequivalent O^{17} sites also yielded many more theoretical lines than the experimental ones to be explained.

The lines centered at $f_B \cong 1715$ kHz are broader than the lines centered at $f_B \cong 858$ kHz, and are at almost twice the frequency. It is possible that the upper lines are first order transitions between two B spin eigenstates and the lower lines correspond to two-quantum transitions between the same eigenstates. The γ_{eff} measured for the upper pair of lines varied from .05 kHz/gauss to .133 kHz/gauss, while γ_{eff} for the lower lines was about .19 kHz/gauss. It is likely that these are Ca^{43} lines because of their low γ_{eff}, high intensity, and narrow width.

The remaining lines in Fig. 57 are much broader and have γ_{eff} in the range from .5 kHz/gauss to 2 kHz/gauss. The breadth of these lines may introduce appreciable error into the measured γ_{eff}, although it is difficult

to say whether this is H_{1B} broadening or inhomogeneous broadening. These are probably S^{33} lines, since the sulphate tetrahedra are known to be distorted in gypsum,[60] and the lines are intense.

An attempt was made at $\Omega = 59°$ to use audio saturation to separate two broad , overlapping resonances located at 2063 and 2080 kHz. The resonance with lower γ_{eff} at 2063 kHz was narrowed from 12 kHz to 5 kHz by using audio saturation rather than phase shifting the B rf. The background caused by the 2080 kHz resonance was still unimportant. But when the audio resonance condition was satisfied for the 2080 kHz resonance, the line was still broad and some background from the 2063 kHz was visible. In conclusion, we have seen resonances in gypsum from naturally-occurring deuterium, and probably from naturally-occurring Ca^{43} and S^{33}. For initial searches it seems best to use phase-shifted B rf for simplicity and because the resonance lines are broader. But the audio saturation technique can be used to help distinguish overlapping resonances, to narrow double resonance lines for more accurate measurements, and to measure the gyromagnetic ratio in the rotating frame, γ_{eff}. Not enough is known about the B spin eigenstates in gypsum either to calculate the expected γ_{eff} or double resonance sensitivity, so no conclusions can be drawn about the importance of spin diffusion among closely coupled proton pairs.

IX. CONCLUDING REMARKS

A. Suggestions for Further Work

The Clough-method evaluation of the cross-relaxation correlation function should be investigated in a case where the distortion of the cross-relaxation spectrum from the exponential form is larger for larger f_{eB} than in CaF_2. This would require larger A-B dipolar interaction and longer τ_c; both these criteria would be satisfied for the case of larger γ_B and smaller γ_A.

If γ_A is smaller and γ_B is larger, the first-order perturbation theory would not be as good, and second order effects might become detectable. Therefore, it would be interesting to repeat the experiments of Lurie and Slichter, but use the pulsed method of evaluating the cross-relaxation parameters ϵ and τ_{AB} for several values of θ. They reported evidence of a second exponential in the cross-relaxation process, but perhaps their data would be completely explained by the assumption of an exponential cross-relaxation spectrum.

Dr. Russell Walstedt has suggested the study of isotropic exchange couplings in CaF_2 type crystals, by measuring the cross-relaxation rates of positive ions heavier than Ca^{++}. For H_o parallel to the [100] direction, $\langle \Delta\omega_{AB}^2 \rangle_{BA}$ drops to about 3% of its value in the [111] direction, so contributions to τ_{AB}^{-1} from exchange couplings may be detectable.

Work should be done on the measurement of cross-relaxation parameters and T_1 of a rare B spin species, when $T_{1B} \lesssim \tau_{AB}$. Presumably no double resonance heating would be necessary for $T_{1B} \ll \tau_{AB}$, and if $T_{1B} \lesssim \tau_{AB}$, perhaps applying larger and larger audio fields during double resonance could help to separate the T_{1B} and τ_{AB} contributions.

It would be interesting to study ADRF double resonance in a sample with several A spin species, such as KDP (KH_2PO_4). It might be possible to study cross relaxation between the A and A' dipolar reservoirs, by doing ADRF on the A species and immediately remagnetizing on the A' species. It would be interesting to see what change in the double resonance sensitivity for a rare B spin occurs, if there are two A spin species.

For the case of a quadrupolar-split B spin transition (as in gypsum), the thermodynamic reservoir model of the A-B cross-relaxation process and the influence of the B spin states on γ_{eff} should be checked. It would also be interesting to measure the T_2 of a quadrupolar-split transition using pulsed double resonance.

B. Conclusions

A detailed study of audio saturation double resonance and pulsed double resonance following adiabatic demagnetization in the rotating frame has shown that these two methods of doing double resonance complement each other nicely. If inhomogeneous broadening of the rare spin resonance line is smaller than the B rf field, audio saturation can be used to locate the B spin resonance line center accurately, to separate dipolar broadening from other broadening mechanisms of the B resonance line, to measure H_{eB} and θ in the rotating frame, to identify quadrupolar-split double resonance lines, and to measure the maximum double resonance rate ϵ/τ_{AB}. The pulsed double resonance method has been used to study the oscillations associated with the approach to equilibrium of the F^{19} dipolar system, to study the validity of a thermal reservoir model of the A-B cross-relaxation process, to make the most accurate and independent measurements of the cross-relaxation parameters ϵ and τ_{AB}, and to measure the free induction decay of a rare

spin species indirectly. If the B spin heat capacity is large enough, and the B spin-lattice relaxation time T_{1B} is long compared to τ_{AB}, the pulsed method can be used to measure T_{1B}.

The thermal reservoir model of the double resonance process, using first-order time dependent perturbation theory, is accurate for Ca^{43} in CaF_2 to about 5%, even for $\theta \neq 90°$. The cross-relaxation spectrum of the F^{19} dipolar reservoir is accurately exponential in the wings, and the major broadening mechanism of the Ca^{43} resonance line in CaF_2 is motionally narrowed dipolar broadening by F^{19} neighbors. The Ca^{43} quadrupolar spin-lattice relaxation mechanism is not greatly affected by the lack of a Ca^{43} spin temperature during relaxation, within the experimental error. No conclusive evidence for spin diffusion weakening of double resonance sensitivity could be found for Ca^{43} in CaF_2.

In gypsum ($CaSO_4 \cdot 2H_2O$), a weak double quantum transition of naturally-occurring deuterium (.0156% abundant) was observed. Other double resonance lines were observed which were tentatively identified as Ca^{43} and S^{33} lines, on the basis of audio saturation measurements of γ_{eff}.

In conclusion, a digital computer can be a great aid in analyzing the dynamic of nuclear double resonance. Most of the work in this thesis would have been impossibly laborious without a computer.

ACKNOWLEDGEMENTS

I wish to thank Professor Erwin L. Hahn for financial support, constant encouragement, and good advice during the course of this research. During the early stages of this work Dr. Russell E. Walstedt contributed many good ideas, in particular the method of measuring T_{1B}, and the possibility of audio saturation double resonance. I gratefully acknowledge stimulating discussions with Professor R. T. Schumacher, and Drs. G. W. Leppelmeier, D. E. MacLaughlin, S. A. Miller, R. E. J. Sears, and R. E. Slusher, and with J. Koo, S. McCall, L. W. Riley, and . M. Schwab.

I am very grateful to my wife, Beverley Bogue McArthur, for typing the rough draft of this thesis, for cheerfully bearing many annoyances and hardships during this research, and for her constant encouragement.

I wish to thank the Woodrow Wilson Foundation for a fellowship during my first year of graduate study, and the National Science Foundation for a Graduate Fellowship during most of the rest of my graduate study. This research program was also supported by grants from the National Science Foundation, the Office of Naval Research, and the United States Atomic Energy Commission through the Inorganic Materials Research Division of the Lawrence Radiation Laboratory. I would also like to thank the Computer Center of the University of California at Berkeley for a grant of computer time.

APPENDIX A

SPIN DIFFUSION AMONG A SPINS

During the double resonance process, disorder is put into the lattice of ordered A spins at randomly located B spin sites. But the dipole-dipole interaction between nuclear spins is a short-range interaction ($H_{dip} \sim \frac{\mu}{r^3}$), so that each B spin affects only its closest A neighbors directly. In fact, the transition probability between A dipolar energy levels will be proportional to the square of the A-B dipolar perturbation,[52] so the strength of the direct double resonance coupling will be proportional to $(1-3\cos^2\theta_{ik})^2/r_{ik}^6$ (here r_{ik} is the distance between the B spin k and the particular A neighbor i it is perturbing). Because of the short range of this direct interaction we must rely on spin diffusion between abundant A neighbors to carry the disorder from the closest A spins out to the rest of the A spins far from the B spin.

To get some feeling for the orders of magnitude involved, we may consider the case of Ca^{43} (.13% abundant) in CaF_2. The average number of F^{19} spins per Ca^{43} spin is about 1540, which occupy a sphere of CaF_2 with radius r = 7.2a (a = F^{19}-F^{19} distance in the cubic lattice of fluorine nuclei in CaF_2). As H_o is rotated with respect to the crystalline axes in CaF_2, the strongest A-B dipolar coupling occurs for the laboratory magnetic field (H_o) parallel to the [111] direction. In this direction about 95% of the A-B coupling ($\sim \sum_i (1-3\cos^2\theta_{ik})^2/r_{ik}^6$) is contributed by the eight fluorine nearest neighbors of the Ca^{43} at a distance $\left(\frac{\sqrt{3}}{2}\right)$ a $\tilde{=}$ .866a (See Fig. 2).[61] If we include the additional 24 second neighbor fluorines at a distance $(\sqrt{11}/2)$ a $\tilde{=}$ 1.66 a, we see that each Ca^{43} interacts directly with only about 32 fluorine neighbors, or $(32/1540) \approx 2\%$

of the average number per Ca^{43} spin. Clearly the spin diffusion process between A spins will be involved if we see double resonance signals corresponding to more than a few percent decrease in the A dipolar signal during the A spin-lattice relaxation time ($T_{1A} \sim 4$sec in CaF_2), because each Ca^{43} must destroy an appreciable amount of the order at all 1540 of the A spins associated with it on the average.

An approximation often used to describe this spin diffusion problem[2,62-64] is to neglect any anisotropy of diffusion and to use a diffusion equation to describe the change of a spatially-varying spin polarization (or spin temperature):

$$\frac{\partial \beta_A(\vec{r},t)}{\partial t} = D \nabla^2 \beta_A(\vec{r},t) - C \sum_n |\vec{r}-\vec{r}_n|^{-6} \beta_A(\vec{r},t) \qquad \text{(A-1)}$$

where

$$C = \left(\frac{3}{8\sqrt{2\pi}}\right)\left(\frac{b}{a}\right)^3 \langle \Delta\omega_B^2 \rangle_{BA} \tau_c \ ,$$

where b is approximately equal to the distance from a B spin to its nearest A neighbor, n ranges over the B spin sites, and $\beta_A \equiv \left(\frac{1}{T_A(r)}\right)$. Lowe and Gade have shown that D is quite isotropic for a simple cubic lattice.[15] The description of the A spins by a spin temperature necessarily means that the spin temperature must not vary too rapidly in space, because we must be able to divide the crystal up into small regions, each of which contains a "macroscopic" number of A spins at nearly the same temperature. Because of the anisotropy of the A-B interaction, and because at most only about 30 (and perhaps as few as 8) A spins interact with each B spin directly in CaF_2 it does not seem likely that a spin temperature can be used to describe the double resonance process close to the B spin. Although

the spin temperature approximation may be a useful one for distances far from the B spin, the question of how best to describe the double resonance process close to the B spin remains open.

It might be thought that the symmetry of CaF_2 would allow us to select only certain F^{19} neighbors of the Ca^{43} and do an exact quantum-mechanical calculation of their eigenstates to treat this problem. Then one could perhaps find the initial absorption of energy from A-B coupling by this subsystem. But for H_o parallel to [111], even though the Ca-F coupling is so anisotropic that 2 of the F^{19} neighbors interact 9 times as strongly with the Ca^{43} spin as do the other 6 F^{19} neighbors, each of these 2 F^{19} neighbors is coupled strongly to at least 12 other F^{19} neighbors. On the other hand, for H_o parallel to [111], not only is each F^{19} spin coupled to many other F^{19} spins (~7 to 8), but the Ca-F coupling is very isotropic so we must consider the direct interaction of many "F^{19} subsystems" with the Ca^{43} spin.

It may be that in a monoclinic system or one involving relatively isolated water molecules, such as gypsum ($CaSO_4 \cdot 2H_2O$), one could choose such a subsystem of A spins to treat quantum-mechanically.[65,66]

SPIN DIFFUSION AND MAXIMUM DOUBLE RESONANCE RATES

To obtain a very crude physical feeling for the possible effect of spin diffusion on the double resonance process we can use the solution of the diffusion equation for a delta-function of heat input at the origin:[67]

$$\beta_A(r,t) \propto [(\sqrt{\pi}\ \rho)^{-3} \exp(-R^2/\rho^2)]$$

where $$\rho(t) = \sqrt{4D\ t},$$

and $$R = x^2+y^2+z^2.$$

To make this very crude estimate we use only the Gaussian spatial dependence of the solution, and require that $\rho(\tau_{SD}) = r$, where r is the radius enclosing the average number of spins per B spin:

$$\rho(\tau_{SD}) = r = \sqrt{4D\,\tau_{SD}} \quad .$$

Then in a time τ_{SD} all the A spins will be appreciably influenced by the B spin at the origin. This yields

$$\tau_{SD} = \frac{r^2}{4D}$$

For H_o parallel to the [111] direction in CaF_2[15], $D \cong 3.4\times10^{-12}$, so $\tau_{SD} \cong 3.3$ msec. Thus for $\tau_{AB} \lesssim \tau_{SD}$, spin diffusion might lower the observed cross-relaxation rates.

APPENDIX B

SIMPLIFIED DERIVATION OF THE MASTER EQUATION

The simplified derivation of the master equation given in this appendix assumes that we are only interested in the change of expectation values of the zero-order parts of the Hamiltonian. If O_1 and O_2 are two commuting parts of the zero-order Hamiltonian which are coupled by the perturbation, and we work in a representation in which O_1 and O_2 are diagonal, we see:

$$\langle O_1 \rangle = \mathrm{Tr}\,\{\rho\, O_i\} = \sum_n \rho_{nn}\,(O_i)_{nn} \quad (i = 1,2) \tag{B.1}$$

and

$$\frac{d\langle O_i \rangle}{dt} = \mathrm{Tr}\,\{\frac{d\rho}{dt}\, O_i\} = \sum_n (\frac{d\rho}{dt})_{nn}\,(O_i)_{nn} \quad (i = 1,2)\,.$$

The spin temperature assumption for the density matrix leads to such a diagonal density matrix.

Equation (18) can be formally solved by iteration:

$$\rho^*(t+\Delta) = \rho^*(t) - i\int_t^{t+\Delta} dt' \,[\mathcal{H}^*(t'),\, \rho^*(t)]$$

$$+ i^2 \int_t^{t+\Delta} dt' \int_t^{t'} dt'' \left[\mathcal{H}^*(t'),[\mathcal{H}^*(t''),\, \rho^*(t'')]\right]\,. \tag{B.2}$$

The observable quantities of interest are $\langle \mathcal{H}_{SS} \rangle$ and $\langle S_z \rangle$, where both of these operators commute with $\rho^*(t)$ and $\mathcal{H}_o$. But if Eq. (B.2) is used to calculate either of these expectation values, the term linear in $\mathcal{H}^*$ does not contribute: using (16), (17) and the fact that $[\mathcal{H}_o,\, \rho_R] = 0$ gives

$$\frac{d}{dt}\langle O\rangle = \mathrm{Tr}\,\{O\rho_R\}$$

$$= \mathrm{Tr}\left\{O\left(-i[\mathcal{H}_o,\ \rho_R] + e^{-i\mathcal{H}_o t}\,\frac{d\rho^*}{dt}\,e^{+i\mathcal{H}_o t}\right)\right\}$$

$$= \mathrm{Tr}\left\{O\ \frac{d\rho^*}{dt}\right\}.$$

But because

$$\mathrm{Tr}\,\{BA\} = \mathrm{Tr}\,\{AB\}\ ,$$

the term linear in $\mathcal{H}^*$ in (B.1) vanishes:

$$-i\int_t^{t+\Delta} dt'\ \mathrm{Tr}\left\{O\,[\mathcal{H}^*(t'),\ \rho^*(t)]\right\}$$

$$= -i\int_t^{t+\Delta} dt'\ \mathrm{Tr}\left\{\mathcal{H}^*(t')\,[\rho_R(t),\ O]\right\} = 0$$

Then if we neglect the linear term in (B.1) and let $\Delta \ll \tau_{AB}$, where τ_{AB} is the cross relaxation time constant, we can write an approximate expression for the derivative of ρ^*:

$$\frac{d\rho^*}{dt} \simeq \frac{\rho^*(t+\Delta) - \rho^*(t)}{\Delta}$$

$$= \frac{(-i)^2}{\Delta}\int_t^{t+\Delta} dt' \int_t^{t'} dt''\ \left[\mathcal{H}^*(t''),\ [\mathcal{H}^*(t''),\ \rho^*(t'')]\right] \tag{B.3}$$

If Δ is sufficiently short compared to τ_{AB} we only need to calculate the lowest order contribution of $\frac{d\rho^*}{dt}$; but t" lies between t and t+Δ, so we can use equation (B.2) to relate $\rho^*(t'')$ to $\rho^*(t)$:

$$\rho^*(t'') \cong \rho^*(t) + \text{items proportional to } \mathcal{H}^*,\ (\mathcal{H}^*)^2$$

Since we are interested in the lowest order change in $\rho^*(t)$ (since $t \ll \tau_{AB}$ and we are calculating the derivative) then for our purposes $\rho^*(t'') = \rho^*(t)$. Thus Eq. (B.3) reduces to

$$\frac{d\rho^*}{dt} \cong \frac{1}{\Delta} \int_t^{t+\Delta} dt' \int_t^{t'} dt'' \left[\mathcal{H}^*(t'), [\mathcal{H}^*(t''), \rho^*(t)] \right]. \quad \text{(B.4)}$$

We will only be interested in the equations for expectation values of operators O that commute with $\mathcal{H}_o$, so let us calculate $\frac{d}{dt}\langle O \rangle$ because an important simplification occurs in (B.4) if we can use the properties of the Tr { }, and the random variation of $\mathcal{H}^*(t)$. Using Tr {BA} = Tr{AB}, $[\mathcal{H}_o, O] = 0$ and $[\rho^*, O] = 0$, we have

$$\frac{d}{dt}\langle O \rangle = -\frac{1}{\Delta} \int_t^{t+\Delta} dt' \int_t^{t'} dt'' \, \mathrm{Tr} \left\{ O \left[\mathcal{H}^*(t'), \left[\mathcal{H}^*(t''), \rho^*(t) \right] \right] \right\}$$

$$= -\frac{1}{\Delta} \int_t^{t+\Delta} dt' \int_t^{t'} dt'' \, \mathrm{Tr} \left\{ \left[O, \mathcal{H}^*(t') \right] \left[\mathcal{H}^*(t''), \rho^*(t) \right] \right\}$$

$$= -\frac{1}{\Delta} \int_t^{t+\Delta} dt' \int_t^{t'} dt'' \, \mathrm{Tr} \left\{ \left[O, \mathcal{H}^*(0) \right] \left[\mathcal{H}^*(t''-t'), \rho^*(t) \right] \right\} \quad \text{(B.5)}$$

or

$$\frac{d\rho^*}{dt} \cong - \frac{1}{\Delta} \int_t^{t+\Delta} dt' \int_t^{t'} dt'' \; \mathrm{Tr} \left\{ o \left[\mathcal{H}^*(0), [\mathcal{H}^*(t''-t'), \rho^*(t)] \right] \right\} \tag{B.6}$$

The trace in (B.5) is the correlation function of the random local field at a B spin site, at times t' and t". This local field must have a correlation time of the order of T_{2A} since mutual spin flips between neighboring flourine nuclei change it. What we have shown in Eq. (B.6) is that this correlation function depends only on the difference of the two times t' and t". If we define

$$t' = t'' + \tau \; ,$$

Eq. (B.6) can be rewritten, after a change of variable:

$$\frac{d}{dt} \langle O \rangle \cong - \frac{1}{\Delta} \int_t^{t+\Delta} dt' \int_0^{t'-t} d\tau \; \mathrm{Tr} \left\{ o \left[\mathcal{H}^*(0), [\mathcal{H}^*(-\tau), \rho^*(t)] \right] \right\} \tag{B.7}$$

But if $\Delta \gg (t'-t) \gg \tau_c$, the integral over τ in (B.7) approaches a constant independent of t; and the first integral can be evaluated:

$$\frac{d}{dt} \langle O \rangle \cong - \int_0^{\infty} d\tau \; \mathrm{Tr} \left\{ o \left[\mathcal{H}^*(0), [\mathcal{H}^*(-\tau), \rho^*(t)] \right] \right\} . \tag{B.8}$$

This is the result obtained by Provotorov and Abragam.[23,25]

APPENDIX C

EVALUATION OF CROSS-RELAXATION CORRELATION FUNCTIONS

Using the formal expansion[68] for $\mathcal{H}_{1x}(\tau)$ and (29), (30) we have

$$g_x(-\tau) \cong \mathrm{Tr}\left\{\mathcal{H}_{1x}\left(\mathcal{H}_{1x} - i\tau\left[\mathcal{H}_{SS}, \mathcal{H}_{1x}\right] + \frac{i^2\tau^2}{2!}\left[\mathcal{H}_{SS}, \left[\mathcal{H}_{SS}, \mathcal{H}_{1x}\right]\right]\right)\right\}$$

$$= \mathrm{Tr}\left\{\mathcal{H}_{1x}^2\right\} - i\tau\ \mathrm{Tr}\left\{\mathcal{H}_{SS}\left[\mathcal{H}_{1x}, \mathcal{H}_{1x}\right]\right\} + \frac{\tau^2}{2!}\ \mathrm{Tr}\left\{\left[\mathcal{H}_{SS}, \mathcal{H}_{1x}\right]^2\right\},$$

$$= \mathrm{Tr}\left\{\mathcal{H}_{1x}^2\right\}\left(1 - \tau^2\left[-\frac{1}{2}\ \mathrm{Tr}\left\{\left[\mathcal{H}_{SS}, \mathcal{H}_{1x}\right]^2\right\} / \mathrm{Tr}\left\{\mathcal{H}_{1x}^2\right\}\right]\right).$$

By a rotation on the B spins, $\mathrm{Tr}\left\{\mathcal{H}_{1x}^2\right\} = \mathrm{Tr}\left\{\mathcal{H}_{1z}^{AB\,2}\right\}$.

Thus

$$g(0) = \mathrm{Tr}\left\{\mathcal{H}_{1Z}^2\right\}$$

$$\frac{1}{\tau_c^2} = -\frac{1}{2}\ \frac{\mathrm{Tr}\left\{\left[\mathcal{H}_{SS}, \mathcal{H}_{1x}\right]^2\right\}}{\mathrm{Tr}\left\{\mathcal{H}_{1x}^2\right\}}$$

Using expressions (7) and (9) and explicitly evaluating traces over the A and B spin systems gives the following values of g(0):

$$g(0) = \frac{\bar{\alpha} I(I+1) S(S+1)}{9} N_B \sum_i \left(A_{ik}^{AB}\right)^2$$

$$= N_B\, \bar{\alpha}\ \frac{S(S+1)}{3}\ \langle \Delta\omega_B^2 \rangle_{BA}, \quad \bar{\alpha} = \mathrm{Tr}\{1\}$$

where the summation index i ranges over the A neighbors of a B spin, and $\langle \Delta\omega_B^2 \rangle_{BA}$ is the Van Vleck second moment of the B spin absorption line caused by A-B dipolar coupling. Evaluation of the lattice sums yields the following approximate expression for $\langle \Delta\omega_B^2 \rangle_{BA}$ for Ca^{43} in CaF_2:

$$\langle \Delta\omega_B^2 \rangle_{BA} = \frac{1}{3} \frac{I(I+1)\gamma_A^2\gamma_B^2\hbar^2}{a^6} \left[38.93 - 37.35\,(\alpha^4+\beta^4+\gamma^4) \right] \qquad (C.1)$$

Here a is the flourine-flourine distance, and α, β, and γ are the direction cosines of the laboratory magnetic field H_o with respect to the cubic crystalline axes of CaF_2. The lattice sums leading to (B.4) were done on a computer for H_o parallel to the [111] and [110] directions, for all A neighbors at $r_{ik} < \sqrt{51/4}\ a$. An integral correction for all farther neighbors was added to the computer results, and the resulting [111] and [110] points were fit to the angular functional form derived for $\langle \Delta\omega_B^2 \rangle_{BA}$. Equation (C.1) is accurate to less than 1/2% error.

Inserting $\mathcal{H}_{SS}$ and $\mathcal{H}_{dz}^{AB}$ from (15) and (11), and noting which $Tr_B\{\ \}$ vanish, we find for $\tau_c(\theta)$

$$\tau_c(\theta)^{-2} = -\frac{1}{2} \frac{\left(Tr\left\{ \left[\mathcal{H}_d^A(s), \mathcal{H}_{lx} \right]^2 \right\} + \cos^2\theta\ Tr\left\{ \left[\mathcal{H}_{lz}^{AB}, \mathcal{H}_{lx}^{AB} \right]^2 \right\} \right)}{Tr\left\{ \mathcal{H}_{lx}^2 \right\}} \qquad (C.2)$$

The numerical values of τ_c calculated from (C.2) in CaF_2 show that τ_c is from 50 to 100% larger than T_2(F-F). The first term in (C.2) is the value of the correlation time when $\theta = 90°$, and the additional term proportional to $\cos^2\theta$ shortens τ_c by about 25% when $\theta = 45°$. It is possible that this shortening of τ_c is related to the broadening of the B spin resonance line in the rotating frame, when $\theta \neq 90°$. At $\theta = 90°$ the B spin line is a delta function, except for lifetime broadening.

Putting $\mathcal{H}_d^A(s)$, $\mathcal{H}_{lx}$, and $\mathcal{H}_{lz}$ from (6), (12), and (11) into (C.2), using the commutation relations between A and B spin operators, and evaluating the traces which appear in (C.2), we find:

$$\tau_c(\theta)^2 = L_1 + L_2$$

where

$$L_1 = \frac{4}{3} I(I+1) \sum_{i \neq j} B_{ij}^{A\ 2} (A_{ik}^{AB^2} - A_{jk}^{AB} A_{ik}^{AB}) / (\sum_i A_{ik}^{AB^2})$$

and

$$L_2 = \frac{\frac{\cos^2\theta}{2} \left[\frac{(3I^2+3I-1)}{15} \sum_i (A_{ik}^{AB})^4 + 2I(I+1) (\sum_i A_{ik}^{AB^2})^2 \right]}{\sum_i (AB_{ik}^{AB})^2}$$

The summation index i ranges over the A neighbors of a rare B spin, and the A_{ik}^{AB}, B_{ij}^{A} are given by (8) and (9). For H_o parallel to [111] in CaF_2 (using only a rough approximation to $\sum_i (AB_{ik}^{AB})^4$) we find for $\tau_c(\theta)$, including the off-resonance correction term L_2:

$$\tau_c(\theta)^{-2} \cong \tau_c(90°)^{-2} \left[1 + \cos^2\theta \ (.78) \right]$$

Thus at $\theta = 45°$, $\tau_c \cong 61$ μs, but at $\theta = 90°$, τ_c is 80.5 μs.

$\tau_c(90°)$ was evaluated by computer to about 1% accuracy for H_o parallel to [111] and [110] in CaF_2, and these values are quoted in connection with experimental results.

APPENDIX D

EFFECT OF SMALL RANDOM QUADRUPOLE SPLITTINGS ON THE CROSS-RELAXATION EQUATIONS

1. Effects on ϵ

We consider here the quadrupole splittings caused at some B spin sites in a cubic crystal by random lattice defects and impurities. We shall make the approximation that the distance between quadrupole satellites of a particular B spin k is $\nu_{Qk} \ll f_{1B}$ and specialize to the case of $\theta = 90°$ for simplicity. If $\langle \nu_{Qk} \rangle \gg f_{1B}$ the double resonance line will be reduced in intensity by $\sim f_{1B}/\langle \nu_{Qk} \rangle \ll 1$, and may not be observable. If $\nu_{Qk} \gtrsim f_{1B}$ the situation cannot be handled by an "effective spin 1/2" formalism[69] since all the quadrupolar split B spin levels will interact strongly with H_{1B}, so the effect of the quadrupole splittings would have to be taken account of exactly.

If $\nu_{Qk} \ll f_{1B}$, then only the secular part of the total quadrupole Hamiltonian $\mathcal{H}_{Qk}$ need be added to the B-spin rotating frame Hamiltonian:

$$\mathcal{H}'_{RQ} = \mathcal{H}_Z^{B'} + \mathcal{H}'_{Brf} + \mathcal{H}_d^A(s) + \mathcal{H}_d^{AB}(s) + \mathcal{H}_{Qk}^B$$

where

$$\mathcal{H}_{Qk}^B = \frac{\hbar}{2} \left\{ \frac{2\pi \ \nu_{Qk}(3\mu^2 - 1)}{2} \right\} \left[S_{zk}^2 - \frac{S(S+1)}{3} \right]$$

$$= \frac{\hbar\omega_{Qk}}{2} \left[S_{zk}^2 - \frac{S(S+1)}{3} \right] \quad .$$

Because we know nothing about the particular value of ν_{Qk} at any B spin site, we shall assume that ν_{Qk} is given by a Gaussian random distribution of width $\bar{\nu}_Q$, normalized to the number N_B of B spins per unit volume:

$$P(\nu_{Qk}) = \frac{N_B}{\sqrt{2\pi}\ \bar{\nu}_Q} \ e^{-\left[\nu_{Qk}^2 / 2\bar{\nu}_Q^2\right]} \quad . \qquad \text{(D.1)}$$

$P(\nu_{Qk})d\,\nu_{Qk}$ then gives the number of B spins with $\nu_Q\left\{\frac{3\mu^2-1}{2}\right\}$ in the region ν_{Qk}, $\nu_{Qk} + d\nu_{Qk}$.

The restriction to $f_{1B} \gg \nu_{Qk}$ or $\bar{\nu}_Q$ is not necessarily very serious, because a "minimum" value of f_{1B} has already entered into the theory: the double resonance rates fall to zero with decreasing f_{1B}, and for the thermal reservoir model to hold we must require that H_{1B} be $\gg H_{LB}$ so that the A-B interaction is a small perturbation on both the A and B systems.

Since $\mathcal{H}_{Qk}$ commutes with $\mathcal{H}_d^A(s)$ is it natural to include it in the zero-order B Hamiltonian:

$$\mathcal{H}_{Bk} = -\omega_{1B}S_{xk} + \frac{\omega_{Qk}}{2}\left[S_{zk}^2 - \frac{S(S+1)}{3}\right]$$

The parameter ϵ is the ratio of the A and B spin energies or heat capacities at the same spin temperature, so the only modification to ϵ consists of adding a new term to the B spin energy:

$$\langle E_B\rangle = \mathrm{Tr}\left\{\rho \sum_k \hbar\mathcal{H}_{Bk}\right\} = \frac{-\hbar^2}{\alpha kT}\sum_k \mathrm{Tr}\left\{\mathcal{H}_{Bk}^2\right\}$$

Therefore

$$\epsilon_Q = \frac{\hbar^2}{(2S+1)k}\sum_k \mathrm{Tr}\left\{\mathcal{H}_{Bk}^2\right\}/C_A H_{LA}'^2$$

But

$$\mathrm{Tr}\left\{\mathcal{H}_{Bk}^2\right\}$$

$$= \frac{\omega_{1B}^2\,(2S+1)S(S+1)}{3}\left[1 + \frac{(4S^2+4S-3)}{60}\left(\frac{\nu_{Qk}}{f_{1B}}\right)^2\right]$$

Since $\int_{-\infty}^{\infty} d\nu_{Qk}\, P(\nu_{Qk}) = N_B$

$$\int_{-\infty}^{\infty} d\nu_{Qk} \quad \nu_{Qk}^2 \, P(\nu_{Qk}) = N_B \, \bar{\nu}_Q^{\,2} \quad ,$$

averaging over the Gaussian distribution of quadrupole splittings yields:

$$\epsilon_Q = \epsilon \left[1 + \frac{\nu_Q^2}{f_{1B}^2} \left(\frac{4S^2+4S-3}{60} \right) \right]$$

$$= \epsilon \left[1 + \frac{\nu_Q^2}{f_{1B}^2} \right] \text{ (for } S = 7/2) \qquad \text{(D.2)}$$

Thus any quadrupole splitting effects on ϵ would noticeable only near $f_{1B} \lesssim \bar{\nu}_Q$, where the perturbation treatment is probably no longer valid.

2. Effects on τ_{AB}^{-1}

If $\mathcal{H}_{Qk}$ is lumped with $-\omega_{1B} S_{xk}$ to form a new B spin Hamiltonian $\mathcal{H}_{Bk}$, then the density matrix derivation for $\frac{dE_A}{dt}$ remains unchanged down to the point:

$$\frac{dE_A}{dt} \cong \frac{\hbar^2}{\alpha k} \int_0^{\infty} d\tau \; \mathrm{Tr} \left\{ \mathcal{H}_d^A \left[\mathcal{H}^*(0); \mathcal{H}^*(-\tau), \mathcal{H}_d^A \right] \right\} \left(T_A^{-1} - T_B^{-1} \right) , \qquad \text{(D.3)}$$

since $\mathcal{H}_{Bk}$ still commutes with the density matrix and with $\mathcal{H}_d^A$, and the correlation function still vanishes for long times.

Here

$$\mathcal{H}^*(t) = \sum_{i,k} A_{ik}^{AB} \, I_{zi}(t) \quad (T_B(t) S_{zk} T_B^{-1}(t))$$

with

$$T_B(t) = \exp\left[i\mathcal{H}_B t \right] = \prod_{k'} \exp\left[i\mathcal{H}_{Bk'} t \right] ,$$

so that we can write the time-dependent B factor as a function of only the kth B spin operator:

$$\mathcal{H}^*(t) = \sum_{i,k} A_{ik}^{AB} I_{zi}(t) S_{zk}(t)$$

$$= \sum_k A_k(t)\, S_{zk}(t) = \sum_k \mathcal{H}_k^*(t),$$

where $$A_k(t) = \sum_i A_{ik}^{AB} I_{zi}(t)$$

and $$S_{zk}(t) = e^{i\mathcal{H}_{Bk}t} S_{zk} e^{-i\mathcal{H}_{Bk}t}.$$

By the properties of the Tr_B { }, terms in (D.3) which are of the following form vanish,

$$\int_0^\infty d\tau\ \mathrm{Tr}\left\{\mathcal{H}_d^A\left[\mathcal{H}_k^*(0); \mathcal{H}_{k'}^*(-\tau), \mathcal{H}_d^A\right]\right\},$$

if $k \neq k'$, because then $S_{zk'}(-\tau)$ and $S_{zk}(0)$ commute with everything, can be taken outside the commutator, and have vanishing trace over the B spins. Then Eq. (D.3) becomes a sum of separate contributions from each B spin in the sample:

$$\frac{dE_A}{dt} \simeq \left(\frac{dE_A}{dt}\right)_k$$

$$= \frac{\hbar^2}{\alpha k}\left(\frac{1}{T_A} - \frac{1}{T_B}\right)\sum_k \int_0^\infty d\tau\ \mathrm{Tr}\left\{\mathcal{H}_d^A\left[\mathcal{H}_k^*(0); \mathcal{H}_k^*(-\tau), \mathcal{H}_d^A\right]\right\}.$$

As before, by the properties of the trace

$$\mathrm{Tr}\left\{\mathcal{H}_d^A\left[\mathcal{H}_k^*(0); \mathcal{H}_k^*(-\tau), \mathcal{H}_d^A\right]\right\}$$

$$= \mathrm{Tr}\left\{\mathcal{H}_k^*(0)\left[\mathcal{H}_d^A; \mathcal{H}_d^A, \mathcal{H}_k^*(-\tau)\right]\right\}$$

Since $S_{zk}(-\tau)$ contains only B spin operators it can be brought outside the commutator:

$$\left[\mathcal{H}_d^A; \mathcal{H}_d^A, \mathcal{H}_k^*(-\tau)\right] = \left[\mathcal{H}_d^A; \mathcal{H}_d^A, A_k(-\tau)\right] S_{zk}(-\tau) \quad .$$

Then the previous relation between a time derivative and a commutator can be applied to yield:

$$\begin{aligned} &\mathrm{Tr}\left\{\mathcal{H}_k^*(0)\left[\mathcal{H}_d^A; \mathcal{H}_d^A, \mathcal{H}_k^*(-\tau)\right]\right\} \\ &= \mathrm{Tr}_A\left\{A_k(0)\frac{d^2}{d\tau^2}A_k(-\tau)\right\}\ \mathrm{Tr}_B\left\{S_{zk}\ S_{zk}(-\tau)\right\} \\ &= \left[\frac{d^2 g_A}{d\tau^2}(-\tau)\right]\ g_B(-\tau), \end{aligned}$$

The major difference between the case with quadrupole splittings and without quadrupole splittings is that the B spin correlation function is simply proportional to $\cos(\omega_{1B}\tau)$ in the latter case. The small quadrupole splitting case then reduces to the evaluation $\mathrm{Tr}_B\left\{S_{zk}S_{zk}(-\tau)\right\}$.

It is at this point that the perturbation approximation $\nu_{Qk} \ll f_{1B}$ becomes necessary, because we shall evaluate $\mathrm{Tr}_B\left\{S_{zk}S_{zk}(-\tau)\right\}$ to second order in the small quantity ν_{Qk}, using the approximate operator identity:[70]

$$e^{A+\lambda B} \simeq e^{A}\left[1 + \lambda S_1 + \lambda S_2\right] \qquad (D.5)$$

where

$$S_1 = \int_0^1 dx\ e^{-Ax}\ B e^{Ax}$$

and

$$S_2 = \int_0^1 \int_0^1 x\,dx\,dx'\, e^{-Ax}\, B e^{Ax(1-x')}\, B e^{Axx'}$$

We intend to evaluate

$$\exp\left[\pm i\tau\left(-\omega_{1B} S_{xk} + \lambda \frac{\omega_{Qk}}{2} S_{zk}^2\right)\right] = e^{\pm i\tau \mathcal{H}_{Bk}}$$

by (D.5) and then set $\lambda = 1$, so

$$A = \pm i\phi S_{xk} \quad \text{and} \quad B = \pm i\, \xi S_{zk}^2$$

where

$$\phi = \omega_{1B}\tau \quad \text{and} \quad \xi = \omega_{Qk}\tau/2$$

The term $\propto S(S+1)$ in $\mathcal{H}_{Bk}$ commutes with everything so it can be neglected in the exponential.

Some of the integrals in $\mathrm{Tr}_B\left\{S_{zk} S_{zk}(-\tau)\right\}$ simplify if quantities such as $e^{-Ax}\, B\, e^{-Ax}$ are first evaluated and $\mathrm{Tr}_B\{\ \}$ is brought under the integrals, since many of the $\mathrm{Tr}_B\{\ \}$ vanish, and parts of the integrands cancel when the sign of τ is changed. Expansion of $e^{\mp i \mathcal{H}_{Bk}\tau}$ using (D.5) yields:

$$e^{\mp i\, \mathcal{H}_{Bk}\tau} \simeq e^{\pm i\, \theta S_{xk}} M(\pm) \tag{D.6}$$

where $M(\pm) = 1 + \lambda\, M_1(\pm) + \lambda^2\, M_2(\pm)$

$$= 1 + \lambda \sum_{i=1}^{3} I_i(+)\, O_i + \lambda^2 \sum_{i=1}^{9} F_i(\pm)\, P_i,$$

and for example

$$I_1(+) = \int_0^1 dx\ (-i\xi)\cos^2(\phi x),\ O_1 = S_{zk}^2$$

$$I_2(+) = \int_0^1 dx(-i\xi)(-\sin\phi x \cos\phi x),\ O_2 = (S_{zk}S_{yk} + S_{yk}S_{zk})$$

$$I_3(+) = \int_0^1 dx(-i\xi)\ \sin^2\phi x,\ 0^3 = S_{yk}^2$$

$$F_1(+) = \int_0^1 xdx\ (-i\xi)^2\ \cos^2\phi x\left(\frac{1}{2} + \frac{\sin 2\phi x}{4\phi x}\right)$$

$$P_1 = S_{zk}^4\ ,$$

etc. The $I_i(-)$ and $F_i(-)$ are obtained from $I_i(+)$ and $F_i(+)$ respectively by changing the sign of τ, that is of both ϕ and ξ. Changing this sign in the explicit expressions yields for the integrals the symmetry properties:

$$I_i(-) = (-1)^i\ \ I_i(+)\ \ ,\ Fi(-) = (-1)^{i+1}\ \ F_i(+)\ . \qquad (D.7)$$

Expansion of the B spin correlation function to second order in λ^2 using (D.5), (D.6), (D.7), and vanishing of some of the $Tr_B\{\ \}$ yields, after a lengthy calculation:

$$Tr_B\left\{S_{zk}\ e^{-\mathcal{H}_{Bk}\tau}\ S_{zk}\ e^{+\mathcal{H}_{Bk}\tau}\right\}$$

$$\cong\ Tr_B\left\{S_{zk}^2\right\}\cos\omega_{1B}\tau$$

$$-\lambda^2\left(\frac{\nu_{Qk}}{4f_{1B}}\right)^2\left[Tr_1\ F_1(\omega_{1B}\tau) + Tr_2\ F_2(\omega_{1B}\tau)\right]$$

where $Tr_1 = Tr_B\left\{S_{zk}^4\ S_{yk}^2\right\}$, $Tr_2 = Tr_B\left\{S_{zk}^2\ S_{yk}\ S_{zk}^2\ S_{yk}\right\}$,

$$F_1(\phi) = \phi^2\ \cos\phi - \phi\ \sin\phi$$

and $$F_2(\phi) = -F_1(\phi)$$

But according to Eqs. (D.4), (D.1), and (24)

$$\left(\frac{dE_A}{dt}\right) \cong \sum_k \frac{\hbar^2}{\alpha k}\left(\frac{1}{T_A} - \frac{1}{T_B}\right)\int_0^\infty d\tau \left[\frac{d^2}{d\tau^2} g_A(-\tau)\right] g_B(-\tau)$$

$$= \frac{\hbar^2}{\alpha k}\left(\frac{1}{T_A} - \frac{1}{T_B}\right)\int_{-\infty}^{\infty} d\nu_{Qk} P(\nu_{Qk}) \int_0^\infty d\tau\, g_B(-\tau)\, \frac{d^2}{d\tau^2} g_A(-\tau)$$

$$= - C_A H'^2_{LA} \frac{d}{dt}\left(\frac{1}{T_A}\right) = - C_A H'^2_{LA} \left\langle \frac{\epsilon}{\tau_{AB}} \right\rangle_Q \left(\frac{1}{T_A} - \frac{1}{T_B}\right) ,$$

so that if we let $\lambda = 1$:

$$\left\langle \frac{\epsilon}{\tau_{AB}} \right\rangle_Q = \left(\frac{\epsilon}{\tau_{AB}}\right)\left[1 + \left(\frac{\bar{\nu}_Q}{4f_{1B}}\right)^2 \int_0^\infty d\tau\, f''(\tau)\, F_1(\omega_{1B}\tau)(Tr_1 - Tr_2)\right] \tag{D.8}$$

and $(Tr_1 - Tr_2) \cong (22.9911 - 16.9911)$ for $S = 7/2$,[71] and if we assume the same form for $g_A(-\tau)$ as in Section II.C.2., Eq. (56).

The correction term in (D.8) has been evaluated numerically for both Lorentzian and Gaussian $g_A(\tau)$ for H_o parallel to the [111] direction ($\tau_c = 80.6$ sec, $\langle \Delta\omega_B^2 \rangle_{BA} = 3.63 \times 10^7$). The value of $(\tau_{AB}^{-1})_Q$ is given by

$$(\tau_{AB}^{-1})_Q = \frac{1}{\epsilon_Q}\left(\frac{\epsilon}{\tau_{AB}}\right)_Q = \left(\frac{1}{\tau_{AB}}\right)_0 \frac{1}{\left(1 + \frac{\bar{\nu}_Q^2}{f_{1B}^2}\right)}\left[1 - \left(\frac{\bar{\nu}_Q}{4f_{1B}}\right)^2 \mathcal{K}(f_{1B})\right] ,$$

if we use Eq. (D.2) for ϵ_Q.

$\mathcal{K}(f_{1B})$ is given by (for $\tau_c = 80.6$ sec; $\langle \Delta\omega_B^2 \rangle_{BA} = 3.63 \times 10^7$):

Table VI: H_{1B} dependence of quadrupolar correction terms

f_{1B}(kHz)	1.0	2.0	3.0	4.0	5.0	6.0	7.0	8.0	9.0	10.0
	7.307	11.80	13.49	12.36	8.43	1.685	-7.86	-20.2	-35.4	-53.3

11.0	12.0	13.0	14.0
-74.0	-97.4	-123.	-152.

The change of sign of $\mathcal{L}(f_{1B})$ occurs also for the Gaussian $g_A(-\tau)$, but at a smaller value of f_{1B}. This behavior could be qualitatively understood by noting that at low f_{1B} the changes in matrix elements of the A-B dipolar perturbation might lead to a smaller τ_{AB}^{-1}, while at high f_{1B} the higher-lying quadrupole satellites allow a greater energy exchange between A and B spin systems. But perhaps the most disturbing feature of this calculation is that as $f_{1B} \to \infty$, the quadrupole effects do not become negligible, since $\mathcal{L}(f_{1B})$ increases faster than f_{1B}^2. This probably is the result of expanding a function for small τ and then using this expansion in an $\int_0^\infty d\tau$, which is obviously dangerous unless the function $g_B(\tau)$ really obeys the approximate form out to where $g_A(-\tau)$ cuts off the integrand. Because the perturbation is obviously becoming relatively more important for large f_{1B}, it would be dangerous to draw any conclusions based on this calculation.

Instead of using the density matrix method of calculating τ_{AB}^{-1}, one can calculate the individual cross-relaxation transition probabilities, and use the expression of Lurie and Slichter[11] for τ_{AB}^{-1}:

$$\tau_{AB}^{-1} \propto \sum_{\substack{r,s \\ k}} g_k \, (\omega_{rs}^k)(\omega_{rs}^k)^2 \, \langle \tilde{s}| S_{xk} |\tilde{r}\rangle \langle \tilde{r}| S_{xk} |\tilde{s}\rangle \ .$$

Here $|\tilde{r}\rangle$ and $|\tilde{s}\rangle$ are the B Zeeman states perturbed by the quadrupole interaction, $\hbar\omega_{rS}^k = \tilde{E}_r - \tilde{E}_S$, and the index k ranges over the B spins in the crystal, each having a different value of ω_{Qk}. By first order perturbation theory,

$$\omega_{m-1,m}^k \cong \omega_{1B} \, (1 + \Delta_m),$$

and

$$|\langle \tilde{m}-1| S_{xk} |\tilde{m}\rangle| \cong |\langle m-1| S_{xk} |m\rangle|_0 \, (1-\Delta_m)$$

where

$$\Delta_m = \frac{\omega_{Qk}}{\omega_{1B}} \, (m - 1/2) \ .$$

Therefore the first-order changes in ω_{rs}^k and the matrix element cancel, leaving only the change of ω in the spectrum:

$$\delta(\tau_{AB}^{-1}) \, \alpha \sum_{k,m} \left(\frac{\partial g}{\partial \omega}\right) \omega_{1B} \left\{ \begin{array}{l} \Delta_m |\langle m-1| S_x |m\rangle|_0^2 \\ + \Delta_{m+1} |\langle m+1| S_x |m\rangle|_0^2 \end{array} \right\}$$

But this term vanishes if Δ_m and Δ_{m+1} are written out, because $\mathrm{Tr}\{S_x^2 S_z\} = 0 = \mathrm{Tr}\{S_x\}$.

APPENDIX E

EXACT SOLUTION OF THE CROSS-RELAXATION EQUATIONS

Equations (79) and (80) of Section II.E.1 may be rewritten as

$$\dot{E}_A = -\alpha_1 E_A + \alpha_2 E_B \qquad (E.1)$$

$$\dot{E}_B = \alpha_3 E_A - \alpha_2 E_B \,, \qquad (E.2)$$

where $\alpha_1 = \epsilon/\tau_{AB} + T_{1A}^{-1}$,

$\alpha_2 = \tau_{AB}^{-1}$,

and $\alpha_3 = \epsilon\, \tau_{AB}^{-1}$.

Equations (E.1) and (E.2) are equivalent to two uncoupled, second-order differential equations for E_A, E_B; in the solutions, the exponential time constants λ_+^{-1}, λ_-^{-1} are the same for both E_A and E_B:

$$E_A(t) = E_{A+}\, e^{-\lambda_+ t} + E_{A-}\, e^{-\lambda_- t} \qquad (E.3)$$

$$E_B(t) = E_{B+}\, e^{-\lambda_+ t} + E_{B-}\, e^{-\lambda_- t} \,. \qquad (E.4)$$

$E_{A\pm}$ and $E_{B\pm}$ are constants to be determined from the initial conditions E_{Ao}, E_{Bo}, and $\lambda_\pm$ are given by

$$\lambda_\pm = \frac{(\alpha_1+\alpha_2)[1 \pm \sqrt{1-4\,y}\,]}{2} \,,$$

where

$$y = x(1+\epsilon)^{-1}\,(1+x^2)^{-1} \,,$$

and

$$x = \tau_{AB}(1+\epsilon)^{-1}\, T_{1A}^{-1} \,.$$

The constants $E_{A\pm}$, $E_{B\pm}$ are found from $E_A(0)$ and $E_B(0)$ using equations (E.1) and (E.2), and the definitions $E_A(0) = E_{Ao}$, $E_B(0) = E_{Bo}$:

$$E_{A+} = \frac{E_{Ao}(\lambda_- - \alpha_1) + \alpha_2 E_{Bo}}{(\lambda_- - \lambda_+)} \equiv \eta_1 E_{Ao} + \eta_2 E_{Bo} \qquad (E.5)$$

$$E_{B-} = \frac{E_{Ao}(\alpha_1 - \lambda_+) - \alpha_2 E_{Bo}}{(\lambda_- - \lambda_+)} \equiv \eta_3 E_{Ao} + \eta_4 E_{Bo} \qquad (E.6)$$

$$E_{B+} = \frac{\alpha_3 E_{Ao} + (\lambda_- - \alpha_2) E_{Bo}}{(\lambda_- - \lambda_+)} \equiv \xi_3 E_{Ao} + \xi_4 E_{Bo} , \qquad (E.7)$$

$$E_{B-} = \frac{-\alpha_3 E_{Ao} + (\alpha_2 - \lambda_+) E_{Bo}}{(\lambda_- - \lambda_+)} \equiv \xi_1 E_{Ao} + \xi_2 E_{Bo} \qquad (E.8)$$

Using (E.3), (E.4) and (E.5) through (E.8) we can finally write out

$$E_A(\tau) = z_1(\tau) E_{Ao} + z_2(\tau) E_{Bo} \qquad (E.9)$$

$$E_B(\tau) = -z_3(\tau) E_{Ao} + z_4(\tau) E_{Bo} , \qquad (E.10)$$

where

$$z_1 = \eta_1 e^{-\lambda_+ \tau} + \eta_3 e^{-\lambda_- \tau}$$

$$z_2 = \eta_2 e^{-\lambda_+ \tau} + \eta_4 e^{-\lambda_- \tau}$$

$$z_3 = \xi_3 e^{-\lambda_+ \tau} + \xi_1 e^{-\lambda_- \tau}$$

and

$$z_4 = \xi_4 e^{-\lambda_+ \tau} + \xi_2 e^{-\lambda_- \tau} .$$

Equations (E.9) and (E.10) only describe what happens to the energies during the B rf pulse. During the time τ_o between B rf pulses $E_A(\tau)$ relaxes according to its exponential law, and the component of M_B perpendicular to H_o decays in a time of order T_{2B}:

$$E_A(t) = E_A(\tau) e^{-t/T_{1A}} \quad (\tau \leq t \leq \tau + \tau_o)$$

and $$M_x^B = - \frac{E_B(\tau)}{H_{eB}} \sin\theta\, f(t) \qquad (\tau \leq t \leq \tau + \tau_o) \ .$$

If $\tau_o \gg T_{2B}$, $M_x^B \to 0$, so we can write (for $\theta = 90^\circ$ case)

$$E_A(\tau+\tau_o) = E_A(n) = z_1 e^{-\tau_o/T_{1A}} E_{Ao}$$

$$\equiv z_1 e^{-\tau_o/T_{1A}} E_A(n-1)$$

Therefore the normalized A signal change for one B rf pulse (for the $\theta = 90^\circ$ case) is given by:

$$\frac{E_A(n)}{E_A(n-1)\, e^{-(\tau_o+\tau)/T_{1A}}} = z_1 e^{+\tau/T_{1A}} \qquad \text{(E.11)}$$

Assuming x is small and expanding Eq. (E.11) to first order in x gives the equation (84) for the first order effect of T_{1A} on the normalized A signal. The exact computer program fits the normalized signals to Eq. (E.11).

To analyze the $\theta = 30^\circ$ data we find the eigenvalues $\lambda_\pm$ of the matrix M:

$$\lambda_\pm = \frac{(C_1' + C_4')}{2} \pm \frac{1}{2} \sqrt{(C_1'-C_4')^2 + 4C_2'C_3'} \ .$$

Then α, β are given by:

$$\alpha = \frac{\lambda_+\lambda_-^N - \lambda_-\lambda_+^N}{(\lambda_+ - \lambda_-)} \ ,$$

$$\beta = \frac{(\lambda_+^N - \lambda_-^N)}{(\lambda_+ - \lambda_-)} \ .$$

Then $E_A(N)$ is given by:

$$E_A(N) = (\alpha + \beta C_1') E_A(0) + \beta C_2' M_Z^B(0) ,$$

The parameter $\left(\frac{\beta C_2'}{\alpha+\beta C_1'}\right)\left(\frac{E_B(0)}{E_A(0)}\right)$, which measures the relative dependence of $E_A(N)$ on $M_Z^B(0)$, varies between 0 for $\tau = 0$ and $\sim \epsilon \cos^2\theta$ for $\tau \gg \tau_{AB}$. Here $E_B(0) \lesssim \epsilon E_A(0)$ since the largest value of M_Z^B is likely to come from contact with the cold A spin reservoir during the preceding B rf pulse.

REFERENCES

1. A. Abragam, The Principles of Nuclear Magnetism (Oxford University Press, London, 1961) Chap. III.
2. S. R. Hartmann and E. L. Hahn, Phys. Rev. 128, 2042 (1962).
3. A. G. Redfield, Phys. Rev. 130, 589 (1963).
4. R. E. Slusher and E. L. Hahn, Phys. Rev. Letters 12, 246 (1964).
5. R. E. Slusher, thesis, University of California, Berkeley (unpublished).
6. A. G. Anderson and S. R. Hartmann, Phys. Rev. 128, 2023 (1962).
7. R. E. Walstedt, D. A. McArthur and E. L. Hahn, Phys. Letters 15, 7 (1965).
8. N. Bloembergen and P. P. Sorokin, Phys. Rev. 110, 865 (1958).
9. A. Hartland, Phys. Letters 20, 567 (1966).
10. R. T. Schumacher, private communication.
11. F. M. Lurie and C. P. Slichter, Phys. Rev. 133, A 1108 (1964).
12. T. P. Das and E. L. Hahn, Nuclear Quadrupole Resonance Spectroscopy (Academic Press, New York, 1958) Chap. III.
13. A. Abragam, The Principles of Nuclear Magnetism Oxford University Press, London, 1961) Chap. V.
14. A. Abragam and W. G. Proctor, Phys. Rev. 109, 1441 (1958).
15. I. J. Lowe and S. Gade, Phys. Rev. 156, 817 (1967).
16. A. G. Redfield, Phys. Rev. 98, 1787 (1955).
17. R. L. Strombotne and E. L. Hahn, Phys. Rev. 133, A 1616 (1964).
18. J. Jeener, H. Eisendrath and R. Van Steenwinkel, Phys. Rev. 133, A 478 (1964).
19. A. Abragam, The Principles of Nuclear Magnetism (Oxford University Press, London, 1961) Chap. IV.
20. J. Philippot, Phys. Rev. 133, A 471 (1964).

21. J. R. Franz and C. P. Slichter, Phys. Rev. 148, 287 (1966).

22. L. D. Landau and E. M. Lifschitz, Quantum Mechanics, Non-Relativistic Theory (Pergamon Press, Oxford, 1965) p. 149.

23. A. Abragam, The Principles of Nuclear Magnetism (Oxford University Press, London, 1961) Chap. VIII.

24. S. Fujita, Non-Equilibrium Quantum Statistical Mechanics (W. B. Saunders Co., Phildelphia, 1966) Chap. 4.

25. B. N. Provotorov, J. Exptl. Theoret. Phys. (USSR) 41, 1582 (1961); Soviet Phys. JETP 14, 1126 (1962).

26. R. E. Walstedt, Phys. Rev. 138, A 1096 (1965).

27. R. T. Schumacher, Phys. Rev. 112, 837 (1958).

28. J. H. Van Vleck, Phys. Rev. 74, 1168 (1948).

29. S. Clough, Phys. Letters 24A, 49 (1967).

30. P. W. Anderson and P. R. Weiss, Rev. Mod. Phys. 25, 269 (1953).

31. R. V. Churchill, Fourier Series and Boundary Value Problems (McGraw-Hill Book Co., New York, 1941) p. 89.

32. I. S. Gradshteyn and I. M. Ryzhik, Table of Integrals, Series and Products (Academic Press, New York, 1965) p. 312.

33. A. Abragam, The Principles of Nuclear Magnetism (Oxford University Press, London, 1961) Chap. X.

34. A. Messiah, Quantum Mechanics, Vol. II (North-Holland Publ. Co., Amsterdam, 1962) Chap. XVI.

35. S. Wilking, Z. für Physik, 173, 509 (1963).

36. P. H. Dederichs and G. Leibfried, Z. für Physik, 184, 521 (1965).

37. H. Margenau and G. M. Murphy, The Mathematics of Physics and Chemistry 2nd Edition (D. Van Nostrand Co., New York, 1956) p. 517.

38. R. E. Walstedt, private communication.

39. B. Friedman, Principles and Techniques of Applied Mathematics (John Wiley and Sons, Inc., New York, 1956) p. 121.

40. J. Reichert and J. Townsend, Rev. Sci. Inst. 35, 1692 (1964).

41. F. Bloch and A. Siegert, Phys. Rev. 57, 522 (1940).

42. M. J. Buerger, Crystal-Structure Analysis (John Wiley and Sons, Inc., New York, 1960) Chap. 5.

43. J. R. White and A. E. Cameron, Phys. Rev. 74, 991 (1948).

44. A. O. Nier, Phys. Rev. 53, 282 (1938).

45. R. M. Sternheimer, Phys. Rev. 146, 140 (1966).

46. P. W. Anderson, J. Phys. Soc., Japan 9, 316 (1954).

47. J. Van Kranendonk, Physica 20, 781 (1954).

48. R. L. Meiher, Phys. Rev. 125, 1537 (1962).

49. R. K. Wangsness and F. Bloch, Phys. Rev. 89, 728 (1953).

50. T. P. Das, D. K. Roy and S. K. Ghosh Roy, Phys. Rev. 104, 1568 (1956).

51. E. G. Wikner, W. E. Blumberg and E. L. Hahn, Phys. Rev. 118, 631 (1960).

52. A. Abragam, The Principles of Nuclear Magnetism (Oxford University Press, London, 1961) Chap. IX.

53. W. A. Wooster, Zeits. f. Kristallographie 94, 375 (1936).

54. M. J. Stevenson and C. H. Townes, Phys. Rev. 107, 635 (1957).

55. T. Chiba, J. Chem. Phys. 39, 947 (1963).

56. D. C. Look and I. J. Lowe, J. Chem. Phys. 44, 2995 (1966).

57. G. E. Pake, J. Chem. Phys. 16, 327 (1948).

58. Cedric J. Gabriel, Thesis, University of California, Berkeley (unpublished).

59. V. Hughes and L. Grabner, Phys. Rev. 79, 829 (1950).

60. M. Atoji and R. E. Rundle, J. Chem. Phys. 29, 1306 (1958).

61. R. W. G. Wycoff, Crystal Structures (Interscience Pub., New York, 1963) Vol. I, Chap. IV.

62. N. Bloembergen, Physica 15, 386 (1949).

63. P. G. deGennes, J. Phys. Chem. Solids 7, 345 (1958).

64. W. E. Blumberg, Phys. Rev. 119, 79 (1960).

65. D. F. Holcomb and B. Pedersen, J. Chem. Phys. 38, 54 (1963).

66. B. Pedersen, J. Chem. Phys. 41, 122 (1964).

67. W. Band, Introduction to Mathematical Physics (D. Van Nostrand Co., Princeton, 1959) Chap. II.

68. J. L. Powell and B. Craseman, Quantum Mechanics (Addison-Wesley Pub. Co., Reading, Mass., 1961) Appendix A-7.

69. A. Abragam, The Principles of Nuclear Magnetism (Oxford University Press, London, 1961) Chap. II.

70. E. J. Jaynes and S. P. Heims, Rev. Mod. Phys. 34, 143 (1962); R. Karplus and J. Schwinger, Phys. Rev. 73, 1020 (1948).

71. E. Ambler, J. C. Eisenstein and J. F. Schooley, J. Math. Phys. 3, 118 (1962).